January 2021

Synthesis Of A Gemini Monomer And Cyclobutane-Containing Bifunctional Building Blocks For Novel Materials

Rahul Kumar Shahni

SYNTHESIS OF A GEMINI MONOMER AND CYCLOBUTANE-CONTAINING BIFUNCTIONAL BUILDING BLOCKS FOR NOVEL MATERIALS

By

Rahul Kumar Shahni
Bachelor of Science in Chemistry, University of Delhi, 2009
Master of Science in Chemistry, Indian Institute of Technology Delhi, 2013

A Dissertation
Submitted to the Graduate Faculty

of the

University of North Dakota

in partial fulfillment of the requirements

for the degree of

Doctor of Philosophy

Grand Forks, North Dakota

August
2021

This dissertation, submitted by Rahul Kumar Shahni in partial fulfillment of the requirements for the Degree of Doctor of Philosophy from the University of North Dakota, has been read by the Faculty Advisory Committee under whom the work has been done and is hereby approved.

_____
Dr. Qianli Chu (Chairperson)

_____
Dr. Irina P. Smoliakova

_____
Dr. Guodong Du

_____
Dr. Alena Kubatova

_____
Dr. Edward Kolodka

This dissertation is being submitted by the appointed advisory committee as having met all of the requirements of the School of Graduate Studies at the University of North Dakota and is hereby approved.

_____
Chris Nelson
Dean of the School of Graduate Studies

_____
Date

PERMISSION

Title SYNTHESIS OF A GEMINI MONOMER AND CYCLOBUTANE-CONTAINING BIFUNCTIONAL BUILDING BLOCKS FOR NOVEL MATERIALS

Department Chemistry

Degree Doctor of Philosophy

In presenting this dissertation in partial fulfillment of the requirements for a graduate degree from the University of North Dakota, I agree that the library of this University shall make it freely available for inspection. I further agree that permission for extensive copying for scholarly purposes may be granted by the professor who supervised dissertation work or, in his absence, by the Chairperson of the department or the dean of the School of Graduate Studies. It is understood that any copying or publication or other use of this dissertation or part thereof for financial gain shall not be allowed without my written permission. It is also understood that due recognition shall be given to me and to the University of North Dakota in any scholarly use which may be made of any material in my dissertation.

Rahul Kumar Shahni

July 7th, 2021

TABLE OF CONTENTS

LIST OF FIGURES

LIST OF TABLES

LIST OF SCHEMES

LIST OF ABBREVIATION

2D: Two-dimensional

2D-GIWAXS: Two-dimensional grazing incidence wide-angle X-ray scattering

BPA: Bisphenol-A

CBAM-1: *trans*-1,3-Cyclobutane diamine

CBDA-1: *trans*-1,3-Cyclobutane diacid

CBDA-2: Di-2-furanyl-1,2-cyclobutanedicarboxylic acid

CBDN: *trans*-1,3-Dinitro-2,4-diphenyl cyclobutane

CBDO-1: *trans*-1,3-Cyclobutane dimethanol

CBPs: Cyclobutane-containing polymers

CBs: Cylocbutane-containing building blocks

CHDM: 1,4-Cyclohexane dimethanol

CPE: Chlorinated polyethylene

DCM: Dichloromethane

DDGS: Dried distillers grains with solubles

DMF: *N*,*N*-dimethyformamide

DMSO: Dimethyl sulfoxide

DMT: Dimethyl terephthalate

DOSY: Diffusion orderedsSpectroscopy

DSC: Differential scanning calorimetry

EBP:	ethylene 1,2-bis (2,4-pentadienoate)
FDCA:	2,5-Furandicarboxylic acid
FT-IR:	Fourier transform infrared spectroscopy
FVP:	Flash vacuum pyrolysis
GPC:	Gel permeation chromatography
HFIP:	hexafluoroisopropanol
HPPs:	High-performance polymers
HRMS:	High resolution mass spectrometer
NMR:	Nuclear magnetic resonance
ORTEP:	Oak ridge thermal ellipsoid plot
PA10T:	polydecamethylene terephthalamide
PA6T/6:	poly(hexamethylene terephthalamide)-co-polycaprolactam
PA9T:	poly-1,9-nonamethylene terephthalamide
PCBA:	polycyclobutane adipate
PCBC:	polycyclobutane-1,3-cyclobutane-dicarboxylate
PCBF:	polycyclobutane furandicarboxylate
PCBG:	polycyclobutane glutarate
PCBM:	polycyclobutane malonate
PCBO:	polycyclobutane oxalate
PCBS:	polycyclobutane succinate
PCBT:	polycyclobutane terephthalate
PCS:	polycyclobutane succinamide
PCT:	polycyclobutane terepthalamide

PEBP:	poly(ethylene 1,2-bis(penta2,4-dienoate))
PEF:	polyethylene 2,5-furandicarboxylate
PET:	polyethylene terephthalate
PMDA:	pyromellitic anhydride
PMMA:	polymethyl methacrylate
PS:	polystyrene
Py:	Pyridine
SC-XRD:	Single crystal X-ray diffraction
SEM:	Scanning electron microscopy
$T_{5\%}$:	Temperature at onset of decomposition
T_d:	Temperature at maximum decomposition
TFA:	Trifluoroacetic acid
T_g:	Glass transition temperature
TGA:	Thermogravimetric analysis
TMCD:	2,2,4,4-tetramethyl-1,3-cyclobutanediol
TMS:	tetramethylsilane
TPP:	triphenyl phosphite
UTM:	Universal testing machine

ACKNOWLEDGMENTS

This journey of half a decade has been transformational for me. These years have helped me not only to grow as a scientist but also to grow as an individual. I want to thank each and every one who had contributed to my growth in their own ways.

I would like to thank my advisor, Dr. Qianli Rick Chu, for believing in me. He has always pushed me out of my comfort zone to tread into the unexplored. He has given me the freedom to address fundamental questions of organic chemistry independently. He has always encouraged me to practice leadership roles in the lab and outside, have worked with me tirelessly during every phase of grad school, and have nurtured in me the ability to think critically. His excellent problem-solving skills and pursuit of cutting-edge techniques are qualities that I have always adored. This journey would have been impossible without his constant support and guidance.

I would also like to thank my current committee members, Dr. Irina P. Smoliakova, Dr. Guodong Du, Dr. Alena Kubatova, and Dr. Edward Kolodka, for their friendly guidance, suggestions, and knowledge they offered to me over the years. I Thank Dr. Smoliakova for her guidance and support in my graduate study. I especially enjoyed working under her as a graduate teaching assistant. I am grateful to Dr. Du, for providing me with suggestions in my research and using NMR for advanced experiments. Thank Dr. Alena Kubatova, who has allowed me to teach the Chem 342 lecture course. I would also like to thank Dr. Kolodka for being a committee member and his support in my doctoral

program. I appreciate the assistance and numerous advices of former advisory committee members Dr. Kathryn Thomasson and Dr. Alexei Novikov. I want to express my gratitude to the University of North Dakota Chemistry Department for giving me the chance to pursue my graduate studies and for the support they have offered, both financially and through the almost daily help and encouragement of the faculty and staff. I would like to thank Kimberly Myrum. If it wasn't her work, I would have been buried in correspondence with the graduate school. Shane Johnson have been a pleasure to work with, whether his help in taking care of the NMR or chatting in the hall.

I'm very grateful for the help from former and current members of Dr. Chu's group. They helped me in research and also gave me valuable feedback. I also want to thank Dr. Angel Ugrinov of NDSU for his help with X-ray crystallography. I would also like to thank my fellow graduate students for all the experiences we shared as a part of the Chemistry Graduate Student Association, for the inspiration they gave me through their hard work, and the assistance they offered in learning new techniques and sharing tips for various small, important or unimportant jobs that we had in common. I would like to thank Muneer Shaik, Audrey Lavallie, Sarah Reagan, Joseph Robertson, Dominic Nkemngong and Brent Kastern for being more than fellow graduate students. I always felt welcome knocking on their door.

Thanks to my wonderful parents, Rajesh and Geeta Shahni, for too many things to list. Furthermore, thanks to my wife, Pinky, for all the ways she loves, helps and supports me.

ABSTRACT

Gemini monomer, a new monomeric class that consists of two monomeric units connected by a covalent linker, can offer a highly dense polymeric framework. Moreover, their ability to form twice the number of covalent bonds than the conventional monomer can afford polymers with high thermal and mechanical strength. The desired Gemini monomer, ethylene 1,2-bis (2,4-pentadienoate) (EBP), was synthesized in two steps. First, an acid precursor 2,4-pentadienoic acid was synthesized by the condensation of malonic acid and acrolein. Second, ethylene glycol was used to connect two 2,4-pentadienoic acid units to obtain the monomer. Later, EBP was polymerized in ambient and solvent-free conditions to yield poly[ethylene 1,2-bis(2,4-pentadienoate)] (PEBP). This polymer was found to be inert with most of the organic solvents (DMSO, DMF, etc.), and was thermally stable ($T_{5\%}$ > 300 °C) and displayed high Young's modulus of up to 10.9 GPa with the mechanical strength of 159MPa.

Semi-rigid, thermally stable, symmetrical aliphatic building blocks suitable for materials synthesis are uncommon. One such class of structures is cyclobutane-containing building blocks (CBs). They bridge the gap between their flexible aliphatic chain and rigid aromatic counterparts. The presence of one or more conformational strained four-membered aliphatic rings in CBs gives them a unique blend of rigidity and processability, making them viable in designing and synthesizing novel polymers, metal-organic material, etc. Herein, we report a novel strategy to synthesize a CB, *trans*-1,3-cyclobutane

dimethanol (CBDO-1), a versatile building block that may also serve as a phenol-free BPA replacement. It was synthesized using a facile photoreaction and subsequent reduction. Specifically, an initial photodimerization of *trans*-cinnamic acid using 365 nm blacklight was carried out to form a *trans*-1,3-cyclobutane diacid, CBDA-1, which was then reduced with either $NaBH_4$ in the presence of I_2, or by catalytic hydrogenation using $CuO\text{-}CrO_3$, to give the desired CBDO-1 in excellent yield. To highlight the potential application of this useful primary diol, CBDO-1 and various diacids were used to synthesize novel polyesters via conventional melt polymerization. The thermal properties of this new series of polyesters were studied, including the glass transition temperature, which ranged from 33 to 114 °C, and the decomposition temperature, which ranged from 381 to 424 °C. The ease of synthesis of this cyclobutane-containing CBDO-1 monomer, coupled with its desirable properties, will help develop alternatives for the widely used BPA, and lead to novel and useful materials that are not accessible employing thermal reactions alone.

A diamine functionalized CB such as *trans*-1,3-cyclobutane diamine (CBAM-1) was obtained by the solid-state photodimerization *trans*-nitrostyrene in the slurry state using brine as a medium for forming a suspension. The characterization of CBAM-1 was done using NMR, FT-IR spectroscopy. For the first time, its structure was also determined by using SC-XRD. It was reckoned that semi-rigid CBAM-1 has the right balance of rigidity and flexibility, which can be translated into polyamides with increased processability and desired T_g suitable for various applications. Polyamides were synthesized using CBAM-1 and diacids such as succinic acid and terephthalic acid. Spectroscopic techniques were employed to characterize the polyamides, and their thermal properties were studied.

A biomass-derived CB such as *rctt*-di-2-furanyl-1,2-cyclobutanedicarboxylic acid (CBDA-2) was used as a semi-rigid polytopic ligand to the synthesis of two different green metal-organic materials with Cu^{2+} and Co^{2+} as the metal centers via a solution method. Both the 2D coordination polymers have been characterized by X-ray crystal structure determination and FT-IR spectroscopy. Also, their thermal properties were studied by using TGA and DSC. During this thermal study, both materials showed visual thermochromic behavior.

Chapter 1

A High-Performance Polymer Synthesized from Sustainable Feedstock-derived Gemini Monomer, Ethylene 1,2-Bis(2,4-pentadienoate)

1.1 INTRODUCTION

High-performance polymers (HPPs) are a unique class of polymers. These materials are designed to have excellent attributes when compared to standard and engineering plastics, and are known for their high mechanical strength and high thermal and chemical resistance.[1] In the past, diverse strategies have emerged to synthesize and characterize these HPPs with a unique combination of properties for a distinct range of military, industry, and electronics applications. Typical examples of HPPs, to name are epoxy resins, polyimides, and polyarylene ethers. In these HPPs, the monomers consist of rigid aromatic rings and are most commonly polymerized via solution condensation. However, the very structural principles that provide the above-mentioned outstanding combinations of properties are also responsible for many problems concerning processability. For instance, the melting and dissolving of stiff chains result in an insignificant change of entropy.[2] Hence, these polymers have high melting point and are

only sparingly soluble in most commonly used solvents.[3] The monomeric precursors for most HPPs are obtained or derived from expensive and hazardous raw materials. For example, one of the popular classes of HPPs, polyimides, contributes almost 35% to the total market shares of HPPs and is used in all major industries such as aerospace, automotive, and medical device manufacturing.[4] Polyimides are typically synthesized from an aromatic tetra carboxylic anhydride such as pyromellitic anhydride (PMDA), accounting for 90% of polyimide synthesis.[5] The thoroughly investigated adverse public health and environmental effects of PMDA,[6] on the other hand, have minimized its production and persuaded investigators to find more benign substitutes leading to polymers with properties similar to polyimides.[7]

Among the diverse approaches in developing novel HPPs, monomers derived from natural products such as carbohydrates have attracted many polymer chemists due to their natural abundance, being non-hazardous, and higher sustainability at low costs. For example, isosorbide, a synthon that contains two cis-fused tetrahydrofuran rings,[8] has been used to develop high-performance thermosetting via gylcidylation with similar thermal and mechanical properties to known high-performance epoxy resins.[9] Another widely studied monomer is 2,5-furandicarboxylic acid (FDCA), which can be derived from sucrose as a primarily available biomass feedstock by a sequential process.[10] FDCA based high-performance polyamides exhibit thermal and mechanical properties similar to aromatic polyamides such as poly(*p*-phenylene terephthalamide) (Kevlar) used in high-tech applications.[11] Additionally, trehalose and β-cyclodextrin based monomers have been used to design and develop novel HPPs with high mechanical and adhesion strength.[12]

Our research group recently developed a novel monomer system called Gemini monomers derived from inexpensive and commercially available synthons. This new monomer class can be envisioned as two identical monomeric units separated by a covalent spacer. The unification of two monomer units results in unique bonding characteristics, which have been utilized to yield vital materials, such as polyladdranes[13], polycyclobutanes[14,] and two-dimensional polymers.[15] These materials possess excellent thermal and electronic properties making them suitable candidates for future applications. If we consider the properties of HPPs, the significant factors which contribute the most are the number of primary bonds and their strength. So for a given material, higher the number of high energy primary bonds it have, higher is the thermal, mechanical and chemical resistance.[16] We previously showed that Gemini monomers tend to form more covalent bonds per monomer than conventional monomers.[13-15] Based on the ability to form multiple covalent bonds, it can be hypothesized that a polymer resulted from Gemini monomer would have desired thermal, mechanical, and chemical stability similar to some known HPPs. At the same time, this unique bonding characteristic of Gemini monomer will help the whole polymeric structure stay intact even if some bonds were lost during the application, making Gemini monomer-based polymers a strong candidate for HPPs. In this study, we report the successful synthesis of novel HPP, poly[ethylene 1,2-bis(2,4-pentadienoate)] (PEBP) from symmetric diester Gemini monomer, ethylene 1,2-bis(2,4-pentadienoate) (EBP) prepared from inexpensive and readily available building blocks such as malonic acid, acrolein and ethylene glycol in good yield. The performance of EBP in synthesizing PEBP, as well as its chemical resistance, thermal stability, and mechanical strength were investigated.

1.2 EXPERIMENTAL SECTION

1.2.1 Materials and methods

All the chemicals and solvents were purchased from Alfa Aesar and Aldrich and used without further purification. NMR spectroscopic experiments were performed on a Bruker AVANCE 500 NMR spectrometer at 500 MHz for ^{1}H and 125 MHz for $^{13}C\{^{1}H\}$. Thermo Scientific Nicolet iS5 ATR spectrometer was employed for FT-IR spectroscopic experiments. TGA analyses were carried out on a Hi-Res TGA Q500 thermogravimetric analyzer from TA Instruments at a heating rate of 5 °C/ min, 10 °C/ min & 20 °C/ min under a nitrogen flow of 100 mL/min with a sample weight of ~10 mg. DSC experiments were performed on a Perkin Elmer Jade differential scanning calorimeter using a hermetic aluminum pan, indium standard for calibration, nitrogen as a purge gas, sample weight of ~ 5 mg, from -30 ^{o}C to 250 ^{o}C, and 10 ^{o}C/min heating rates. Tensile testing was performed using a universal testing system with a 5 kN load cell on samples with a dog bone geometry at a 5 mm/min crosshead rate. Scanning electron microscopy (SEM) was used to study the surface properties of polymer on a Hitachi SU8010 UHR cold-emission field emission scanning electron microscope.

1.2.2 Synthesis

1.2.2.1 Synthesis of (E)-2,4-pentadienoic acid

Malonic acid (2.31 mol) was dissolved in 250 mL of pyridine at 30 – 40 °C in a 1-L, three-necked round-bottom flask fitted with a stirrer, reflux condenser, and dropping

funnel. To this stirring solution, a 100 mL (1.50 mol) portion of acrolein was added. After the addition of this first portion of acrolein, the temperature rose to between 65 and 75 °C, and the reaction mixture was stirred for another 15 min. In an analogous manner, second and third portions of acrolein (75 and 25 mL, respectively) were added. After the addition of acrolein, the reaction mixture was allowed to cool down to room temperature, and approximately 1500 g of ice and 500 mL of DCM were added to it. Then the reaction mixture was acidified by dropwise addition of 175 mL of concentrated H_2SO_4. The original 500 mL of DCM was separated, and the aqueous solution was extracted with DCM (50 mL x 3). Hydroquinone (1.5 g) was added to the combined extracts and dried for 12 h over Na_2SO_4. After removing DCM, a yellow residue was transferred to a 2 L Erlenmeyer flask containing 1200 mL of warm (40 °C) petroleum ether, and resulting solution was stirred for 20 min. The solution was then filtered and stored in a refrigerator to allow crystallization. Evaporation of the mother liquor and treatment with more petroleum ether afforded additional (*E*)-2,4-pentadienoic acid. The combined fractions (1.61 mol, 60%) were white crystalline solids and had a melting point range of 71-72 °C. The FT-IR (solid) $\overline{\nu}_{max}$ (cm^{-1}): 3000 (br, O—H), 1685 cm^{-1} (vs, C=O), 1640–1600 (s, C=C), 1400 (w, O—H in plane bending), 1220 (m, C—O), and 690 (m, O—H out-of-plane). ^1H NMR ($CDCl_3$, 500 MHz,): δ, ppm 12.20 (s, 1H), 7.35 (m, 1H), 6.48 (m, 1H).

1.2.2.2 Synthesis of (E)-2,4-pentadienoyl chloride

2,4-Pentadienoic acid (0.20 mol), 80 mL of DCM, and 12 g of molecular sieves (3 Å) were added to a 500 mL, three-necked flask fitted with a stirrer, reflux condenser, dropping funnel, and external sodium hydroxide trap. $(COCl)_2$ (0.42 mol) was then added

dropwise to the reaction mixture. After the addition of $(COCl)_2$, it was stirred continuously for two hours, and the solution was then allowed to stand. The solution was filtered, and removal of solvent yielded *(E)*-2,4-pentadienoyl chloride (0.15 mol, 73%). The FT-IR (KBr, thin film) $\overline{\nu}_{max}$ (cm^{-1}): 1735 (vs, C=O), 1615–1575 (s, C=C), 1020 (s, O=C—C) and 628 (m, C—Cl) The spectrum was devoid of absorption above 3000 cm^{-1}, near1400 cm^{-1}, and 1200 cm^{-1}.

1.2.2.3 Synthesis of the Gemini monomer

Ethylene glycol (0.06 mol), 280 mL of DCM, and 30 g molecular sieves (3Å) were added to a 500 mL, three-necked round bottom flask fitted with a stirrer, reflux condenser, and dropping funnel. The reaction was stirred for 30 min at room temperature followed by dropwise addition of a solution of 15 g of 2,4-pentadienoyl chloride in 30 mL of DCM. The reaction was exothermic, and temperature rose to 40-45°C during the addition of the acid chloride. After the addition, the reaction mixture was stirred for an additional 72 h while temperature was maintained at 60-65 °C. The molecular sieves were then removed by filtration, and flash chromatography by using ethyl acetate /hexane (1% ethyl acetate) as eluent afforded the symmetric diester Gemini monomer, ethylene 1,2-bis(2,4-pentadienoate) (EBP), with a total yield of 70%. The FT-IR (solid) $\overline{\nu}_{max}$ (cm^{-1}):1712 (vs, C=O), 1641 – 1600 (m, C=C), 1140 (s, C—O), and 745 (w, C=C—H bending). ^{1}H NMR ($CDCl_3$): δ 7.21 (m, 2H), 6.40 (m, 2H), 5.87 (d, J = 15 Hz, 2H), 5.55 (dd, J = 15 Hz, 2H), 5.45 (d, J = 10 Hz, 2H), 4.33 (s, 4H). $^{13}C\{^1H\}$ NMR ($CDCl_3$, 125 MHz): δ 165, 144, 133, 124, 120, 61.

1.2.3 Polymerization and tensile bars preparation

1.2.3.1 Method A, thermal preparation

The monomer EBP was weighed and put into a 20-mL scintillation glass vial, which was subsequently heated at 50 °C under a high vacuum in a convection oven for 2 h yielding PEBP.

1.2.3.2 Method B, room temperature synthesis:

The monomer EBP was weighed and was put into a 20-mL scintillation glass vial which kept closed at room temperature for 72 h, yielding PEBP. In the same way, EBP was transferred to a dog-bone shape mold of chlorinated polyethylene (CPE) and allowed to polymerize at room temperature for 72 h. Later it was removed from molds and post cured at 170 °C overnight and used for testing mechanical properties.

1.3 RESULTS AND DISCUSSION

1.3.1 Synthesis of the Gemini monomer

(E)-2,4-Pentadienoic acid was synthesized in good yield by the direct Knoevenagel-Doebner condensation between acrolein and malonic acid in the presence of pyridine. The stereocontrol of the reaction in favor of thermodynamically more stable E-isomer was achieved at 50 °C in dark. Afterward, the carboxylic acid was converted into corresponding acyl chloride by reacting with an excess of oxalyl chloride at room temperature. Later, acyl chloride went under esterification reaction with ethylene glycol in

DCM containing molecular sieves (3Å). A 2:1 mole equivalent ratio of acyl chloride to ethylene glycol and low reactants concentrations were optimal to obtain EBP in 77 % yield. The chemical structure of EBP was confirmed by ^{1}H, ^{13}C NMR, and FT-IR spectroscopy. The proton signal at about 4.33 ppm was assigned to the methylene protons of the linker. The resonances at 5.44 to 7.23 ppm were attributed to the protons attached to the double bonded carbons. Moreover, the observed integral ratio of all protons was in accord with expected values.

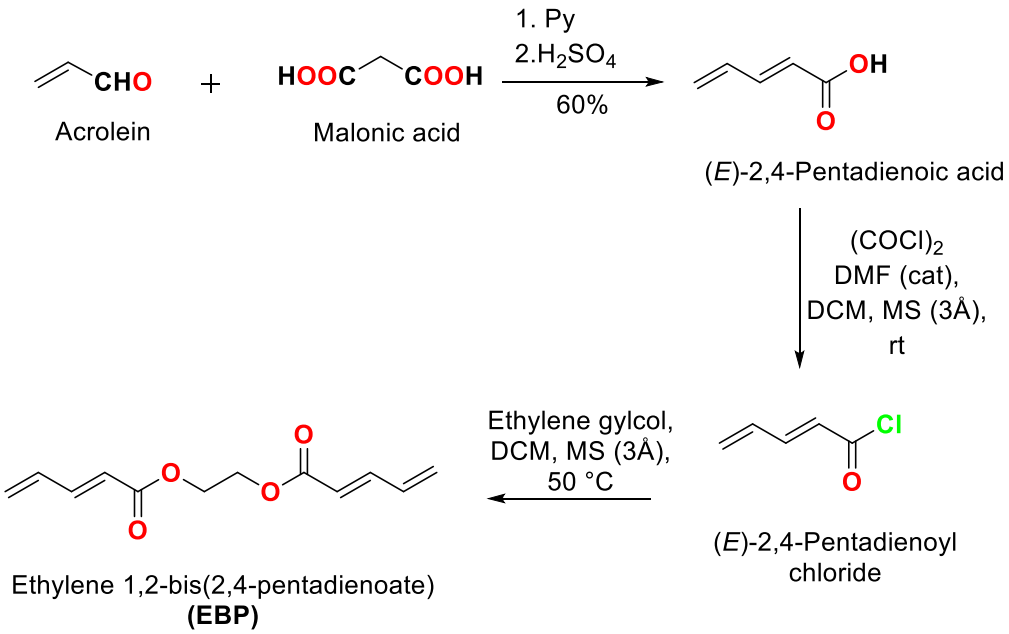

Scheme 1.1. Synthesis of the Gemini monomer EBP from malonic acid, acrolein and ethylene glycol.

Figure1-1 presents the FT-IR spectra of EBP. The characteristic absorptions of conjugated ester, including strong stretching vibration of the C=O group around 1708 cm^{-1}, medium intensity absorption of C=C bonds around 1640 and 1600 cm^{-1}, the C–O bond around 1010 cm^{-1}, and weak out-of-plane bending vibration of C–H near to 745 cm^{-1}, were observed, confirming the desired functional groups in the EBP.

1.3.2 Synthesis of polymer from EBP

EBP was polymerized in the absence of light at different temperatures without any solvents making it a sustainable process to obtain the polymer PEBP. The polymerization process was monitored by using FT-IR. It was found that the temperature of 50 °C for two hours (Figure 1.1) was optimal for the polymerization, which was marked by the disappearance of C=C bond stretching vibration and out-of-plane C–H bending vibrations at 1600 cm^{-1} and 950 cm^{-1}, respectively. No further change was observed at temperature and time higher than 50 °C.

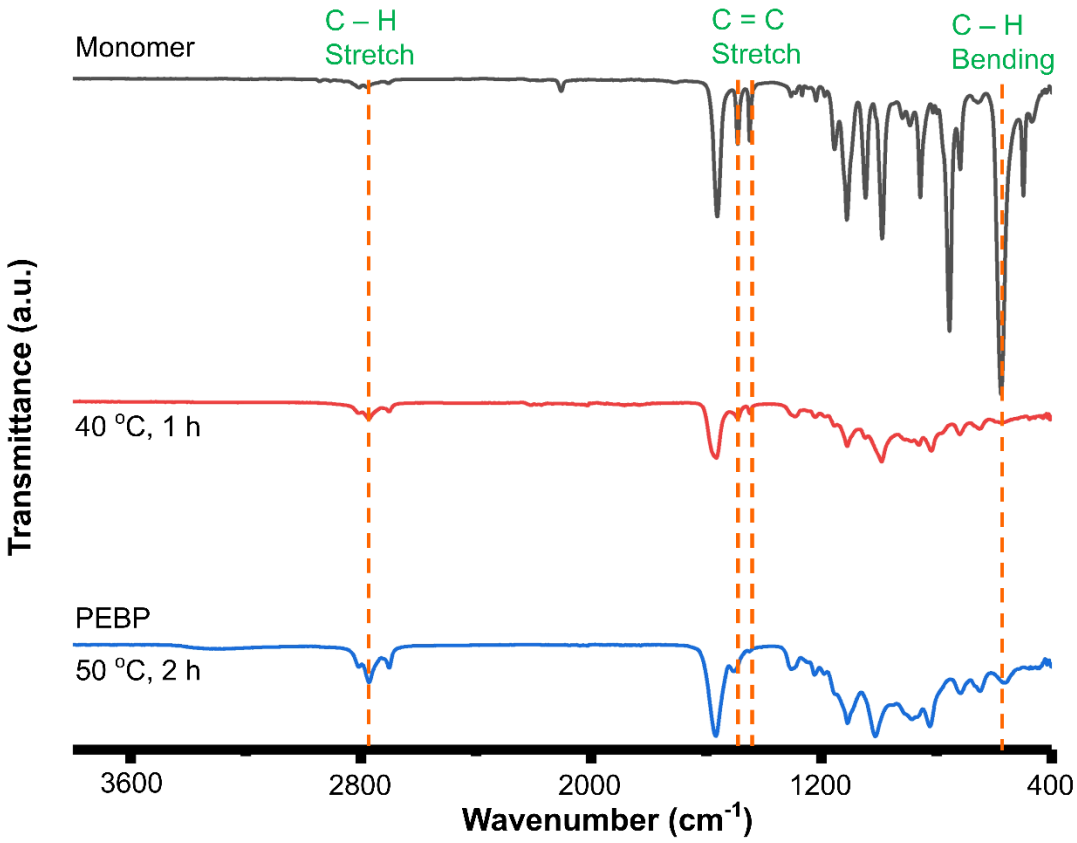

Figure 1.1. FT-IR spectra of EBP showing the polymerization completed by heating.

Also, due to the high reactivity of EBP, it was found to undergo polymerization at room temperature. Interestingly, the final polymer obtained by this method was transparent when compared with opaque product formed at elevated temperatures. The resulting polymer had similar IR characteristics in both processes, indicating both PEBP samples are chemically identical, but they might differ structurally. Also, it was found that the room-temperature method of polymerizing EBP at room can be an effective way to obtain different forms of PEBP depending upon application or requirement, as shown in Figure 1.2.

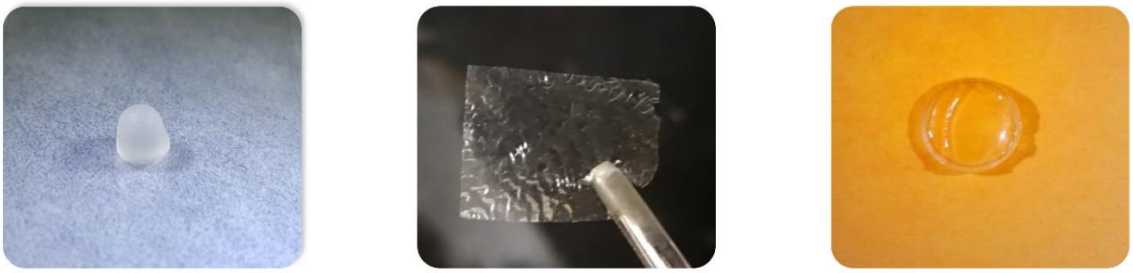

Figure 1.2. Photographs of the PEBP in different shapes.

1.3.3 Thermal properties of PEBP

Thermal properties of the PEBP were initially investigated by differential scanning calorimetry (DSC) under N_2 atmosphere. A PEBP sample was heated from -25 to 250 °C at a rate of 20 °C per min. After heating at that rate, it was isothermally held at 250 °C for 5 min, then allowed to cool down to -25 °C at a rate of 20 °C per min. PEBP did not show any melting and glass transition temperature in three continuous DSC cycles. However, an exothermic peak around 150 °C was observed in the first heating cycle, as shown in Figure 1.3, which was not present in the subsequent second and third heating cycles. Also, with

the decrease in heating rate, the curing peak became broad and dropped to a lower temperature. This exothermic transition reflected in the DSC thermogram was attributed to the curing, where the polymer chain cross-links. In practical application, post-curing can be extremely important in that it not only expedites the cross-linking process, but let the polymer chains align in a more organized way.[17] In order to determine an activation energy (E_a) to cross-link the PEBP, multiple DSC experiments were performed at different heating rates to measure the cross-linking temperature. These cross-linking peak temperatures were fitted in to the Kissinger's equation[18] which relates the E_a to the peak temperatures of exothermic processes observed in DSC as shown in equation 1.1:

$$-ln\left(\frac{q}{T_p^2}\right) = \frac{E_a}{RT_P} + ln\frac{AR}{E_a} \qquad \textbf{1.1}$$

Where q is the heating rate DSC scans, T_p is the exothermic peak temperature, E_a is the activation energy, R is the gas constant (8.314 J mol^{-1} K^{-1}), and A is the pre-exponential factor.

A plot of $-\ln(q/T_p^2)$ versus $1/T_p$ allows the determination of the apparent activation energy from the slope of the equation 1.1.[19] The linear fit of Kissinger's equation is shown in Figure 1.3b. Accordingly, the E_a for the thermal curing reaction for the sample of PEBP was calculated as 8.4 $kJ.mol^{-1}$. This value Indicates that PEBP can easily be cured at elevated temperatures and can be used with other prepolymers to introduce thermal curability. Therefore, a hybrid polymer with valuable properties can be tailored with an adept combination of a different class of polymers.[20]

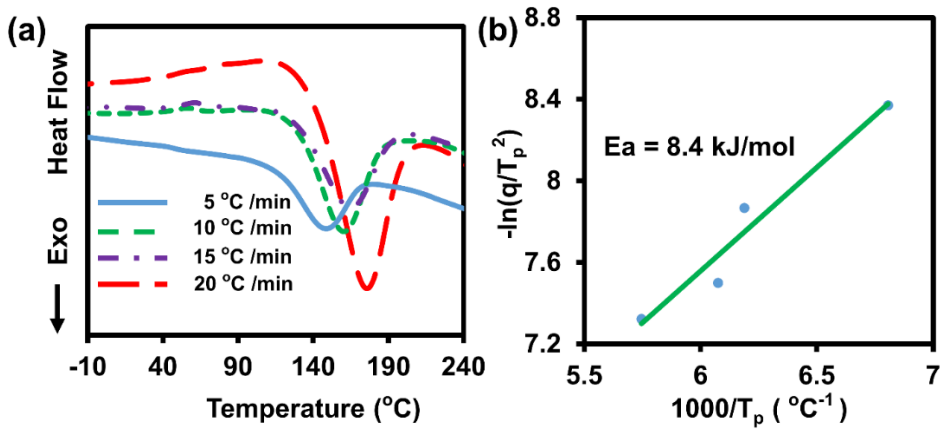

Figure 1.3. (a) DSC thermograms of PEBP under nitrogen showing the crosslinking at different heating rates. (b) Linear plot of - ln (q/T_p^2) versus $1/T_p$ based on Kissinger's equation

High thermal decomposition temperature is an important property of polymers and probably the most distinguished property of HPPs.[21] Therefore, we have evaluated the thermal stability of PEBP by thermogravimetric analysis (TGA) under a N_2 atmosphere (Figure 1.4a). PEBP exhibited high thermal stability without any weight loss below 300 °C. The onset decomposition temperature ($T_{5\%}$) was found to be in the range of 370 to 380 °C, and the maximal decomposition temperature of PEBP was in the range of 412 to 433 °C. The plausible explanation for this unusually high thermal stability can be attributed to the lower shearing forces at the middle of polymer chains induced during thermal motion, resulting in the free rotation of a flexible aliphatic linker connecting the monomers.[22] To understand decomposition behavior of PEBP and how it is related to the polymeric structure of PEBP, thermal decomposition kinetics were performed using TGA and differential thermogravimetry (DTG) (Figure 1.4b). According to Kissinger's method described by the equation 1.2, dynamic heating experiments can be quantitatively used to calculate activation energy, E_a of the solid-state reactions such as decomposition.[20a, 23]

$$ln\left(\frac{\beta}{T_p^2}\right) = ln\frac{AR}{E_a} + ln[n(1-\alpha)^{n-1}] - \frac{E_a}{RT_P} \quad 1.2$$

Where β is the heating rate (°C/min), T_p is the peak temperature from DTG, A is frequency factor (s^{-1}), R is the gas constant (8.314 J mol^{-1} K^{-1}), E_a is the apparent (kJ mol^{-1}), α is defined as the fractional conversion at any time t, and n is reaction order.

At maximum decomposition temperature, $n(1-\alpha)^{n-1n}$ equals to 1, based on this approximation the equation 1.2 can be simplified to the equation 1.3. Therefore, E_a can be obtained by plotting $\ln(\beta/T_p^2)$ versus $1/T_p$, as shown in Figure1.4c.

$$ln\left(\frac{\beta}{T_p^2}\right) = ln\frac{AR}{E_a} - \frac{E_a}{RT_P} \quad 1.3$$

The slope of the line was used to calculate the E_a of the decomposition of PEBP, which was 84.22 kJ mol^{-1}. The order of decomposition reaction was also estimated by Crane's equation (equation 1.4),

$$\frac{d(ln\,\beta)}{d(1\,/\,T_P)} = -\left(\frac{Ea}{nR} + 2T_P\right) \quad 1.4$$

when $E_a/nR >> 2T_p$, the slope of plot $\ln(\beta)$ vs. $1/T_p$ (Figure 3.4d) can be approximately equaled to E_a/nR. Thus, the calculated reaction order was 0.92, suggesting the decomposition was first-order process.

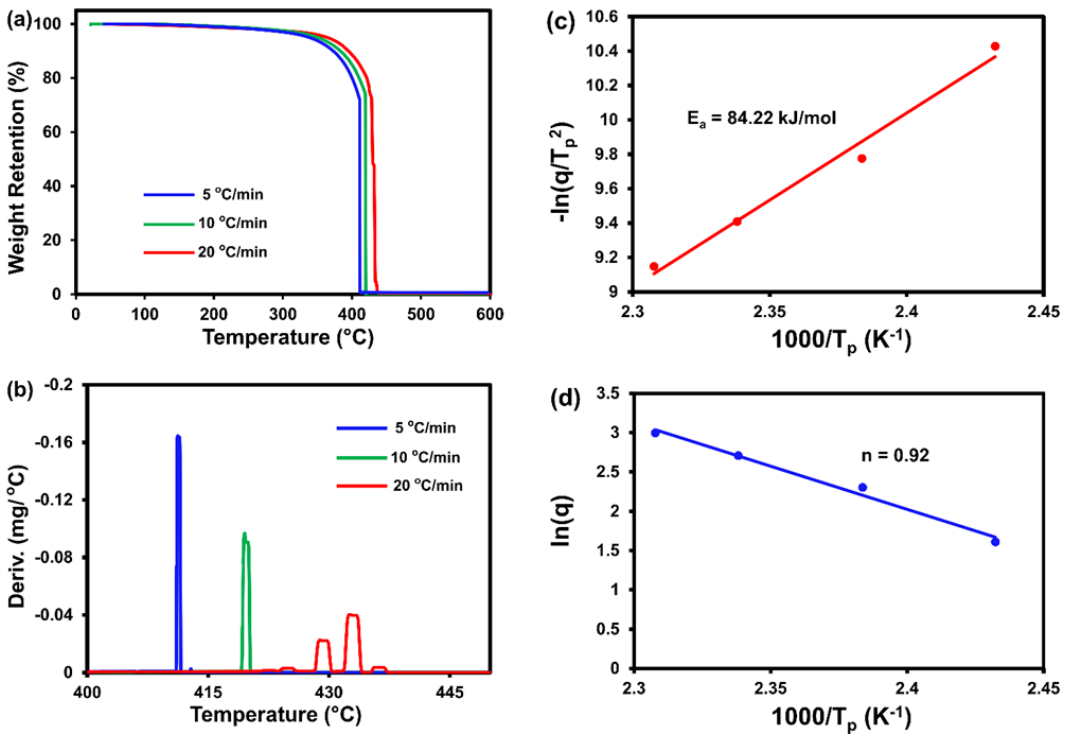

Figure 1.4. (a) TGA curves of PEBP at different heating rates under nitrogen. (b) DTG curves of PEBP at different heating rates. (c) Linear plot of $-\ln(q/T_p^2)$ versus $1/T_p$ based on Kissinger's equation. (d) Linear plot of $\ln(\beta)$ vs. $1/T_p$ based on Crane's equation.

The above analysis indicated that a significant amount of energy was necessary to decompose PEBP, which is affirmed by the high decomposition temperature (T_d) ranging from 412 to 433 °C at different heating rates. The thermal stability of PEBP was a little inferior to previously known HPPs.[24] The possible reasons that could be accounted for the differences are as follow (1) The degradation of aliphatic units is easier than aromatic ones, as suggested by earlier studies.[25] (2) The absence of strong interactions (such as hydrogen bonds) among PEBP chains prevented thermal motion and decomposition. (3) The relative lower molecular weight of PEBP. These reasons indicated that improvement in molecular weight by implementing various polymerization methods could further increase the heat resistance to the desired level because the first two reasons are intrinsic properties of

aliphatic polymers. Although the thermal stability was a little inferior, it is still high enough for some high-temperature applications where a temperature lower than 300 °C is required.

1.3.4 Mechanical properties of the PEBP

The monomer EBP was loaded onto dog-bone shape molds at room temperature and allowed to polymerize at the room temperature. Some PEBP tensile bars were kept in a convection oven for heating at 170 °C for overnight to achieve curing. After the preparation of tensile bars, the mechanical properties such as Young's modulus (E), tensile strength at break (σ) and elongation at break (ε) were determined by using a universal testing machine (UTM) at a crosshead rate of 5 mm/min under 5 kN load cell at room temperature. In general, the mechanical properties of a given polymer are significantly influenced by its chemical structure and cross-link density of the polymer network. As shown in Figure 1.5, the PEBP exhibited a high tensile strength up to 159 MPa with a strain of 3.9 %, while post cured PEBP showed a slightly lower tensile strength of 146 MPa with a strain of 2.4%. Also, post-cure PEBP fractured without much plastic deformation compared to the uncured PEBP sample, as shown in the stress-strain curve (Figure1.5). The Young's Moduli of the uncured and post-cured sample was ~ 10.9 GPa and 12.9 GPa. It is noteworthy to mention the tensile strength of uncured and post-cure PEBP was found to be more than that of commercially, best known, and widely used polyimide Kapton[26].

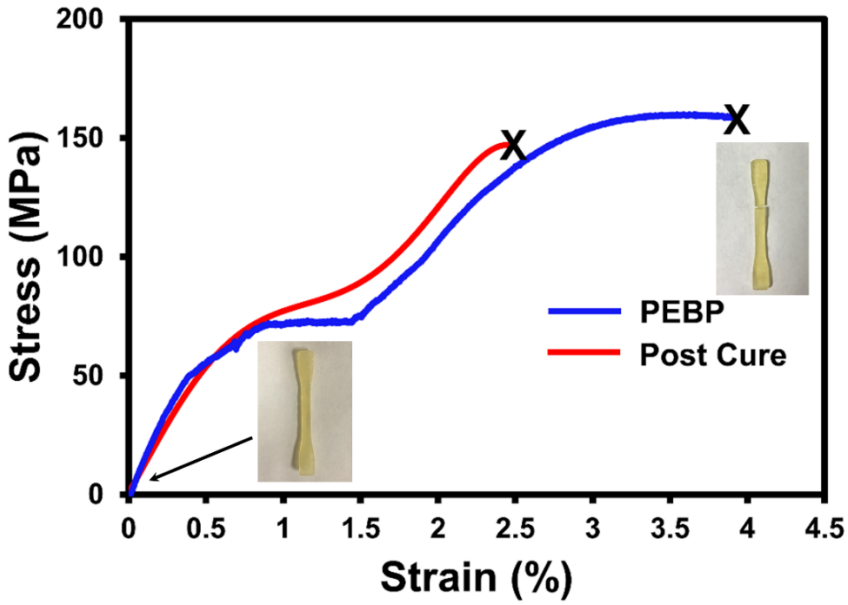

Figure 1.5. Representative stress-strain curve of PEBP by tensile testing from polymer tensile bars.

1.3.5 Chemical properties of PEBP

The solubility of PEBP was tested in several commonly used solvents such as NMP, DMAc, DMSO, DMF, THF, $CHCl_3$ and MeOH. It was found that PEBP was insoluble in all the tested solvents even with the addition of LiCl and heating the solution to 100 °C for 2h in the case of DMSO and DMF. It also tolerated bases (Et_3N and NaOH) and acids (1M HCl and TFA) at room temperature. This excellent chemical resistance can be attributed to a rigid framework present in PEBP and makes it suitable for developing protective coatings where contact with harsh chemicals, gases, detergent, or oils are intended or cannot be avoided. Under strongly acidic conditions, such as in the presence of conc. H_2SO_4, the PEBP, exhibited unusual behavior (Figure 1.6). PEBP swelled into a dark brown material about 6 – 7 times the original volume of PEBP in 24 h, as shown in Figure 1.6b.

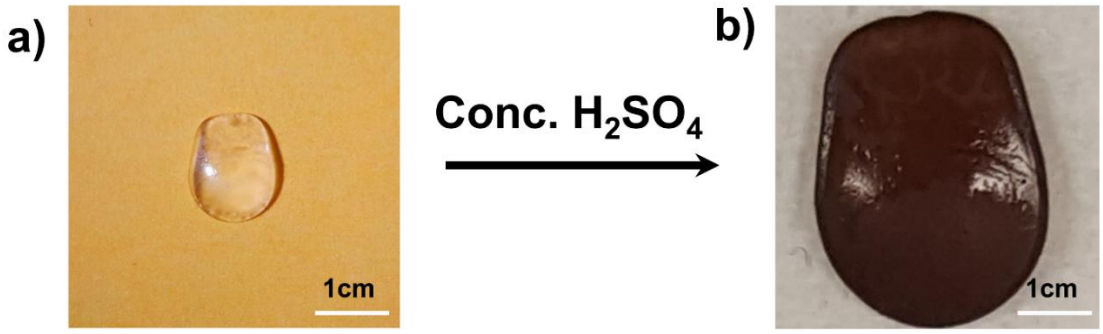

Figure 1.6. Photographs of PEBP (a) before treatment with conc. H_2SO_4. (b) After treatment with conc. H_2SO_4.

The swelled form of PEBP was further investigated. a TGA was performed on this swelled material after removing most of conc. H_2SO_4, and it was found to degrade in two steps. The first stage of decomposition happened at approximately 216 °C with a weight loss of 26%, which was near to the boiling point of sulfuric acid. The second decomposition occurred around 430 °C, indicating the decomposition of swelled PEBP. Interestingly, it is found that the thermal stability of this form of PEBP was almost similar to that of original PEBP. Although the char yield of this conc.H_2SO_4 PEBP was about 20% of the total weight (Figure 1.7a), while the untreated PEBP left no char product after heated above 450 ^oC (Figure 1.4a). To better understand the properties of swelled material, SEM was done to compare the polymer surface before and after the treatment with conc. H_2SO_4 (Figure 1.8). Before the conc H_2SO_4 treatment the polymer surface was smooth and plain, which is typical for polymers. After the treatment, a rough surface with tiny pores were observed, indicating the formation of a porous material. This unique swelling response to the change in pH has been proven instrumental in various applications ranging from superabsorbents to catalyst supports. Moreover, the material with this property would be suitable for segregation, such as filtration, gas separation, and pervaporation.[27]

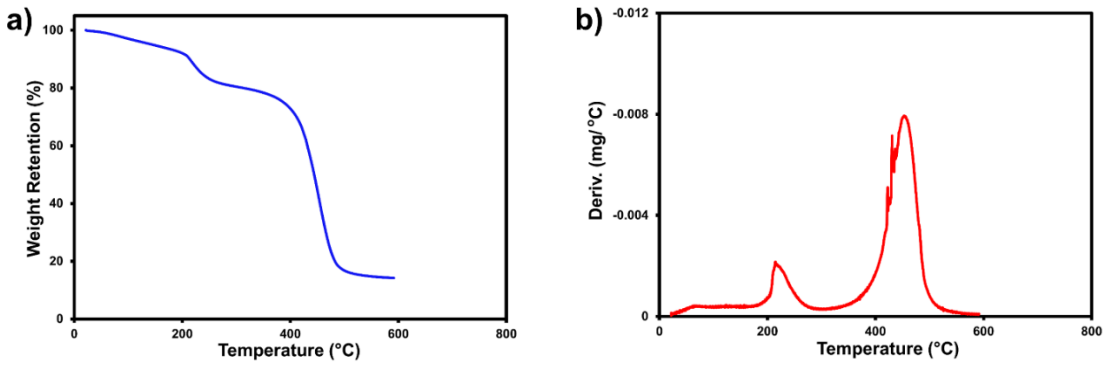

Figure 1.7. TGA and DTG curves of PEBP after treatment with conc. H_2SO_4 under nitrogen.

1.3.6 Sustainability

The PEBP synthesized from the Gemini monomer EBP could synthesized from biomass-derived building blocks such as glycerol, malonic acid,[28] and ethylene glycol.[29] Glycerol is a particularly important precursor because of its availability as a by-product in biodiesel production and its conversion into high-value chemical intermediates like acrolein[28] and ethylene glycol. Therefore, this compound has been recognized as a valuable synthon in the sustainable chemical industry by the U.S. Department of Energy.[30] An expanding demand for biodiesel will always ensure that a large amount of cheap glycerol is available. Moreover, malonic acid can be either obtained directly from natural sources like molasses of sugarbeets[31] or prepared from malic acid, one of the twelve most valuable sugar-derived agrochemicals,[32] via a multistep process including one-pot oxidative de-carboxylation and esterification followed by hydrolysis.[33]

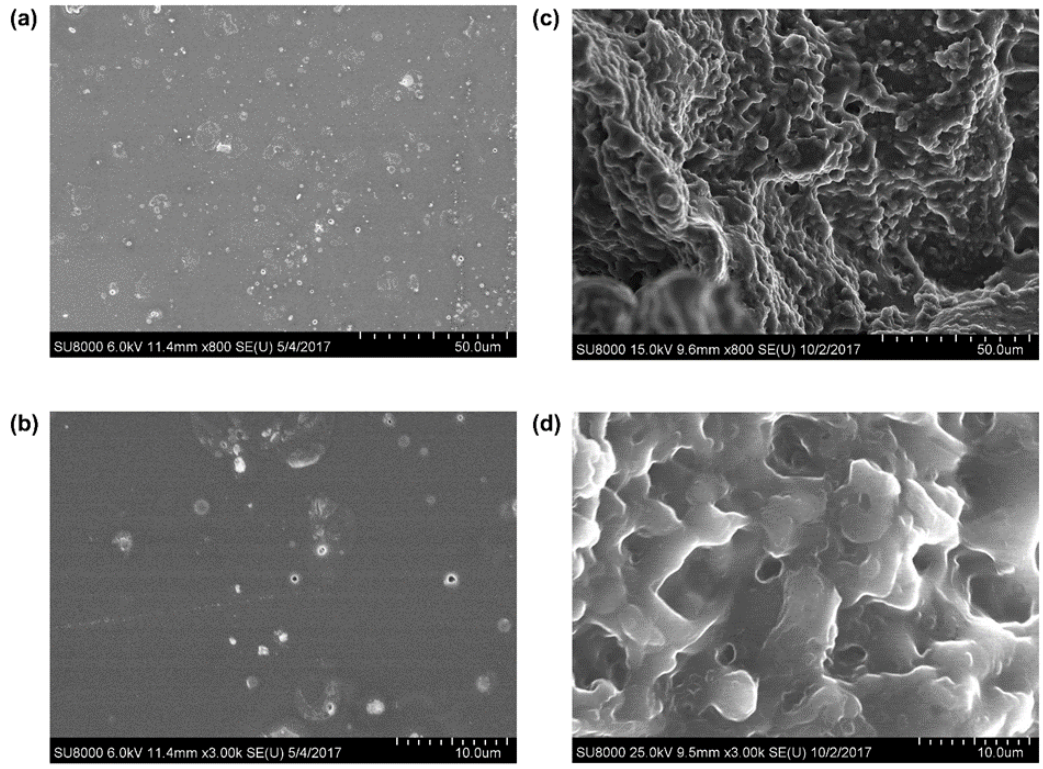

Figure 1.8. (a) and (b) SEM images of the PEBP surface before treatment with conc. H_2SO_4. (c) and (d) SEM images of a cross-section of PEBP after treatment with conc. H_2SO_4.

1.4 CONCLUSION

The sustainably sourced ethylene 1,2-bis(2,4-pentadienoate) (EBP) Gemini monomer was prepared by solvent-free polymerization and formulated into the high-performance polymer, PEBP. The synthesized HPP showed good chemical resistance towards most organic solvents due to its high cross-linking. The DSC experiments demonstrated that the synthesized HPP could undergo post-curing at approximately 170 °C. The HPP composed from the Gemini monomer EBP exhibited excellent thermal and mechanical properties. Specifically, the synthesized PEBP showed the T_d, E, σ, and ε values (412 °C, 11 GPa, 160 MPa, and 4%, respectively), demonstrating its enormous

potential for implementation as engineering plastics. Also, the Gemini monomer based HPP PEBP was found to swell seven times to its original volume under strongly acidic conditions. However, the thermal stability of the PEBP was still inferior to the known HPPs, suggesting efforts were still needed to improve the properties further. This study provided an innovative approach to synthesizing novel HPPs using a Gemini monomer. The results presented here might serve as clues for the future development of new HPPs with high chemical resistance and mechanical strength.

Chapter 2

Synthesis and Characterization of BPA-Free Polyesters by Incorporating a Semi-rigid Cyclobutanediol Monomer

2.1 INTRODUCTION

Synthetic polymers[34] have become prime materials of choice around the globe because of their diverse applications, ranging from commodity to high tech, such as food and beverage packaging, electronics, as well as the automotive and architectural industries. Among these, bisphenol A (BPA) based polymers have proven to be essential thermoplastics. For example, BPA-based polycarbonates[35] and epoxy resins[36] exhibit exceptional thermal, mechanical, and optical properties, making them perfect for durable goods and engineering applications. Their success can be attested by their considerable market consumption of 2.7 billion pounds worldwide annually. Some of these uses include reusable water bottles, food can linings, spectacle lenses, and construction materials. The application of BPA-based polymers, however, has recently come under scrutiny due to the potential carcinogenic and disruptive endocrine effects of BPA.[37] This has boosted widespread research and development of health- and environment-friendly polyesters with similar thermal and mechanical properties.[14b, 38,39,40] One strategy to achieve excellent thermal and mechanical properties similar to those of BPA-derived polymers is to incorporate semi-rigid cyclic monomers such as octahydro-2,5-pentalenediol and isohexides into the polymer structure.[14b, 38a-h] These cyclic monomers bridge the gap in

rigidity between their flexible aliphatic chains and rigid aromatic counterparts. Some of them have been proven to be useful in synthesizing polyesters with the desired properties. Introduction of the semi-rigid aliphatic units can be used to tune the glass transition temperature, to improve optical clarity of the polymeric materials by reducing their crystallinity, and to make them more UV-stable due to the absence of phenol groups. Cyclic aliphatic diol monomers for example 1,4-cyclohexane dimethanol (CHDM)[39, 41] and 2,2,4,4-tetramethyl-1,3-cyclobutanediol (TMCD or CBDO)[40-41] have achieved significant commercial success (Figure 2-1). They have been used in a variety of polyester and co-polyester products, including BPA-free water and baby bottles, which are now hugely popular.[41,42] However, the ability to introduce functional groups onto the cyclobutane ring of TMCD to tune the properties of the corresponding polymers (e.g., Tritan copolyester) is inherently limited because TMCD is mainly produced through flash vacuum pyrolysis (FVP).[41, 43] Moreover, it is challenging to synthesize polymers with high molecular weight using TMCD due to the low reactivity of the secondary diol (a mixture of trans and cis isomers) and its relatively high melting point (126 to 134 °C). Because of these limitations, copolymers are usually synthesized using a mixture of TMCD and another diol (e.g., CHDM).[41 44]

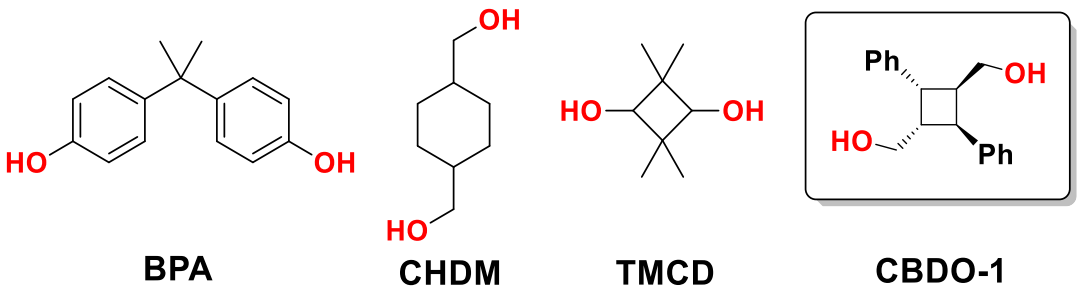

Figure 2.1. Comparison of different diols with BPA: CBDO-1 shares the structural similarities with BPA, CHDM, and TMCD.

trans-1,3-Cyclobutane dimethanol (CBDO-1), on the other hand, has not gained much attention from researchers, although it was discovered contemporaneously with TMCD. Characterization of the diol was limited to melting point determination and elemental analysis at that time.[45] To the best of our knowledge, no detailed investigation of CBDO-1's physical properties and its application in synthesizing polymers can be found in the literature up to now. In this study, we report the synthesis and application of CBDO-1 monomer as a part of our systematic efforts in designing and constructing useful cyclobutane-containing building blocks (CBs) using photoreactions.[46] The performance of CBDO-1 in synthesizing a series of cyclobutane-containing polyesters, as well as their thermal properties, molecular weight distribution, and structural details were investigated. On the one hand, CBDO-1 does not contain a phenol group, which enables BPA to trigger estrogenic pathways in the body.[37b-h] On the other hand, this novel primary diol building block has two rigid phenyl rings like BPA and shares structural similarities with both CHDM and TMCD. Thus, it may also serve as a novel BPA replacement like the monomers shown in Figure 2.1. Besides CBDO-1, other CBDOs with different substituents can also be readily prepared via reduction from the cyclobutane diacids (CBDAs) reported by our group and others,[46] which allow the properties of the corresponding polymers to be tuned by changing the structure of the CBDOs according to specific needs. In addition, since CBDO-1 is a primary diol, it can be easily used in polymer synthesis without the need of adding another diol due to its higher reactivity and lower melting point compared to those of TMCD.

2.2 EXPERIMENTAL SECTION

2.2.1 Materials and methods

All chemicals were purchased from Alfa Aesar, Sigma-Aldrich, or Acros and used without further purification. Blacklight used in photoreactions was produced by E27 40-watts HD 159 compact fluorescent bulbs or 15W Eiko EK15526 F15T8 blacklight bulbs. The solution phase nuclear magnetic resonance (NMR) spectra were recorded with a Bruker AVANCE 500 NMR spectrometer (^{1}H: 500 MHz, ^{13}C{^{1}H}: 125 MHz). Proton and carbon chemical shifts were reported in ppm downfield from tetramethylsilane (TMS) or using the resonance of the corresponding deuterated solvent as an internal standard. ^{1}H NMR data were reported as follows: chemical shift (ppm), s = singlet, d = doublet, t = triplet, q = quartet, dd = doublet of doublets, m = multiplet, and integration. Single crystal X-ray data were collected on a Bruker Kappa Apex II Duo X-Ray diffractometer with Cu Kα (λ = 1.54178 Å). Infrared (IR) spectra were recorded on a Thermo Scientific Nicolet iS5 FT-IR spectrometer. The mass spectrometric analyses were performed using a high-resolution time of flight G1969A mass spectrometer with electrospray (atmospheric pressure chemical) ionization (Agilent, Santa Clara, CA, USA) and reported as m/z. All MALDI-MS spectra were acquired using Waters SYNAPT G2-Si MALDI-TOF mass spectrometer. The instrument is equipped with a laser emitting at 355 nm. Spectra were collected in the reflectron mode, the ion source and reflector lens potentials were fixed at 20 and 22.5 keV, respectively. The *α*-cyano-4-hydroxycinnamic acid (CHCA) was used as matrix in all experiments. THF solution of polymer (10 mg/mL) and matrix (20 mg/mL) and a THF solution of sodium trifluoroacetate (5 mg/mL) were used for sample

preparation. The polymer, matrix, and salt solutions were mixed in a 2:10:1 ratio, and ca. 0.50 μL of the final mixture was applied to the MALDI sample target.

DSC experiments were performed on a Perkin Elmer Jade differential scanning calorimeter using a hermetic aluminum pan, indium standard for calibration, nitrogen as a purge gas, sample weight of ~ 5 mg with a ramping rate of 20 °C/min. Heat flow was recorded from both the first heating and cooling curves. TGA analyses were carried out on a Hi-Res TGA Q500 thermogravimetric analyzer from TA Instruments using alumina pans at a heating rate of 20 °C/min under nitrogen with a sample weight of about 10 mg. Molecular weight distribution data were obtained using a GPC system (EcoSEC HLC-8320GPC, Tosoh Bioscience, Japan) with a differential refractometer (DRI) detector. Separations were performed using two TSKgel SuperH3000 6.00 mm ID× 15 cm columns with an eluent flow rate of 0.35 m min^{-1}. The columns and detectors were thermostated at 40 ºC. The eluent used was Tetrahydrofuran (THF). Samples were prepared at about 10 mg ml^{-1} in THF and allowed to dissolve at ambient temperature for several hours, and the injection volume was 40 μL for each sample. Calibration was conducted using PS standards (Agilent EasiVial PS-H 4ml).

2.2.2 Diffusion ordered spectroscopy (DOSY) experiments

NMR tubes were flame-dried in advance, and experiments were performed at 25 ± 1 °C. The data collection was done after stabilizing the NMR sample at RT for 30 min. For polystyrene standard samples, each NMR tube contained 0.5 mg of polystyrene and 1 mL of deuterated chloroform ($CDCl_3$). For CBP samples, each NMR tube contained 0.5 mg of polyester and 1 mL of $CDCl_3$. DOSY experiments were performed on a Bruker AVANCE

500 spectrometer equipped with a z-axis gradient coil. All experiments were run without spinning to avoid convection. The maximum gradient strength was 0.214 T/m. The standard Bruker pulse program, stebpgp1s, employing a stimulated echo sequence and 1 spoil gradient, was utilized. Bipolar rectangular gradients were used with a total duration of 0.5−10 ms. Gradient recovery delays were 0.5−1 μs. Diffusion times were between 100 and 2000 ms. The number of gradient steps was set to be 16. Individual rows of the quasi-2-D diffusion databases were phased and baseline corrected. DOSY spectra were processed by Topspin 1.3 software. The diffusion dimension was generated using inverse Laplace transform driven by the maximum entropy method. Diffusion coefficients of a chosen narrow chemical shift range were extracted from the T_1/T_2 analysis module of Topspin 1.3.

2.2.3 Synthesis of CBDA-1

2.2.3.1 Method 1: Solid-state approach

The solid-state method was modified from the previously reported procedure by our group. It involves the use of operator-friendly household blacklights as a source of irradiation. The photosynthesis was carried out on an 8 x 4-inch glass plate. 13.49 mmol of powdered *trans*-cinnamic acid was dispersed uniformly over the glass plate. This plate was irradiated with six 15W Eiko EK15526 F15T8/BL bulbs, three on top, and the other three on the bottom. The distance between the light source and glass plate was about 1.5 cm, as shown in Figure 2.2. The progress of the reaction was monitored by ^{1}H NMR spectroscopy. The powder was periodically re-blended uniformly to ensure even irradiation. After a total of about 60 h, the powder was collected and washed with 3 mL

ethanol to obtain the product as a white solid (6.55 mmol, 97% yield). The product was determined as the CBDA-1, consistent with the previous reports.

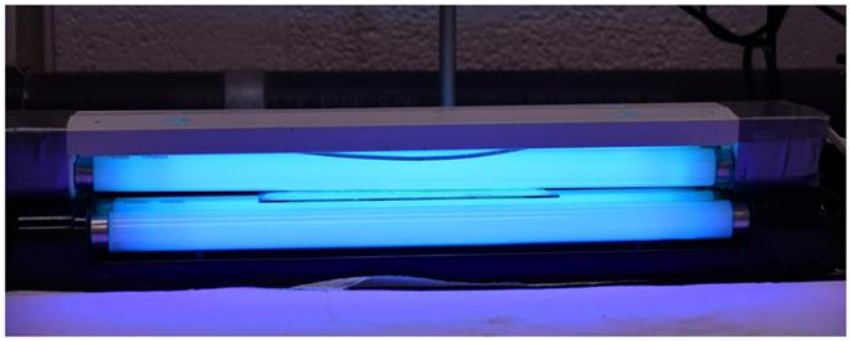

Figure 2.2. Setup for the solid-state synthesis of CBDA-1.

2.2.3.2 Method 2: Brine slurry approach

The brine slurry approach is suitable for larger-scale reactions and is more operator friendly. Specifically, 33.74 mmol *trans*-cinnamic acid powder was suspended in 2 L of brine solution in a 2000 mL crystallizing dish or beaker with magnetic stirring. Three E27 40W HD 159 blacklights bulbs were immersed in the crystallizing dish, as shown in Figure 2.3. The slurry was continuously stirred under the blacklights for 72 h. To ensure that the brine was as transparent as possible, 25 mL water was added into the brine before the reaction and each day during the slurry photoreaction. The slurry was then filtered, and the solid was washed with 10 mL ice-cold water. After air-drying, the desired product was obtained as a white solid (16.02 mmol, 95% yield). The same slurry photoreaction that was done by suspending cinnamic acid powder in water only gave a yield of 78% (13.16 mmol) mainly due to the solubility of *trans*-cinnamic acid and CBDA-1 in water. Additionally, it is much easier to disperse *trans*-cinnamic acid powder in brine than in water because

cinnamic acid can easily accumulate on the surface of the glassware in the latter case, which slows down the reaction and makes it difficult to collect the product.

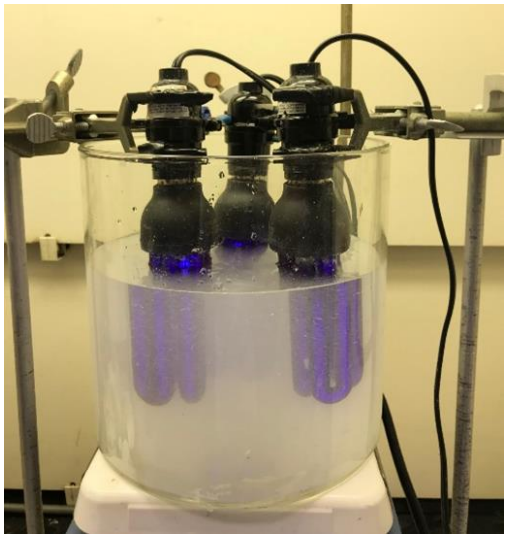

Figure 2.3. The setup for synthesis of CBDA-1 in brine slurry.

2.2.4 Synthesis of CBDO-1

2.2.4.1 Method 1: Reduction with $NaBH_4/I_2$

In a 100 mL round bottom flask fitted with a Claisen head adaptor, a magnetic stir bar and fine powered of $NaBH_4$ (23.59 mmol) was added to 25 mL of THF. This suspension was stirred for 10 min, and then CBDA-1 (3.37 mmol) was added to the suspension. The addition resulted in bubbling (CAUTION: hydrogen gas is flammable). When the reaction mixture stopped bubbling, a solution of I_2 (6.74 mmol) in THF (15 mL) was added dropwise using a dropping funnel attached to the Claisen head over a period of 45 – 60 min. The addition of I_2 was an exothermic reaction and resulted in significant evolution of H_2 gas. During this addition, the color of the mixture changed from red to yellow first and then to colorless, indicating the disappearance of I_2. After the disappearance of I_2, a water

condenser was attached to the Claisen head, and the solution was heated to reflux. After 16 h of refluxing, the reaction mixture was analyzed using TLC (10 % MeOH in DCM as eluent) to verify the absence of the starting material. Approximately 40 mL of THF was removed using a rotavapor, and a white solid was collected from the flask. To this white solid, 20 mL of cyclohexane and 30 mL of 10% aqueous solution of NaOH were added and the mixture was stirred until the bubble from the mixture ceased (approximately 30 min). After 1 h, a white solid separated from the solution. It was filtered using a Buchner funnel and washed 3 x 10 mL with 3M NH_4OH solution and later with 10 mL of 12 % aqueous solution of $NaHSO_3$ to remove traces I_2. The white solid obtained after filtration was dissolved in chloroform, and the organic layer was washed three times with a saturated brine solution. The chloroform removal yielded the desired product CBDO-1 (3.13 mmol; 93% yield) as a white solid. Its structure was confirmed by NMR using $CDCl_3$ as the solvent. Melting point: 106.4–107.0 °C. ^{1}H NMR ($CDCl_3$, 500 MHz) δ (ppm): 7.13–7.27 (m, 12H), 3.49–3.52 (m, 2H), 3.40–3.47 (m, 4H), 3.12–3.18 (m, 2H), 1.07 (s, 2H); $^{13}C\{^1H\}$ NMR ($CDCl_3$, 125 MHz) δ (ppm): 134.9, 123.9, 122.9, 121.8, 58.5, 37.6, 36.4; FT-IR (solid) $\overline{\nu}_{max}$ (cm^{-1}): 3307, 2931, 1448, 1496, 1014, 1600, 743, and 696. HRMS (ESI/TOF): Calculated for $[M+Na]^+$, $C_{18}H_{20}O_2Na^+$: 291.1361; Found: 291.1370.

2.2.4.2 Method 2: Catalytic hydrogenation

CBDA-1 (1.69 mmol) and $CuO\text{-}CrO_3$ (0.32 mmol) in 20 mL of water-dioxane (1:1) as solvent were added into a stainless-steel reactor equipped with a magnetic stirrer and pressure regulator. Afterwards, the reactor was sealed and purged with argon, and then with hydrogen, and this process was repeated three times. The hydrogen gas was introduced at

a pressure of 15 MPa, and then the temperature was raised to 180 °C. The reaction mixture was allowed to stir for 12 h. After that, the reaction mixture was filtered through celite, and the filtrate was extracted with EtOAc (3 x 5 mL). The extract was dried over $MgSO_4$, and then the solvent evaporation afforded the product, CBDO-1, as a white solid.

2.2.5 General methods of polycondensation

Polycondensation was conducted in a 15 mL two-neck round bottom flask containing a magnetic stir bar equipped with a Claisen head. One neck was attached to an argon gas inlet and the other neck was connected to a water condenser. A finely grounded mixture of CBDO-1 (1.06 mmol) and a dicarboxylic acid (1.28 mmol) was charged in the reaction flask. The setup was placed under a vacuum and purged with argon gas. This process was repeated three times. The method of polycondensation involves two steps. In the first step, the reaction was carried out under argon gas to promote the formation of oligomers. The reaction mixture was heated in the sand bath at 130 °C for 15 min with constant stirring. When complete melting of the mixture was observed, a solution of titanium isopropoxide $Ti(OiPr)_4$ (1.25 mol%) in 1 mL of toluene was then added to the reaction flask under the continuous flow of argon. Afterward, the temperature was increased to 170 °C and the reaction mixture was allowed to stir for 12 h, and finally to 200-215 °C for 1.5 h to complete the pre-polymerization step. In the second step of polycondensation to connect the oligomers to form a long chain, a vacuum was gradually applied to the reaction setup at 210-215 °C for 2 h (Figure 2.6). After reaction completion, the mixture was cooled to room temperature under the flow of argon. The polymer was further purified by dissolving it in 5 mL of a $CHCl_3$-TFA mixture (6:1). After the addition

of 50 mL of methanol polymer was precipitated. Polymer was filtered and dried in vacuum at 40 °C for 12 h. In the case of an external mechanical stirrer, a 3-neck 100 mL round bottom flask was used, one neck was attached as argon inlet and the other two necks for mechanical stirrer and water condenser.

PCBO: ^{1}H NMR ($CDCl_3$) δ (ppm): 7.30 (s, 10H), 4.05 (s, 4H), 3.29–3.72 (m, 4H); $^{13}C\{^{1}H\}$ NMR ($CDCl_3$) δ (ppm): 129.2, 129.0, 128.3, 128.1, 127.4, 67.0, 63.4, 41.9, 39.1; FT-IR (solid) $\overline{\nu}_{max}$ (cm^{-1}): 3027, 2939, 1740, 1234, 1081.

PCBM: ^{1}H NMR ($CDCl_3$) δ (ppm): 7.23–7.31 (m, 10H), 3.89 (s, 4H), 3.58 (s, 2H), 3.34 (s, 2H), 2.91 (s, 2H); $^{13}C\{^{1}H\}$ NMR ($CDCl_3$) δ (ppm): 166.4, 138.9, 128.9, 128.1, 127.2, 66.01, 42.0, 41.3, 39.1; FT-IR (solid) $\overline{\nu}_{max}$ (cm^{-1}): 2944, 1728, 1143, 1005.

PCBS: ^{1}H NMR ($CDCl_3$) δ (ppm): 7.23–7.32 (m, 10H), 3.93 (m, 4H) 3.63 (s, 2H), 3.37 (s, 2H), 2.20 (s, 4H); $^{13}C\{^{1}H\}$ NMR ($CDCl_3$) δ (ppm): 172.3, 139.2, 128.9, 128.1, 127.1, 65.3, 42.1, 39.4, 29.1; FT-IR (solid) $\overline{\nu}_{max}$ (cm^{-1}): 2925, 1728, 1151.

PCBG: ^{1}H NMR ($CDCl_3$) δ (ppm): 7.22–7.32 (m, 10H), 3.94 (s, 4H), 3.64 (s, 2H), 3.39 (s, 2H), 1.98 (s, 4H), 1.57 (s, 2H); $^{13}C\{^{1}H\}$ NMR ($CDCl_3$) δ (ppm): 173.0, 139.3, 128.9, 128.2, 127.1, 65.0, 42.2, 39.6, 33.3, 20.1; FT-IR (solid) $\overline{\nu}_{max}$ (cm^{-1}): 2942, 1727, 1147.

PCBA: ^{1}H NMR ($CDCl_3$) δ (ppm): 7.23–7.32 (m, 10H), 3.94 (m, 4H), 3.67 (m, 2H), 3.43 (m, 2H), 2.02 (s, 4H), 1.34 (s, 4H); $^{13}C\{^{1}H\}$ NMR ($CDCl_3$) δ (ppm): 173.5, 139.3, 128.9, 127.1, 65.0, 42.2, 39.5, 34.0, 24.4. FT-IR (solid) $\overline{\nu}_{max}$ (cm^{-1}): 2943, 1728, 1139.

PCBT: ^{1}H NMR ($CDCl_3$) δ (ppm): 7.29 (m, 4H), 6.76-6.93 (m, 10H), 3.80 (m, 4H), 3.35 (s, 2H), 3.16 (m, 2H); $^{13}C\{^{1}H\}$ NMR ($CDCl_3$) δ (ppm): 160.6, 133.9, 128.7, 124.4, 123.8, 123.0, 122.0, 60.6, 37.0, 34.6. FT-IR (solid) $\overline{\nu}_{max}$ (cm^{-1}): 2941, 1709, 1264, 1100.

PCBF: ^{1}H NMR ($CDCl_3$) δ (ppm): 7.18–7.24 (m, 10H), 6.83 (s, 2H), 4.16–4.24 (m, 2H), 3.76 (m, 2H), 3.53–3.60 (m, 2H); $^{13}C\{^{1}H\}$ NMR ($CDCl_3$) δ (ppm): 157.5, 146.5, 138.4, 128.5, 127.8, 127.6, 118.1, 65.5, 41.8, 39.2. FT-IR (solid) $\overline{\nu}_{max}$ (cm^{-1}): 2943, 1716, 1267, 1220, 1130.

PCBC: ^{1}H NMR ($CDCl_3$) δ (ppm): 7.17–7.26 (m, 10H), 7.04–7.08 (m, 4H), 2.70–4.17 (m, 6H); $^{13}C\{^{1}H\}$ NMR ($CDCl_3$) δ (ppm): 172.00, 139.24, 139.16, 128.81, 128.22, 127.92, 127.63, 127.41, 127.05, 64.74, 41.97, 41.37, 39.27. FT-IR (solid) $\overline{\nu}_{max}$ (cm^{-1}): 3028, 1724, 1168, 695.

2.3 RESULTS AND DISCUSSION

2.3.1 Synthesis of CBDO-1

Solvent-free dimerization of *trans*-cinnamic acid under residential blacklight (365 nm) resulted in the *rctt*-2,4-diphenylcyclobutane-1,3-dicarboxylic acid (CBDA-1), in nearly quantitative yield. The photoreaction can also be carried out in slurry conditions, using brine as a medium in which the commercially available crystalline powder of cinnamic acid is stirred under blacklight. Compared to reported procedures,[46a,47] this innovative slurry photoreaction using brine and blacklight has merits of simplicity and easy scalability Figure 2.3. CBDO-1 (*rctt*-2,4-diphenyl-1,3-cyclobutanedimethanol) was then synthesized in 93% isolated yield by the reduction of CBDA-1 using sodium borohydride ($NaBH_4$) in the presence of iodine (I_2) as an electrophile and tetrahydrofuran (THF) as the solvent (Scheme 2.1).

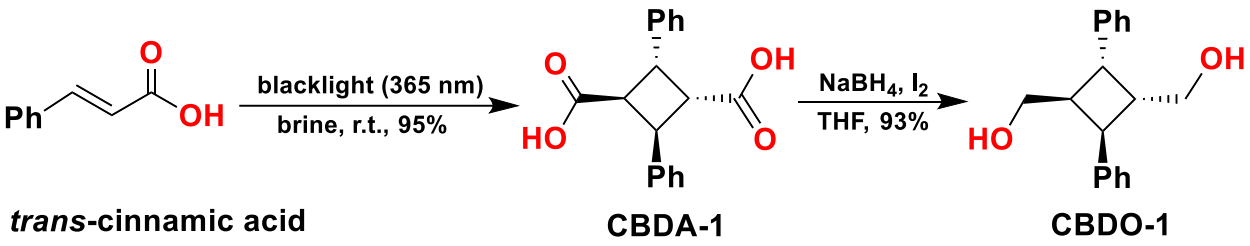

Scheme 2.1. Synthesis of CBDO-1 from *trans*-cinnamic acid.

Although $LiAlH_4$ is known to be able to reduce carboxylic acids to alcohols, its high reactivity makes it difficult to handle, and extra precautions are required.[48] The milder reagent $NaBH_4$ is not reactive enough to reduce carboxylic acids to alcohols by itself. However, the combination of $NaBH_4$ and I_2[49] reduced CBDA-1 to CBDO-1. The role of I_2 is unique because of its ability to work either as an electrophile or nucleophile. The mechanism of the reduction of acids to alcohols by metal hydrides shows that the rate-determining step is the hydride transfer from the metal hydride to the carbonyl carbon. Unfortunately, the carbonyl carbon on the acid is not susceptible to a hydride attack in the case of the $NaBH_4$. However, the presence of I_2 can facilitate the hydride transfer in this reaction.[50] CBDA-1 has good solubility in THF, so using this solvent gave a better yield (93%) of CBDO-1 when compared to the yield with diethyl ether (74%). As a side note, the solvent does not need to be dried before use in this reaction, unlike when using $LiAiH_4$. In terms of reaction stoichiometry, for every mole of the diacid, a significant excess of the hydride regent (7 moles, 3.5 equivalents for each acid functional group) was required to assure the completion of the reduction. CBDO-1 was obtained as a white solid, which was further purified by recrystallization from ethyl acetate and hexane. The chemical structure was fully characterized by HRMS, FT-IR, and ^{1}H and $^{13}C\{^{1}H\}$ NMR spectroscopy.

Besides having optimized reaction conditions to synthesize CBDO-1 from CBDA-1 in the lab using $NaBH_4/I_2$, we have also successfully applied a model protocol used in industry to this reduction. Specifically, the transformation was accomplished by an efficient and cost-effective heterogeneous catalytic hydrogenation method using an inexpensive and commercially available catalyst, $CuO\text{-}CrO_3$, at elevated pressure and temperature in a stainless-steel reactor (47% yield).

To further characterize this promising diol, rhombic crystals of CBDO-1 were obtained from a 3:1mixture of ethyl acetate and hexane by slow evaporation at room temperature. Single crystal X-ray diffraction was used to elucidate the structure of CBDO-1. The crystal structure revealed that the two methanol groups are on the 1 and 3 positions of the cyclobutane ring and are trans to each other, which is the same configuration as their parent carboxylic acid groups in the starting material of CBDA-1 (Figure 2.4a). The space group is Pna21, and there are two molecules in each asymmetric unit cell. The two cyclobutane rings in each asymmetric unit adopt about 18.61 and 22.02° puckered conformations (Figure 2.4b and Figure 2.5), respectively, indicating a certain degree of flexibility of the four-membered ring structure. [51] The angles in the cyclobutane ring are 89.00, 88.55, 90.06, and 88.13° (Figure 2.5a & b).

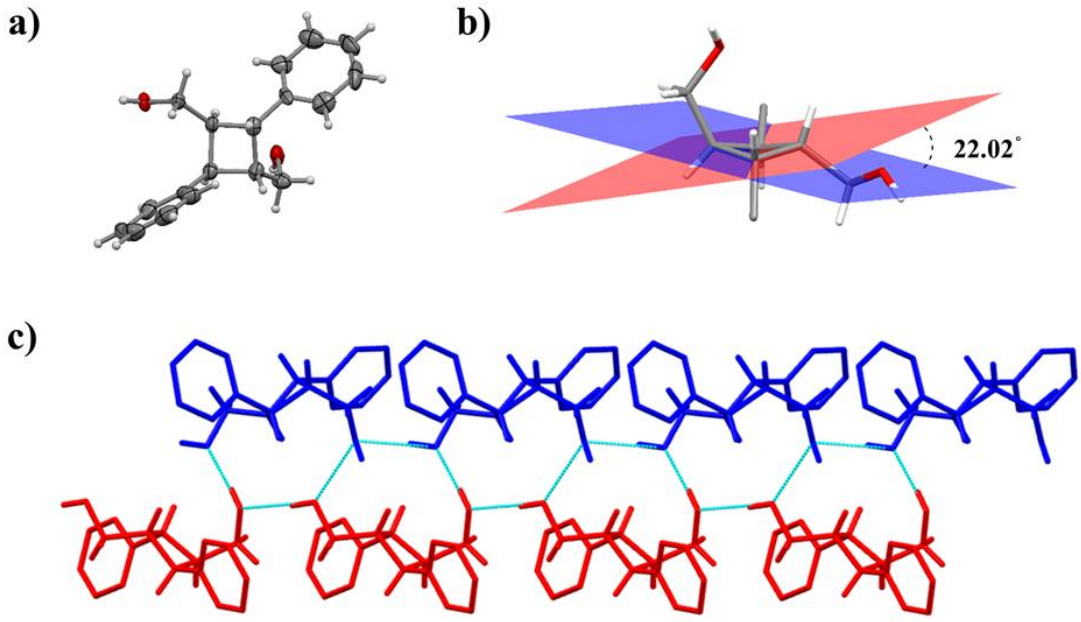

Figure 2.4. X-ray single-crystal structure of CBDO-1: (a) One molecule shown as Oak Ridge Thermal Ellipsoid Plot (ORTEP) representing 50% electron density; (b) The puckered conformation adopted by cyclobutane rings (the phenyl groups are replaced with carbon atoms for clarity); (c) Side view of supramolecular helix formed via hydrogen bonding (the molecules with the same symmetry equivalence are shown in the same color).

Each hydroxyl group forms two hydrogen bonds with the two hydroxyl groups of the two neighboring molecules (Figure 2.4c) to form a supramolecular helix, which plays an important role in determining the melting point of CBDO-1 (m.p. 106.4–107.0 °C). For comparison, the melting point of its diacid parent molecule, CBDA-1, is about 175 ^{o}C higher. The distance between oxygen atoms in the four hydrogen bonds is 2.734, 2.758, 2.764, and 2.769 Å, respectively. Although the hydrogen-bonded helix is chiral, each crystal is racemic. CBDO-1 is soluble in many common organic solvents, such as acetone, ethyl acetate, diethyl ether, and chloroform. Its relative low melting point and high solubility reinforce CBDO-1 application in polymer synthesis.

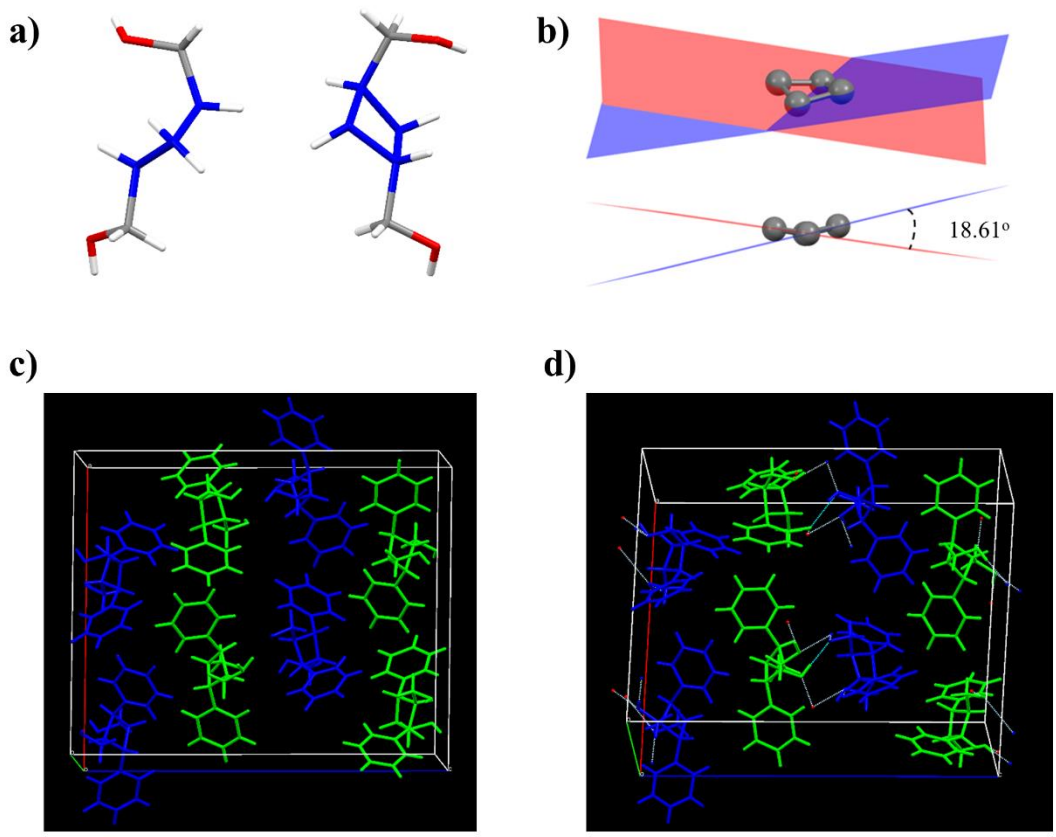

Figure 2.5. a) Two CBDO-1 molecules in the asymmetric unit cell (cyclobutane moiety highlighted in blue and the phenyl groups are omitted for clarity), b) Conformation of a cyclobutane ring in the crystal: The puckered cyclobutane ring of CBDO-1 with an angle of 18.61°, and the other one is 22.02° as shown in Figure 2.4, c) The packing of CBDO-1 in crystal (In the unit cell, the molecules with the same symmetry equivalence are shown in the same color.), d) The packing of CBDO-1 in crystal with the hydrogen bonds shown in blue dash lines.

2.3.2 Synthesis of CBDO-1 based polymers

To demonstrate the potential application of CBDO-1 in synthesis of materials, a series of polyesters were synthesized using a conventional polycondensation procedure.[52] The two-step polycondensation was performed using titanium isopropoxide as a catalyst (1.25 mol %). The pre-polymerization was first carried out at 160 °C for 12 h, followed by further polycondensation at 210–215 °C for 2 h under reduced pressure in the second step

(Scheme 2.2). This melt polycondensation involved the reaction of CBDO-1 with one equivalent of an aromatic or aliphatic diacid. Specifically, these diacids were oxalic, malonic, succinic, glutaric, adipic, terephthalic, 2,5-furandicarboxylic acid, and CBDA-1, which yielded eight corresponding cyclobutane-containing polymers (CBPs):[15, 53] polycyclobutane oxalate (PCBO), polycyclobutane malonate (PCBM), polycyclobutane succinate (PCBS), polycyclobutane glutarate (PCBG), polycyclobutane adipate (PCBA), polycyclobutane terephthalate (PCBT), polycyclobutane furandicarboxylate (PCBF), and polycyclobutane-1,3-cyclobutane dicarboxylate (PCBC). Out of the eight polyesters synthesized, PCBS, PCBT, and PCBC appears as white amorphous solids, PCBO had an earth color, and PCBM had a very distinct bright orange color. PCBF, PCBG, and PCBA were found to have a light yellow, tan, and brown color, respectively.

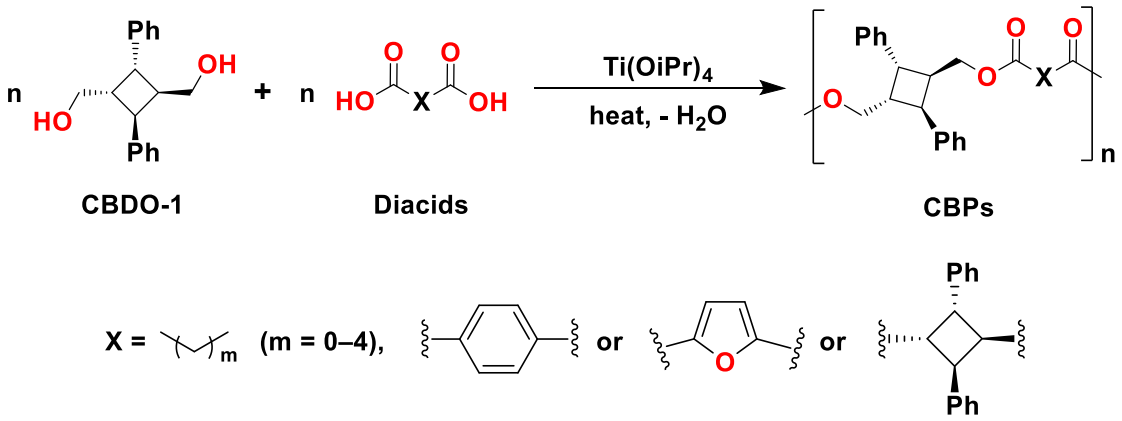

Scheme 2.2. Synthesis of CBDO-1 based polyesters.

The color observed in the polymers prompted us to replace magnetic stirring with external mechanical stirring in the polycondensations, which resulted in polyesters with negligible color (Figure 2.6) The success of this subtle change of the process supported our hypothesis that ineffective magnetic stirring of the melted reaction mixture with high viscosity might result in localized overheating and degradation of some polymer at high

temperature. The tiny amount of the degraded products might be responsible for the color in the final polymers although they were undetectable using NMR and FT-IR. Furthermore, a white translucent film (2 cm x 1 cm) of PCBS, as shown in Figure 2.7, was obtained by solution casting using DCM as solvent, showing the processability of these polyesters.

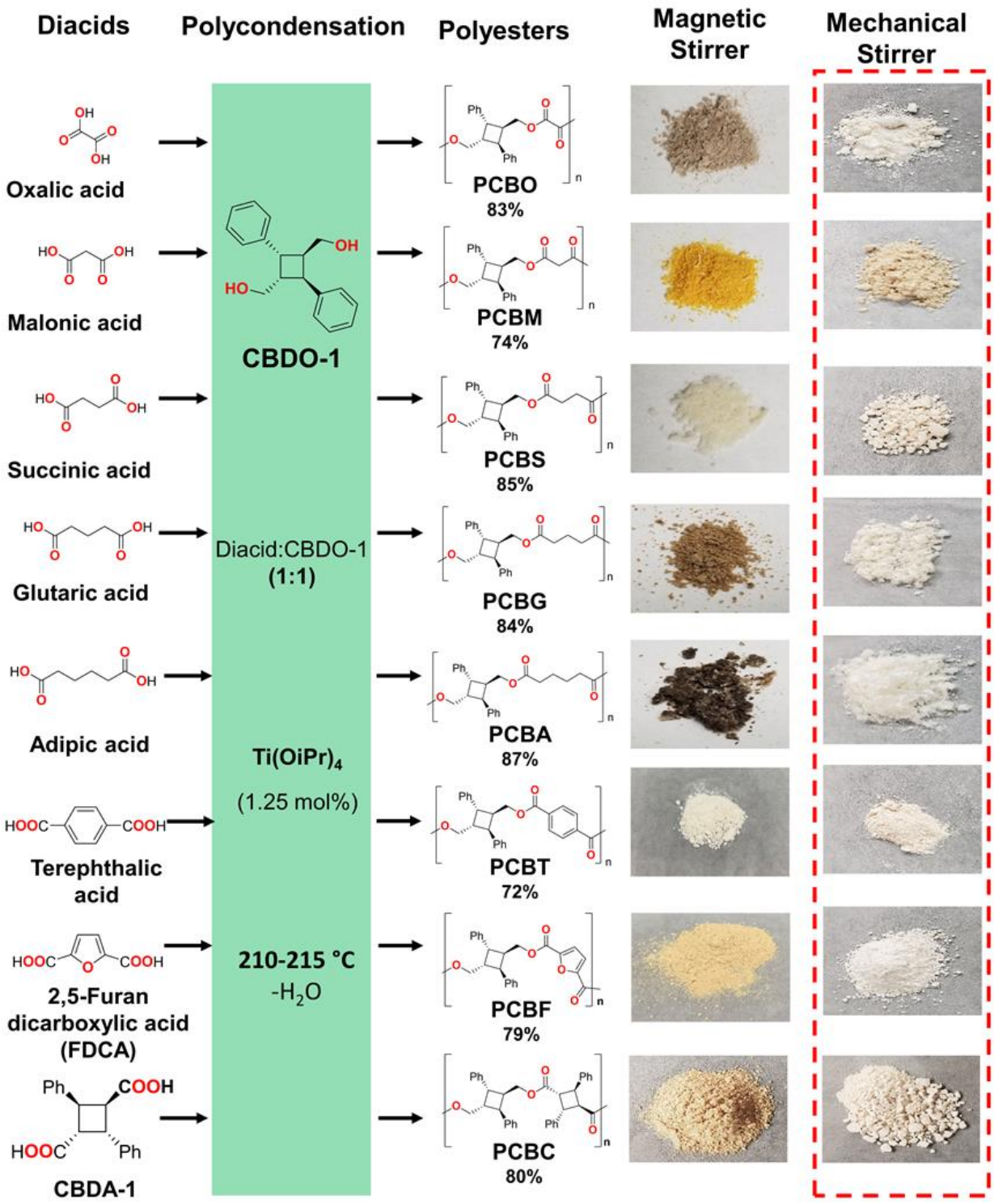

Figure 2.6. Synthesis of CBDO-1 based polyesters and the product color difference by using magnetic stirrer and external mechanical stirrer.

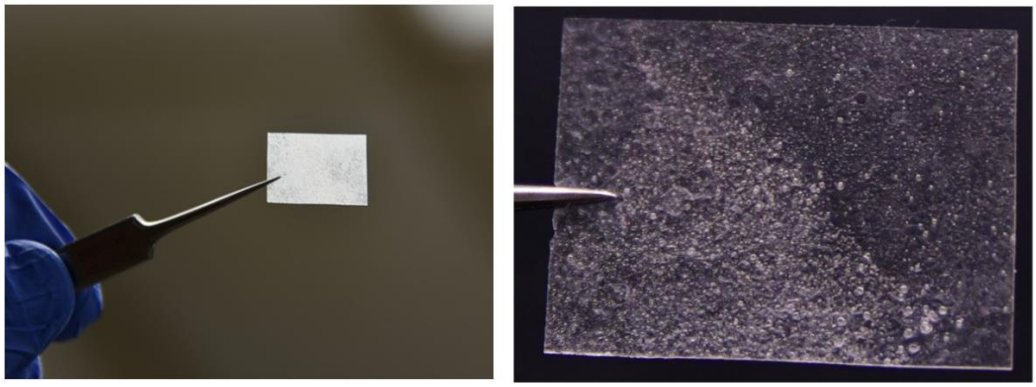

Figure 2.7. Images of the synthesized polycyclobutane succinate (PCBS).

It is worth noting that some of the diacids, such as succinic[54] and 2,5-furandicarboxylic acid,[55] used in the polyester syntheses can be produced from various biomass-derived precursors. The starting material for making both CBDA-1 and CBDO-1, *trans*-cinnamic acid, can also be obtained from glucose or Dried Distillers Grains with Solubles (DDGS), which is generated as a side product of dry mill ethanol production on a large scale and used as livestock feed.[56] Due to the possible environmentally friendly origin of the starting materials, the CBPs are even greener compared to BPA-based polymers.

The polymers synthesized by the polycondensation were subjected to further purification by first dissolving them in a solution of chloroform and trifluoroacetic acid (TFA) in a 6:1 ratio and then precipitating them by adding methanol. All the polyesters precipitated as amorphous powders with excellent isolated yields of 72–87%. NMR and FT-IR spectroscopy confirmed the structures of the CBPs (see Appendix B). The molecular weight and molecular weight distribution of CBPs were measured by gel permeation chromatography (GPC) and compared with the weight average molecular weight (M_w) data

obtained from Diffusion Ordered NMR Spectroscopy (DOSY) data.[57] DOSY linearly relates the ^{1}H NMR chemical shifts to the translational diffusion coefficient of a particular molecular species, which could be applied to determine M_w of polymers in dilute solutions. In infinite dilution, viscosity and density remain consistent throughout the solution, hence the linear relation is observed between Log D^a and Log M_w using the Stokes-Einstein equation.[58] The commercial polystyrene (PS) standards were selected to obtain the D - M_w calibration curve due to its widespread use as GPC standards. $CDCl_3$ was used as a solvent due to its ability to dissolve most of the polyesters. Table 2.1 and Figure 2.8 show the PS calibration curve in $CDCl_3$, good linearity of Log D_a - Log M_w is demonstrated by a high value of r^2 of 0.9969. Furthermore, by extrapolating the calibration curve to the low molecular weight range, the M_w of $CDCl_3$ was estimated as 122.97 g/mol with only 2.1% deviation of its calculated value, 120.38 g/mol. After the establishment of a calibration curve, diffusion coefficients of the CBPs samples were fitted to the PS calibration curve to calculate the M_w. As shown in Table 2.2 and Figure 2.9, the M_w of CBPs obtained from the DOSY spectra ranged between 7,200 and 35,600 g/mol, which were consistent with the results from GPC (6,900–34,900 g/mol). The polydispersity index (PDI) of CBPs were from 1.55 to 2.91.

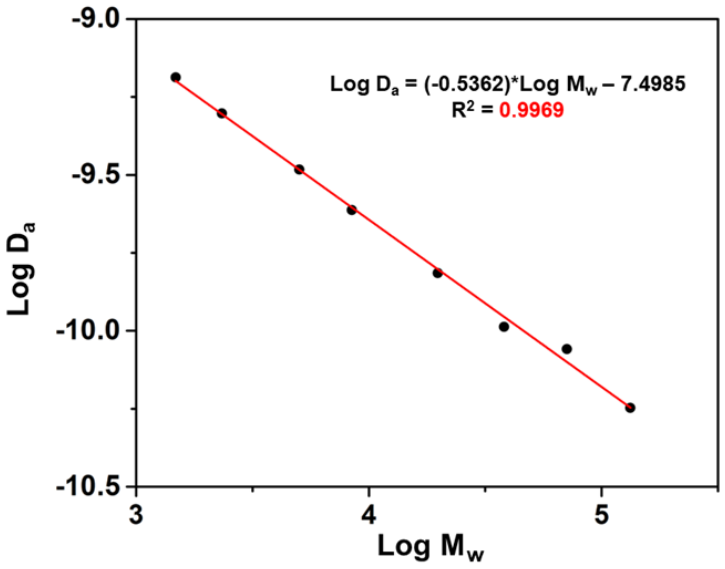

Figure 2.8. PS calibration curve in $CDCl_3$ for M_w prediction.

Table 2.1. Diffusion Coefficient – Molecular weight results of PS calibration curve using DOSY spectra.

samples	M_p (g/mol)	D^a (10^{-10}) (m^2/s)	Log D^a	Log M_p
PS	1480	6.50 ± 0.02	-9.18	3.17
PS	2340	4.98 ± 0.03	-9.30	3.36
PS	5030	3.29 ± 0.04	-9.48	3.70
PS	8450	2.44 ± 0.01	-9.61	3.92
PS	19760	1.53 ± 0.04	-9.81	4.29
PS	38100	1.03 ± 0.02	-9.98	4.58
PS	70950	0.87 ± 0.01	-10.05	4.85
PS	132900	0.56 ± 0.01	-10.24	5.12

^1H DOSY measurement was performed at 25 °C in $CDCl_3$with a concentration of 1 mg/mL.

Table 2.2. Molecular weight distribution calculated from GPC and externally referenced DOSY data.

	Molecular weight distribution GPC			Molecular weight data DOSY[a]	
Sample	M_n (g mol^{-1})	M_w (g mol^{-1})	PDI	D_a (m^2 s^{-1}) (10^{-10})	M_w (g mol^{-1})
PCBA	8800	25 600	2.91	1.38	25 700
PCBG	5300	8900	1.66	2.33	9500
PCBM	4400	6900	1.55	2.71	7200
PCBO	6300	14 900	2.28	1.79	15 700
PCBS	12 100	26 800	2.21	1.33	27 100
PCBT	11 000	23 100	2.11	1.48	22 300
PCBF	3600	6900	1.89	2.66	7500
PCBC	23 400	34 900	1.49	1.15	35 600

[a] M_w (DOSY) were calculated using the PS calibration curve incorporating the experimental D values of the CBP samples.

To obtain more details about the structural information, MALDI-TOF mass spectra of CBPs were recorded. Fragments and oligomers with low masses (< 5000 D_a), which have the same repeat units and possible end groups as high mass components, were studied to get structural information. The positive ion MALDI-TOF spectra were obtained for PCBS, PCBT, PCBF, and PCBC, and their results are summarized in the Figures C.1–4 (see Appendix C for the spectra and proposed structures). In general, the spectra of CBPs were highly asymmetric and had dispersed fragment and oligomer distributions, which was expected for polycondensates. The individual repeated units are well displayed, 350 Da for PCBS, 398 Da for PCBT, 388 Da for PCBF, and 528 Da for PCBC, respectively.

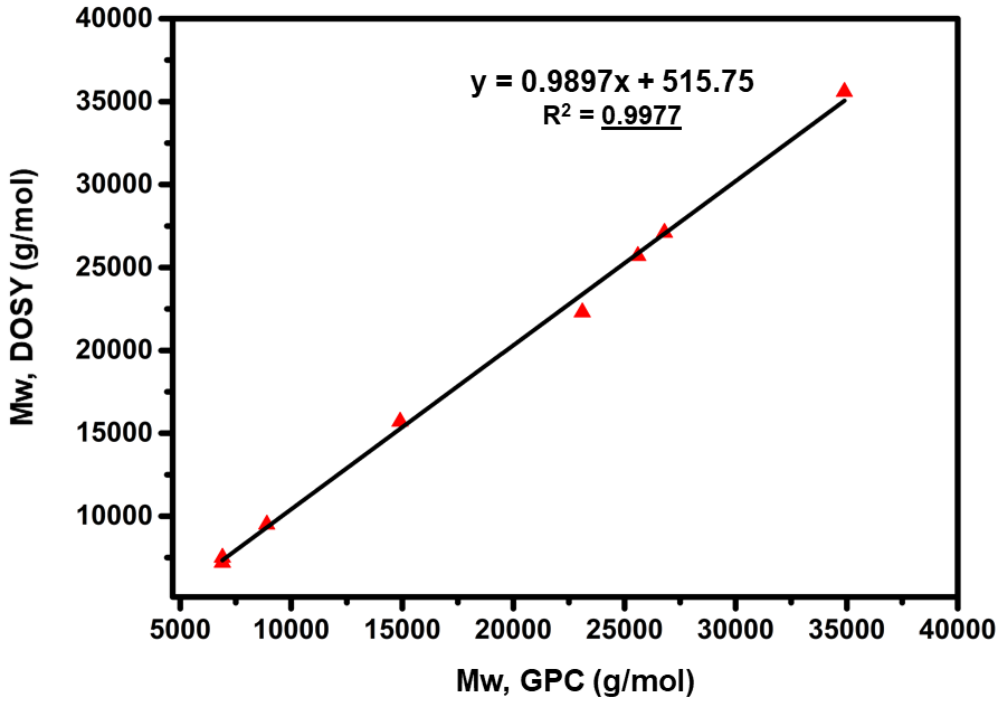

Figure 2.9. Comparison of M_w data of CBPs samples obtained by DOSY and GPC.

In PCBS and PCBF, four main series of repeated units and oligomers are marked in Figures C.1 and C.3 and shown in different colors: cyclic (blue), linear with two carboxyl end groups (yellow), linear with one carboxyl and one hydroxyl end groups (red), and linear with two alcohol end groups (purple). In contrast, peaks corresponding to the cyclic oligomers were not found in PCBT and PCBC as shown Figures C.2 and C.4 due to the linear orientation and rigidity of the diacid moieties (i.e., terephthalic acid and CBDA-1). PCBT showed a series of high-intensity peaks from linear fragments with two alcohol end groups and a series of low-intensity peaks from linear fragments with both acid and alcohol end groups. In case of PCBC, a series of peaks from linear fragments with two acid end groups were prominent, and two series of medium-intensity peaks were also observed, corresponding to the other two possible linear fragments. Interestingly, one additional

series of strong peaks with the mass 148 Da less than the high-intensity peak at 2962 Da were observed. These peaks were presumably due to the cleavage of cyclobutane ring in CBDA-1 moieties present in the polymer chains during the process of MALDI experiment, which led to formation of the fragments with one end group as cinnamate (coded with black in Figure C.4 of Appendix C).

Thermal properties of the polyesters were analyzed using differential scanning calorimetry (DSC) under N_2 atmosphere. The samples were heated from 0 to 200 °C at a rate of 20 °C/min. After this step, they were isothermally held at 200 °C for 5 min, then cooled to 0 °C at a rate of 20 °C/min. DSC did not show a melting transition in any of the polymer samples, suggesting that all the materials are amorphous thermoplastics. As anticipated, the semi-rigid structure of the CBDO-1 monomer unit has a profound effect on the thermal properties such as the glass transition temperatures (T_gs) of the final polyesters (Figure 2.10a). For instance, the substitution of the ethylene glycol unit with the cyclobutane unit increased the T_gs of the polymers substantially. The T_gs of the polyesters derived from CBDO-1 and aliphatic diacids such as succinic acid (PCBS) and adipic acid (PCBA) were approximately 50 °C and 80 °C higher than their ethylene glycol analogs: polyethylene succinate and polyethylene adipate, respectively (see Table 2.3). The effect of the carbon chain length of the homologous diacid on the T_g of the polyesters is graphically represented in Figure 2.10b. This representation shows a considerable decrease in T_g with an increasing length of the carbon chain of the diacid; the PCBG was found to have the lowest T_g of 33 °C amongst all the aliphatic polyesters while PCBO had a highest T_g of 62 °C. This anticipated decrease can be attributed to the increase in chain mobility with higher flexible aliphatic content from 2-carbon oxalic acid to 6-carbon adipic acid. Interestingly, the

polyesters with an even-number carbon chain (PCBO, PCBS, and PCBA) showed a higher T_g than the polyesters with odd-number carbon chain (PCBM, PCBG). This odd-even difference in T_gs shows that the packing and stereochemical properties of the even-number carbon chain form a better-organized structure in a solid phase, which requires more energy to move apart. [59]

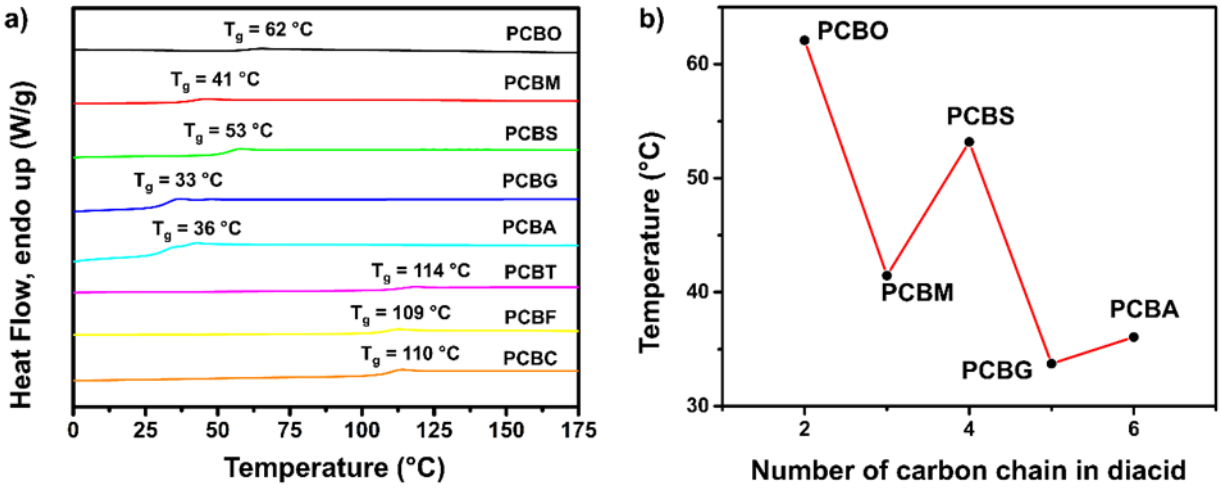

Figure 2.10. The DSC analyses of CBDO-1 polymers: a) second heating DSC curves of polymers derived form CBDO-1 at a heating rate of 20 °C/min under N_2. b) The plot of T_gs of polymers against carbon chain length of aliphatic diacids showing the odd-even difference.

Table 2.3. Thermo-physical properties of some known polyesters compared with synthesized polyester.

Polyester	Glass Transition Temperature, T_g (°C)
Polyethylene Succinate	-11 to -1
PCBS	53
Polyethylene Adipate	-70 to -40
PCBA	35
Polyethylene Terephthalate	64 to 84
PCBT	114
Polyethylene Furan 2,5 dicarboxylate	80 to 87
PCBF	109

Similarly, the introduction of CBDO-1 in conjunction with the rigid aromatic diacids also showed a clear impact on the T_g of the polyesters. It was observed that the T_gs of polyesters synthesized from CBDO-1 with terephthalic acid (PCBT) and 2,5-furan dicarboxylic acid (PCBF) were higher than those of the polyesters derived from aliphatic diacids, with PCBT and PCBF having T_gs of 114 and 109 °C, respectively. It should be noted that PET (polyethylene terephthalate) and PEF (polyethylene 2,5-furandicarboxylate) synthesized under similar conditions were shown to have T_gs of 80 °C and 87 °C, correspondingly, meaning that the replacement of flexible ethylene glycol with the semi-rigid CBDO-1 with two phenyl substituents in the above two polymers significantly improved their T_gs. Furthermore, a sample of the popular Tritan copolyester, which is produced from polycondensation between DMT (dimethyl terephthalate) with both CHDM and TMCD (Figure 2.1), was shown to have a T_g of 109 °C.[10a] When CBDO-1 was used to replace CHDM and TMCD in this Tritan polyester, it was also not a surprise to observe higher T_g (PCBT: 114 ^{o}C) even at relatively low M_w under the current experimental conditions (see Table 2.2). The obvious improvement in T_g can be attributed to the unique structure of the CBDO-1 monomer, which contains a semi-rigid cyclobutane backbone as well as two rigid and bulky phenyl substituents roughly perpendicular to the backbone. The phenyl groups sticking out from the polymer backbone restrict the movement between the polyester chains, resulting in the high T_g. For the same reason, the T_g of PCBC (the polyester synthesized from CBDO-1 and CBDA-1) was as high as 110 °C, which is comparable to corresponding polyesters made from CBDO-1 and a rigid diacid such as terephthalic acid (PCBT with T_g of 114 °C) or 2,5-furan dicarboxylic acid (PCBF with T_g of 109 °C). Compared to the polyesters derived from CBDO-1 and the other

aliphatic diacids, incorporating CBDA-1 in the polymer chain boosts T_g of the polyester by more than 50 °C (Figure 2.10a).

The thermal stabilities of the CBPs were examined by comparing the temperatures at which the onset of decomposition occurs, $T_{5\%}$ (5% weight loss), and maximum rate of decomposition (T_d) occur. Thermogravimetric analysis (TGA) was employed to measure these characteristics under a N_2 atmosphere, as shown in Figure 2.11. As expected, the morphology of CBDO-1 does affect the decomposition temperatures of the synthesized polyesters. Figure 2.11a reveals that most of the CBPs showed high thermal stability without any significant weight loss below 300 °C. Onset decomposition temperature ($T_{5\%}$) of PCBM was 266 °C, while PCBA exhibited the highest $T_{5\%}$ at 350 °C. The thermal stability of CBPs increases slightly with the increase of the length of the linear diacids used in the preparation of the polyesters.[60] In the case of the aromatic diacids, PCBT and PCBF showed similar $T_{5\%}$, 363 °C and 341 °C, respectively. When diacid monomer was replaced with CBDA-1, PCBC was obtained, having a $T_{5\%}$ of 383 °C, among the highest of all CBPs synthesized in this study. Notably, the maximum decomposition temperature (T_d) of the CBPs were in the range of 381 to 424 °C, without any significant difference as that of $T_{5\%}$, suggesting the decomposition of these polyesters might be governed by the cleavage of cyclobutane moieties.

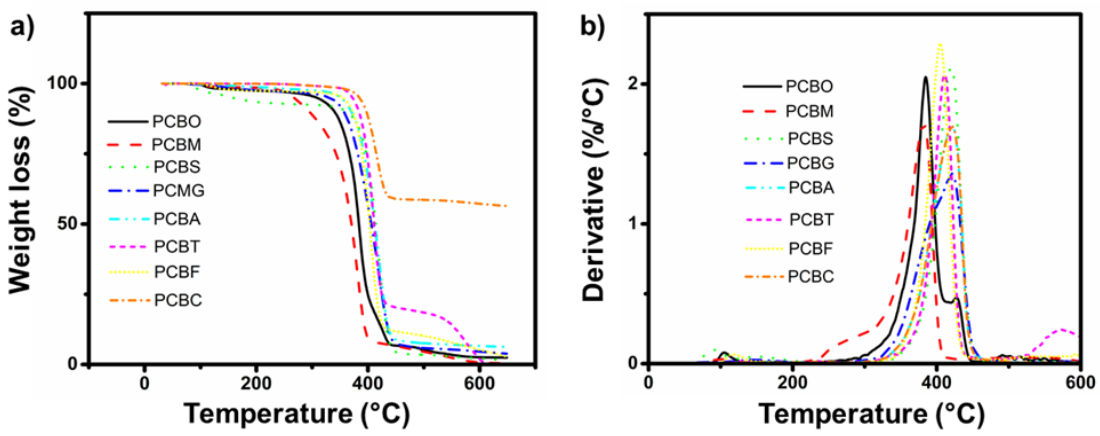

Figure 2.11. The TGA of CBDO-1 polymers: a) TGA traces of CBDO-1 based polymers recorded from 30 to 600 °C at 20 °C/min under N_2. b) The plot of derivative of TGA traces (%/°C) against temperature.

It is important to point that, besides polyesters, CBDOs can also be used to produce other industrially relevant polymers such as polyurethanes, polycarbonates, and polysilylethers, which are challenging to obtain from the previously reported CBDAs. Thus, exemplified with CBDO-1 in this work, the use of CBDOs will largely extend the scope of novel polymers with desirable properties that CBs can make.

2.4 CONCLUSION

The *trans*-1,3-cyclobutane-containing diol, CBDO-1 has been synthesized and introduced to materials science as a versatile monomer. In the first stage of the CBDO-1 synthesis, a diacid was yielded by dimerizing *trans*-cinnamic acid using 365 nm residential blacklight. The carboxyl group was then reduced using a reliable and operator-friendly $NaBH_4/I_2$ system or by catalytic hydrogenation with an inexpensive catalyst $CuO\text{-}CrO_3$ used in industry. This whole synthetic route is safe, efficient, and scalable. CBDO-1 was fully characterized, and its single crystal structure confirmed that the two methanol arms

attached to the cyclobutane ring are trans to each other, showing this molecule's potential to serve as a monomer. As a phenol-free monomer, CBDO-1 shares structural similarities to BPA, as well as its replacements CHDM and TMCD, which have been used in producing the popular Tritan copolyester. The unique semi-rigid nature and thermal stability of the primary diol were then translated into a series of novel polyesters via a two-step melt polycondensation using titanium isopropoxide as a catalyst. The thermal properties, molecular weight distribution, and structural details of the CBDO-1 polyesters were investigated. Potential utilizations of these polymers as BPA-free polyesters were evaluated. Compared to the polyesters with industrial importance such as PET, PEF, and Tritan copolyester, the amorphous cyclobutane-containing polyesters derived from CBDO-1 showed excellent thermal properties (e.g., high T_g, $T_{5\%}$, and T_d) due to the unique structure of CBDO-1. However, under the current polymerization conditions, the M_w was still inferior to commercially available Tritan-based counterparts, suggesting efforts are still needed to further improve the molecular weight of the CBPs. Nevertheless, the successful synthesis of Tritan-like polymers, possessing desirable thermal properties, and not relying on the required petroleum feed of TMCD monomer, support CBDO-1 as a promising building block for BPA-free thermoplastics.

Chapter 3
A Cyclobutane-1,3-Diamine Building Block Prepared by a Slurry Photocyclizaion for Polymeric Materials with Enhanced Properties

3.1 INTRODUCTION

The design and synthesis of novel building blocks enable human beings to produce innovative materials that drive technological advancement and improve our daily lives. The nucleophilic character and polarity conferred to amines make them a key intermediates in various chemical industries such as agrochemicals, drugs, detergents, lubricants, food additives, and polymers.[61] An excellent example is diamines, as they have found extensive applications in synthesizing polyamides. As one of the most attractive engineering plastics, polyamides have been widely used in developing industrial and commercial materials due to their comprehensive properties.[62] According to the composition of their main chains, polyamides are classified as aliphatic and aromatic polyamides containing aliphatic and aromatic main chains, respectively. Due to reasonable chain regularity and the high content of hydrogen bonds, aliphatic polyamides or nylons such as nylon-6 and nylon-6,6 have remarkable properties such as good mechanical performance and processability.[62a, 63] However, the moderate thermal properties of nylon and high sensitivity to moisture limit its applications, mainly when used in surface mount technology and other applications.[64] Aromatic polyamides or aramids, such as Kevlar and aramid-1313, are well known for their excellent thermal, mechanical, and corrosion resistance.[65] They are irreplaceable

specialty polymers but have a drawback of poor processable properties. For example rigid rodlike aromatic polymer chains and intermolecular hydrogen bonding in Kevlar exhibit a high degree of intermolecular association.[62a] These crystalline materials with high thermal transitions and poor solubility are challenging to process in melt or solution,[66] which limits their wide applications.

Various efforts have been made to enhance the processability and solubility of aromatic polyamides by decreasing the rigidity of the polymer backbone, thus reducing the interchain interactions by structure modification. One such approach is to design semi-aromatic polyamides combining thermal resistance of aramids with the good processability of nylon.[67] Nonetheless, only a few semi-aromatic polyamides, such as PA9T,[68] PA10T,[69] and copolymers of PA6T/66, PA6T/6, etc.,[70] are commercial and processable. Typically, semi-aromatic polyamides with short-chain (less than seven) diamine moieties such as PA4T, PA6T, etc., are difficult to process thermally due to their poor solubility and decomposition before the melting temperature.[71] These limitations associated with semi-aromatic polyamides has inspired the research focusing on chemical modification of the polyamide backbone as a way to improve their processability, such as the incorporation of ester units,[72] sulfide groups,[73] cyclodextrin units,[74] long carbon chains (C_{12} to C_{18})[69a, 75] to lower the thermal characteristics and improve melt processability. Also, there has been research on the introduction of hyperbranched units,[76] pendant groups,[71, 77] nonplanar biphenyl rings[75a, 78] into the main polymer chain to lower the molecular regularity, thus increasing solubility. The moisture sensitivity of commercial semi-aromatic polyamides such as the copolymer of PA6T/66 is better than that of nylons, but it can still be troublesome to affect the thermal and mechanical properties.[79]

Herein, we report the design, synthesis, and application of a unique semi-rigid cyclobutane-containing 1,3-diamine building block (CBAM-1, Figure 3.1), which can introduce many enhanced properties (e.g., high T_g, good solubility, and low moisture sensitivity) to materials that the currently popular aliphatic diamines (e.g., hexamethylenediamine) and aromatic diamines (e.g., *p*-phenylenediamine) cannot. This is because the cyclobutane core of *trans*-1,3-cyclobutane diamine (CBAM-1) monomer allows functional groups, such as phenyl rings, as shown in Figure 3.1, to be installed and stay perpendicular to the polymer backbone. We hypothesize that incorporating a four-membered semi-rigid ring is expected to reduce interchain interactions and increase processability. This modification will eventually enhance the glass transition temperature, T_g, of the polyamides to a more desirable range for various applications when compared with polyamides containing analogous backbones and at the same time weaken their molecular arrangement to improve their solubility. Finally, the CBAM-1 based polyamides will have low amide content leading to reduced moisture sensitivity.

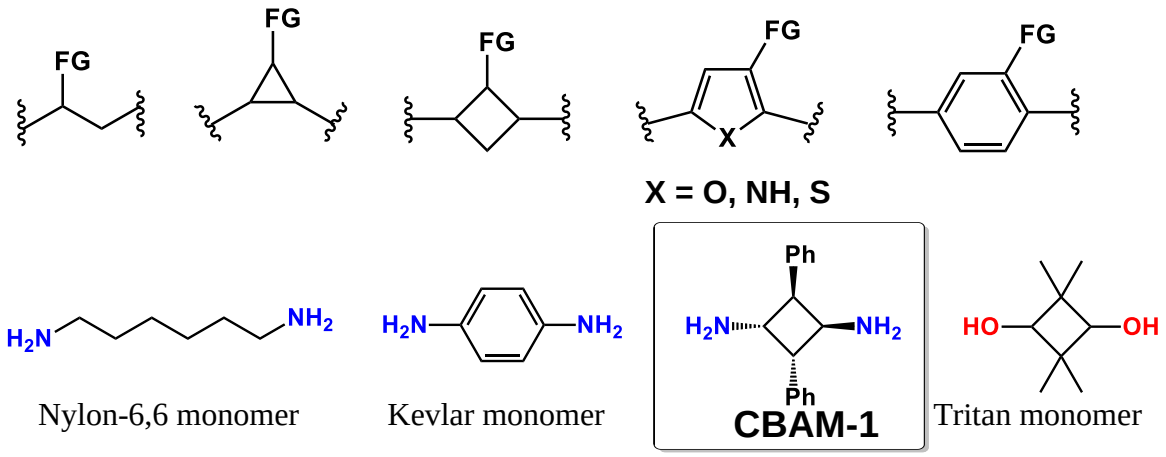

Figure 3.1. a) Compared to other possible structures, cyclobutane represents an ideal backbone for introducing bulky group(s) to enhance T_g of a polymer. b) Comparison of novel CBAM-1 with three popular monomers in industry: hexamethylenediamine, *p*-phenylenediamine, and 2,2,4,4-tetramethyl-1,3-cyclobutanediol.

Figure 3.2 shows the retrosynthetic analysis to produce CBAM-1 from readily available and inexpensive starting materials. CBAM-1 can be obtained by reduction of *trans*-1,3-dinitro-2,4-diphenylcyclobutane (CBDN-1), and the corresponding CBDN-1 can be synthesized by photodimerization of *trans*-nitrostyrene, which can be yielded from nitromethane with benzaldehyde via Henry reaction (nitroaldol condensation).

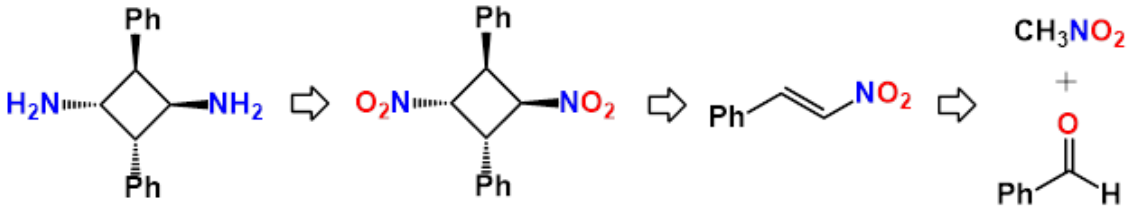

Figure 3.2. Designed synthetic route (retrosynthetic analysis) for making CBAM-1 from inexpensive starting materials: nitromethane with benzaldehyde.

3.2 EXPERIMENTAL SECTION

3.2.1 Materials and methods

All chemicals were purchased from Alfa Aesar, Sigma-Aldrich, or Acros, and used without further purification. Blacklight used in the photoreaction was 7W Fiet electric LED bulb. The solution phase NMR spectra were recorded with Bruker AVANCE 500 spectrometer (^{1}H: 500 MHz, ^{13}C{^{1}H}: 125 MHz). Proton and carbon chemical shifts were reported in ppm downfield from TMS or using the resonance of the corresponding deuterated solvent as an internal standard. ^{1}H NMR data were reported as follows: chemical shift (ppm), s = singlet, d = doublet, t = triplet, q = quartet, dd = doublet of doublets, m = multiplet, and integration. Single crystal X-ray data were collected on a Bruker Apex or Bruker Kappa Apex II Duo X-Ray diffractometer with Cu Kα (λ = 1.54178 Å). Infrared

(IR) spectra were recorded on a Thermo Scientific Nicolet iS5 FT-IR spectrometer. The mass spectrometric analyses were performed using a high-resolution time of flight G1969A mass spectrometer with electrospray (atmospheric pressure chemical) ionization (Agilent, Santa Clara, CA, USA) and reported as m/z. DSC experiments were performed on a Perkin Elmer Jade differential scanning calorimeter using a hermetic aluminum pan, indium standard for calibration, nitrogen as a purge gas, sample weight of ~ 5 mg with a ramping rate of 20 °C/min. Heat flow was recorded from both the first heating and cooling curves. TGA analyses were carried out on a Hi-Res TGA Q500 thermogravimetric analyzer from TA Instruments using alumina pans at a heating rate of 20 °C/min under nitrogen with a sample weight of about 10 mg.

3.2.2 Diffusion ordered spectroscopy (DOSY) experiments

NMR tubes were flame-dried in advance, and experiments were performed at 25 ± 1 °C. The data collection was done after stabilizing the NMR sample at RT for 30 min. For polymethyl methacrylate (PMMA) standard samples, each NMR tube contained 0.5 mg of PMMA and 1 mL of DMSO-d_6. For polyamide samples, each NMR tube contained 0.5 mg of polyamide and 1 mL of DMSO-d_6. DOSY experiments were performed on a Bruker AVANCE 500 spectrometer equipped with a z-axis gradient coil. All experiments were run without spinning to avoid convection. The maximum gradient strength was 0.214 T/m. The standard Bruker pulse program, stebpgp1s, employing a stimulated echo sequence and 1 spoil gradient, was utilized. Bipolar rectangular gradients were used with a total duration of 0.5−10 ms. Gradient recovery delays were 0.5−1 μs. Diffusion times were between 100 and 2000 ms. The number of gradient steps was set to be 16. Individual rows of the quasi-

2-D diffusion databases were phased, and baseline corrected. DOSY spectra were processed by Topspin 1.3 software. The diffusion dimension was generated using inverse Laplace transform driven by the maximum entropy method. Diffusion coefficients of a chosen narrow chemical shift range were extracted from the T_1/T_2 analysis module of Topspin 1.3.

3.2.3 Synthesis of *trans*-nitrostyrene

A 1 L beaker packed in a crystallizing dish with a freezing mixture of ice and salt and containing a magnetic stirrer, thermometer, and dropping funnel, was charged with an equimolar mixture of 0.23 mol of nitromethane and 0.23 mol of benzaldehyde, and 50 mL of methanol. A solution of sodium hydroxide was prepared by dissolving 0.29 mol of sodium hydroxide in 50 mL of water. The NaOH solution was poured into a dropping funnel, and added upon stirring to the nitromethane mixture at such a rate that the temperature was kept at 10–15 °C. During the addition, a white precipitate formed by adding the alkali, which later converted to a clear solution upon addition ice water containing crushed ice. The resulting mixture was transferred to the dropping funnel and added dropwise to the hydrochloric acid solution made by diluting 50 mL of concentrated HCl with 100 mL of water. A pale-yellow precipitate separated immediately as the alkaline solution comes in contact with the acid. The precipitate was filtered by using a Buchner funnel and washed with water until it is free from chlorides. The crude *trans*-nitrostyrene was recrystallized using ethyl alcohol. The yield of the recrystallized is 82 % (0.19 mol).

3.2.4 Synthesis of CBDN-1

In a 1000 mL crystallizing dish, 67.04 mmol g of *trans*-nitrostyrene powder was suspended in 800 mL of brine solution with magnetic stirring. Three 7W Fiet electric LED blacklight bulbs were immersed in the dish as shown in Figure 3.3. The resulting slurry of *trans*-nitrostyrene in brine was continuously stirred under the blacklight. After the completion of the reaction (8 h), the slurry was filtered, and the resulting solid was washed with 15 mL of ice-cold water. After drying the desired product, CBDN was obtained as a beige solid (32.31 mmol, 96%). ^{1}H NMR (DMSO-d_6, 500 MHz) δ (ppm): 7.49−7.31 (m, 10H), 6.15 (dd, J = 6.3, 9.8 Hz, 2H), 5.09 (dd, J = 6.5, 9.6 Hz, 2H). ^{13}C NMR (DMSO-d_6, 125 MHz,) δ (ppm) 133.3, 128.9, 128.6, 128.2, 82.1, 47.1.

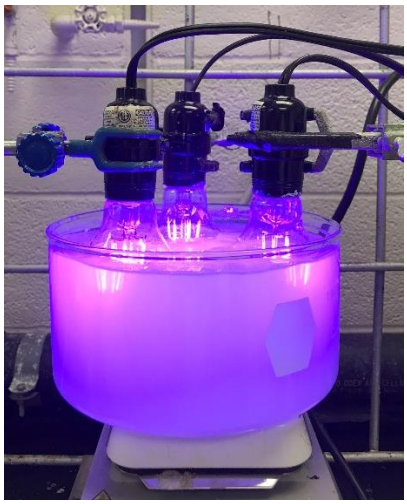

Figure 3.3. Setup for the synthesis of CBDN

3.2.5 Synthesis of CBAM-1

In a typical procedure, 1.67 mmol of CBDN, activated zinc (48.94 mmol) and 40 mL methanol were added in a 100 mL round bottom flask equipped with a dropping funnel, magnetic stirrer, and a slow stream of nitrogen. To this mixture, 30 mL of a 6N

hydrochloric acid was added over 30 minutes, and the reaction temperature was maintained at around 25 °C. The reaction mixture was allowed to stir for 3 h at room temperature under the nitrogen atmosphere. After the completion of the reaction, unreacted zinc was removed by filtration. The resulting solution was extracted with chloroform to remove methanol, and the aqueous layer was made strongly alkaline with a 3M sodium hydroxide solution and extracted four times with ethyl acetate (4 x 20 mL). The combined organic extracts were dried using anhydrous magnesium sulfate, and the solvent removal afforded desired product CBAM-1 in 84% without any further purification. The CBAM-1 was characterized by NMR using $CDCl_3$ as the solvent. ^{1}H NMR ($CDCl_3$) δ (ppm): 7.41−7.27 (m, 10H), 4.06 (dd, J = 15.0, 9.0 Hz, 2H), 3.33 (dd, J = 15.0, 9.0 Hz, 2H), 2.17 (s, 4H); $^{13}C\{^1H\}$ NMR ($CDCl_3$) δ (ppm): 138.4, 129.0, 128.1, 127.1, 53.7, 51.5. FT-IR (KBr, thin film) $\overline{\nu}_{max}$ (cm^{-1}):3338, 3181, 1664, 1643, 1619, 1097, 767, 655. HRMS (ESI/TOF): Calculated for $[M+H]^+$, $C_{16}H_{18}N_2H^+$: 239.1548; Found: 239.1547. It was observed that the CBAM-1 was not stable in air, so it was stored in nitrogen and immediately used in the polyamide synthesis.

3.2.6 General method to synthesize CBAM-1 based polyamides

A typical polymerization method, polyamides were synthesized in a 50 mL round bottom flask equipped with a mechanical stirrer and nitrogen inlet. 1 mmol of corresponding diacid and 2.36 mmol lithium chloride were dissolved in 5 mL *N*-methyl pyrrolidone (NMP), and an equimolar molar amount of CBAM-1 together with 2 mL pyridine and 2.21 mmol triphenyl phosphite (TPP) were added to the mixture to form a homogenous yellow solution. The mixture was then gradually heated to 130 °C and maintained at that temperature for 14 h under the protection of nitrogen. After the completion of the reaction,

the polyamide solution was precipitated by adding excess of acetone. The precipitate was filtered and washed with acetone and distilled water four times, after which crude polyamides were further purified by dissolving in 5 mL of a 1:4 solution of TFA: $CHCl_3$. Then 100 mL of methanol was added to precipitate the polyamide out of the solution. After it was filtered and dried in a vacuum at 60 °C for 12 h to yield the desired polyamide.

PCS ^{1}H NMR (DMSO-d_6) δ (ppm): 8.02 (s, 2H), 7.38−7.02 (m, 10H), 4.86 (s, 2H), 3.74 (s, 2H), 2.11−1.64 (m, 4H); $^{13}C\{^1H\}$ NMR (DMSO-d_6) δ (ppm): 138.4, 129.0, 128.1, 127.1, 53.7, 51.5; FT-IR (solid) $\overline{\nu}_{max}$ (cm^{-1}): 3303, 1641, 1533, 1451, 1032, 751, 698.

PCT ^{1}H NMR (DMSO-d_6) δ (ppm): 8.75 (s, 2H), 7.56 (m, 4H), 7.42 - 7.23 (m, 10H), 5.37 (s, 2H), 4.26 (s, 2H); $^{13}C\{^1H\}$ NMR (DMSO-d_6) δ (ppm): 165.8, 138.3, 128.6, 128.4, 127.2, 126.7, 49.9, 48.8; FT-IR (solid) $\overline{\nu}_{max}$ (cm^{-1}): 3292, 1633, 1527, 1450, 1031, 863, 698.

3.3 RESULTS AND DISCUSSION

3.3.1 Synthesis of *trans*-nitrostyrene

In the first step of the reaction sequence, the synthesis of *trans*-nitrostyrene was achieved by performing nitroaldol condensation between nitromethane and benzaldehyde in the presence of sodium hydroxide as a catalyst (Scheme 3.1). This method provided the purified *trans*-nitrostyrene in good yield (82%) and high purity (99% based on NMR). The product structure was determined using NMR and FT-IR spectroscopy, and the data were consistent with the literature. It should be noted that the basic solution of nitromethane and benzaldehyde was found to be temperature sensitive, so it is important to keep the reaction at low temperature using an ice-water bath. To achieve a good yield, it was essential to add

basic reaction mixture into the HCl aqueous solution dropwise. It was observed that the reverse addition, i.e., the addition of HCl aqueous solution into basic reaction mixture, resulted in the undesirable unsaturated nitro compound.

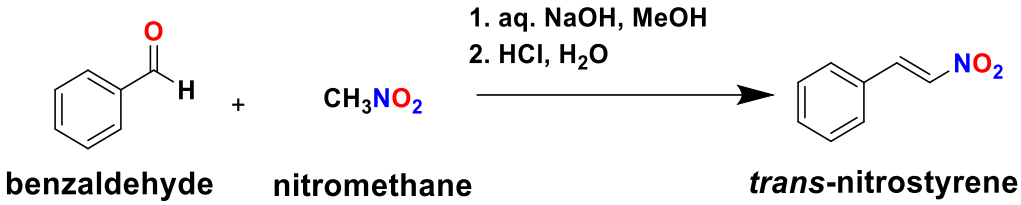

Scheme 3.1. Nitroaldol condensation of nitromethane with benzaldehyde to obtain *trans*-nitrostyrene.

The crude *trans*-nitrostyrene upon recrystallization in ethanol resulted in yellow, long needle-shaped crystals, and the structure of *trans*-nitrostyrene was determined by NMR and conformed using a single-crystal X-ray diffraction (SC-XRD) analysis. The XRD crystallographic data were consistent with the literature report,[80] but had less disorder and better quality, as shown in Table F.2 (Appendix F). In the crystal structure, the neighboring molecules with the opposite orientation were related by inversion, and the center to center double bond distance was 3.82 Å, which is well within the required length to undergo solid-state [2+2] photocycloaddition explained by Schmidt.[81]

3.3.2 Solid-state photodimerization of *trans*-nitrostyrene

The crystalline powder of *trans*-nitrostyrene was dimerized into *trans*-1,3-dinitro-2,4-diphenylcyclobutane**,** CBDN-1, using the method reported by Cambell et al.[82] with some modifications. In this process, CBDN-1 was synthesized in 30 % yield from a ground crystalline powder of *trans*-nitrostyrene using a medium pressure mercury lamp as the radiation source, as shown in Scheme 3.2 and Entry 1 of Table 3.1. Another method was

also employed, in which CBDN-1 was synthesized (42%) by irradiating a crystalline sample of dispersed on the water under magnetic agitation. Both methods suffered the drawback of low yields, which was initially attributed to the decomposition of *trans*-nitrostyrene under the heat produced by mercury lamp.

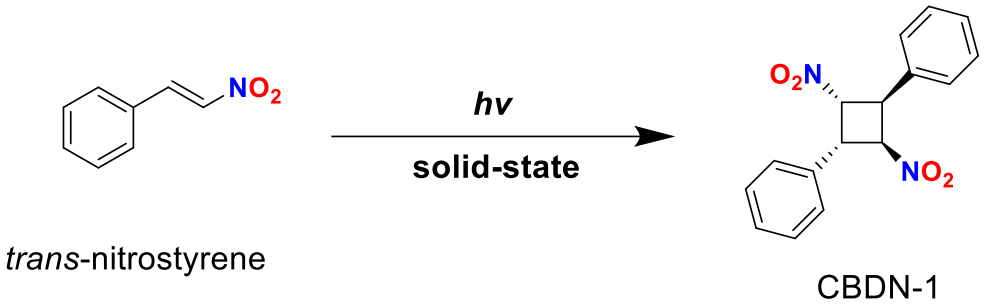

Scheme 3.2. Photocycloaddition of *trans*-nitrostyrene using UV radiation.

The nitro group is a strong chromophore and can shift the absorbance wavelength of *trans*-nitrostyrene towards a low-energy region of electromagnetic spectrum when compared to that of styrene. This red shift could lead to the resonance of its UV absorbance with the energy produced from domestic blacklights, which do not produce the undesired heat as the medium pressure mercury lamp generate. Meanwhile, the blacklight generated much less heat than the medium-pressure mercury lamp. Thus, we replaced the medium pressure mercury lamp with a LED blacklights (Feit Electric 7 watts) as the source of irradiation in the above protocols. As a result, the isolated yields of CBDN-1 were improved to 73% in the solvent-free reaction and 53% in the water slurry (Entries 3 and 4 in Table 3.1). Considering the scalability of the slurry process and the energy-efficient, cost-effective, and operator-friendly UV (ECO-UV) nature of blacklights, these were adopted for all the experiments in this study.

During a close examination of the photodimerization process, we noticed that the heat-caused decomposition was not solely responsible for the low yield of the desired dimer product. The photodimerization of *trans*-nitrostyrene gave a mixture of products as suggested by ^{1}H NMR spectra (Figure 3.4). At room temperature, it was found that the desired dimer CBDN-1 and byproducts (including other photodimers) were in a ratio of 2:1.

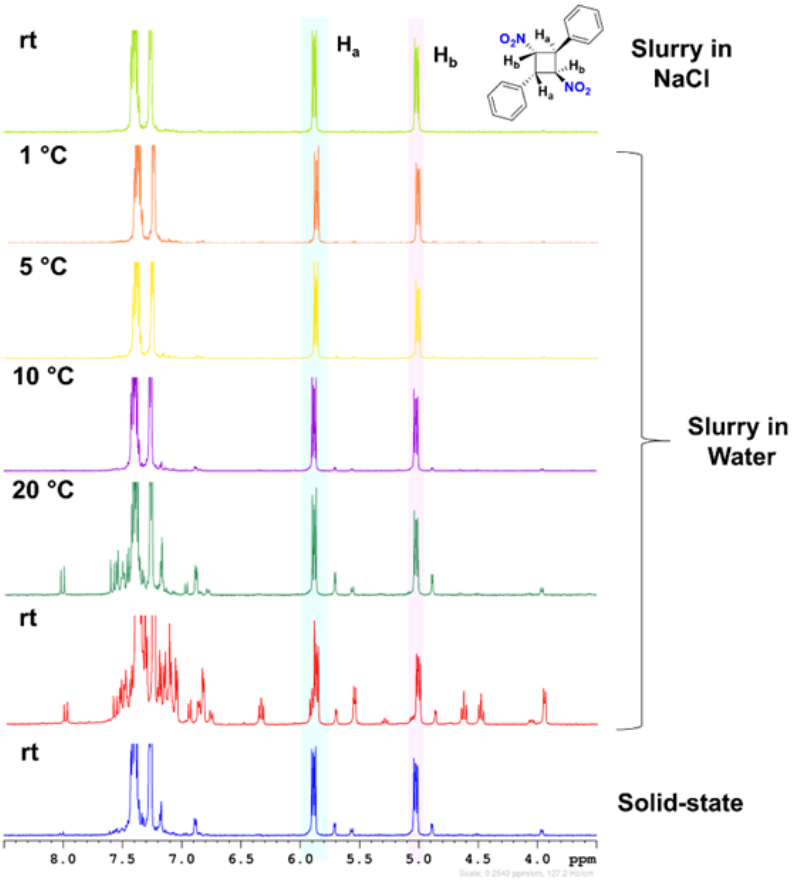

Figure 3.4. ^{1}H NMR spectra of photodimerization of *trans*-nitrostyrene under different reaction conditions.

A similar observation was reported by Shechter and coworkers[80a] who studied the solid-state photodimerization of *trans*-nitrostyrene under winter exposure conditions. Later, Desiraju et al.[80b, 83] obtained the same results, confirmed the structure of CBDN-1

by SC-XRD, and suggested that the unusual outcome of photodimerization was caused by the crystallographic disorder. Specifically, the disorder around the alkenic bridge in the *trans*-nitrostyrene molecule implies some free space in the crystal packing, allowing some molecules to undergo cis-trans isomerization before 2+2 photocycloaddition and led to the formation of the undesired dimers. They also found that this conversion happened during the early stage of irradiation and low temperature suppresses the formation of undesired side products to about 25%. In corroboration of these results, a mixture of products were also observed even when we carried out the photoreaction using LED blacklight in a water slurry (see Figure 3.4 and Table 3.1). It was also confirmed that a decrease in temperature favors the formation of dimer CBDN-1. There was a 72 % formation of the desired CBDN-1 at room temperature with an isolated yield of 54 % (Entry 5). When the temperature is close to 0 °C, there was a 98% formation of CBDN-1 with a good isolated yield of 88% (Entry 8).

Table 3.1. Optimization of reaction conditions of photodimerization of *trans*-nitrostyrene.

Entry	Irradiation Source	Method of Irradiation	Temp. (°C)	Time (h)	Formation of CBDN-1 (%)[a]	Yield of CBDN-1 (%)[b]
1	medium pressure Hg lamp	Solvent-free	rt	6	47	30
2	medium pressure Hg lamp	Slurry in water	rt	6	56	42
3	LED blacklight	Solvent-free	rt	14	84	73
4	LED blacklight	Slurry in water	rt	14	65	53
5	LED blacklight	Slurry in water	20	14	72	54
6	LED blacklight	Slurry in water	10	14	95	78
7	LED blacklight	Slurry in water	5	14	96	86

8	LED blacklight	Slurry in water	1	14	98	88
9	LED blacklight	Slurry in brine	rt	8	> 99	95

[a] Conversion is based on the integration of the peaks in ^{1}H NMR spectrum of reaction mixture.
[b] Isolated yield after washing and purification.

Since this photocycloaddition was performed by irradiating a slurry of crystalline powder suspended in water rather than conventional solvent-free solid-state photocycloaddition, there was a reason to believe that isolated yield could be improved by reducing the solubilities of *trans*-nitrostyrene and CBDN-1 in water. Thus, a saturated sodium chloride solution (brine) was used as a reaction medium for dispersing *trans*-nitrostyrene in photodimerization. The isolated yield of CBDN-1 further increased to 95% (Entry 9 in Table 3.1). Interestingly, the application of brine improved the overall yield of this process and suppressed the formation of the side products even at room temperature. To the best of our knowledge, it is unprecedented to use a salt solution to control product selectivity on solid-state photocycloaddition. We tested and compared photodimerization of *trans*-nitrostyrene in various saturated salt solutions to learn more about this interesting phenomenon. The results are summarized in Table 3.2 and the corresponding NMR spectra are compared in Figure 3.5. It was found that halide salts such as KCl and KBr showed a similar effect as NaCl by favoring the formation of CBDN-1 with high isolated yields of 93% and 89%, respectively. In contrast, halide salt NaI only gave the desired dimer product CBDN-1 with a 30% yield and some unidentified insoluble solid byproduct. The salt with a bulky anion, Na_2CO_3 gave a high yield of 90% while Na_2SO_4 offered 82% yield. When the photodimerization of *trans*-nitrostyrene was performed in saturated KNO_3 solution, no selectivity for CBDN-1 was observed. The results were almost similar to the case of slurry

in water (Entry 4, Table 3.1), indicating that bulky anions such as NO_3^- do not affect photodimerization.

Table 3.2. Effect of salt solution on photodimerization of *trans*-nitrostyrene

Entry	Salt Solution	Formation of CBDN-1[a] %	Yield of CBDN-1[b] %
1	NaCl	99	95
2	Na_2SO_4	87	82
3	KCl	97	93
4	KBr	94	89
5	NaI	59	30
6	Na_2CO_3	97	90
7	KNO_3	62	54

[a] Conversion is based on the integration of the peaks in ^{1}H NMR spectrum of reaction mixture.
[b] Isolated yield after washing and purification.

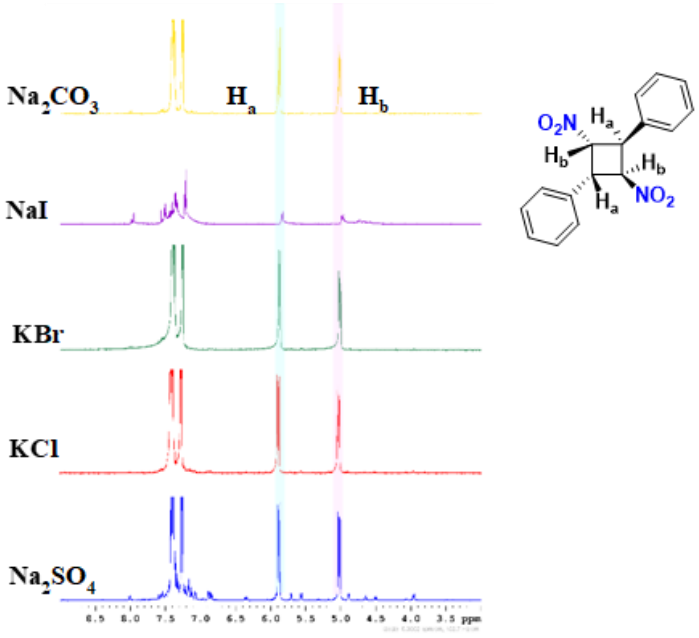

Figure 3.5. ^{1}H NMR spectra of photodimerization of *trans*-nitrostyrene reaction mixtures in the presence of different salt solutions.

3.3.3 Reduction of CBDN-1 to CBAM-1

The last step of the reaction sequence in the synthesis of CBAM-1 involved the reduction of CBDN-1. Activated Zn in HCl (6N) solution worked well for reducing CBDN-1 to CBAM-1. To optimize the reaction conditions, different amounts of Zn were tested ranging from 15 to 110 equivalents. It was found that a combination of 30 equivalents of Zn in the presence of 6N solution of HCl and methanol as the solvent gave the 83% isolated yield of CBAM-1 (Scheme 3.3). It is worth mentioning that the product diamine, CBAM-1, can be easily purified by performing a simple acid-base extraction. The product obtained was a viscous liquid at room temperature with slight yellow color, and its structure was characterized by NMR and FT-IR spectroscopy. The diamine was crystallized in $CDCl_3$ by forming an ammonium chloride salt, which was analyzed by SC-XRD as shown in Figure 3.6. The CBAM-1 has good solubility in most commonly used organic solvents such as acetone, methanol, chloroform, and ethyl acetate.

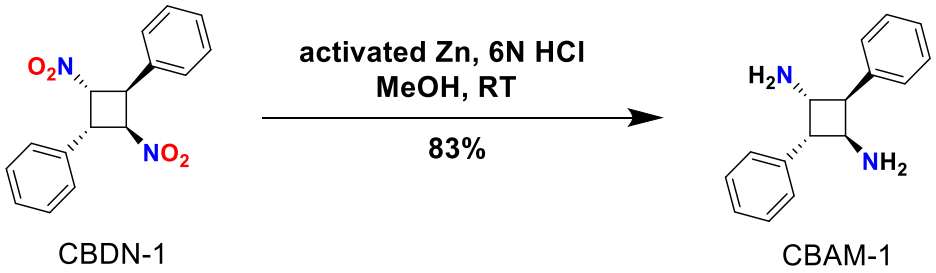

Scheme 3.3. Reduction of CBDN-1 to CBAM-1 using activated zinc and acid

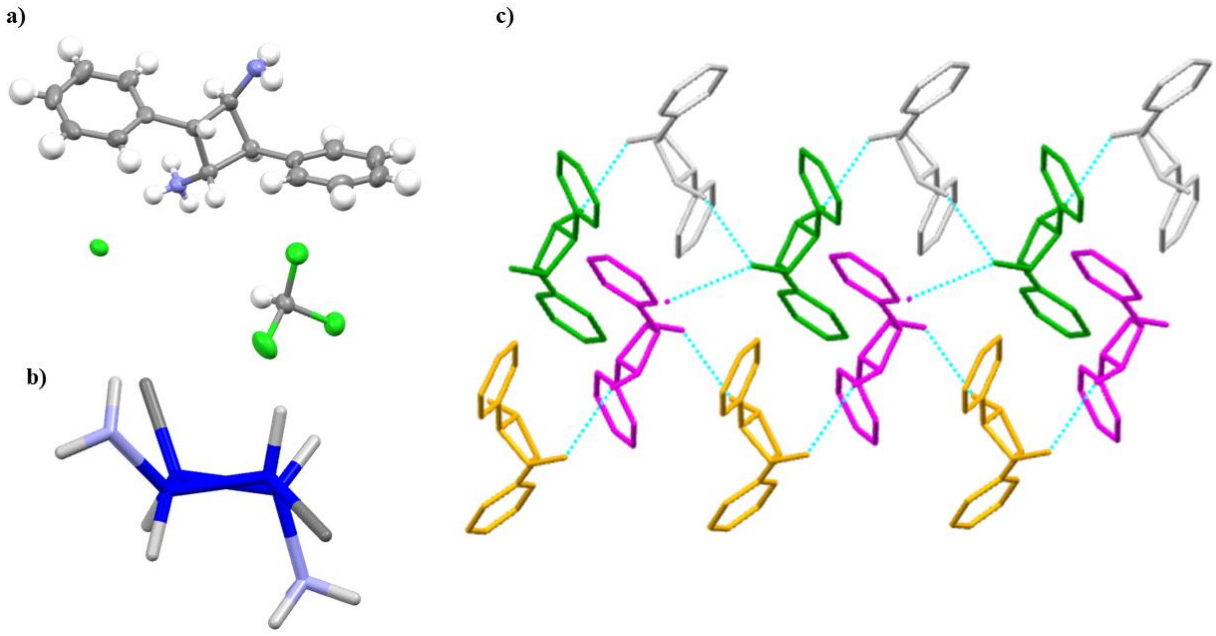

Figure 3.6. X-ray single-crystal structure of CBAM-1: (a) One molecule shown as ORTEP representing 50% electron density; (b) The puckered conformation adopted by cyclobutane rings (the phenyl groups are replaced with carbon atoms for clarity); (c) Side view of supramolecular helix formed via hydrogen bonding (the molecules with the same symmetry equivalence are shown in the same color).

3.3.4 Polyamide synthesis

To demonstrate the application of CBAM-1 in material synthesis, two polyamides were synthesized. The polyamides were obtained by reacting CBAM-1 with two commercially available diacids (i.e., succinic acid and terephthalic acid, respectively) in a *N*-methyl-2-pyrrolidone (NMP) solution using Yamazaki–Higashi direct condensation[84] method in the presence of triphenyl phosphite (TPP), pyridine (Py) and lithium chloride as shown in Scheme 3.7. The condensation of CBAM-1 with succinic and terephthalic acids yielded two corresponding cyclobutane-containing polyamides: polycyclobutane succinamide (PCS) and polycyclobutane terepthalamide (PCT). The obtained polyamides were subjected to further purification by dissolving them in a 1:4 solution of TFA and

$CHCl_3$. A large volume of methanol was then added to precipitate the polyamides out of the solution. PCS (75%) was precipitated as a white fibrous powder, while PCT (73%) was slightly tan in appearance. The polyamides were further washed with hot water and kept in ethanol overnight to remove the traces of the high boiling point NMP solvent.

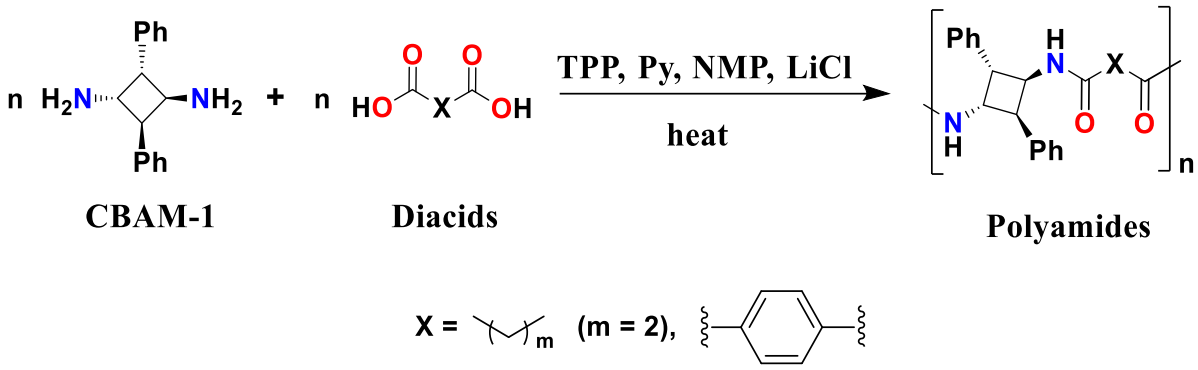

Figure 3.7 . Synthesis of CBAM-1 based polyamides.

The structures of PCS and PCT were characterized by FT-IR as well as ^{1}H and $^{13}C\{^{1}H\}$ NMR. spectroscopy The NMR signals corresponding to the protons of the cyclobutane ring present in the polymer backbone were found in the spectra of both the polyamides. The chemical shifts of cyclobutane rings in PCT were slightly more downfield than those in PCS, as shown in Figures A.30 and A.33 (see Appendix A). The resonances at 8.09 ppm in the spectrum of PCS and at 8.67 ppm in PCT were assigned to the amide protons. Moreover, the ratios of the integral area of proton signals were as predicted based on the proposed structures. Figure 3.8 presents the FT-IR spectra of PCS and PCT. The absence of the carbonyl absorption bands of the carboxyl group at 1720 cm^{-1} and the presence of the amide vibration band at around 1660 cm^{-1} confirmed the presence of the

amido group in the polymers. The peak at 3285 cm^{-1} was attributed to hydrogen-bonded N-H stretching vibrations suggesting the presence of hydrogen bonds in these polyamides.

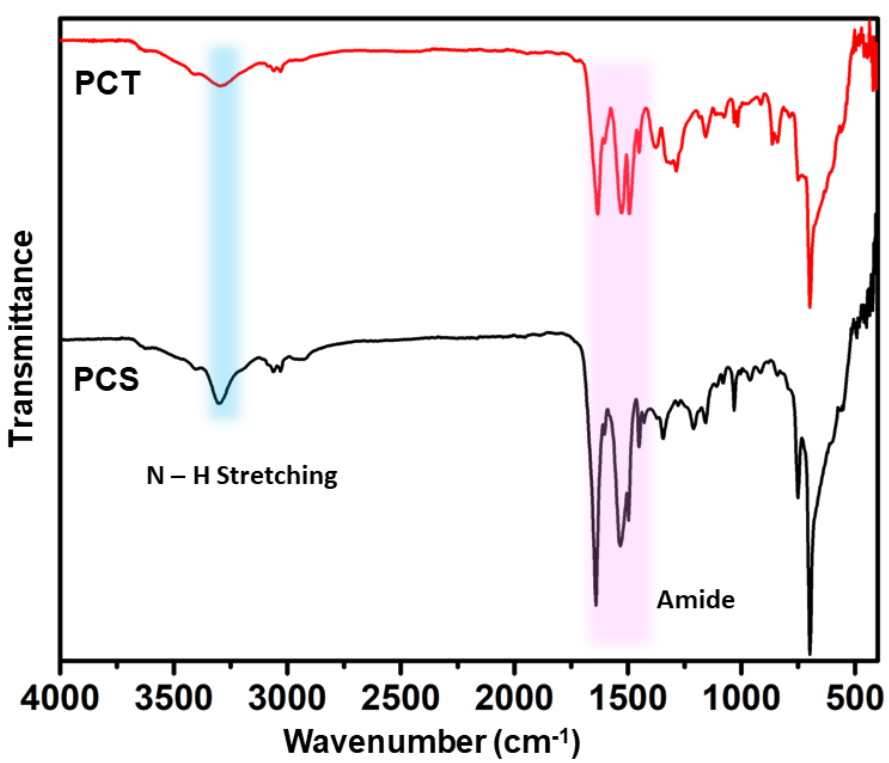

Figure 3.8. FT-IR spectra of PCS and PCT stacked together for comparison.

The solubilities of these CBAM-1 polyamides in several common solvent are listed in Table 2.3. It was observed that PCS and PCT not only soluble in fluorinated solvents such as hexafluoroisopropanol (HFIP) and trifluoroacetic acid (TFA) but also found to dissolve in some polar aprotic solvents, e.g., DMAc, DMSO, and DMF at room temperature when compared with poly(*p*-phenylene terephthalamide) Kevlar, and nylon-4,4 synthesized under similar condition were insoluble in all tested solvents except HFIP and TFA. This characteristic solubility of PCS and PCT in organic solvents for PCS and PCT can be attributed to the presence of the semi-rigid CBDM-1 fragments and phenyl

rings moieties perpendicular to the four-membered ring which reduced the polymer chain rigidity and interactions, respectively.

Table 3.3. Solubility of polyamides in various solvents[a]

Sample	Acetone	CH_3OH	$CHCl_3$	THF	DMF	DMSO	DMAc	TFA	HFIP	$CHCl_3$:TFA (4:1)
PCT	-	-	-	-	+	+	+	++	++	+
PCS	-	-	-	-	+	+	+	++	++	+

Note: ++ soluble at room temperature; + soluble upon sonication; - insoluble

A rotational rheometer measured the shear viscosity behavior of a PCS and PCT solutions in HFIP and DMF at 25 °C by employing different shear rates. Figure 3.9a shows simple shear viscosity data for a PCT and PCS solution in HFIP at a shear rate from 1 s^{-1} to 700 s^{-1}. The 10% w/w PCT solution showed a classic shear thinning behavior over a wide range of shear rates (11–0.12 Pa·s), while PCS solution at the same concentration appeared fairly Newtonian and showed little change (0.03–0.01 Pa·s) in the viscosity over a wide range of shear rates. PCT exhibited more than two orders of magnitude higher viscosity at a low shear rate than PCS, indicating a more robust interaction between the polymeric chains than in PCS. Interestingly, PCS and PCT at 10% w/w formed gels when dissolved in DMF.

In contrast to the solutions, the PCS gel showed a shear thinning and a higher viscosity than the PCT gel (Figure 3.9b). This dramatic change in the PCS/DMF system is likely caused by the strong H-bonding interaction between PCS and DMF molecules. Therefore, the excellent solubility and shear thinning behavior make PCS and PCT potential candidates for the practical application in the spin-on and casting processes.

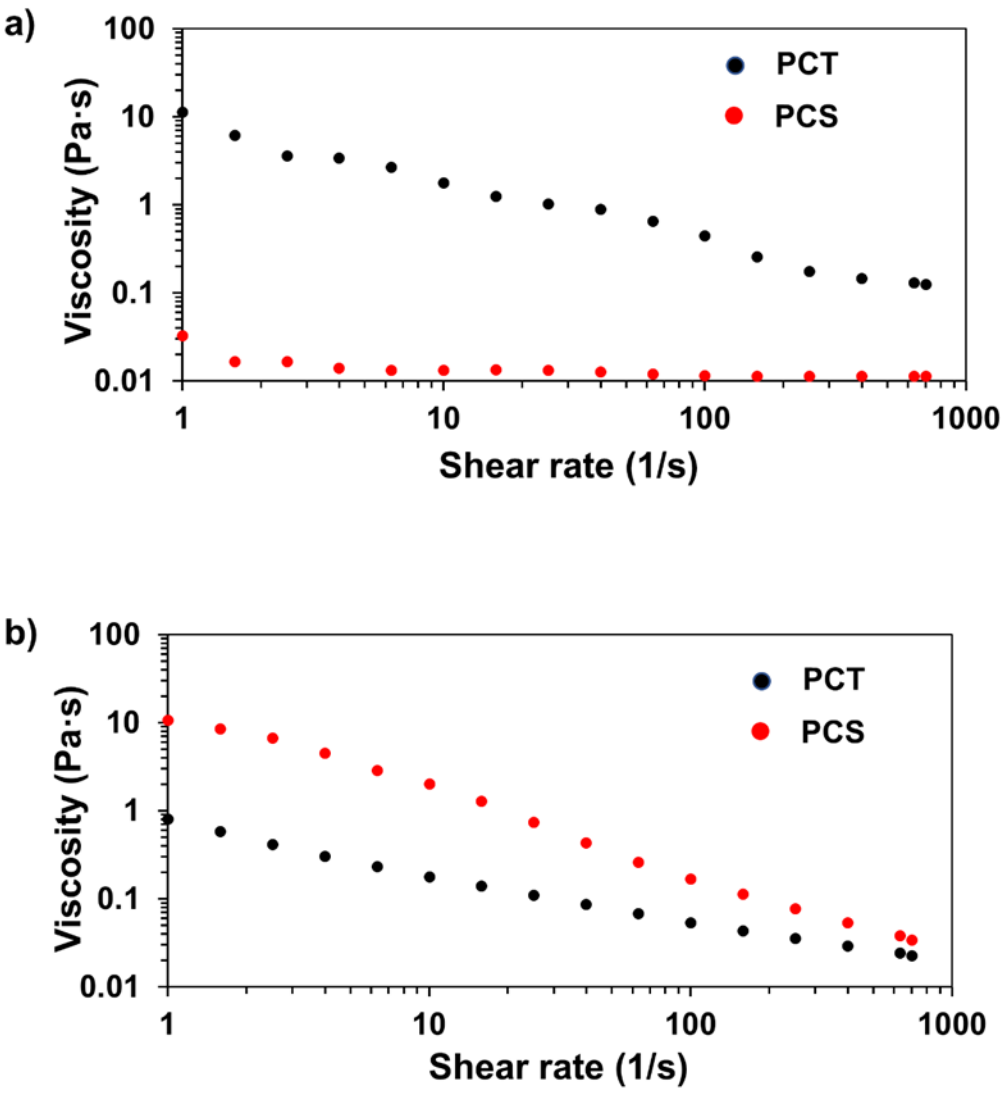

Figure 3.9. Shear viscosity data for a) a 10% PCT and PCS solution in hexafluoro-2-propanol at 25°C. b) a 10% PCT and PCS gel form in DMF at 25°C.

Based on the solubility in DMSO, the weight average molecular weight (M_w) of the PCS and PCT was determined using diffusion-ordered spectroscopy (DOSY). DOSY is a well-studied NMR method that linearly relates the chemical shifts of ^{1}H NMR resonances to the translational diffusion coefficient (D^a) of a particular molecular species. Optimizing the acquisition and processing parameters can be applied to determine M_w of polymers in dilute solutions. Dilute conditions are essential to ensure viscosity and density remain

consistent throughout the solution, hence the linear relation between Log D^a and Log M_w using the Stokes-Einstein equation. Commercial polymethyl methacrylate (PMMA) standards were selected to obtain the D^a-M_w calibration curve due to its widespread use in GPC standards. DMSO-d_6 was used as a solvent due to its ability to dissolve both the polyamides and standards. The PMMA calibration curve in DMSO-d_6 showed good linearity between logarithmic values of D^a and M_w with a high value of r^2 of 0.992 (Figure 3.10).

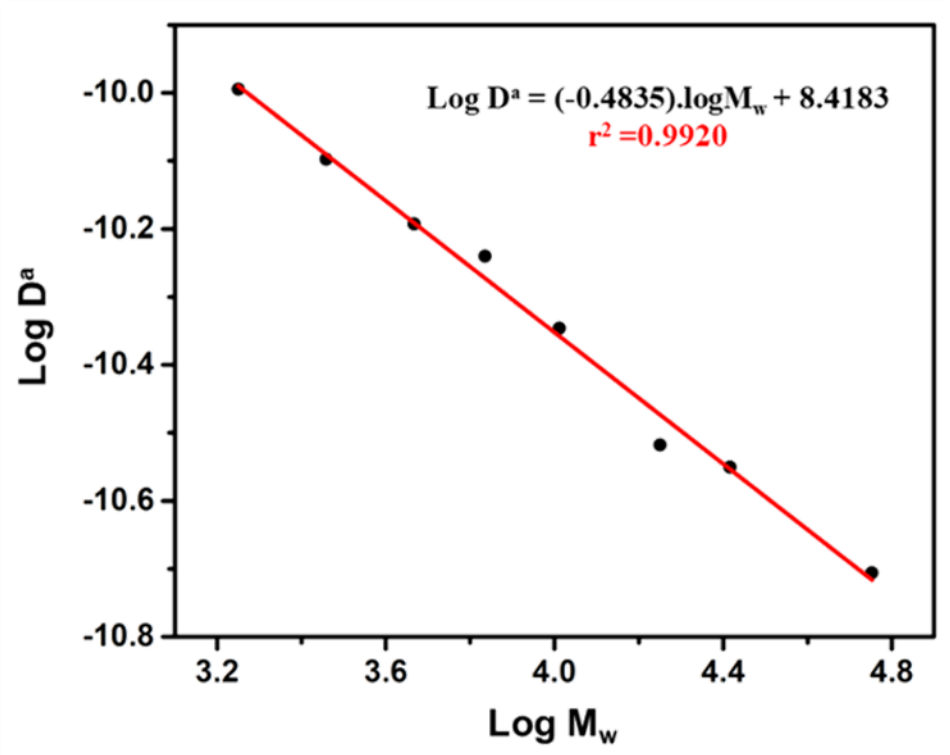

Figure 3.10. PMMA calibration curve in DMSO-d_6 for M_w prediction.

Two polystyrenes (PS) standards (i.e., PS 5030 and PS 17960) with narrow dispersity were used to verify the calibration curve. The M_w of PS 5030 and 17690 were estimated as 4200 Da and 15300 Da, respectively, with an approximate deviation of 13 to 16 % from their reported M_w. After establishing the calibration curve D^a of the PCS and

PCT samples were fitted to the PMMA calibration curve to calculate the M_w. The M_w of PCS and PCT obtained from DOSY are 14,400 and 11,300 Da, respectively (Table 3.5).

Table 3.4. Molecular weight data of PS standards and polyamides sample using externally referenced DOSY.

Sample	D^a m^2/s (10^{-11})	Log D^a	M_w (Da)
PS 5030	6.753 ± 0.005	-10.171	4200
PS 17960	3.620 ± 0.004	-10.441	15300
PCS	3.724 ± 0.007	-10.429	14400
PCT	4.177 ± 0.006	-10.379	11400

The thermal properties of PCS and PCT were first investigated by differential scanning calorimetry (DSC) to determine the essential thermal parameters such as glass transition temperature, T_g, as shown in Figure 3.11. PCT showed a T_g of 160 °C when compared with Kevlar T_g ~ 370 °C, suggesting that a less rigid backbone enables the thermal motion of polymeric chains, hence bringing the T_g to a range where it can be processed without the use of advanced techniques. In comparison, PCS showed a T_g of 109 °C, which is due to flexible succinic acid in the polyamide backbone. Meanwhile, PCS showed T_g approximately 50–60 °C higher than those of nylon-4,6 and nylon-6,6, two important aliphatic polyamides used in industry, confirming that the CBAM-1 molecule is more rigid than the aliphatic counterparts. The presence of rigid planer phenyl groups perpendicular to the backbone restricts the movement of the polymer chains, resulting in a high T_g while maintaining the good processability of aliphatic polyamide. These results suggest that CBAM-1 represents an ideal structure designed to tune the thermal and other

properties (e.g., solubility) of the corresponding polyamides, considering the phenyl ring can be readily modified using scalable and inexpensive reactions such as Friedel-Crafts alkylation.

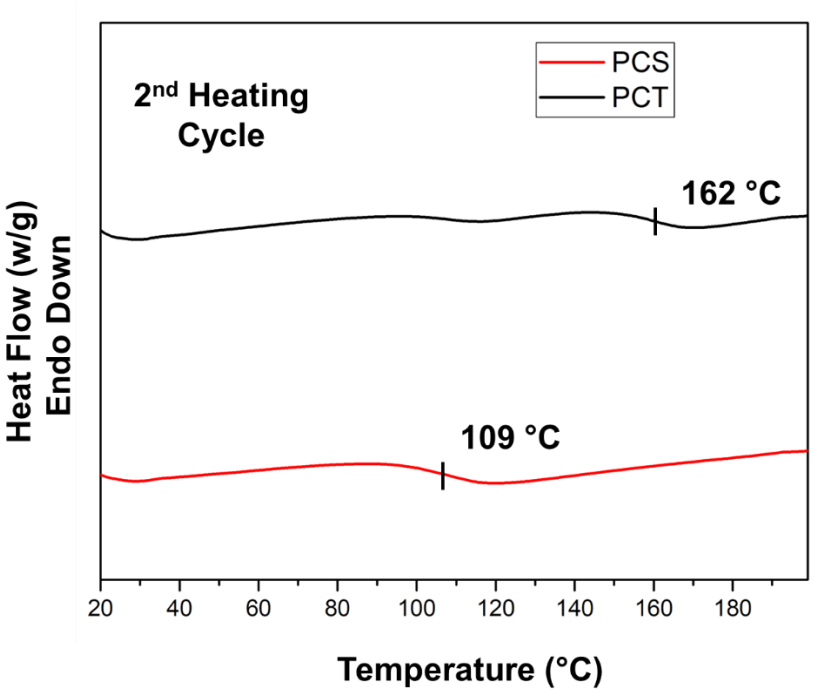

Figure 3.11. DSC curves of CBAM-1 based polyamides.

One characteristic property of polyamides is a high thermal decomposition temperature. Therefore, the thermal stability of PCS and PCT was evaluated by thermogravimetric analysis (TGA) and compared with the known aromatic and aliphatic polyamides (i.e., Kevlar and nylon-4,4) synthesized under similar conditions as shown in Figure 3.12. PCS exhibited an onset of decomposition temperature ($T_{5\%}$) at 314 °C while nylon-4,4 has $T_{5\%}$ of 236 °C. PCT showed the highest $T_{5\%}$ of 365 °C, and Kevlar has $T_{5\%}$ of 323 °C. In the case of decomposition temperature (T_d), nylon-4,4 has the lowest T_d of 343 °C, and Kevlar has the highest T_d of 528 °C, while T_d of PCS and PCT were 368 °C and 415 °C, respectively. These results confirmed that thermal cleavage of cyclobutane in

the polymeric backbone is a thermally forbidden process with a high energy barrier according to Woodward-Hoffmann rules,[85] showing the high stability of the novel polyamides.

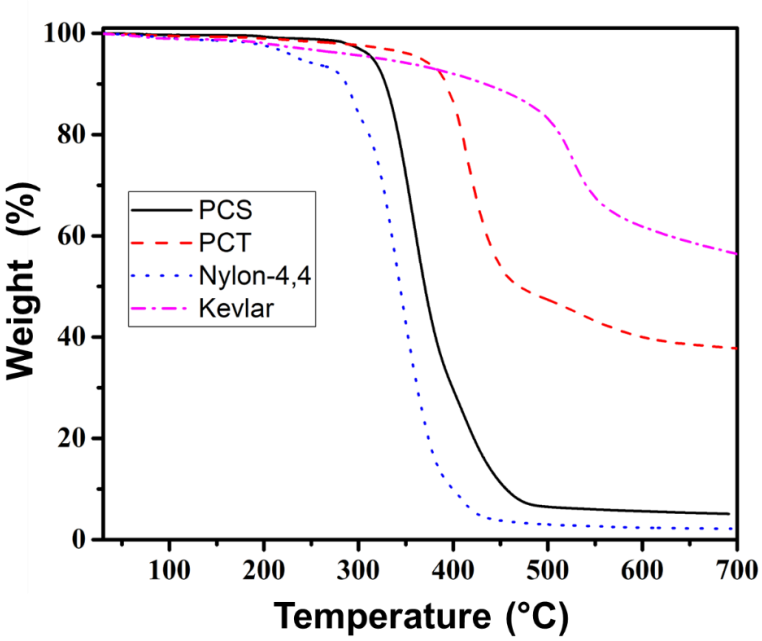

Figure 3.12. Thermogravimetric analysis of polyamides.

In polyamides, hydrogen bonding between the amido functional groups is well known to influence physical properties, such as excellent thermal properties, toughness, and abrasion resistance. Unfortunately, these amido groups, which serve as the source of hydrogen bonds, also cause significant moisture absorption. The absorbed water molecules can effectively disrupt the hydrogen bonding between amido groups, resulting in the loss of excellent thermal and mechanical properties. The amount of moisture absorbed in aliphatic polyamides at relative humidity is high due to their high amide content. In contrast, for the aromatic polyamides, the packing of rigid chains often results in voids within the polymeric structure leading to moisture absorption. For instance, nylon-4,4 and

Kevlar were reported to have 15 and 7.5 weight percentage moisture content at 23 °C and 100% relative humidity.

Based on the structure of CBAM-1, PCS and PCT will have relatively low amide content and flexible polymeric chains. They were expected to absorb a relatively low amount of moisture compared with classic aliphatic and aromatic polyamides. Thus, an experiment was designed to quantify the moisture uptake in PCS and PCT. First, the uniform polyamide powder samples were dried in a vacuum oven at 70 °C overnight to eliminate any possible moisture absorption during polyamide synthesis. Second, after cooling it down to room temperature, the samples were kept in the incubator with 50 % relative humidity, maintained at 25 °C for 24 h. After incubation, the change in weight of polyamide samples was recorded and correlated with TGA experiments before and after the moisture absorption experiment. As shown in Figure 3.13, the moisture absorption of PCS and PCT after exposure to moisture was 0.05, and 3.1 uptake %, respectively, which was significantly lower than 17.2 uptake % of nylon-4,4 and 6.1 uptake % of Kevlar synthesized under similar conditions. These results clearly approved that PCS and PCT were less sensitive to moisture than the well-known polyamides such as nylon-4,4 and Kevlar.

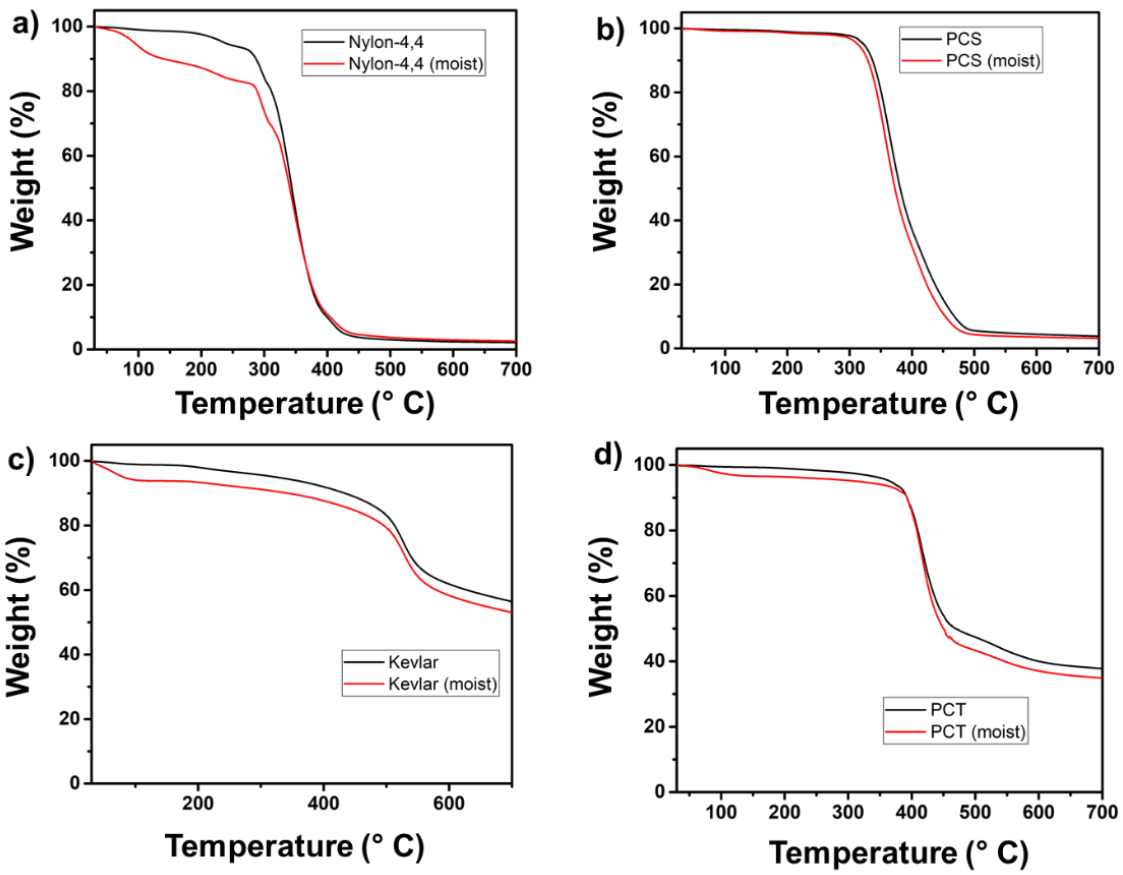

Figure 3.13. Thermogravimetric analysis of different polyamide samples before and after moisture absorption test.

A crystalline film of PCS and PCT was prepared by Doctor blade coating technique[86] using a 10% w/ w solution of PCS and PCT in HFIP, respectively, on a surface of indium tin oxide substrate. PCS formed a continuous film covering the substrate while PCT did not. In contrast to PCT being easy to peel off the substrate, PCS showed a smooth and stable coating. The two-dimensional grazing incidence wide-angle X-ray scattering (2D-GIWAXS) was employed to determine the crystallinity and orientation of the crystalline domains in the film. In the PCS film, the reflections were weakly observed, respectively, at 9.3 and 4.6 Å (Figure 3.14a–b), indicating a relatively low crystallinity. However, the intensity is higher along in-plane direction than that of out-of-plane direction,

suggesting these periodicities are primarily perpendicular to the surface. On the other hand, after two hours of annealing at 160 °C showed slightly increased d-spacing and more spread intensity along the Debye-Scherrer ring, indicating that the thermal movement during annealing decreased the preferred orientation of the polymer chains. Figure 3.14c-d shows 2D X-ray diffraction patterns of PCT films. On the one hand, reflections were more substantial than the PCS film, suggesting PCT was more crystalline than PCS. On the other hand, PCT polymer chains preferred the in-plane orientation in the film without annealing, while the preferred orientation is diminished after annealing at 160°C for 2 h, similar to the case of PCS. The two broad diffraction peaks indicating periodicities of 9.5 Å and 4.7Å were observed at room temperature without annealing.

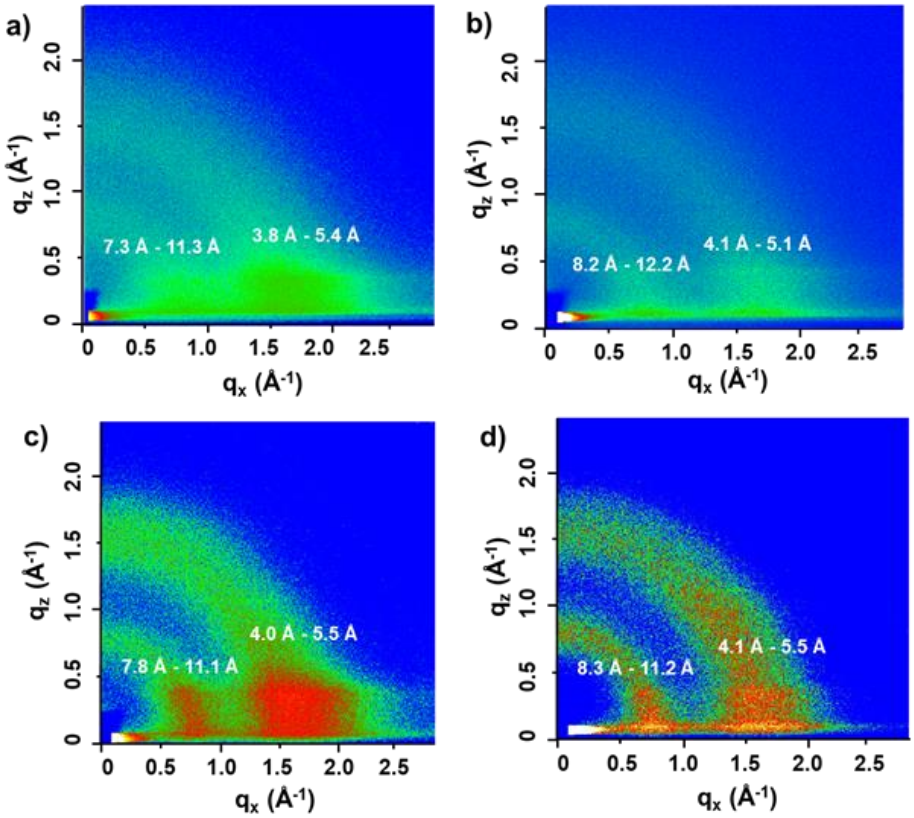

Figure 3.14. X-ray diffraction patterns of the PCT and PCS films with different annealing conditions. (a) PCS film without annealing. (b) PCS film after 160 °C 2 h annealing. (c) PCT film without annealing. (d) PCT film after 160 °C 2 h annealing.

Based on the 2D-GIWAXS, a schematic arrangement of a possible PCT crystalline model is depicted in Figure 3.15. Figure 3.15a shows the polymer repeating unit of PCT with a length of about 9.6 Å and the distance between two neighboring polymer chains in the xy plane around 4.7 Å. Figure 3.15b shows the packing of two neighboring polymer chains along the *z*-axis. Because the phenyl groups are perpendicular to the polymer backbone, the space between these phenyl groups on each polymer chain is filled by the phenyl groups of the neighboring polymer chains. As a result, the neighboring polymer chains are packed like meshing gears to achieve close packing.

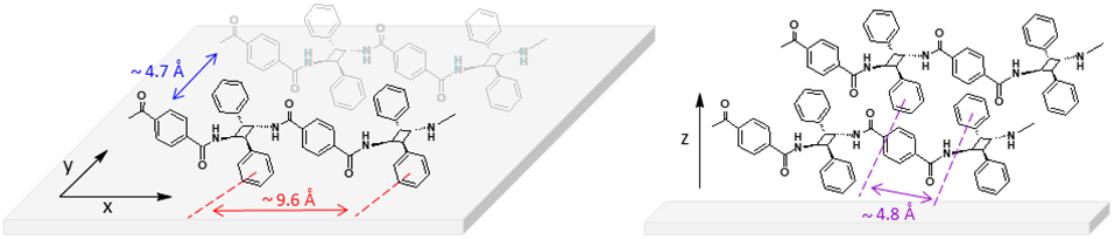

Figure 3.15. Suggested crystalline model of PCT based on the results of 2D-GIWAXS.

3.4 CONCLUSION

A semi-rigid cyclobutane-containing diamine (CBAM-1) building block has been synthesized and applied to materials science. During the synthesis of CBAM-1, the cyclobutane-containing dinitro compound CBDN-1 was obtained by dimerization of *trans*-nitrostyrene via an operator-friendly photodimerization process using 380 nm residential LED blacklights in a saturated brine solution. It was found that saturated salt solutions promoted the formation of CBDN-1 with excellent selectivity and isolated yield even at room temperature. CBDN-1 was then reduced to CBAM-1 using inexpensive and readily available zinc metal in the presence of a dilute acid. The CBAM-1 was fully characterized,

and the single-crystal structure of the CBAM-1 ammonium chloride salt was reported for the first time. The crystal structure confirmed that CBAM-1 has a unique characteristic where the two phenyl groups are perpendicular to the direction of the two amine groups, showing its potential to introduce interactions between polymer chains to tune the thermal properties. The semi-rigid nature of CBAM-1 was then transferred to two novel polyamides via the Yamazaki-Higashi polyamidation process. The CBAM-1 based polyamides were characterized, and their physical and thermal properties were investigated to evaluate their potential utilization. Compared to polyamides of the established industrial importance, the cyclobutane-containing polyamides derived from CBAM-1 showed enhanced solubility in common organic solvents, classic shear thinning behavior, and remarkably low moisture sensitivity, indicating they can be processed into polymeric material using solution casting and spin-coating methods. These desirable properties can be attributed to the fact that the introduction of semi-rigid CBAM-1 provides the polymer chains with a decreased rotational barrier. At the same time, the phenyl rings perpendicular to the polymer backbone offer a means to interact between polymer chains hence allowing its T_g in the desired range, as evidenced by the WAXS data. Compared with previously known approaches to enhance the properties of polymers, the introduction of semi-rigid cyclobutane-containing building blocks with substitutes perpendicular to the polymer backbone put forward an innovative direction to achieve these desired properties of polymeric materials.

Chapter 4
Biomass-Derived *rctt*-3,4-Di-2-furanyl-1,2-cyclobutanedicarboxylic Acid: a Polytopic Ligand for Synthesizing Green Metal-Organic Materials

4.1 INTRODUCTION

Increasing awareness of environmental protection and continuous shrinking of the earth's finite fossil resources have inspired extensive studies into the use of biomass-derived compounds to replace fossil feedstocks in the manufacture of a variety of products.[87] Petrochemicals are still the major starting materials for synthesizing all kinds of ligands used in coordination chemistry. However, the inherent composition of carbon, hydrogen, and oxygen in biomass leads its suitability as a starting material for the synthesis of oxygen-rich ligands (Figure 4.1). As important members of the polytopic ligand family, oxygen-rich ligands,[88] are crucial in constructing metal-organic materials with different potential applications such as catalysis, gas separation, and detection of volatile organic compounds.[89] To the best of our knowledge, there is still no polytopic ligand specifically designed and synthesized from biomass-derived chemicals.[90]

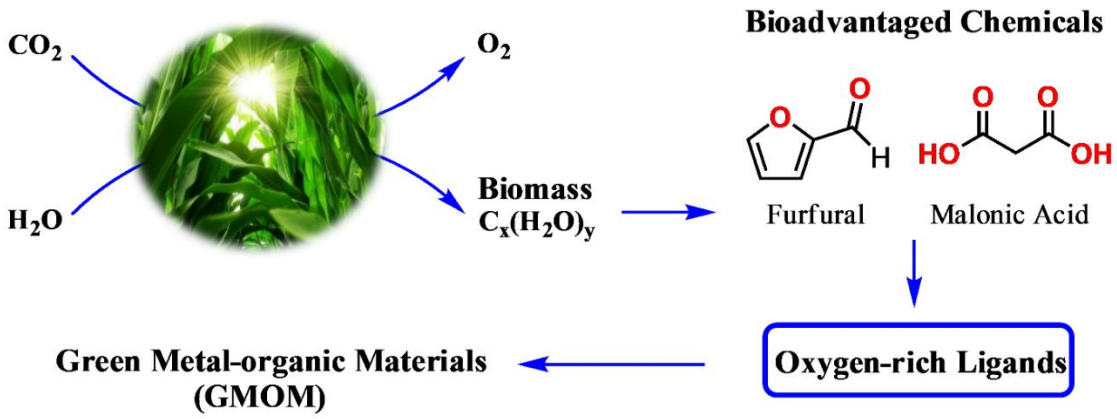

Figure 4.1. Synthesis of green metal-organic materials from biomass via bioadvantaged chemicals and oxygen-rich ligands.

In this study, we report a polytopic ligand, *rctt*-3,4-di-2-furanyl-1,2-cyclobutanedicarboxylic acid (CBDA-2), synthesized from two bioadvantaged chemicals furfural and malonic acid.[46a, 46b, 46d] Furfural is an important renewable feedstock, which is mainly produced from hemicellulose of crop residues such as corncobs, sugarcane bagasse, and wheat bran.[91] Bio-production of malonic acid involves the use of genetically modified yeast cells to ferment sugar directly into malonic acid with up to over 100% yield due to carbon dioxide sequestration during the process.[37g, 37h] The polytopic ligand,. CBDA-2, yielded from biomass has the potential to become a useful green building block, which will make metal-organic materials more environmentally friendly. To demonstrate the potential application of this multifunctional ligand, two different two-dimensional (2D) coordination polymers have been synthesized via a conventional solution method using copper and cobalt salts. We hope that our study will initiate more work into the design, synthesis, and application of biomass-derived ligands to make coordination chemistry more sustainable.

4.2 EXPERIMENTAL SECTION

4.2.1 Materials and methods

All chemicals were purchased from Alfa Aesar, Sigma-Aldrich, or Acros, and used without further purification. Blacklight used in the photoreaction was 15W Eiko EK15526 F15T8/BL. The solution phase NMR spectra were recorded with a Bruker AVANCE 500 spectrometer (^{1}H: 500 MHz, ^{13}C{^{1}H}: 125 MHz). Proton and carbon chemical shifts were reported in ppm downfield from (TMS) or using the resonance of corresponding deuterated solvent as an internal standard. ^{1}H NMR data were reported as follows: chemical shift (ppm), s = singlet, d = doublet, t = triplet, q = quartet, dd = doublet of doublets, m = multiplet, and integration. SC-XRD data were collected on a Bruker Kappa Apex II Duo X-Ray Diffractometer with Cu Kα (λ = 1.54178 Å). FT-IR was recorded on Thermo Scientific Nicolet iS5 FT-IR spectrometer. Abbreviations used in the description of FT-IR data are as follows: br, broad; s, strong; m, medium; w, weak. DSC experiments were performed on a Perkin Elmer Jade differential scanning calorimeter using a hermetic aluminum pan, indium standard for calibration, nitrogen as a purge gas, sample weight of ~ 5 mg with a ramping rate of 20 °C/min. Heat flow was recorded from both the first heating and cooling curves. TGA analyses were carried out on a Hi-Res TGA Q500 thermogravimetric analyzer from TA Instruments using alumina pans at a heating rate of 20 °C/min under nitrogen with a sample weight of about 10 mg.

4.2.2 Synthesis of *rctt*-3,4-di(furan-2-yl)cyclobutane-1,2-dicarboxylic acid (CBDA-2)

The synthetic procedure of CBDA-2 reported herein is developed by improving our previous approach.[46b] Specifically, CBDA-2 was synthesized by photodimerization of 2-furanacrylic acid in a slurry using hexane as a reaction medium. The typical process involves suspending 5.0 g of crystalline FAA in the hexane in a 250 mL Erlenmeyer flask with magnetic stirring. The vigorously stirred suspension was kept between six 15-watt Eiko blacklights for 12 hours. The powder clustered on the inside wall of the flask was loosened using a spatula or sonication when necessary, during the reaction. The slurry was then filtered and CBDA-2 was obtained as a white solid in 91 % yield (4.5 g, m.p. 170 – 171 °C).^{1}H NMR (DMSO-d_6) δ (ppm): 12.52 (s, 2H), 7.43 (d, J = 2.5 Hz, 2H), 6.28 (dd, J = 3.3, 1.1 Hz, 2H), 6.11 (d, J = 3.5 Hz 2H), 4.03(m, 2H), 3.68 (m, 2H); ^{13}C{^{1}H} NMR (DMSO-d_6) δ (ppm): δ 173.6, 153.1, 142.6, 110.4, 107.9, 43.0, 38.3; FT-IR (solid) $\overline{\nu}_{max}$ (cm^{-1}): 3072 (br, O—H) 2959 (w, C—H), 1696 (s, C=O), 1503–1415 (s, C=C aromatic str), 1257 (m, C—O), 1011 (m, in-plane O—H).

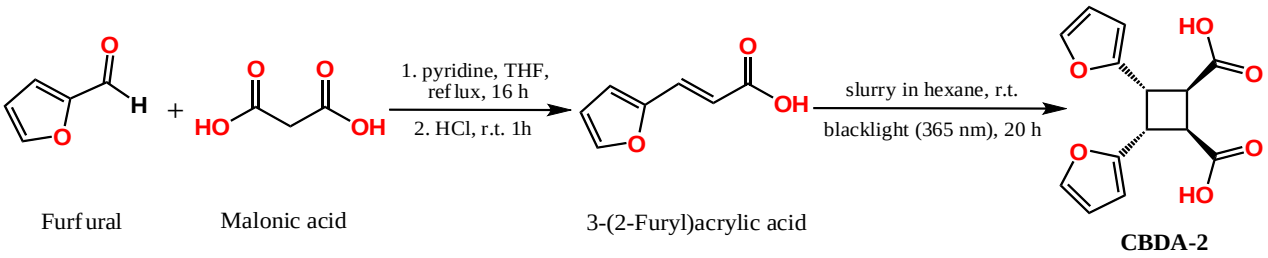

Scheme 4.1. Synthesis of a polytopic ligand, CBDA-2, from two bioadvantaged chemicals: furfural and malonic acid.

4.2.3 Synthesis of CBDA-2·Et_3N

CBDA-2 (1 mmol) was dissolved in 5 mL methanol. Triethylamine (2 mmol) was first diluted with 3 mL methanol, and then added into the CBDA-2 solution dropwise upon magnetic stirring. After filtration, the solution was kept in a 15 mL vial with a porous lid. Colorless crystals formed in two weeks. Only one of the two carboxylic acid was deprotonated although two equivalents of triethylamine were used (see Figure 4.2).

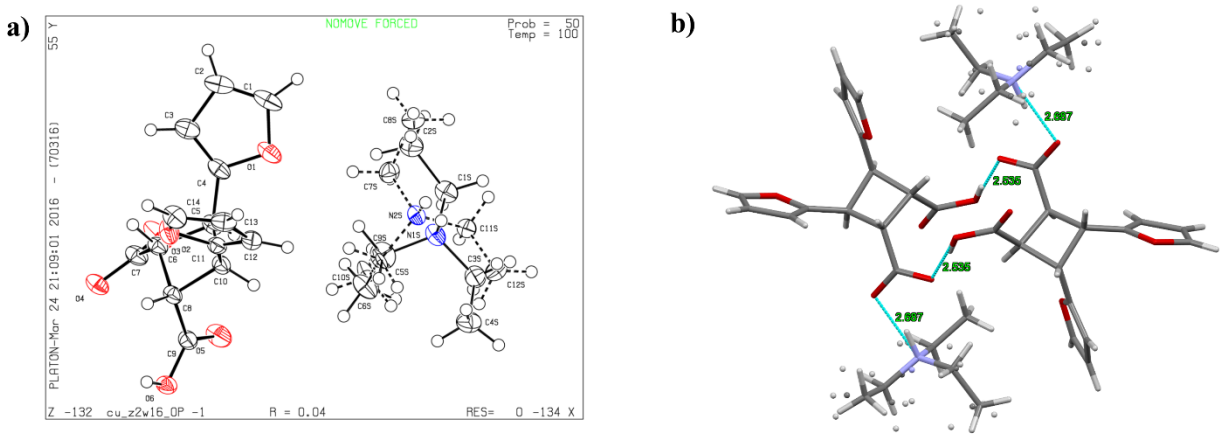

Figure 4.2. X-ray crystal structure of CBDA-2·Et_3N: a) image with labels of the atoms, a) image with hydrogen bonds.

4.2.4 Synthesis of Cu-CBDA-2 complex I

CBDA-2 (2 mmol) was dissolved in a 10 mL of methanol and to this a solution of $Cu(NO_3)_2 \cdot 3H_2O$ (0.1 mmol) in 10 mL of deionized water was added dropwise. Then this reaction mixture was allowed to stir for 30 minutes. After that, a 1M aq NaOH solution was added dropwise to the reaction mixture until a slight amount of precipitate began to form. The precipitate was then filtered out, and the filtrate was kept at room temperature.[92] After several days, the turquoise crystals were produced. The crystals were washed with water and methanol, respectively, and then dried in vacuum overnight. The yield of

complex I was 52% based on the metal salt. FT-IR (solid) $\overline{\nu}_{max}$ (cm^{-1}): 3147 (br, O—H), 2943 (w, C—H), 1696 (s, C=O from carboxyl), 1549 (m, C=O asymmetric for carboxylate ion), 1613 (w, C=C aromatic), 1418 (m, C=O symmetric carboxylate ion), 1276 (m, C—O), 1013 (w), 727 (s), 596 (m).

4.2.5 Synthesis of Co-CBDA-2 complex (II)

A similar process was used as in the case of complex I, but $Co(NO_3)_2 \cdot 6H_2O$ (0.1 mmol) was used with an equimolar amount of CBDA-2 (0.1 mmol). After a few days, light pink colored crystals of complex II were obtained. The yield was 61% based on the metal salt. FT-IR (solid) $\overline{\nu}_{max}$ (cm^{-1}): 3316 (br, O—H water), 1564 (s, C=O asymmetric for carboxylate ion), 1435 (m, C=O symmetric carboxylate ion), 1019 (w), 722 (s).

Table 4.1. Crystal data of CBDA-2, CBDA-2 Et_3N, complexes I and II.

Crystal	**CBDA-2***	**CBDA-2·Et_3N**	**Cu-CBDA-2 Complex (I)**	**Co-CBDA-2 Complex (II)**
CCDC #	1578122	2049902	2049903	2049905
Formula	$C_{14}H_{12}O_6$	$C_{20}H_{27}NO_6$	$C_{30}H_{30}CuO_{14}$	$C_{30}H_{32}Co_2O_{16}$
FW	276.24	377.42	678.08	766.41
Crystal size [mm]	0.34*0.08*0.04	0.39*0.23*0.20	0.20*0.15*0.04	0.19*0.14*0.04
Crystal system	Monoclinic	Triclinic	Orthorhombic	Orthorhombic
Space group	P $2_1/c$	P-1	Pbca	$Pna2_1$
a (Å)	15.8528(7)	9.1495(3)	7.5903(3)	6.9274(3)
b (Å)	5.4219(3)	9.9671(4)	14.4036(7)	33.4102(12)
c (Å)	15.2918(7)	11.0579(4)	26.3037(11)	6.8234(3)
α (°)	90	82.6770(10)	90	90
β (°)	113.218	76.9120(10)	90	90
γ (°)	90	75.4290(10)	90	90
V ($Å^3$)	1207.92	947.97(6)	2875.72	1579.25
Temp. (K)	100(2)	100(2)	106(2)	105(2)
ρcalc ($g \cdot cm^{-3}$)	1.519	1.322	1.566	1.612
μ (mm^{-1})	1.023	0.804	1.736	8.913
Radiation type	CuK\a	CuK\a	CuK\a	CuK\a
F(000)	576	404	1404	788.0
No of measured refl.	7726	12048	14792	7413
No of independent refl.	2099	3264	2541	2368

4.3 RESULTS AND DISCUSSION

4.3.1 Description of CBDA-2 structure

The crystal structure of CBDA-2 is revealed in Figure 4.3a, while Figure 4.3b displays a CBDA-2 anion with one of the two carboxylic acids deprotonated. The disordered counter ion, triethylammonium, is omitted in Figure 4.3b for clarity. Both crystal structures are shown in ORTEP at the 50% probability level except for the hydrogen atoms. While the two furan rings in Figure 4.3a are roughly pointing towards the same direction, they are orientated towards the opposite directions in Figure 4.3b, confirming the furan rings can rotate around the carbon-carbon single bond between the five and four membered-rings.

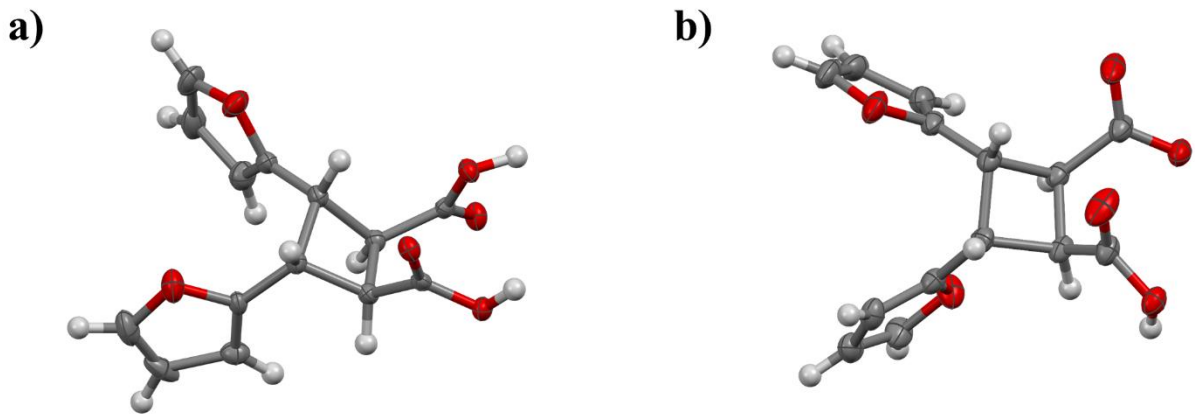

Figure 4.3. Crystal structures of (a) CBDA-2 and (b) CBDA-2 anion (a disordered Et_3NH^+ is omitted for clarity) in (ORTEP) at the 50% probability level except for the hydrogen atoms.

As shown in Figure 4.4, each CBDA-2 molecule contains two carboxylic acids and two furan rings, which can interact with metals or metal cations to form complexes. Figure 4.4b-c displays that the two sp^2 hybridized oxygen atoms in the furan rings of CBDA-2

may interact with metal collaboratively or individually.[38i, 93] Figure 4.4d-h exhibits five different ways that the two carboxylic acids or the corresponding carboxylate ion may interact with metal or metal cation.[94] Although the furan rings and carboxylic acids within the same CBDA-2 molecule may interact with different metal atoms or cations simultaneously, it is unlikely that they will interact with the same metal/metal cation since they are bonded to the same cyclobutane ring and trans to each other. It is worth mentioning that, besides what are shown in Figure 4.4, there are other possible ways that CBDA-2 may interact with metal or metal cation. For example, the electron-rich furan ring may interact with metal cation via its π electrons.[95]

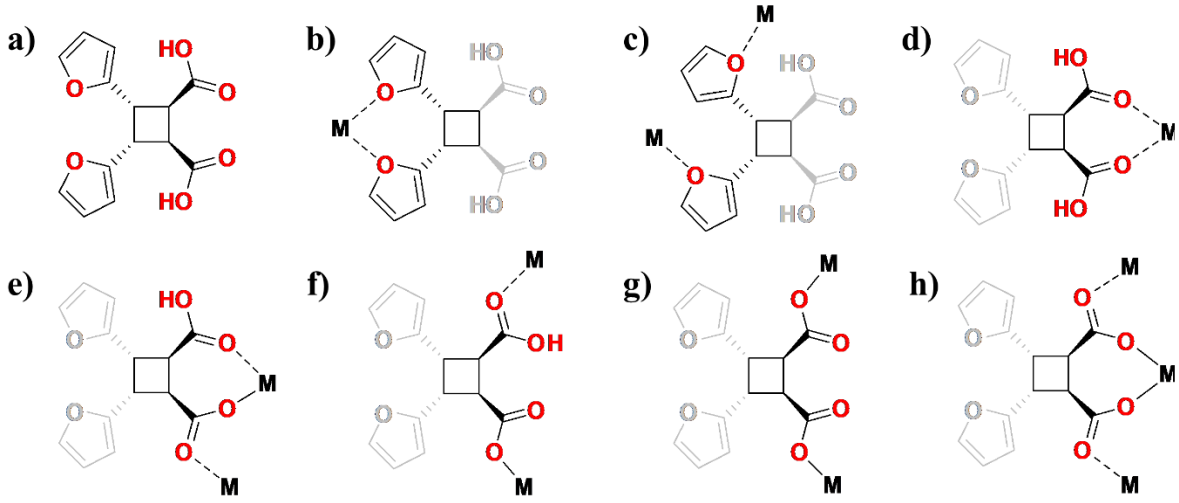

Figure 4.4. Chemical structure of CBDA-2 (shown in black and red), and seven coordination modes that furan rings and carboxylic acid/carboxylates of CBDA-2 may adopt to interact with metal or metal cation (shown in black, red, and gray).

Meanwhile, the cyclobutane core/linker of CBDA-2 has two exchangeable conformations (i.e., puckered vs. planar) with approximately 23° difference between them.[46a-c, 51, 96] The semi-rigid nature of cyclobutane will offer CBDA-2 a unique and useful

balance between typical flexible aliphatic or rigid aromatic linkers in forming metal-organic materials.

4.3.2 Structure description of Cu-CBDA-2 complex I

Figure 4.5a presents the asymmetric unit of Cu-CBDA-2 Complex I in ORTEP. The ratio of Cu:CBDA-2:MeOH in the complex is 1:2:2. As shown in Figure 4-5b, the Cu^{2+} center adopts an octahedral geometry with four CBDA-2 molecules interacting with the metal cation in the equatorial basal plane and two methanol molecules at the axial positions. Two of the four CBDA-2 molecules are deprotonated, which balance the charges on the Cu cation. The two deprotonated carboxylate oxygen atoms are located on the opposite sides of the Cu^{2+} center with the O—Cu^{2+}—O angle 180.0° and O—Cu^{2+} bond distance 1.923 Å. The two carbonyl groups of the non-deprotonated carboxyl acid group and two oxygen atoms in the two MeOH molecules are also located at the exact opposite direction of the Cu^{2+} center, with O—Cu^{2+} bond distances 2.446 and 1.984 Å, respectively.

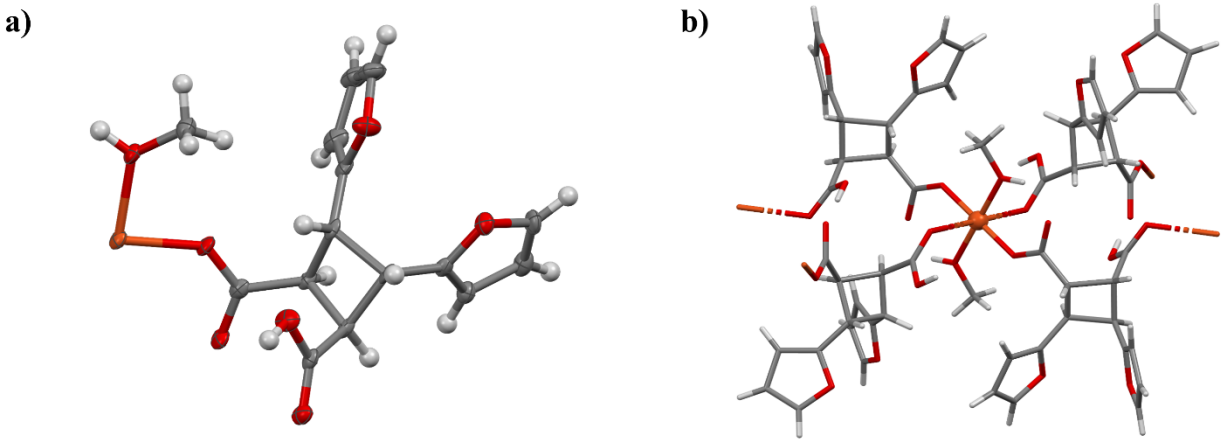

Figure 4.5. a) Asymmetric unit of Cu-CBDA-2 Complex (I) in ORTEP at the 50% probability level except for the hydrogen atoms; b) Octahedral Cu^{2+} center with four CBDA-2 molecules and two MeOH molecules.

The Cu^{2+} ion interacts with CBDA-2 in the way as illustrated in Figure 4-4f, forming a 2D coordination polymer. Figure 4-6b shows a top view of one layer of the 2D structure with the furan substituents omitted for clarity. The Cu^{2+} center is highlighted in polyhedral style. Figure 4-6c shows the side view of the 2D coordination polymer along the crystallographic a axis. In the 2D structure, the Cu^{2+} cations are sandwiched between two layers of CBDA-2 molecules with the furan substituents pointing outward.[97] The oxygen atom in the furan ring does not participate in the interactions with Cu^{2+} cation or any hydrogen bond. However, the oxygen atom in the carbonyl group of the deprotonated acid forms two hydrogen bonds (Figure 4-6a): one with the hydrogen atom in the acid of a neighboring CBDA-2 molecule [O···OH distance: 2.601(6) Å] and the other with the hydrogen atom in the hydroxyl group of a MeOH molecule [O···OH distance: 2.604(5) Å].

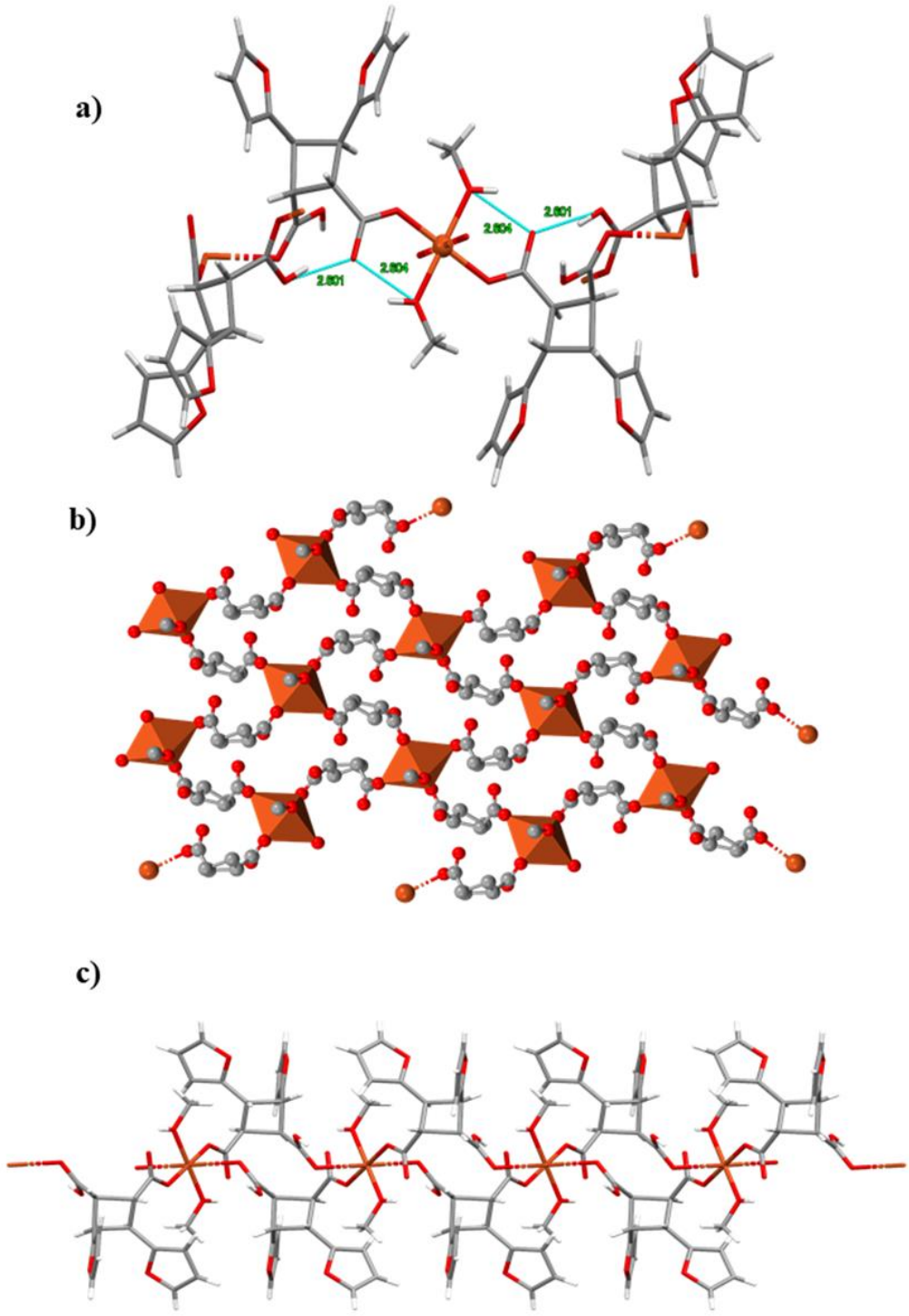

Figure 4.6. X-ray crystal structure of Cu-CBDA-2 complex II with hydrogen bonds; b) Top view of the Cu-CBDA-2 complex (II) shown in polyhedral style (the furan substituents are omitted for clarity); c) Side view of the 2D complex (II) along crystallographic an axis shown in Capped Sticks style.

4.3.3 Structure description of Co-CBDA-2 complex II

SC-XRD analysis of complex II revealed that the ratio of Co:CBDA-2:MeOH:H_2O in the compound is 1:1:1:1. Figure 4.7a exhibits the asymmetric unit of Complex II ORTEP. As shown in Figure 4.7b, the Co^{2+} center adopts a slightly distorted octahedral geometry with three CBDA-2 molecules interacting with the metal cation in the equatorial basal plane while one MeOH and one H_2O molecule occupy the two opposite axial positions. The O—Co^{2+}—O angle of MeOH, Co^{2+}, and H_2O is 172.4(1)°, and the O—Co^{2+} distances are 2.163(4) and 2.132(4) Å, respectively. Both of the carboxylic acid groups in each CBDA-2 molecule are deprotonated, and they are bonded to the same Co^{2+} cation balancing the charges. The O—Co^{2+}—O- angle is 95.1(1)°, and the two O—Co^{2+} bond distances are 2.051(4) and 2.112(3) Å, respectively. Two carbonyl groups from two neighboring CBDA-2 molecules' carboxylates occupy the other two corners of the equatorial basal plane of the octahedral, and the two corresponding O—Co^{2+} distances are nearly identical, which are 2.077(3) and 2.077(4) Å.

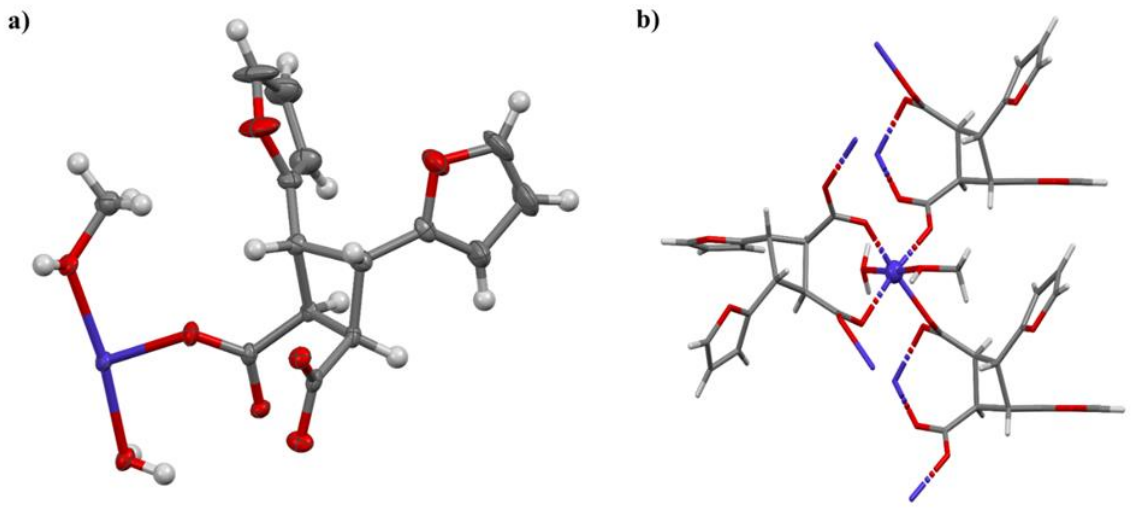

Figure 4.7. a) Asymmetric unit of Co-CBDA-2 Complex (II) in ORTEP at the 50% probability level except for the hydrogen atoms; b) Octahedral Co^{2+} center interacting with three CBDA-2 molecules, one MeOH, and one H_2O molecule.

The Co^{2+} cation interacts with CBDA-2 in the way as illustrated in Figure 4.4h, which is completely different from that (Figure 4.4f) of Complex (I). Nevertheless, Complex (II) is also a 2D coordination polymer. Figure 4.8c presents a top view of one layer of the 2D structure with the furan substituents omitted for clarity. The Co^{2+} center is highlighted in polyhedral style. Figure 4.8b displays the side view of the 2D coordination polymer along crystallographic axis. Just as the Complex (I), the Co^{2+} cations are sandwiched between two layers of CBDA-2 molecules with the furan substituents pointing outside. The oxygen atom in the furan ring does not participate in the interactions with Co^{2+} cation or any hydrogen bond. However, the MeOH molecule in complex II forms a hydrogen bond with a carboxylate group of a neighboring CBDA-2 ion with a O···OH distance of 2.792(5) Å (Figure 4.8a). The H_2O in the complex II forms two hydrogen bonds with two different carboxylate groups from its two neighboring CBDA-2 ions with O···OH distances of 2.655(5) and 2.991(5) Å.

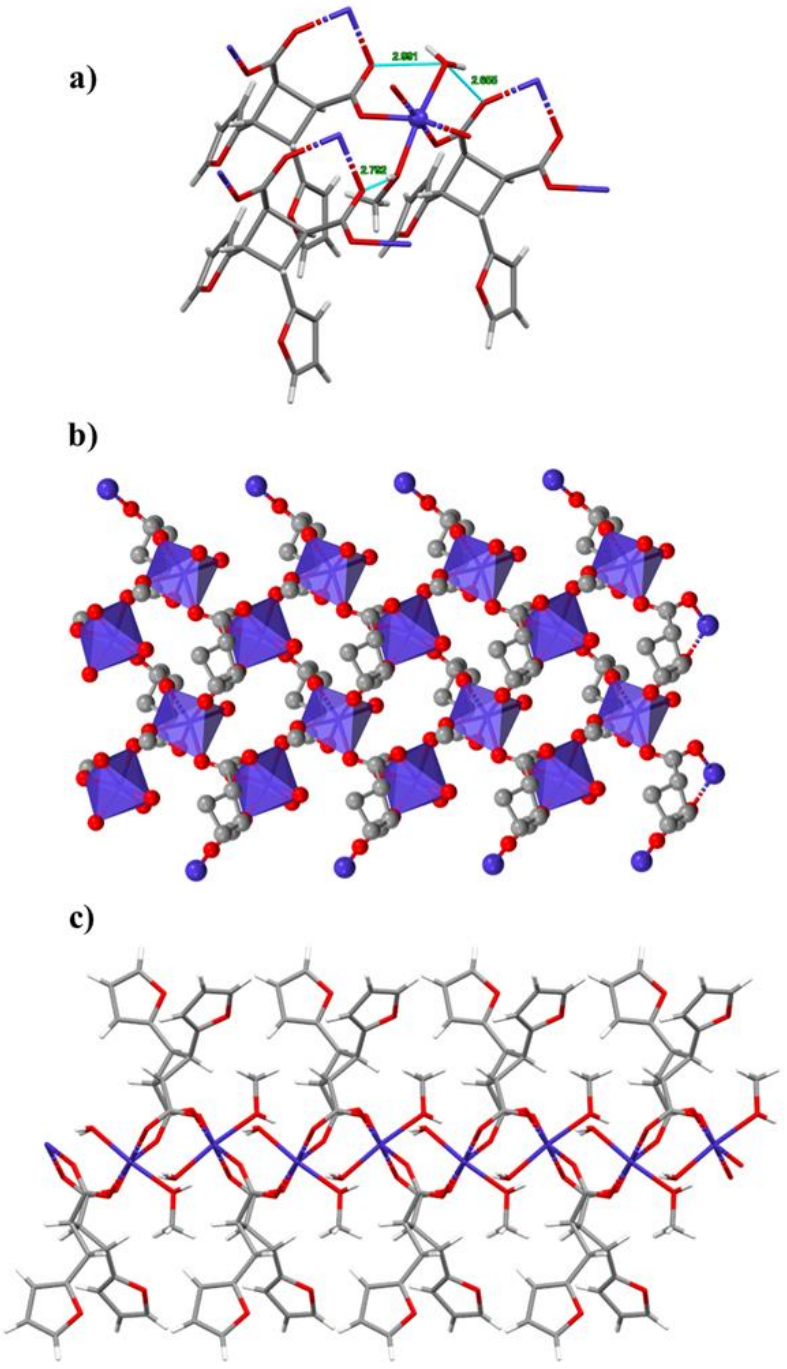

Figure 4.8. a) X-ray crystal structure of complex II with hydrogen bonds; b) Top view of the complex II shown in polyhedral style (the furan substituents are omitted for clarity); c) Side view of the 2D complex II along crystallographic axis shown in Capped Sticks style.

4.3.4 FT-IR spectrum of the complexes

The FT-IR spectra of complex I and II are reported in Figure 4.9 for comparison. The strong band at 1698 cm^{-1} in the spectrum of complex I is characteristic to the carbonyl stretching of a carboxylic acid because only one of the two acid groups in CBDA-2 ligand is deprotonated in the compound. In contrast, the peaks at 1564 and 1453 cm^{-1} in the spectrum of complex II are attributed to symmetric and asymmetric stretching vibrations of the carboxylate anion, respectively, since both carboxylic acid groups of CBDA-2 are deprotonated in the complex. The broad absorption at 3200–3500 cm^{-1} indicates the presence of coordinated H_2O and MeOH molecules in complex II, which is consistent with its single-crystal X-ray structure. For the spectrum of complex I, the signals of hydroxyl stretching vibration of the carboxylic acid are shown beside a weak, broad peak of the hydroxyl stretching of the coordinated MeOH molecules in the copper 2D coordination polymer.

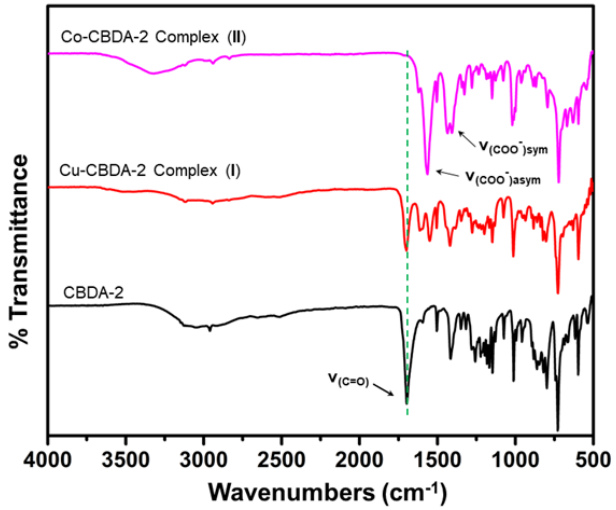

Figure 4.9. FT-IR spectra of CBDA-2, complex I and II.

4.3.5 Thermal properties of the complexes

TGA and DSC curves of complex I and II under a nitrogen atmosphere at a heating rate of 20 °C/min are shown in Figure 4.10. The thermal decomposition profile of CBDA-2 reported in our previous study indicated no degradation below 200 °C.[46b] According to the TGA curves in Figure 4.10a, both complexes were found to undergo decomposition in two stages. Complex I exhibited a weight loss of 9.1% due to removal of the coordinated MeOH molecules (calcd.: 9.4%) in the crystalline sample around 150 °C, and started to decompose at approximately 200 °C. The TGA curve of complex II showed a weight loss of 12.5%, which accounts for the loss of coordinated MeOH and H_2O molecules in the complex around 140 °C (calcd.: 13.1%), but did not decompose until near 300 °C. The latter observations were in accordance with the endothermic transitions seen in the DSC curve shown in Figure 4.10b. Interestingly, the DSC curve of complex I displays three overlapped peaks between 120 and 180 °C, indicating possible phase transitions due to the loss of MeOH in the complex. Thermal analysis results indicated a similar thermal decomposition behavior of both the complexes, among which the complex I decomposes faster than the complex II, presumably due to the different ways CBDA-2 coordinates to the two metals (i.e., Figure 4.4f *vs*. 4.4h). In short, the two-step decomposition pattern of these 2D coordination polymers is consistent with the SC-XRD structural results in terms of ligands' coordination to the metal centers.

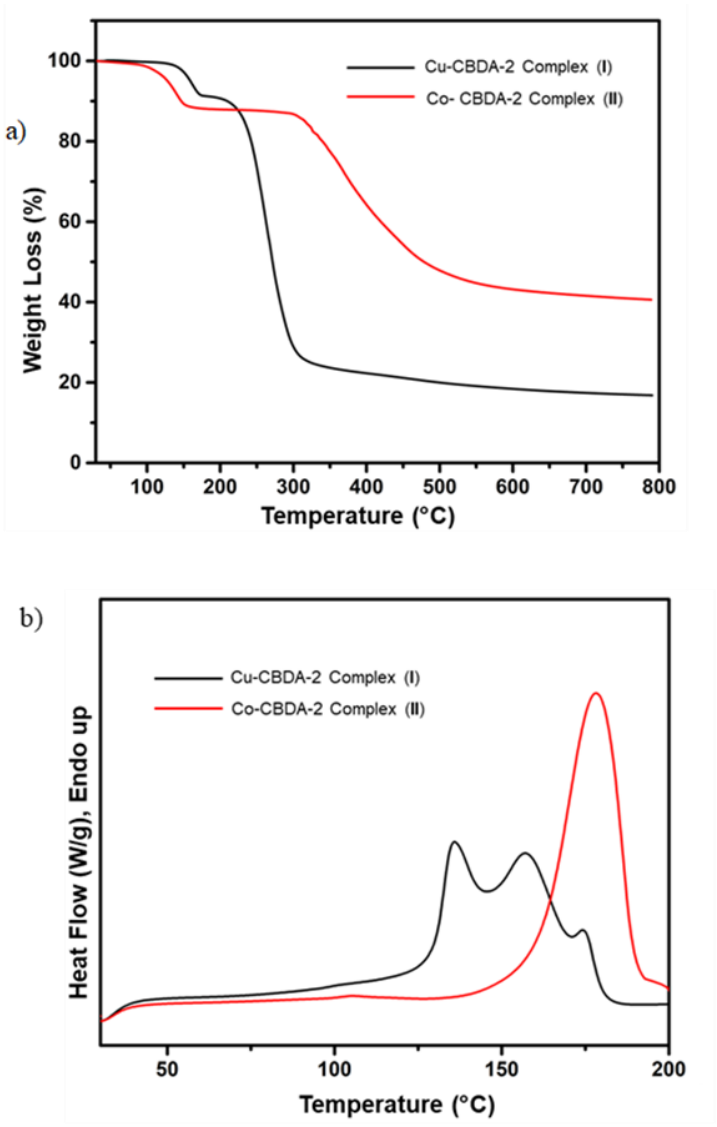

Figure 4.10. a) TGA curves of complex I and II with a heating rate of 20 °C min^{-1} under N_2 atmosphere. b) DSC curves of the two complexes from 25 to 200 °C with a heating rate of 20 °C min^{-1} under N_2 atmosphere.

4.3.6 Thermochromic properties

At room temperature, the microcrystalline powder of complex I is turquoise while complex II is pink. The single crystals of the two complexes exhibited the same colors, respectively, but they appeared somewhat lighter. Both complexes I and II showed fascinating visual thermochromic behaviors during the study of their thermal properties.

When heated to 200 °C for 15 minutes in a vacuum oven, complexes I and II turned into black and purple, respectively (see Figure 4.11). Complex II was chosen for further investigation considering its desolvated form showed higher thermal stability and exhibited more interesting color change. In addition, cobalt complexes are present in nature and are included in many synthetic materials with varied applications.[98] For example, cobalt is the principle metal center of four vitamers of B12, which are deeply red-colored complexes essential to the function of cells.

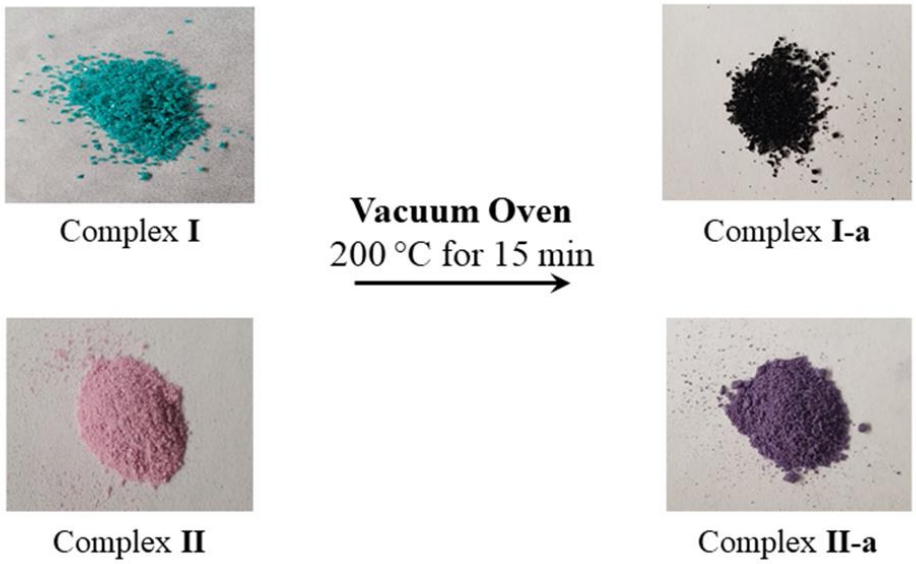

Figure 4.11. Thermochromic behavior of complex I and II: left) samples at room temperature; right) sample after heated at 200 °C under vacuum for 15 min.

The purple color of complex II-a did not change even when the sample was cooled down to room temperature and exposed to air. Color changes of metal complexes resulting from temperature variation are mainly caused by solid-solid phase transition due to changes in metal coordination geometry, coordination number, and/or the coordinated ligands.[99] The FT-IR spectrum of complex II-a qualitatively indicates that this thermochromic process is likely due to the loss of coordinated MeOH and H_2O molecules, which might

have caused the Co^{2+} center to go under coordination geometry change (Figure 4.12). The TGA curve of complex II in Figure 4.10a also confirmed that most of the coordinated MeOH and H_2O molecules were removed at 250 °C.

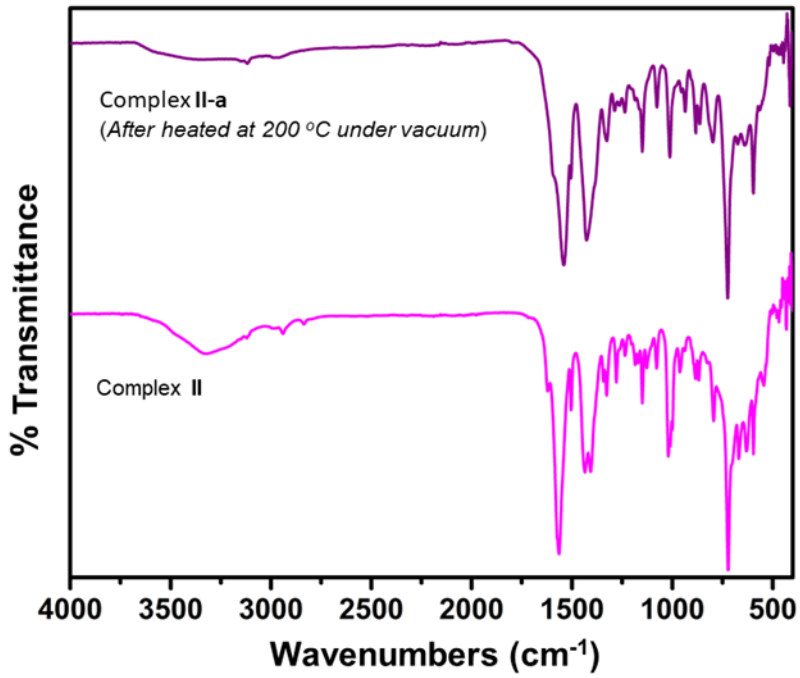

Figure 4.12. Comparison of the FT-IR spectra of complex II before and after the thermal treatment.

Visual thermochromic materials have found applications in designing security markers in currency bills and bonds,[100] smart coatings,[101] thermal printing,[102] and leuco dyes.[103] The successful synthesis and characterization of visual thermochromic complexes I and II, whose ligand was obtained from bioadvantaged starting materials, may stimulate more research and development more environmentally friendly ligands in the field of coordination chemistry.[104]

4.4 CONCLUSION

A promising biomass-derived ligand, CBDA-2, was introduced to coordination chemistry in this study. This polytopic ligand was yielded from furfural and malonic acid, which are two bioadvantaged chemicals. A scalable and straightforward synthetic method of CBDA-2 was documented, and single-crystal X-ray data of a mono-carboxylate triethylammonium derivative of CBDA-2 was reported for comparison with other crystal structures. The potential application of CBDA-2 in preparing green metal-organic materials (GMOM) has been demonstrated through the synthesis of two 2D coordination polymers via a conventional solution method using $Cu(NO_3)_2$ and $Co(NO_3)_2$ as metal sources. The two 2D complexes have been characterized using single-crystal X-ray diffraction analysis, FT-IR, and TGA/DSC. Although both Cu^{2+} and Co^{2+} in the two 2D structures adopt octahedral geometry while interacting with CBDA-2 and two solvent molecules, this novel ligand coordinates with the metal cations in two different ways demonstrating its flexibility and adaptability. Moreover, both complexes exhibited visual thermochromic behaviors when heated at 200 °C under vacuum. This oxygen-rich ligand, CBDA-2, and its congeners provide opportunities to make various GMOM,[90b, 105] electronic and optoelectronic devices,[106] and functional nanostructured materials with interesting properties and potential applications in the future.[107]

Chapter 5
Summary and Outlook

Cyclobutane-containing bifunctional building blocks (CBs) and the Gemini monomer are uncommon. It is especially true for CBs despite their ubiquity in many synthetic drugs and natural products.[108] During the metabolism, cyclobutane derivatives are generated, which play a vital role in ensuring proper biological functions.[108a, 108c, 109] Due to their inherent ring strain and lower stability compared to five- and six-membered rings, they are rarely employed in developing industrially relevant materials. Based on the concepts of conservation of orbital symmetry devised by Woodward and Hoffmann, cyclobutane is stable towards thermal [2+2] cycloelimination and near UV radiation.[85] This thermal and photochemical stability substantiates their candidacy in developing materials of choice. In addition, their unique semi-rigid characteristics due to the planer and puckered conformation of the cyclobutane ring[110] bridge the performance gap between flexible aliphatic and rigid aromatic counterparts and provide CBs the balance of processability and rigidity, which is crucial in synthesizing novel materials with desired properties, as shown in Figure 5.1. Moreover, the solid-state photochemical process to synthesize CBs limits organic solvents and harsh conditions creating a more environmental-friendly approach for synthesizing materials.[111]

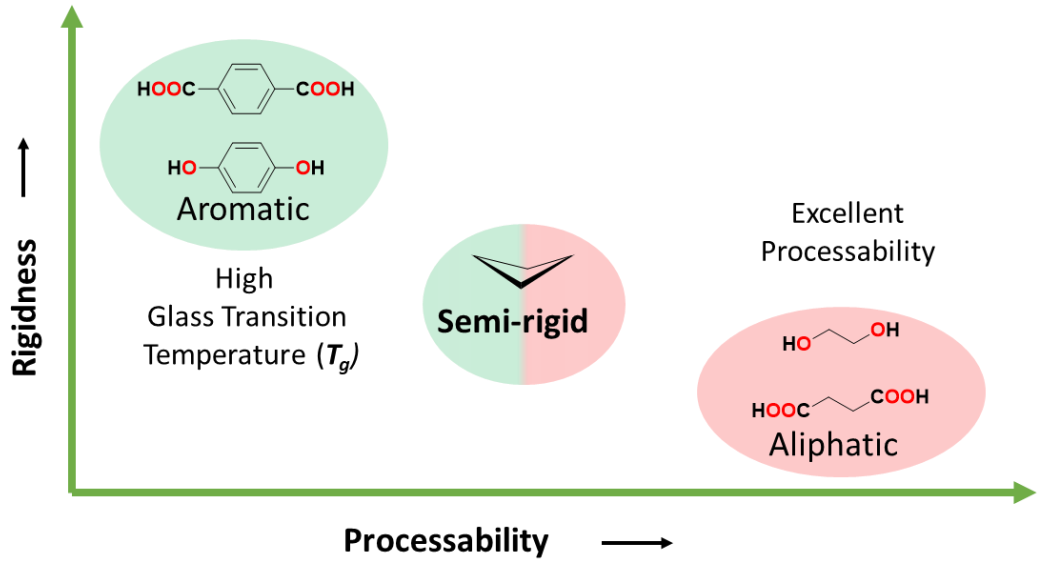

Figure 5.1. Classification of bifunctional building blocks based on rigidity.

This dissertation describes the synthesis of bifunctional CBs such as CBDO-1, CBAM-1, and CBDA-2 using an interdisciplinary approach of modern photochemical methods and conventional organic synthesis. To highlight the potential applications of these valuable CBs, different materials were synthesized, e.g., high T_g polyesters as an alternative to BPA-based polyesters, polyamides with enhanced physical and processing properties, and 2-D green metal-organic materials with interesting morphology (Figure 5.2). This study focuses on synthesizing various CBs and novel materials and characterizing and comparing their properties with similar and commercial materials.

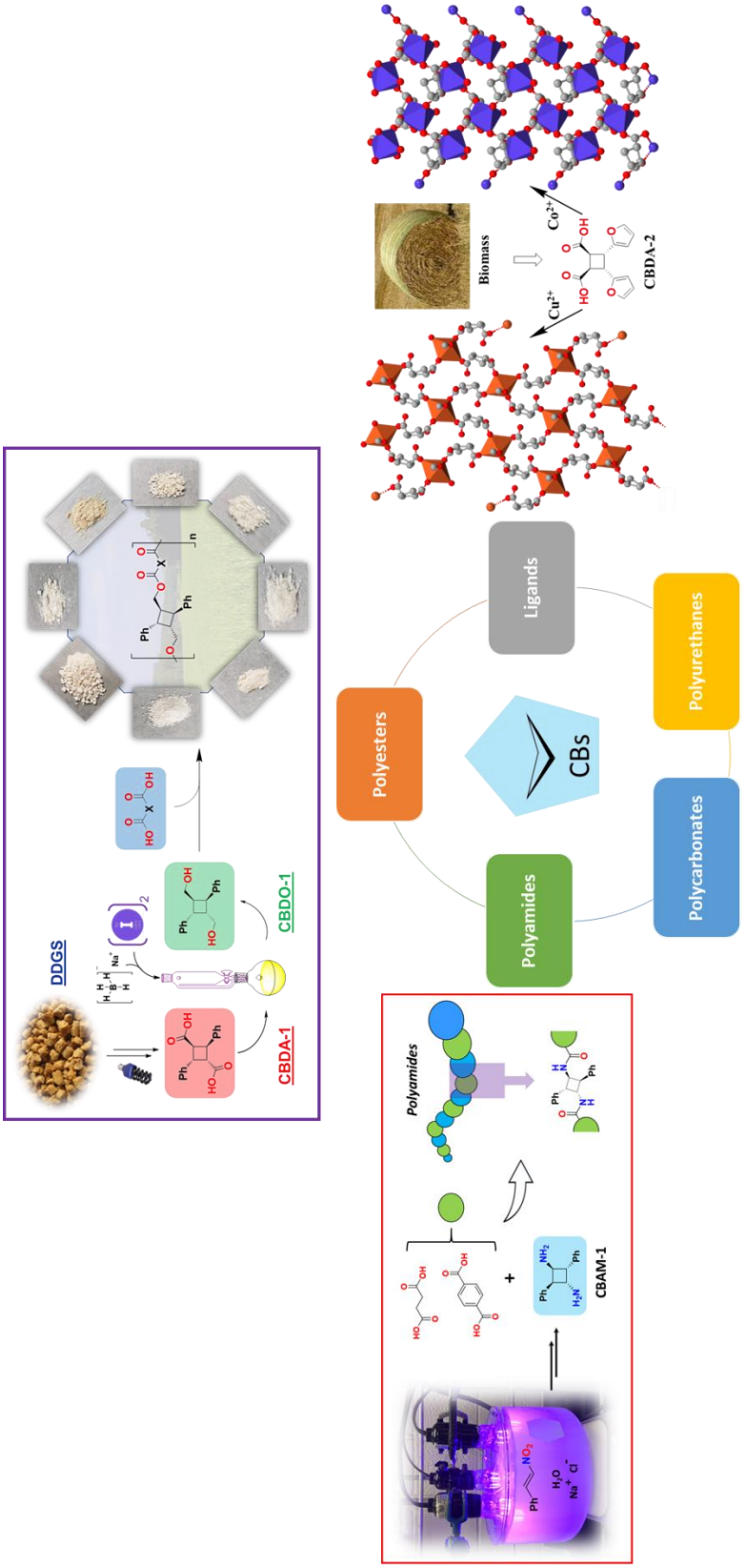

Figure 5.2. Applications of CBs in the synthesis of novel materials.

The examples mentioned in this dissertation will pave the way to explore other possible CBs with different substituents synthesized under similar conditions (Figure 5.3). This approach can be used to tune the properties of the corresponding materials by changing the structure of the CBs according to specific needs. Also, it will allow exploration of other industrially relevant materials such as polyurethanes, polycarbonates, and polysilylethers.

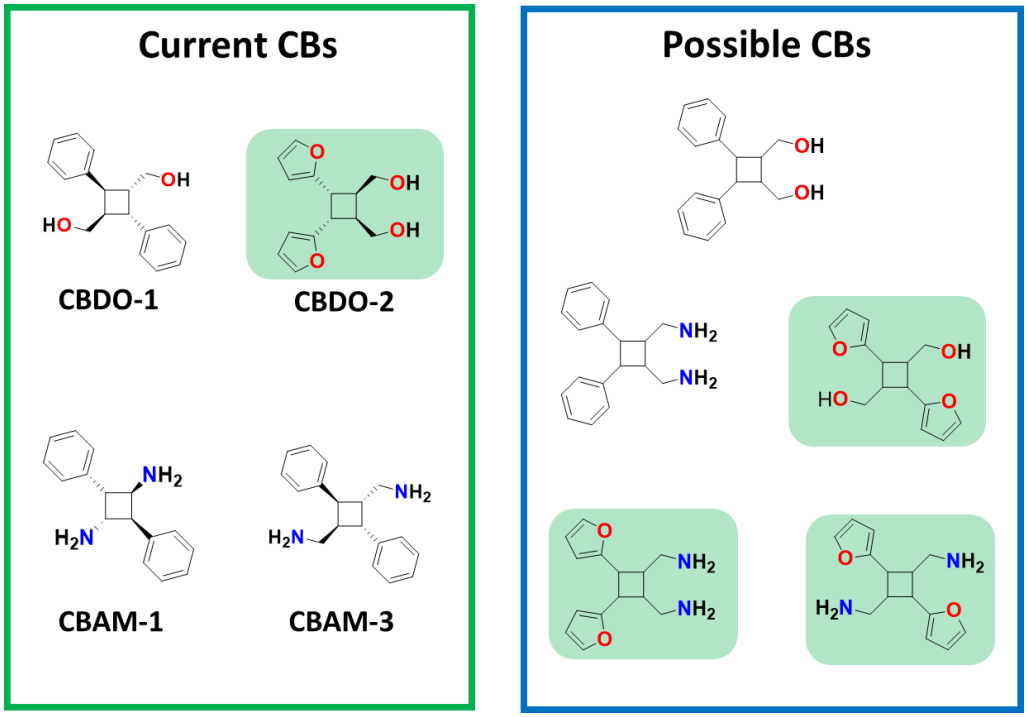

Figure 5.3. Diverse CBs that can be synthesized using the method studied in this study. CBs with green highlights can be derived from biomass.

Appendix A

Selected NMR spectra

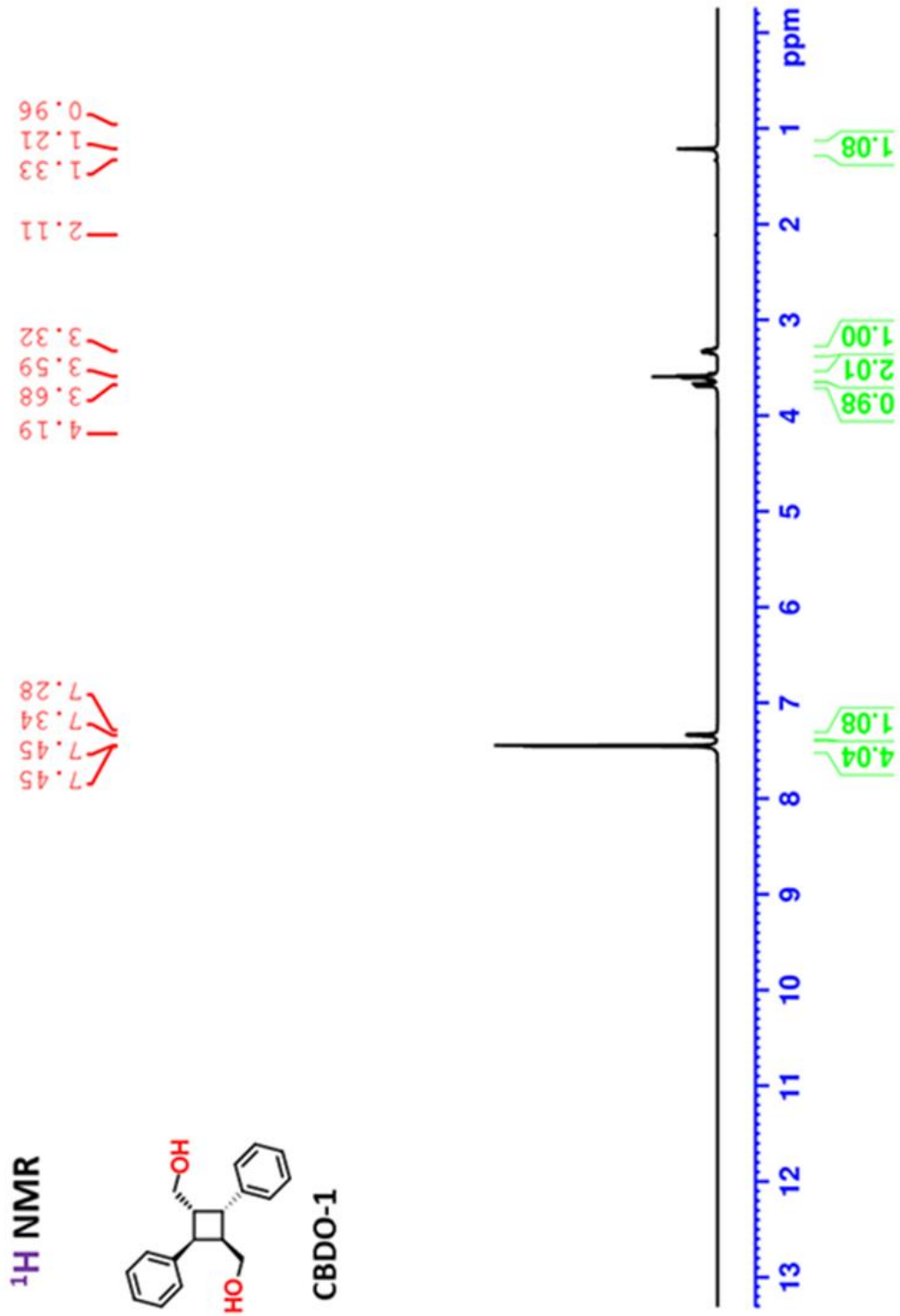

Figure A.1. ^{1}H NMR spectrum of CBDO-1 in $CDCl_3$ at room temperature.

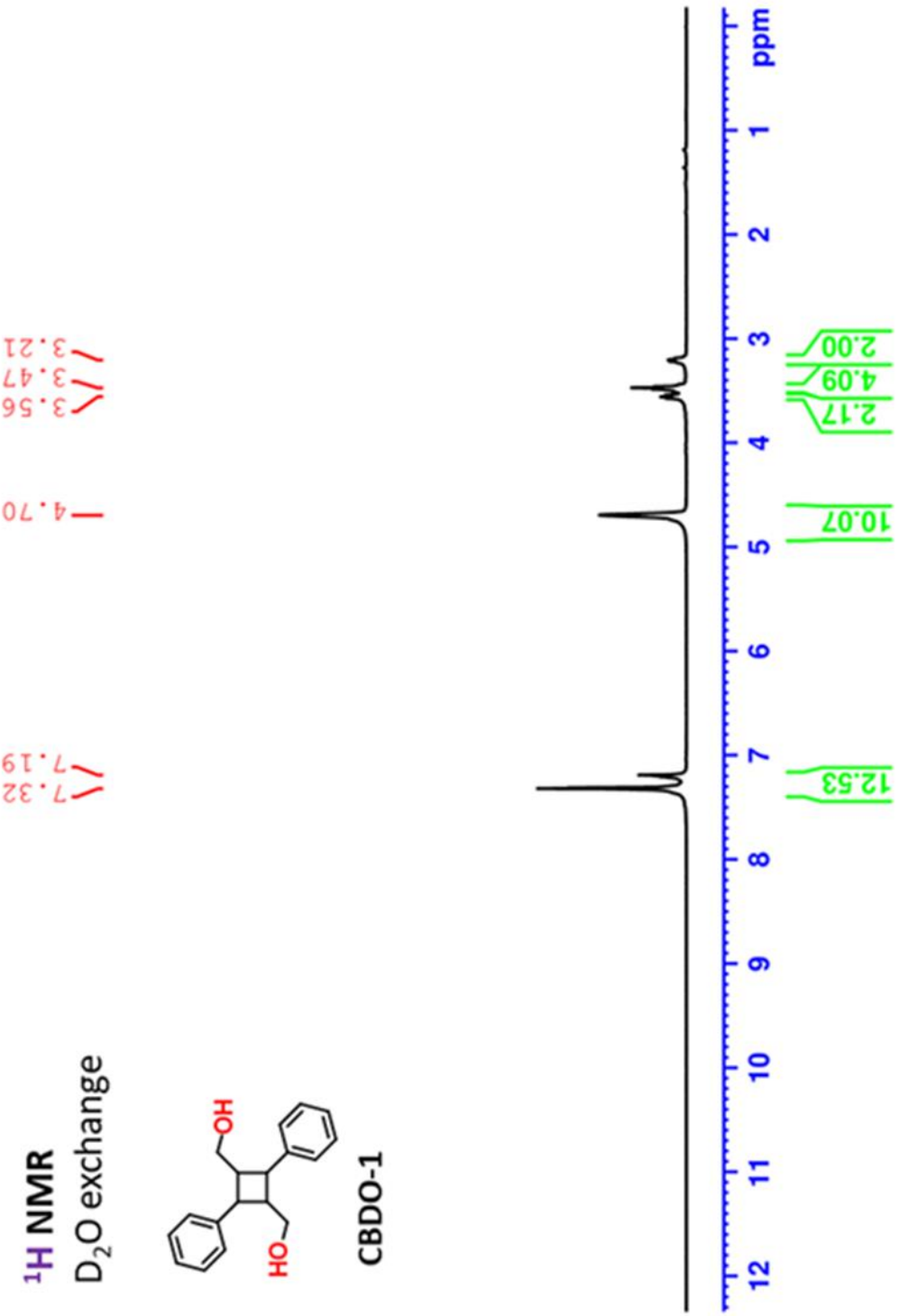

Figure A.2. ^{1}H NMR D_2O exchange spectrum of CBDO-1 in $CDCl_3$ at room temperature.

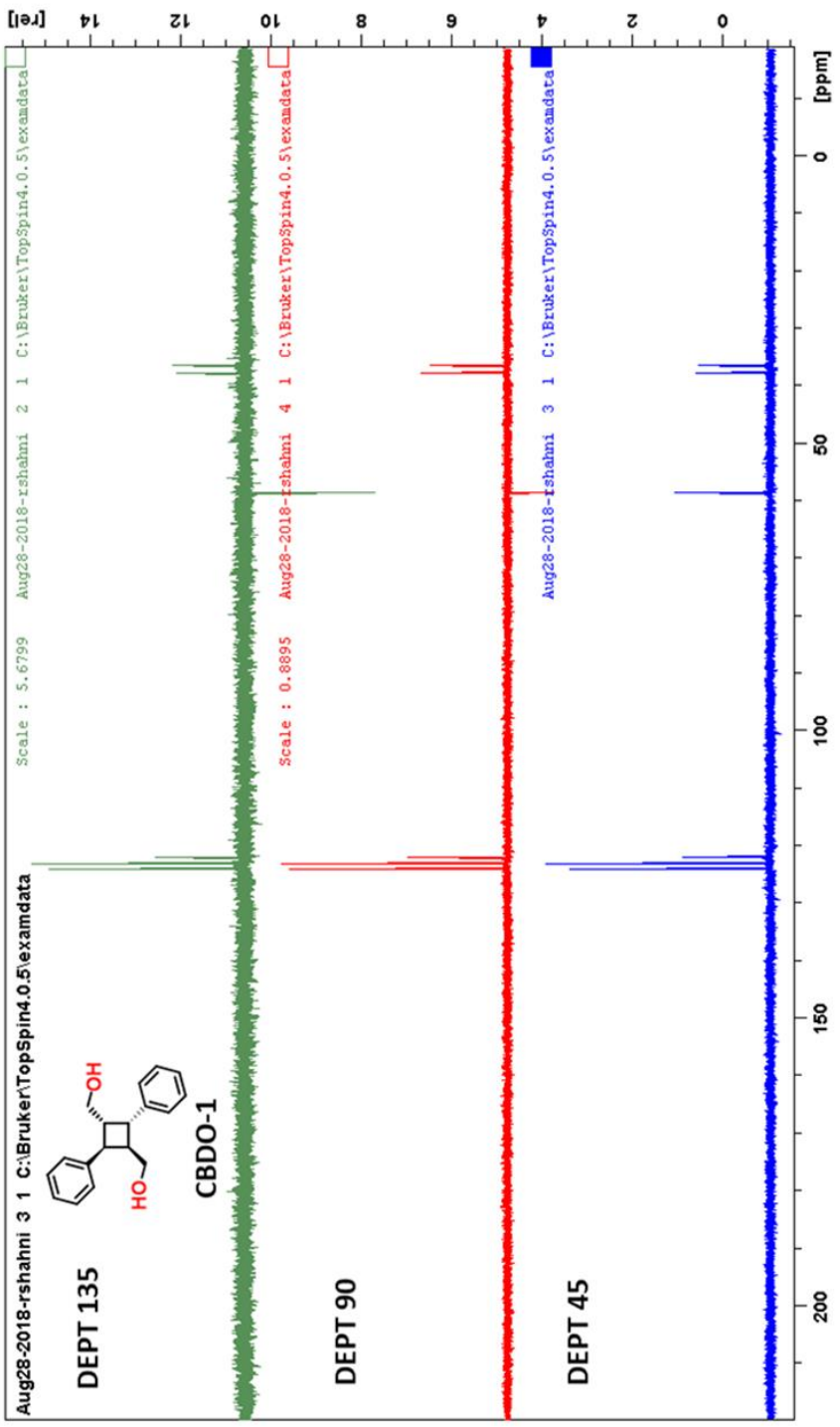

Figure A.3. DEPT 45, 90 and 135 spectra of CBDO-1 in $CDCl_3$ at room temperature.

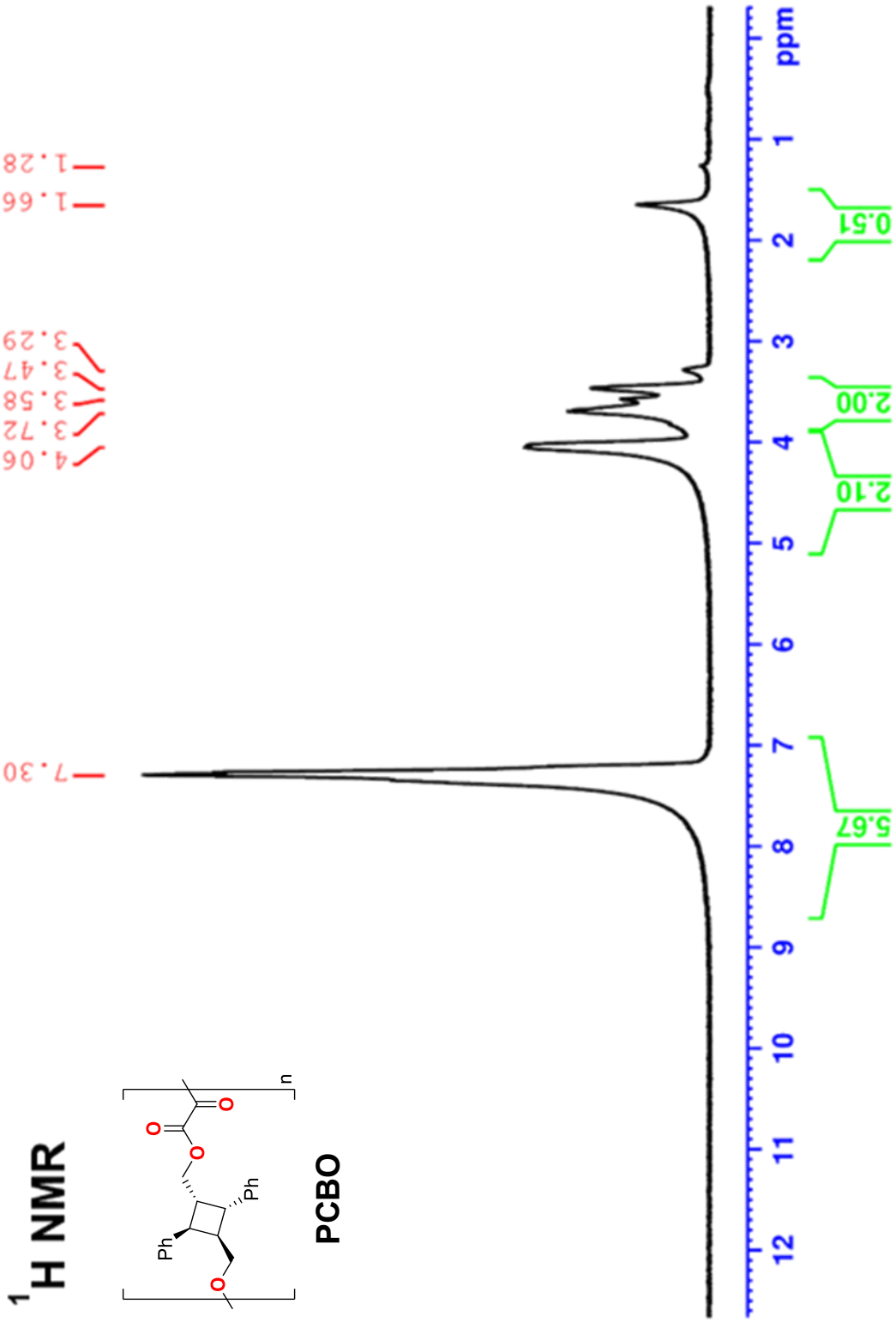

Figure A.4. ^{1}H NMR spectrum of PCBO in $CDCl_3$ at room temperature.

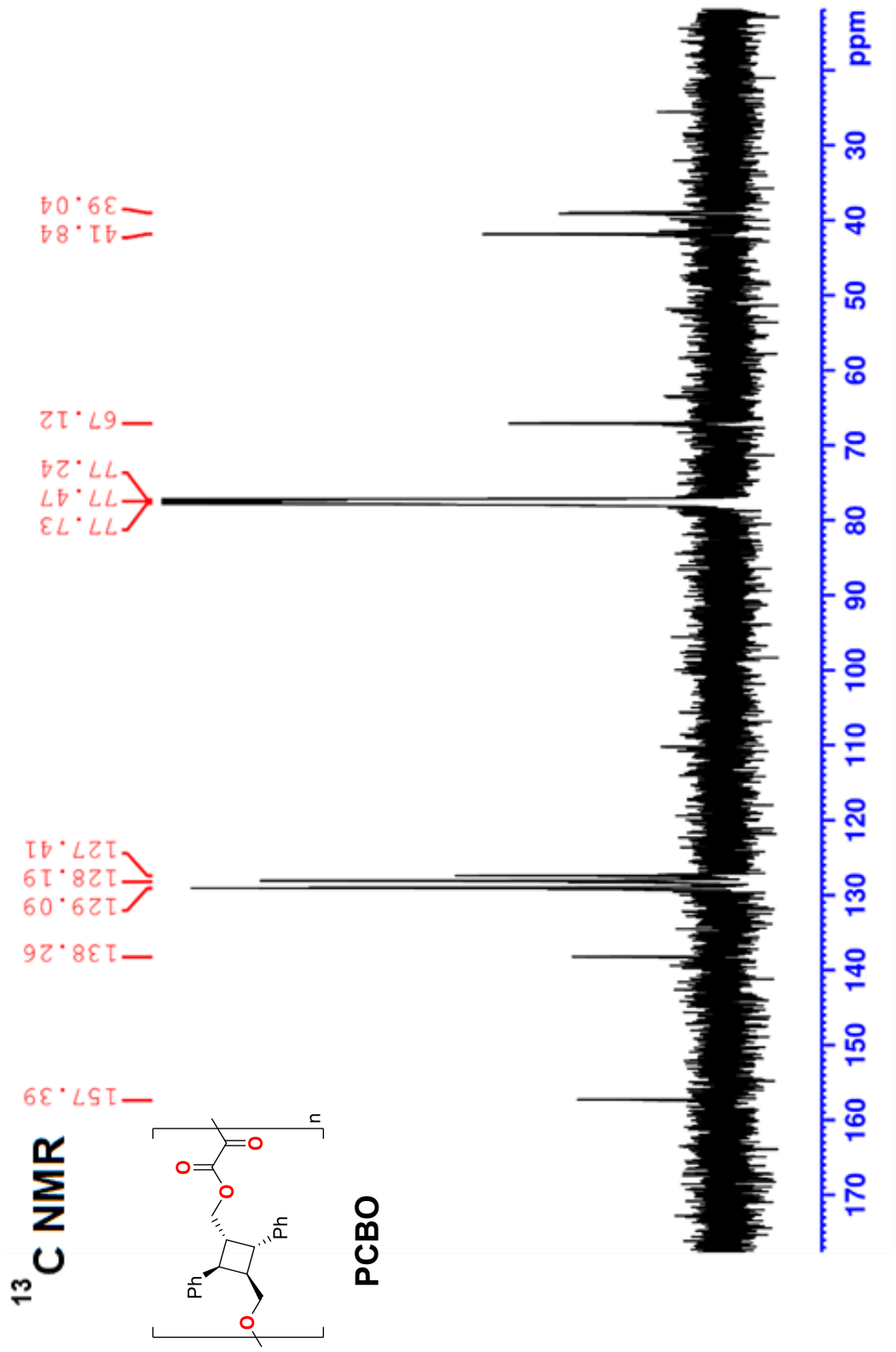

Figure A.5. $^{13}C\{^{1}H\}$ NMR spectrum of PCBO in $CDCl_3$ at room temperature.

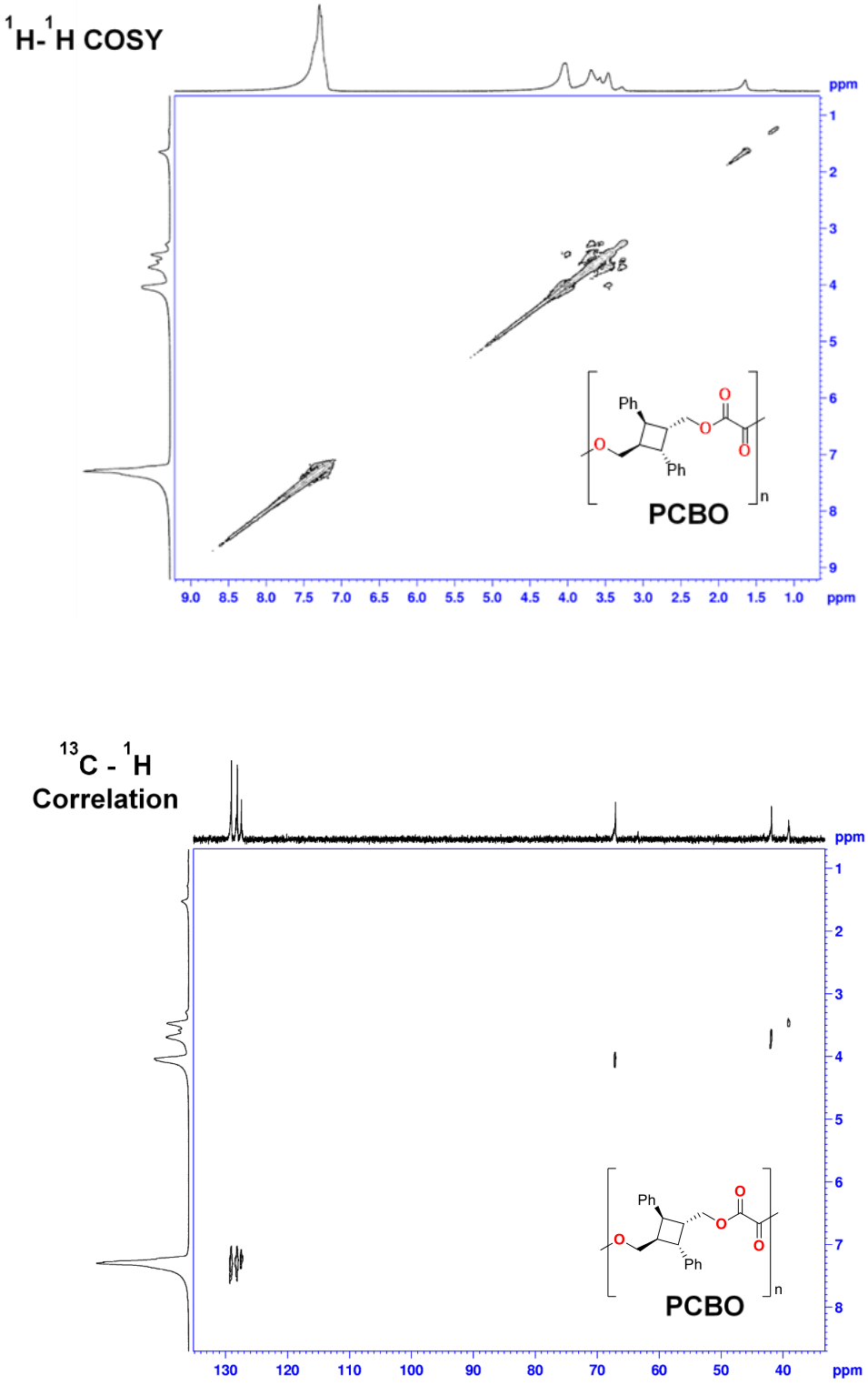

Figure A.6. COSY and CH-correlation spectra of PCBO in $CDCl_3$ at room temperature.

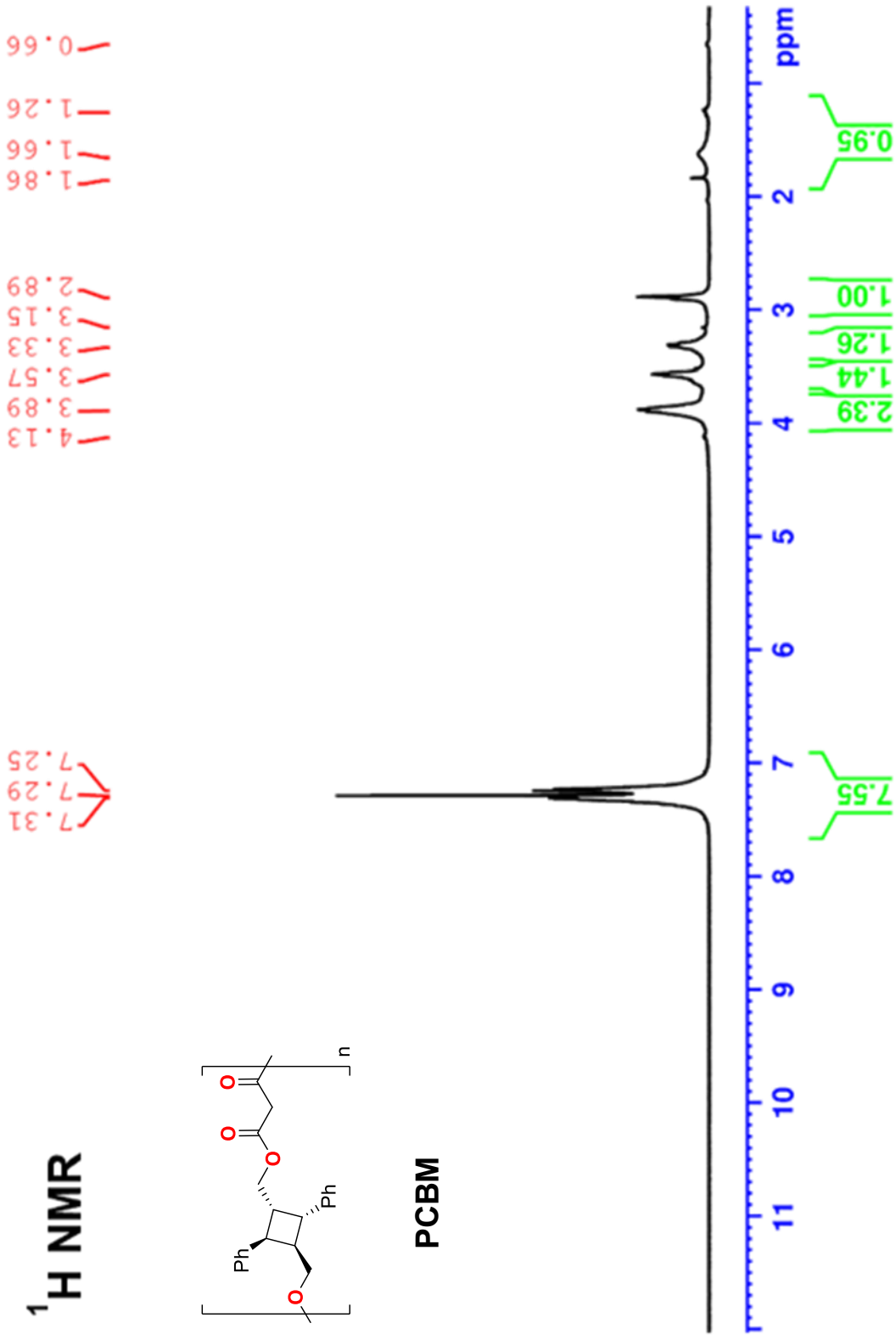

Figure A.7. ^{1}H NMR spectrum of PCBM in $CDCl_3$ at room temperature.

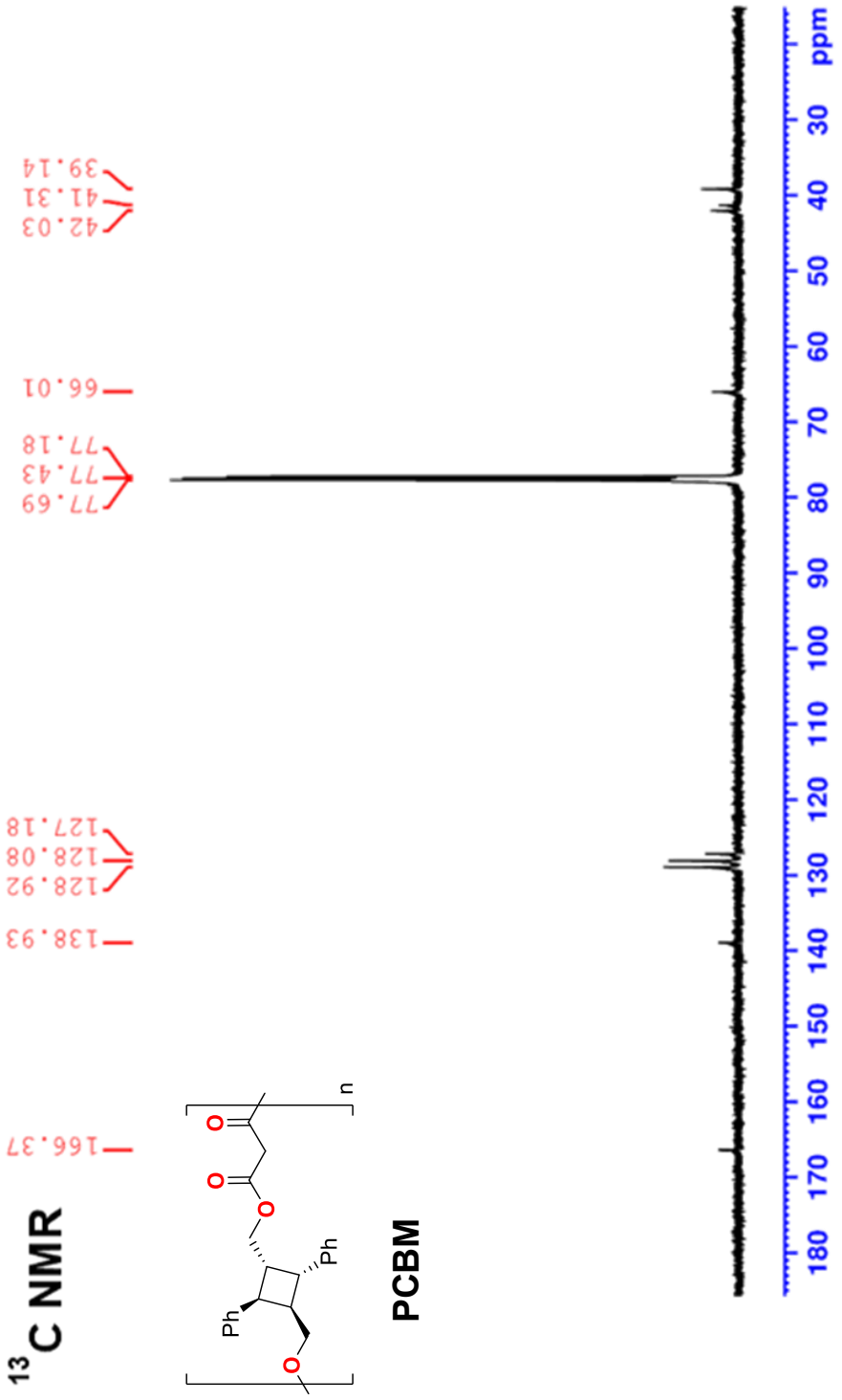

Figure A.8. $^{13}C\{^{1}H\}$ NMR spectrum of PCBM in $CDCl_3$ at room temperature.

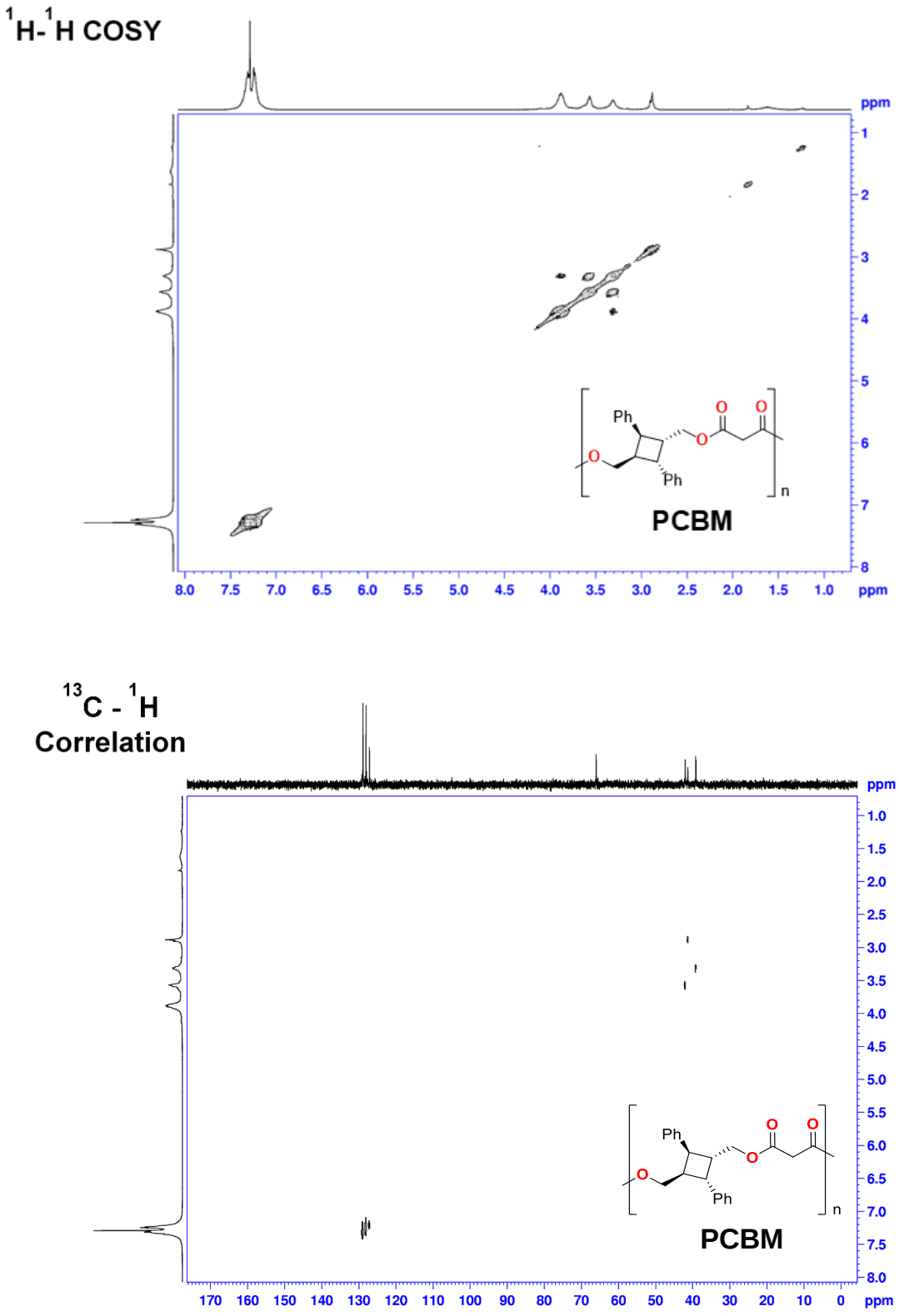

Figure A.9. COSY and CH-correlation spectra of PCBM in $CDCl_3$ at room temperature.

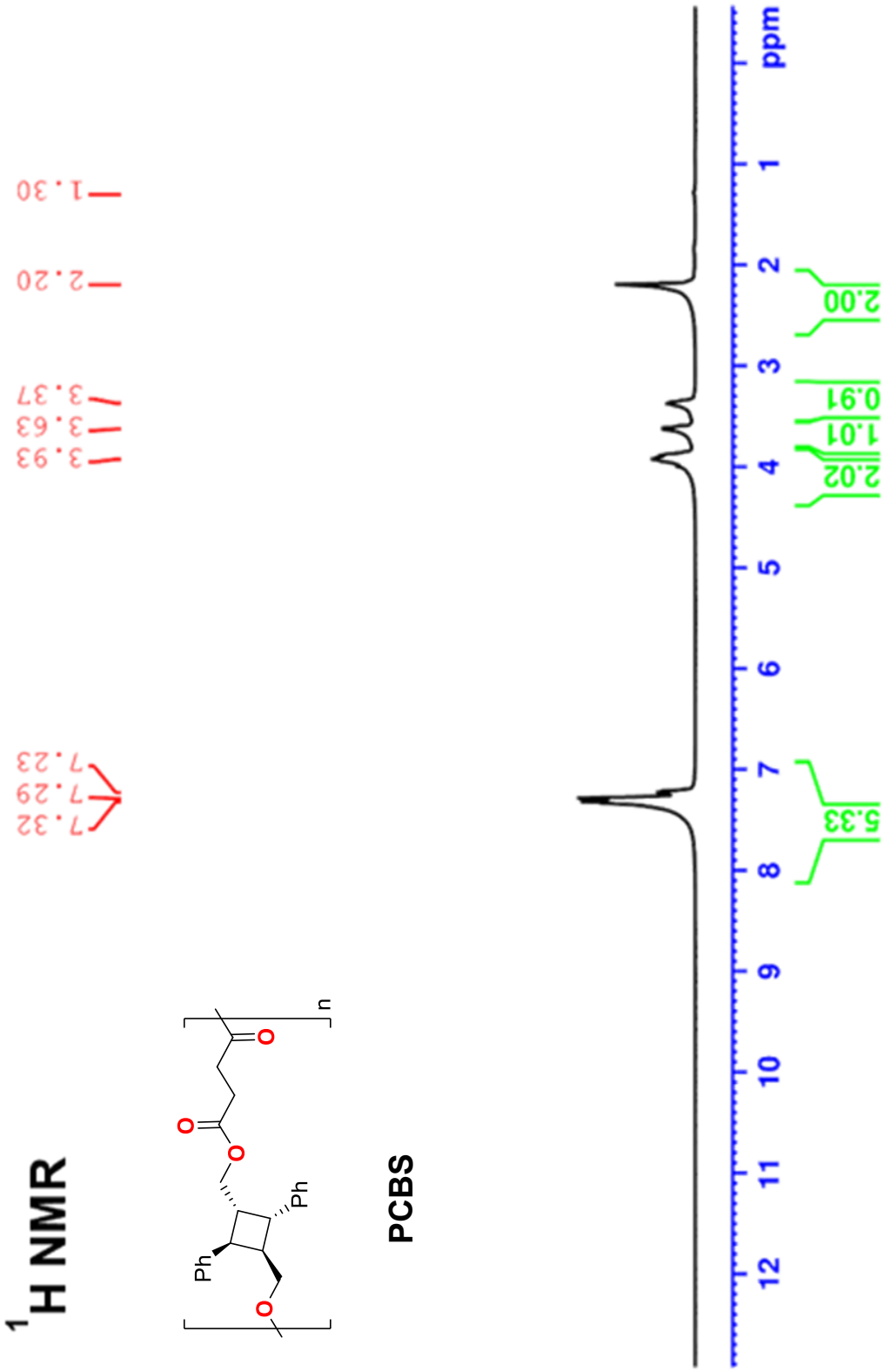

Figure A.10. ^{1}H NMR spectrum of PCBS in $CDCl_3$ at room temperature.

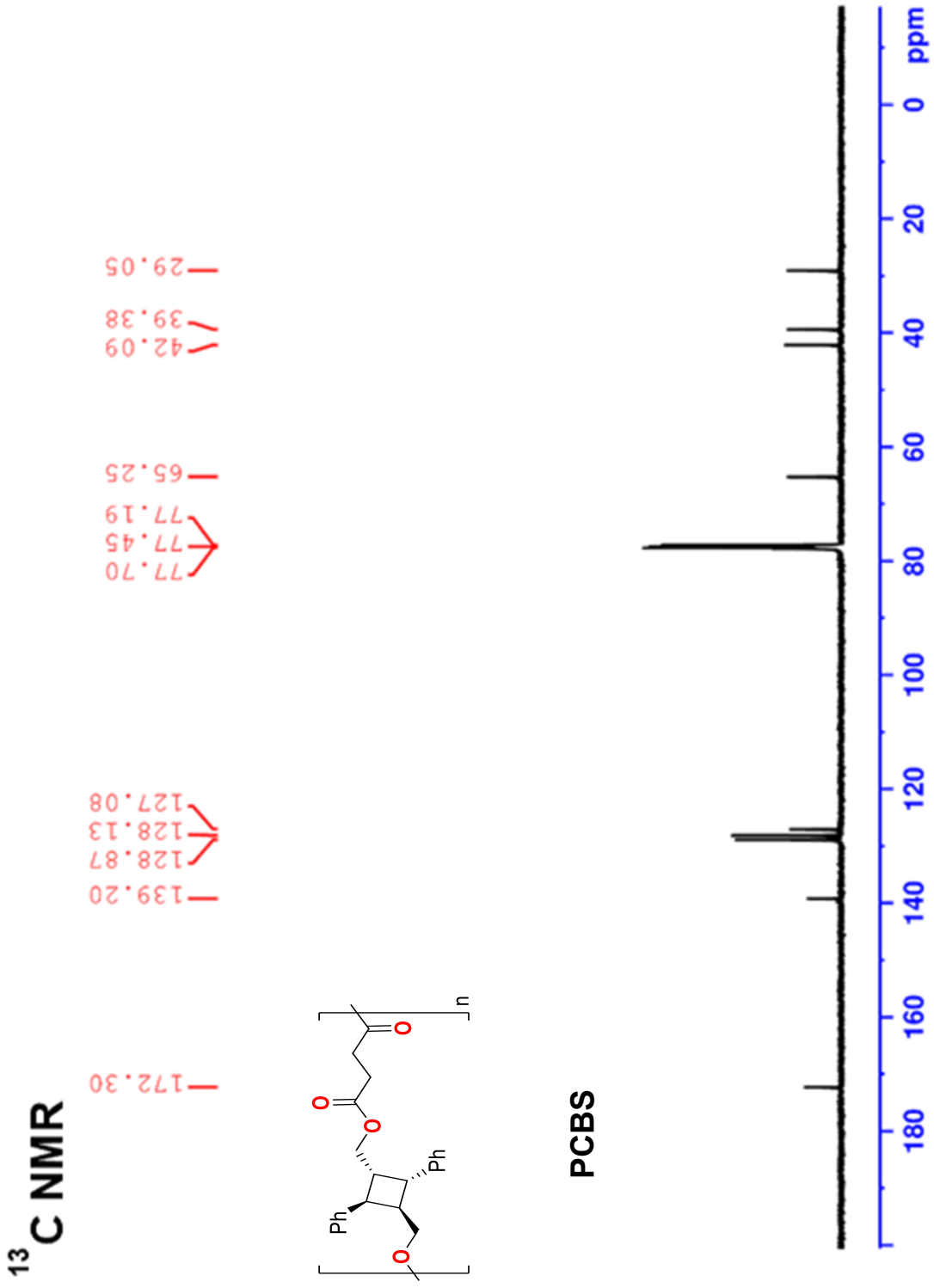

Figure A.11. $^{13}C\{^{1}H\}$ NMR spectrum of PCBS in $CDCl_3$ at room temperature.

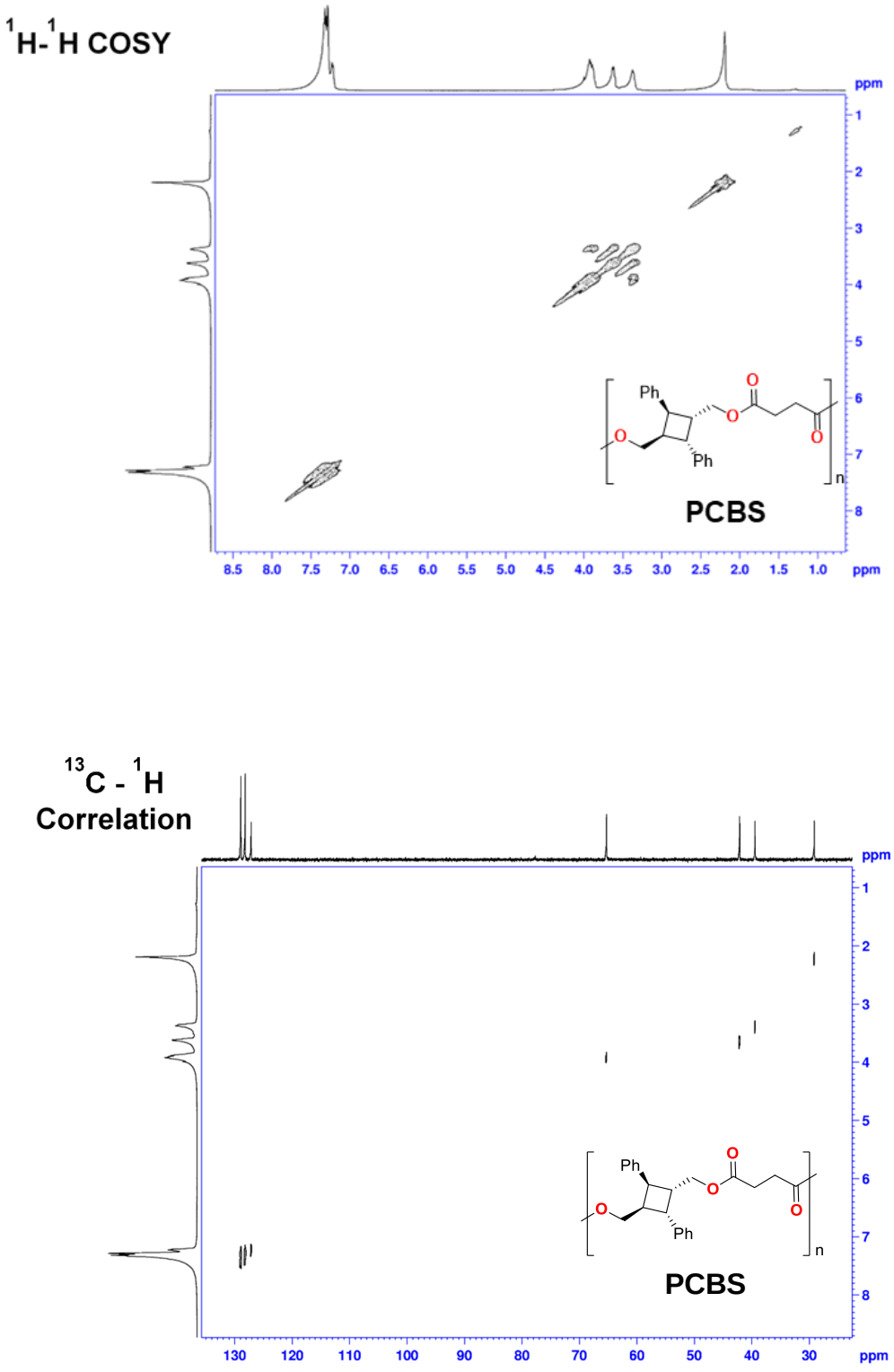

Figure A.12. COSY and CH-correlation spectra of PCBS in $CDCl_3$ at room temperature.

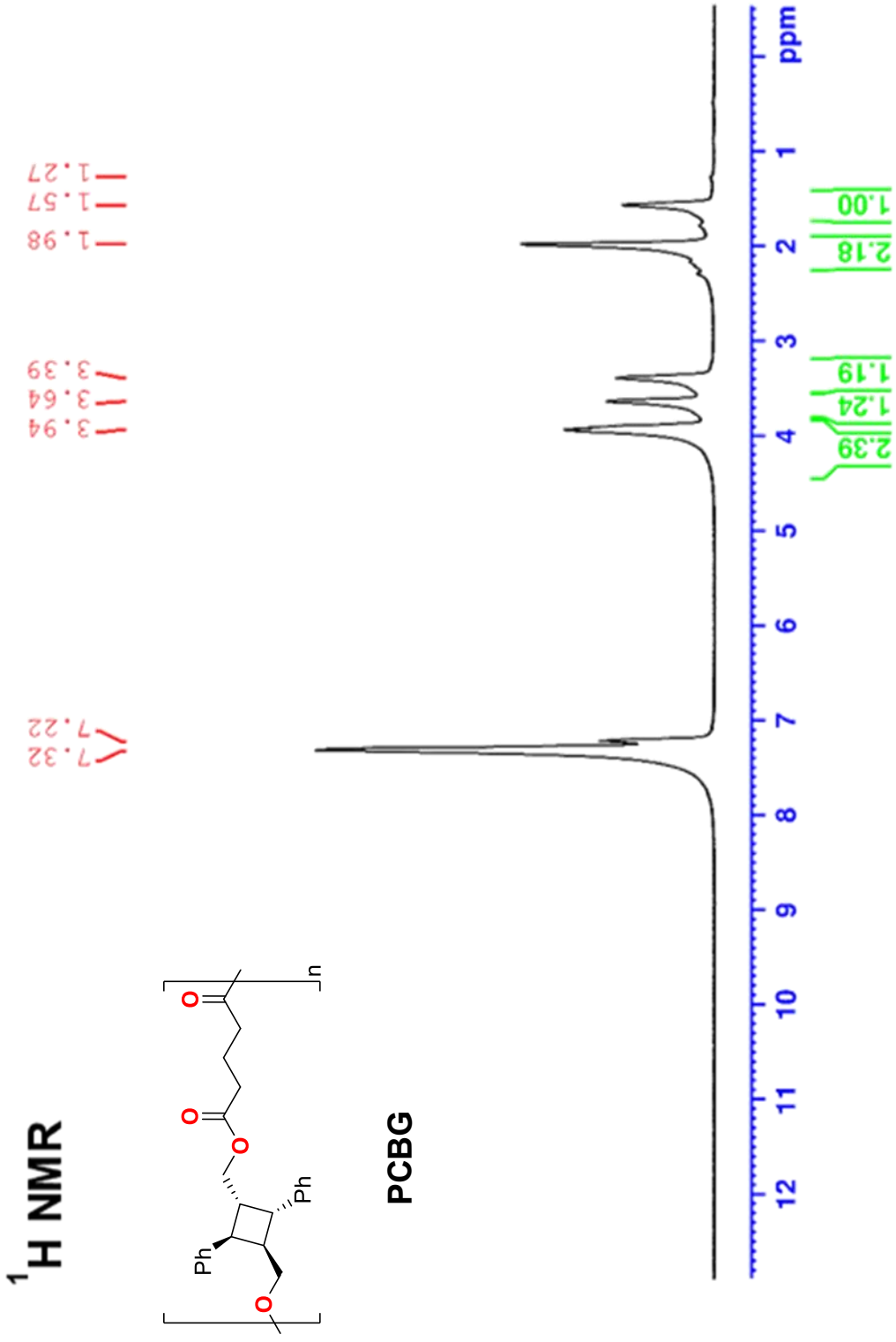

Figure A.13. ^{1}H NMR spectrum of PCBG in $CDCl_3$ at room temperature.

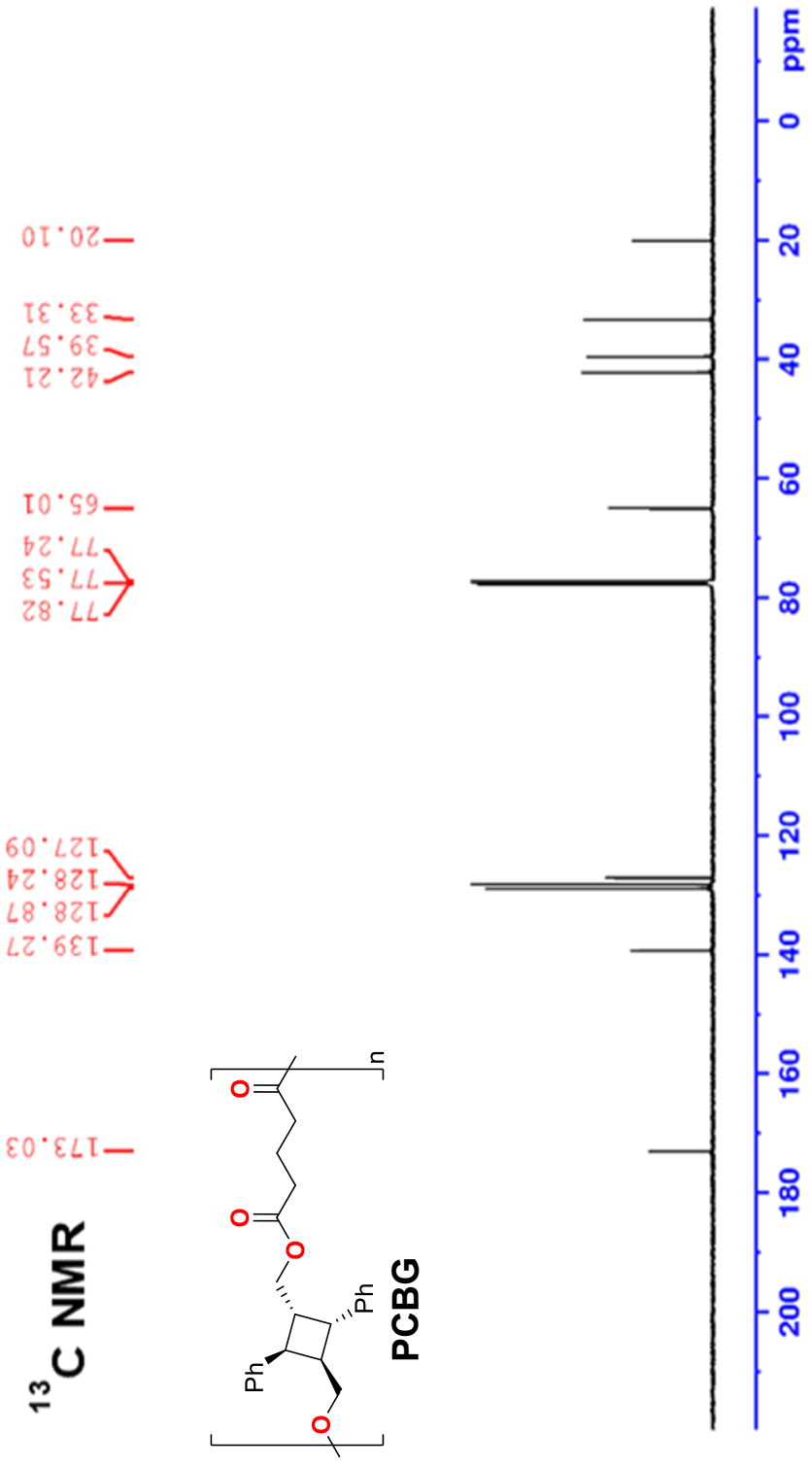

Figure A.14. $^{13}C\{^{1}H\}$ NMR spectrum of PCBG in $CDCl_3$ at room temperature.

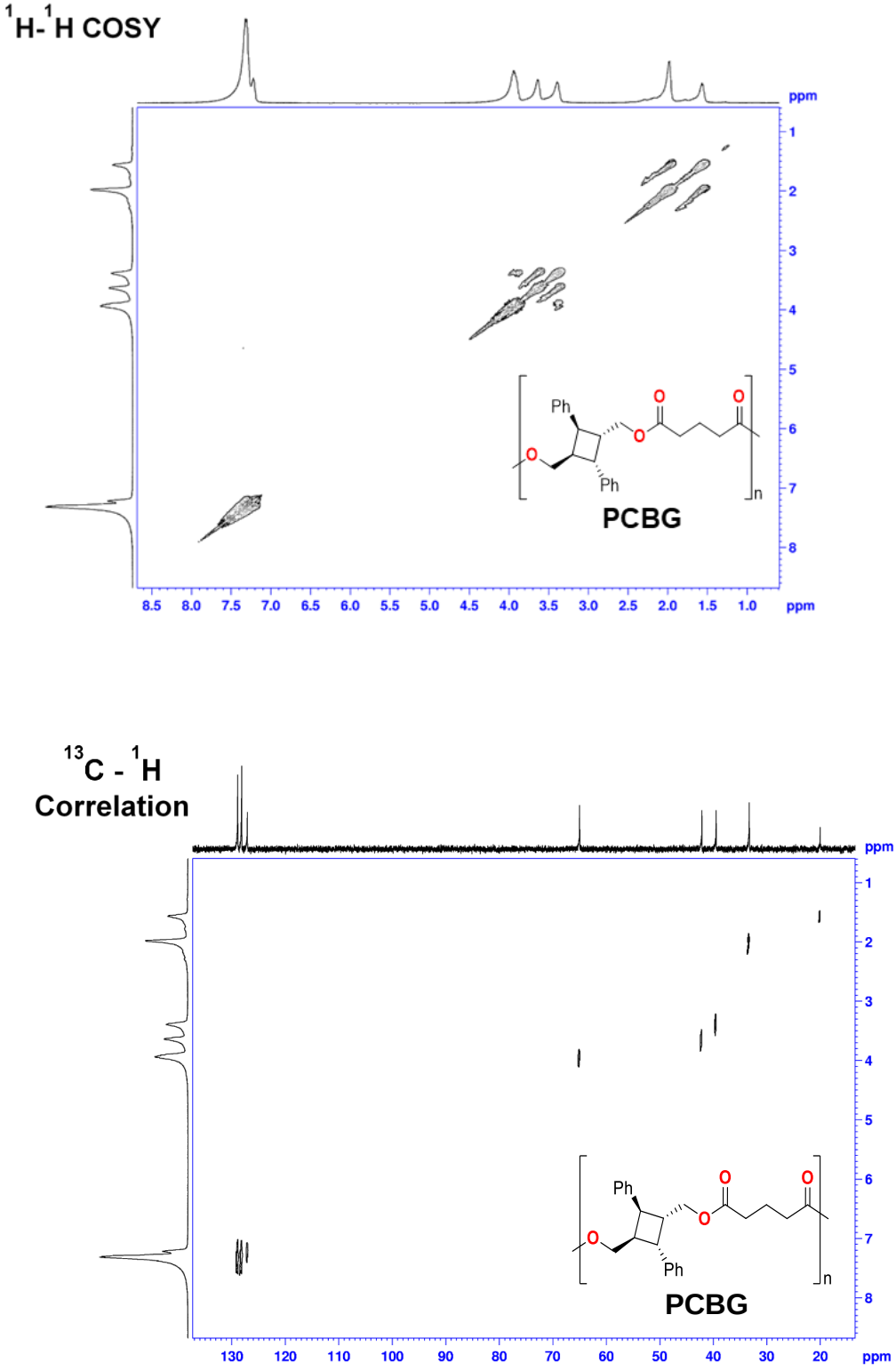

Figure A.15. COSY and CH-correlation spectra of PCBG in $CDCl_3$ at room temperature.

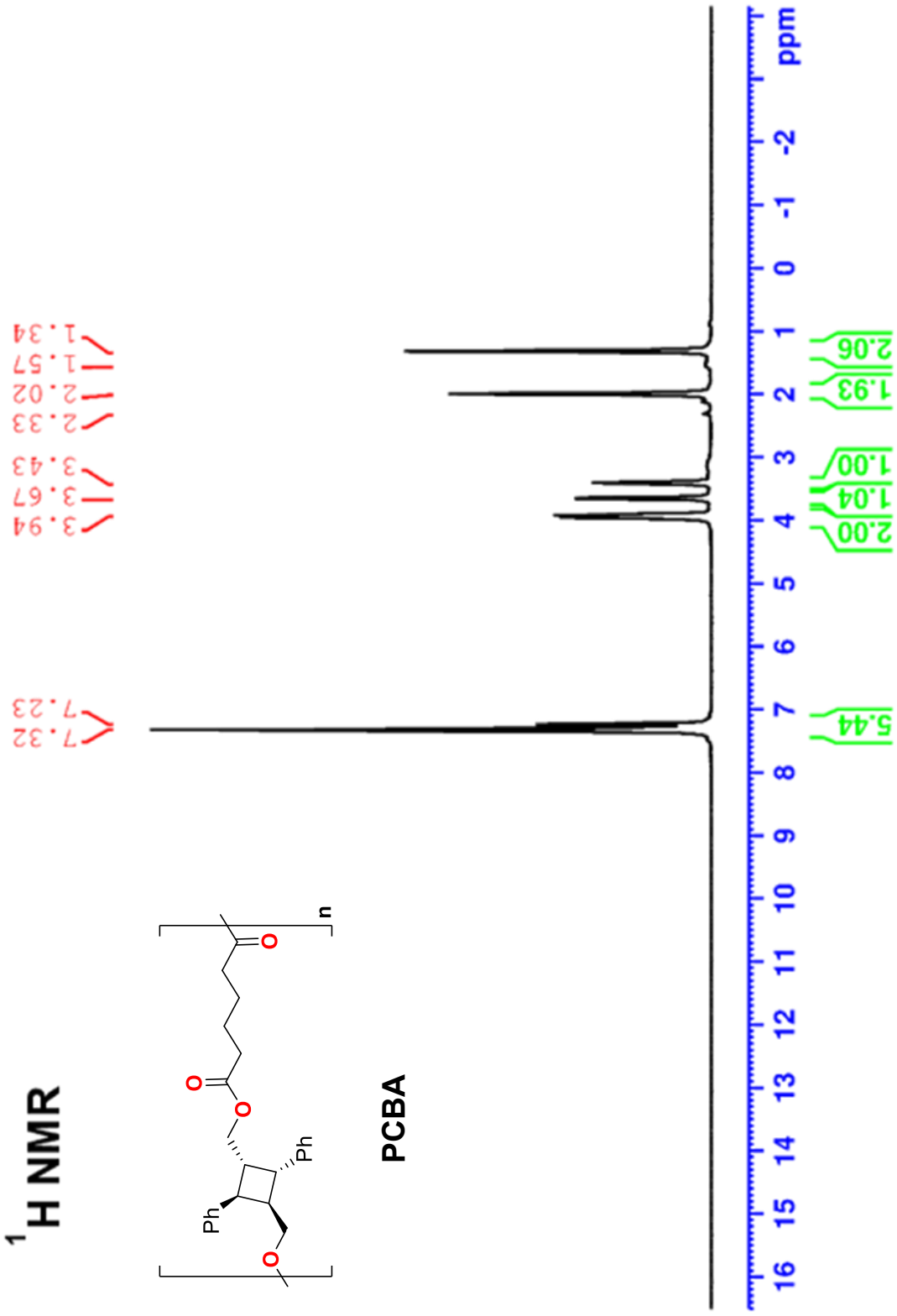

Figure A.16. ^{1}H NMR spectrum of PCBA in $CDCl_3$ at room temperature.

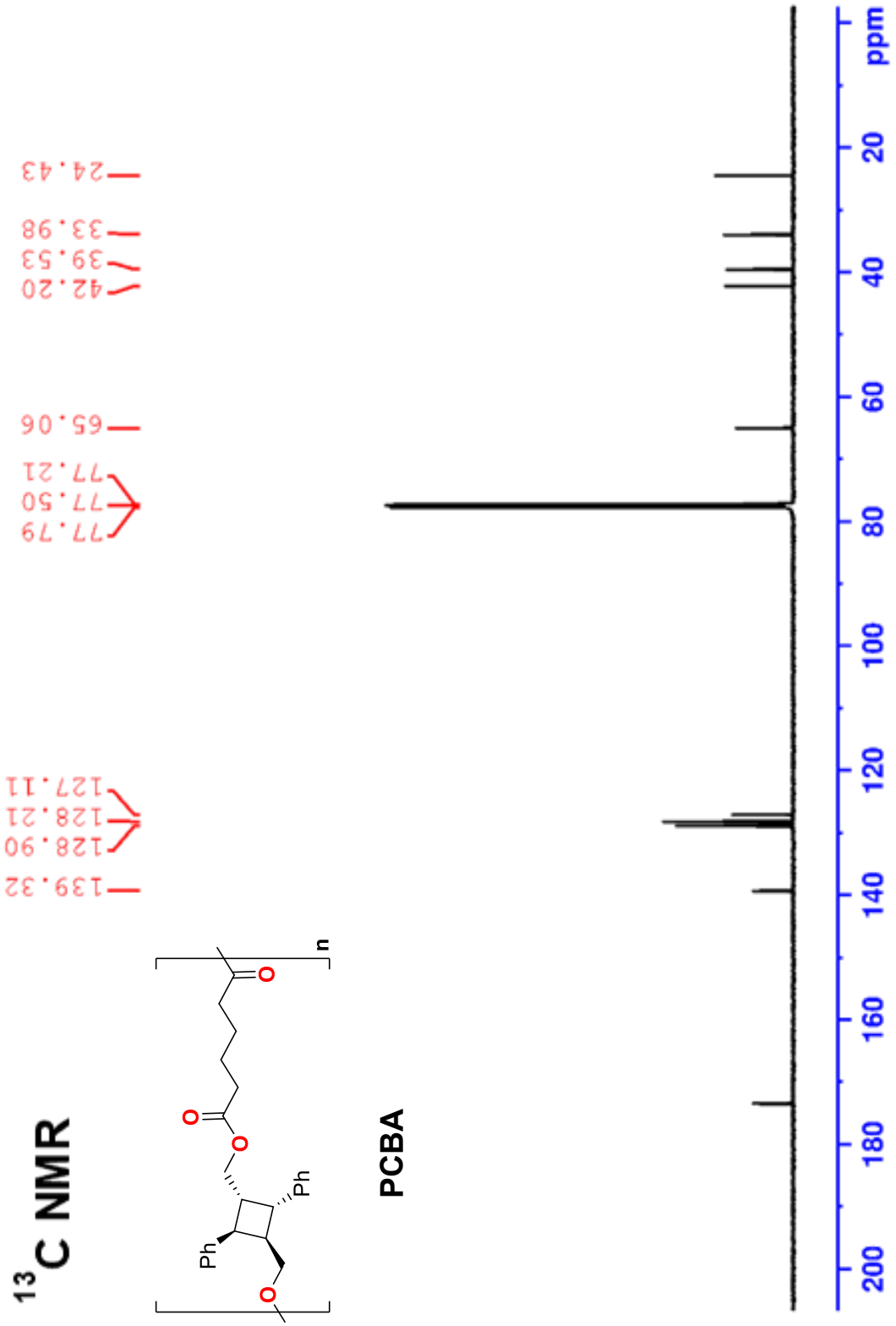

Figure A.17. $^{13}C\{^{1}H\}$ NMR spectrum of PCBA in $CDCl_3$ at room temperature.

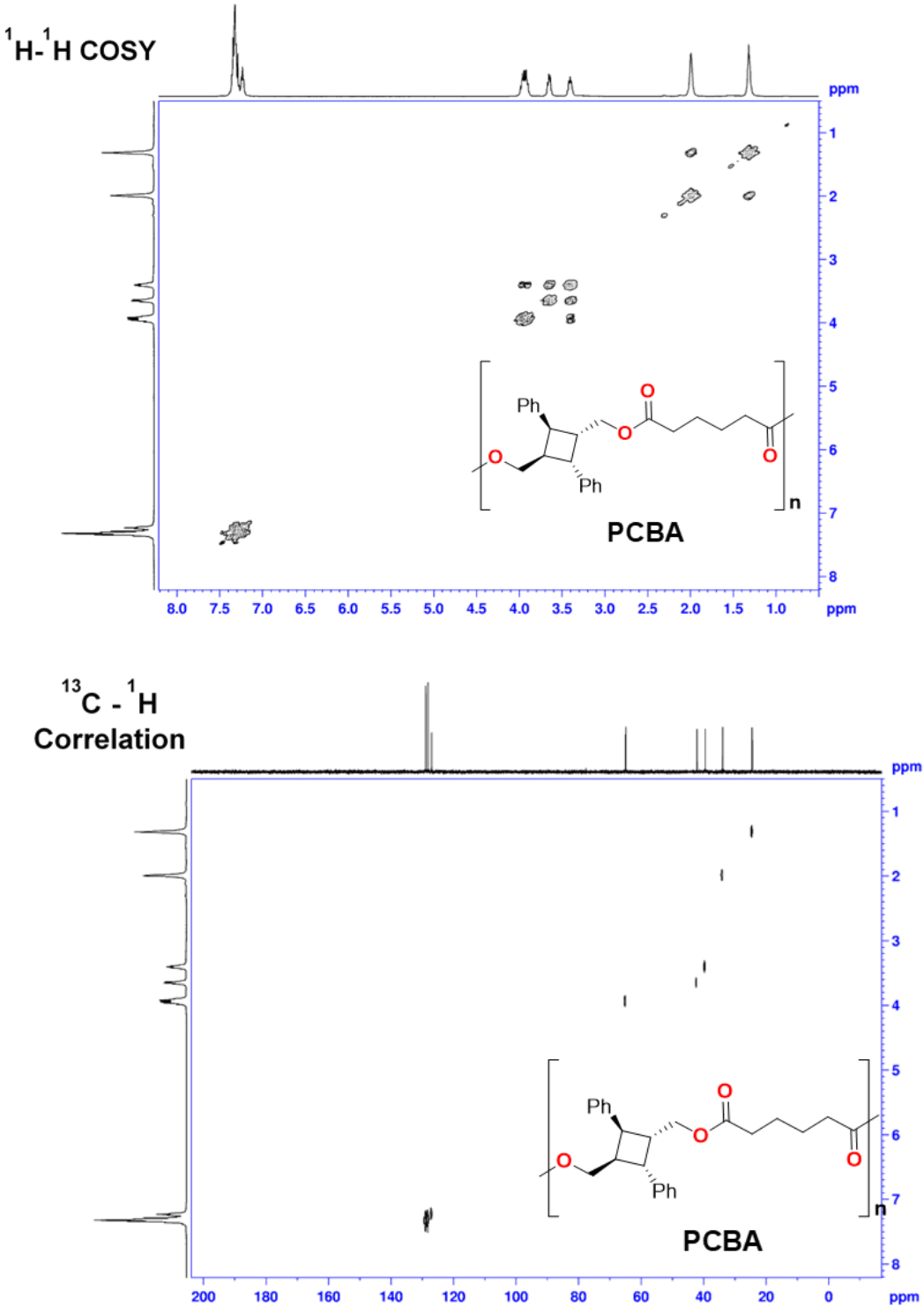

Figure A.18. COSY and CH-correlation spectra of PCBA in $CDCl_3$ at room temperature.

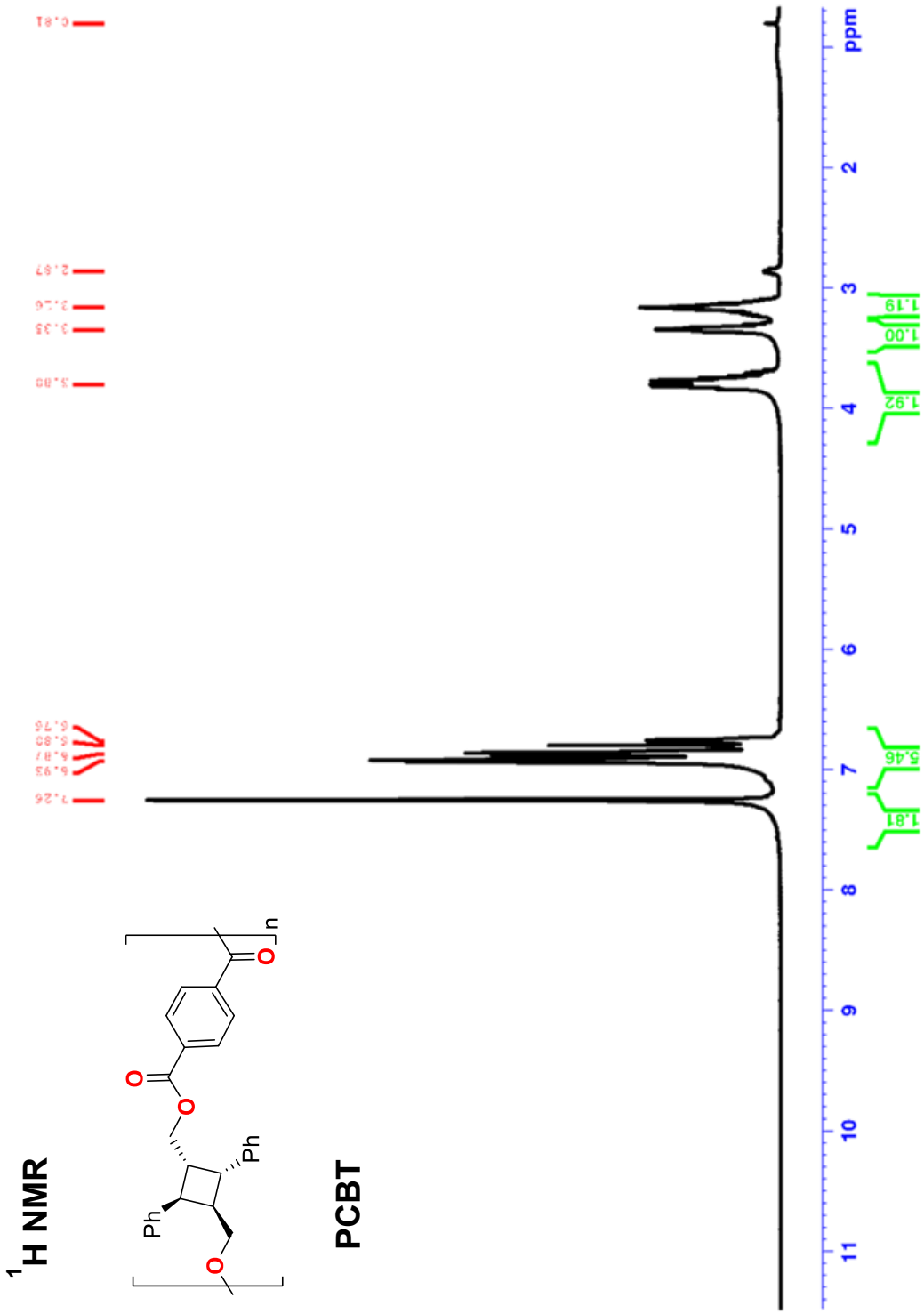

Figure A.19. ^{1}H NMR spectrum of PCBT in $CDCl_3$ at room temperature.

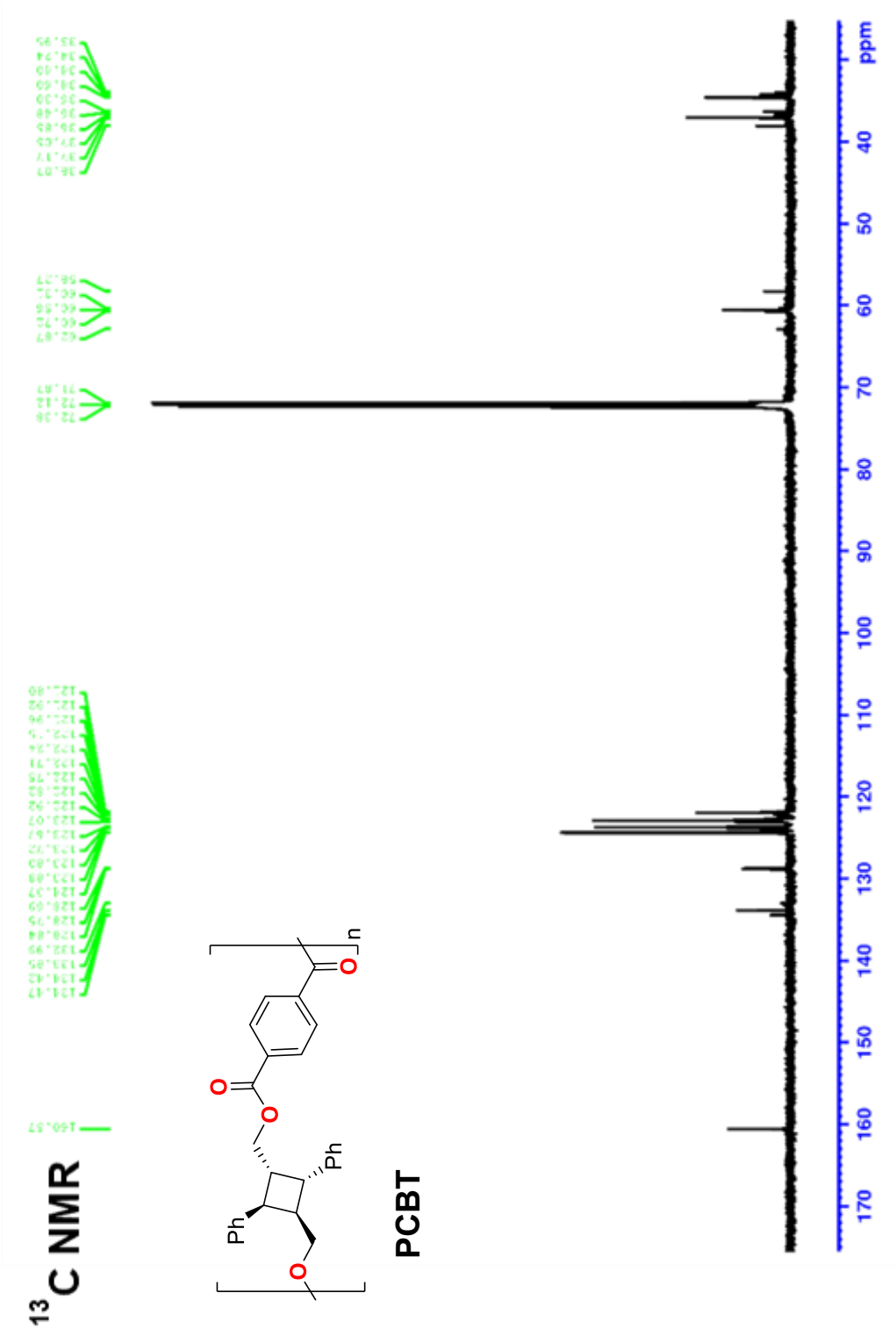

Figure A.20. $^{13}C\{^{1}H\}$ NMR spectrum of PCBT in $CDCl_3$ at room temperature.

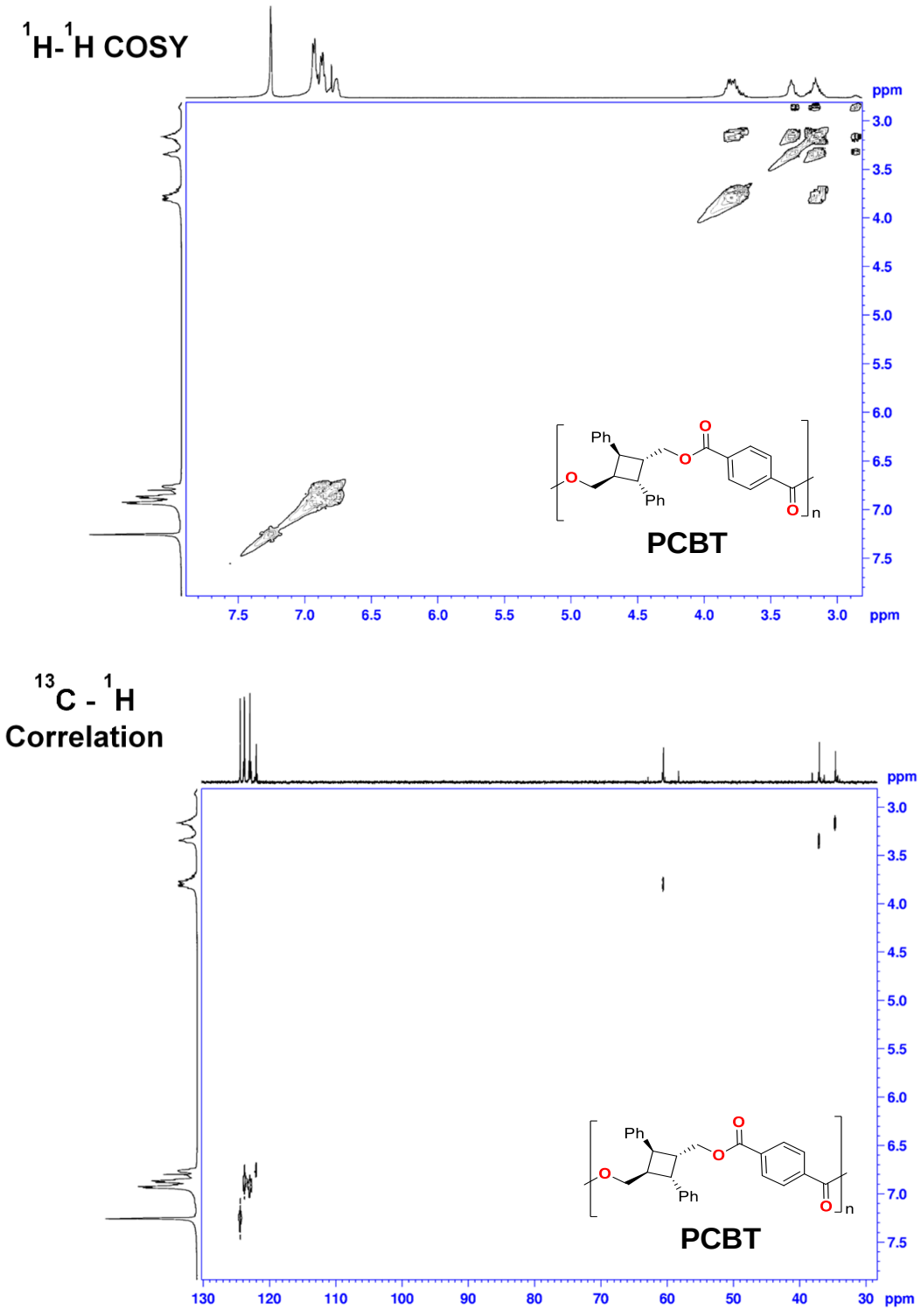

Figure A.21. COSY and CH-correlation spectra of PCBT in $CDCl_3$ at room temperature.

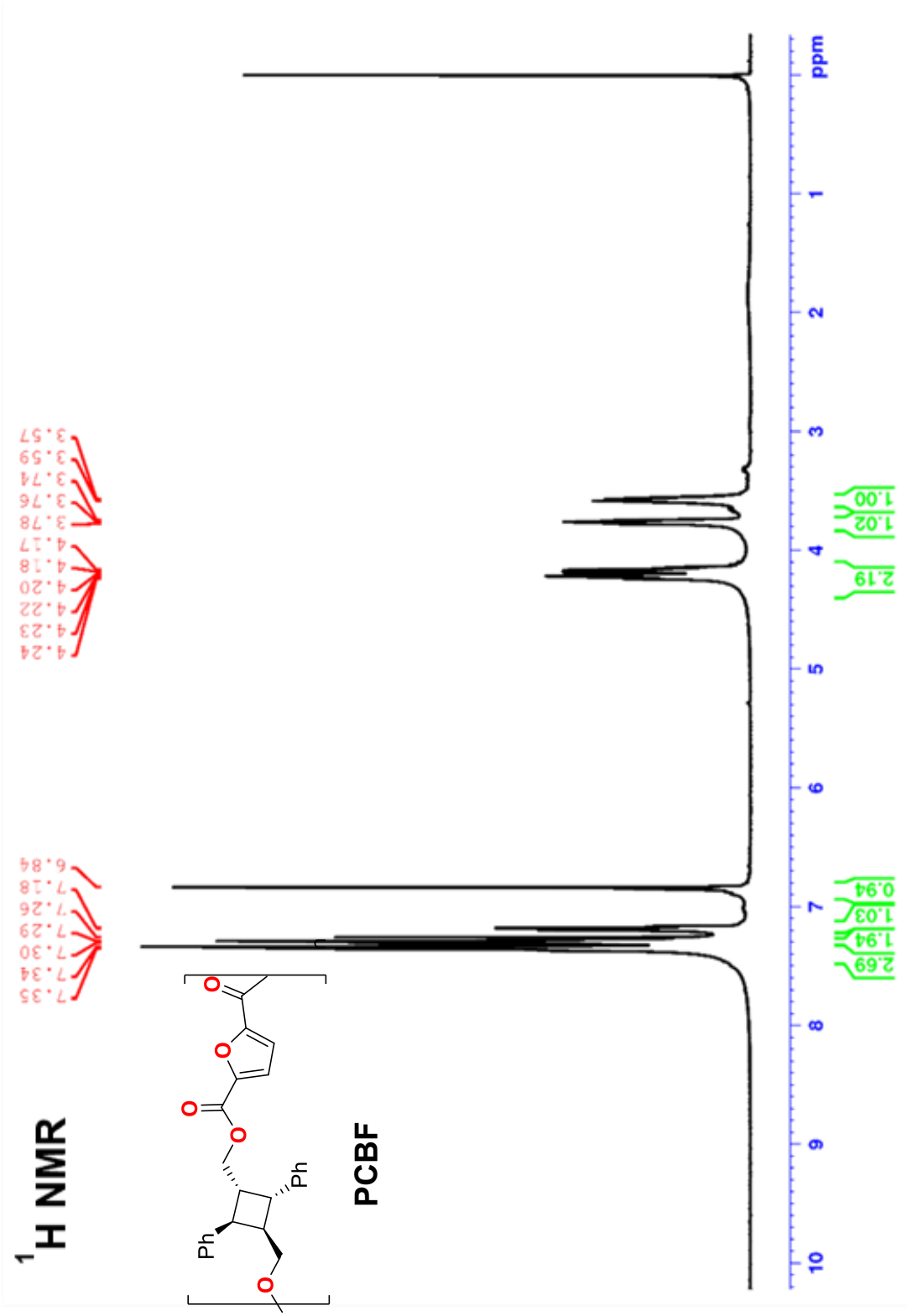

Figure A.22. ^{1}H NMR spectrum of PCBF in $CDCl_3$ at room temperature.

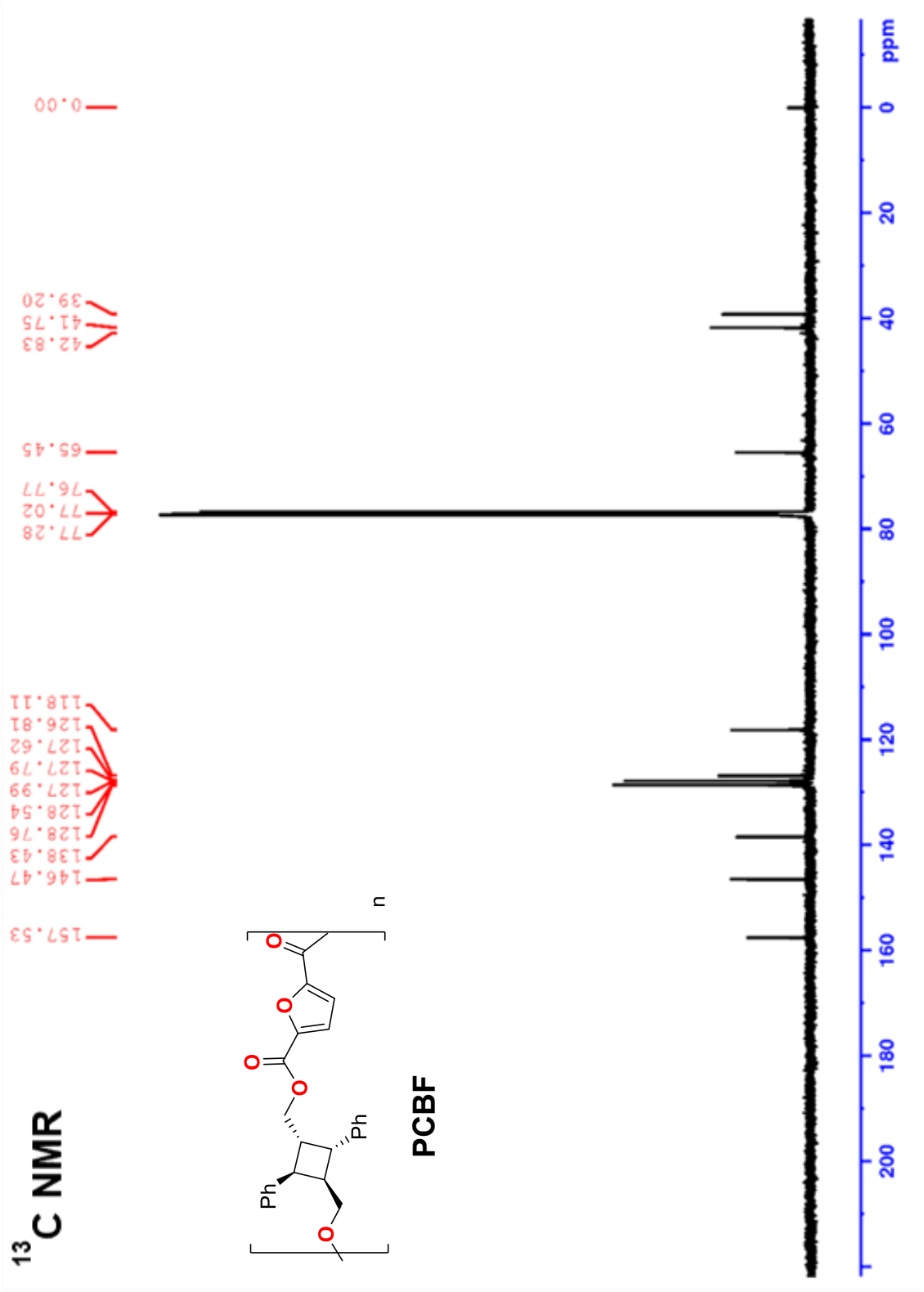

Figure A.23. $^{13}C\{^{1}H\}$ NMR spectrum of PCBF in $CDCl_3$ at room temperature.

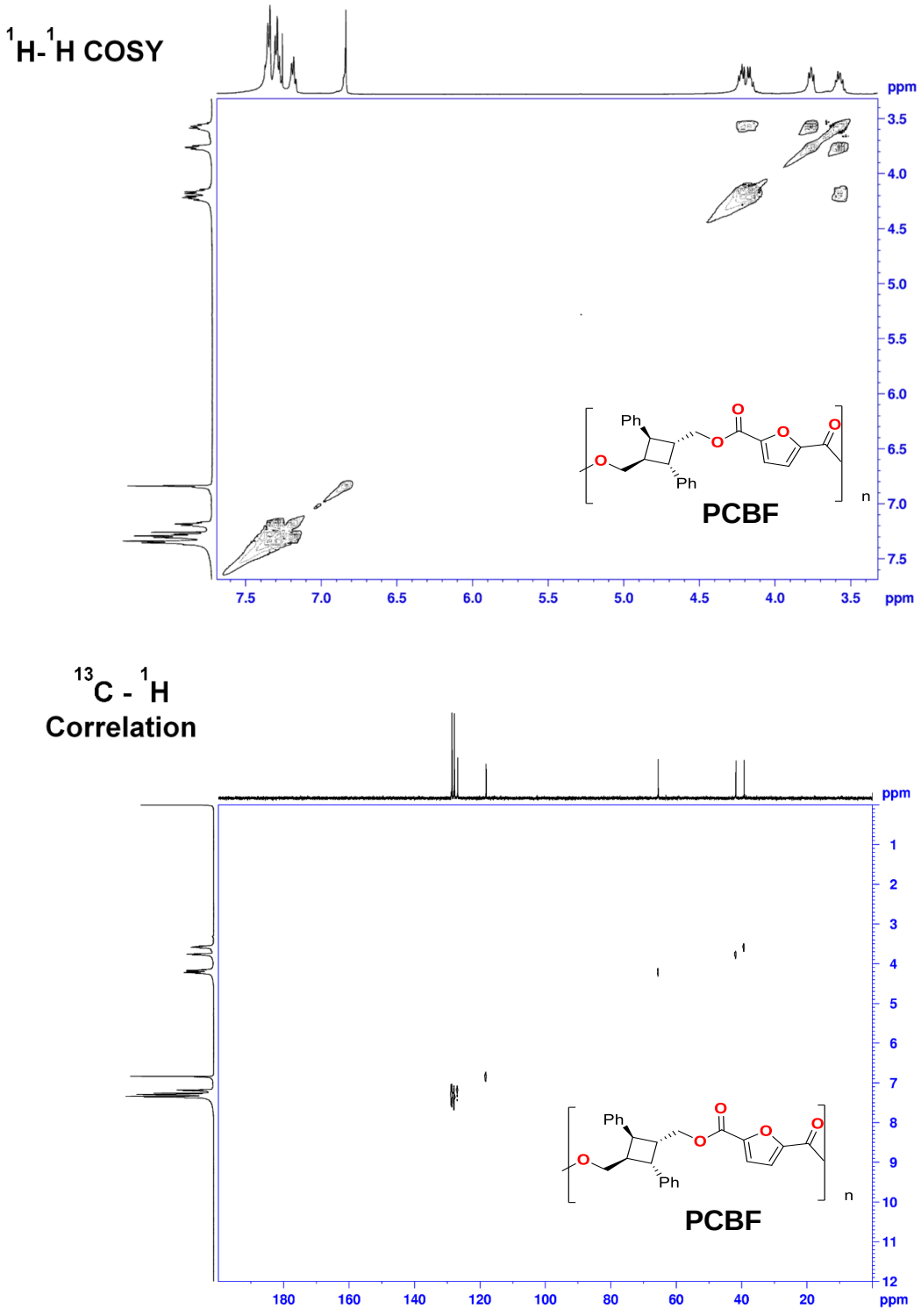

Figure A.24. COSY and CH-correlation spectra of PCBF in $CDCl_3$ at room temperature.

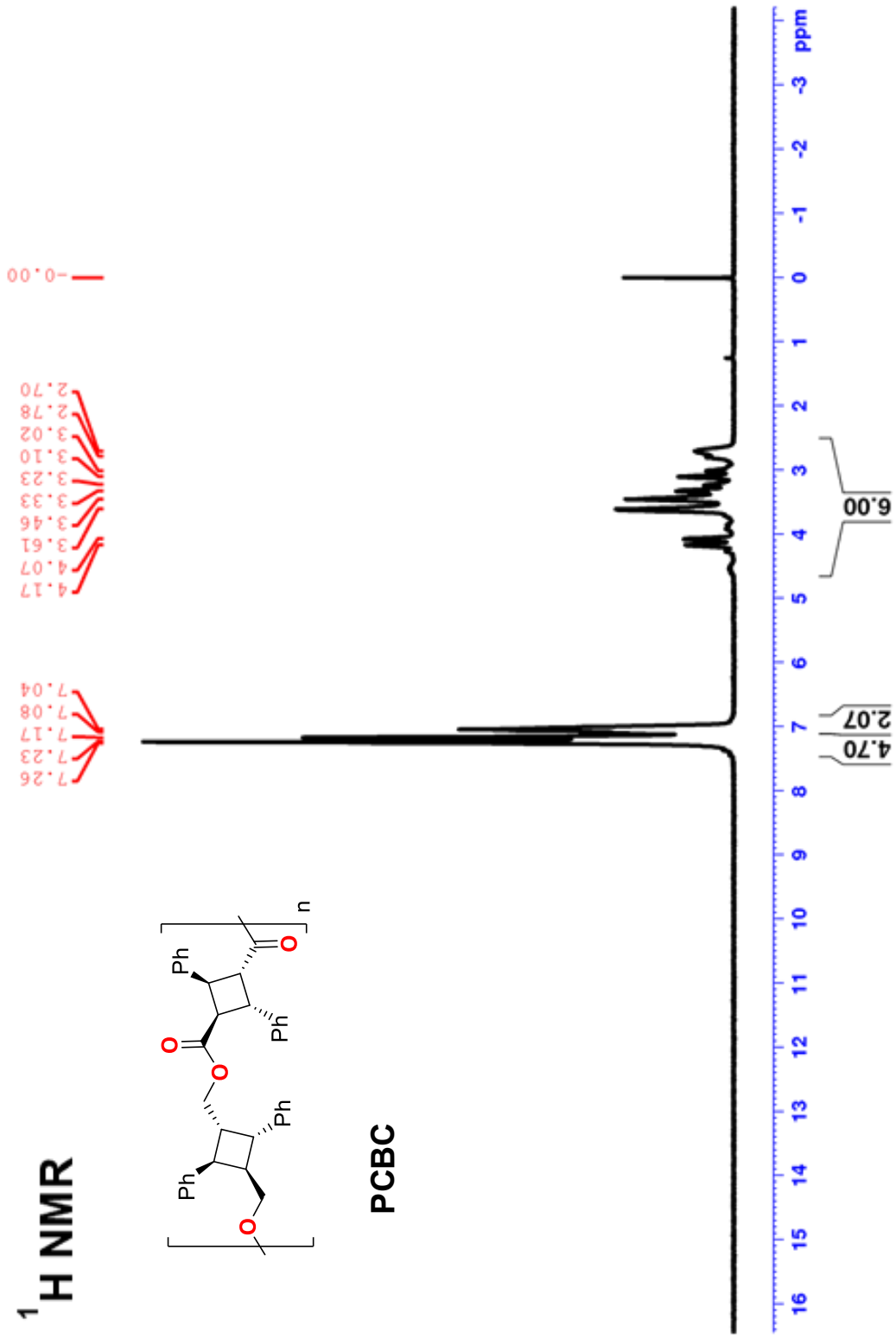

Figure A.25. ^{1}H NMR spectrum of PCBC in $CDCl_3$ at room temperature.

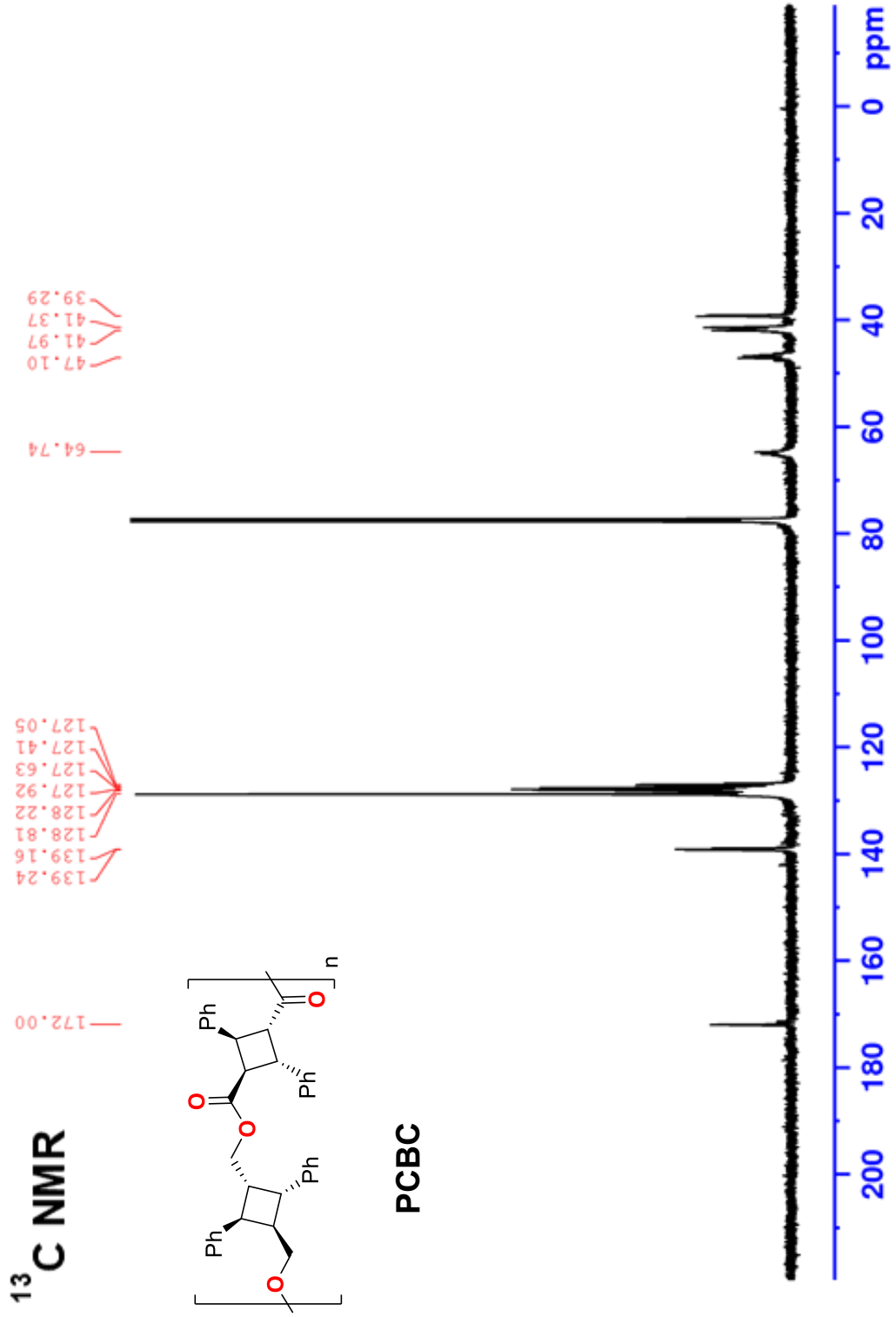

Figure A.26. $^{13}C\{^{1}H\}$ NMR spectrum of PCBC in $CDCl_3$ at room temperature.

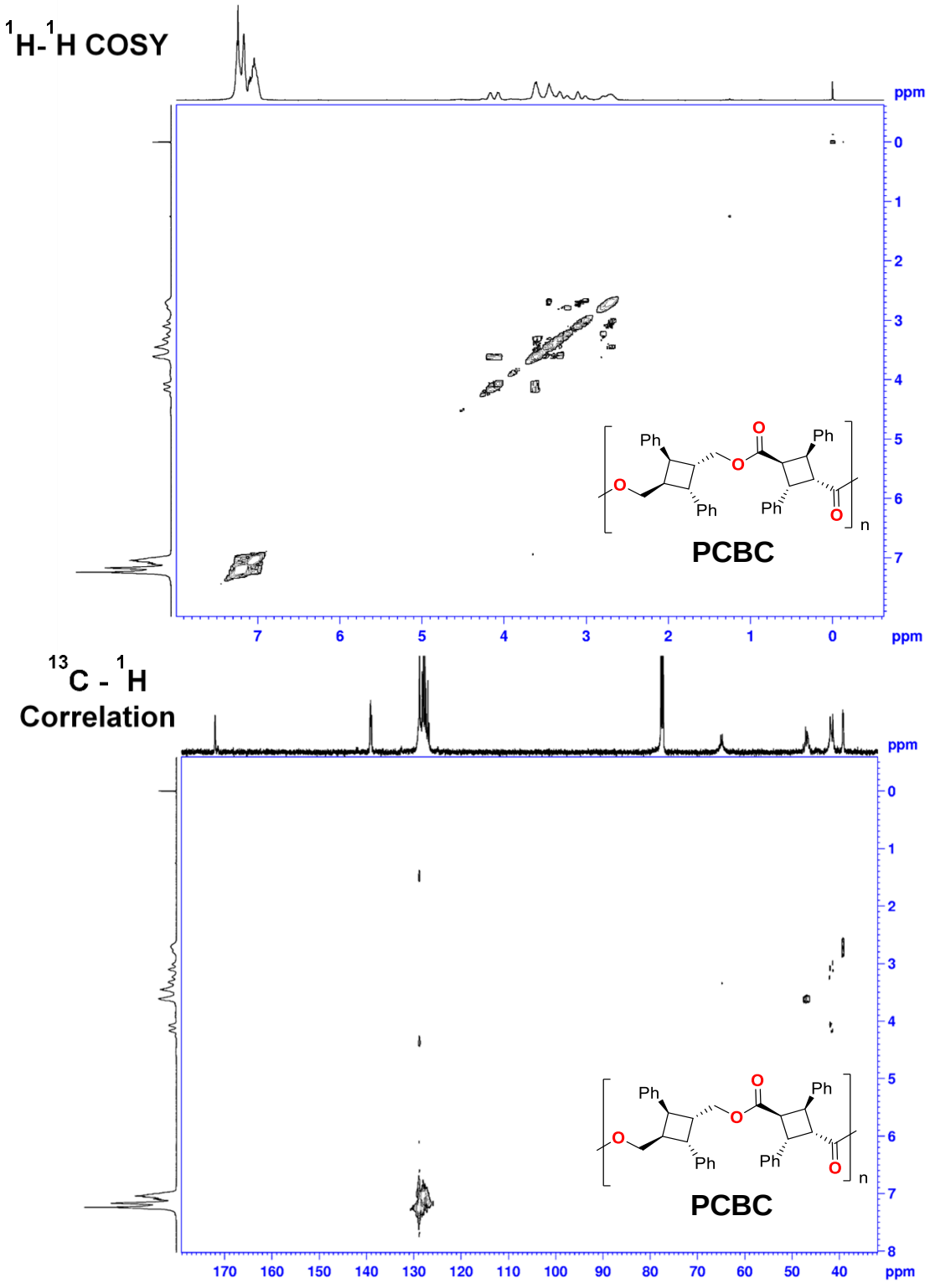

Figure A.27. COSY and CH-correlation spectra of PCBC in $CDCl_3$ at room temperature.

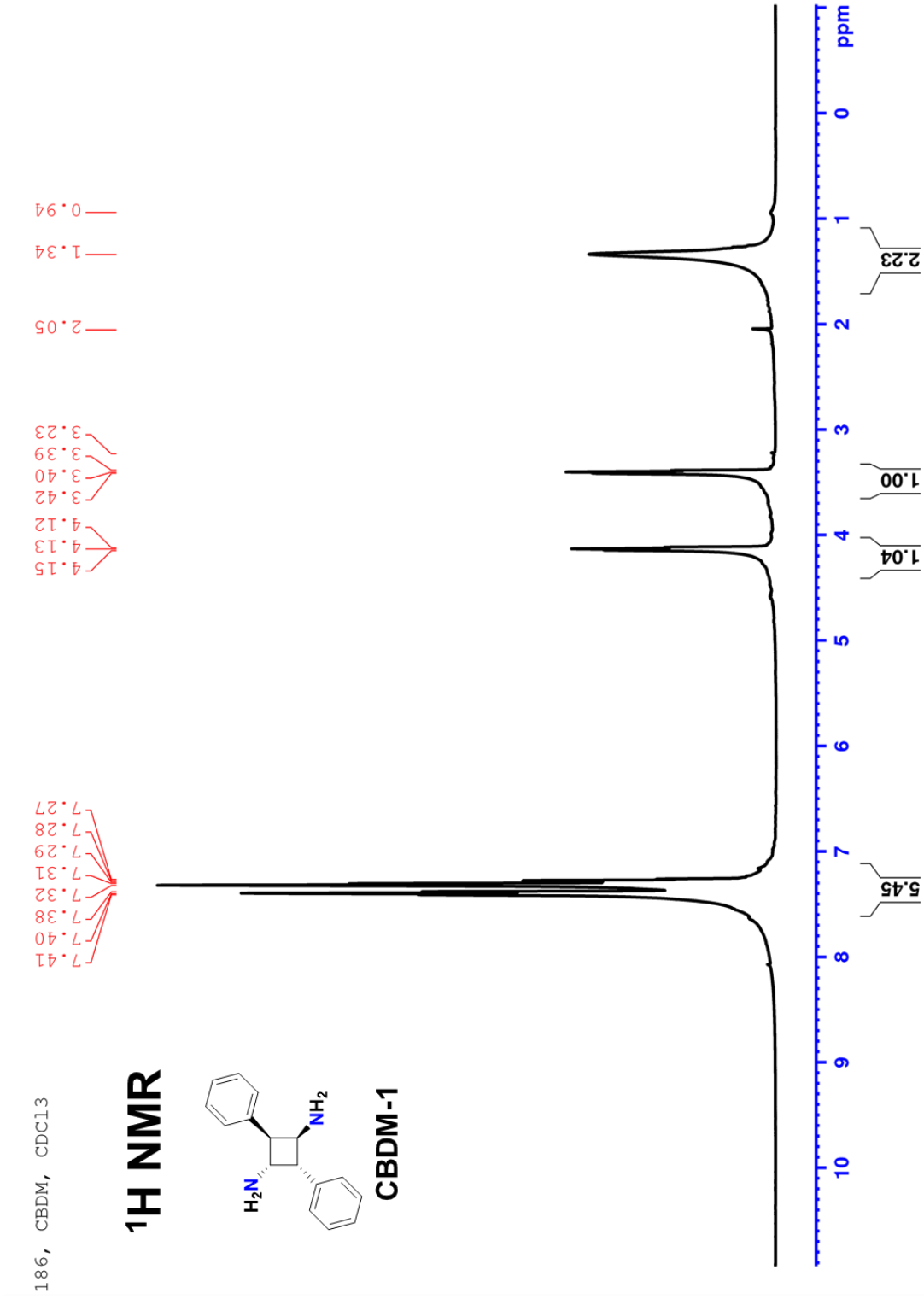

Figure A.28. ^{1}H NMR spectrum of CBAM-1 in DSMO-d_6 at room temperature.

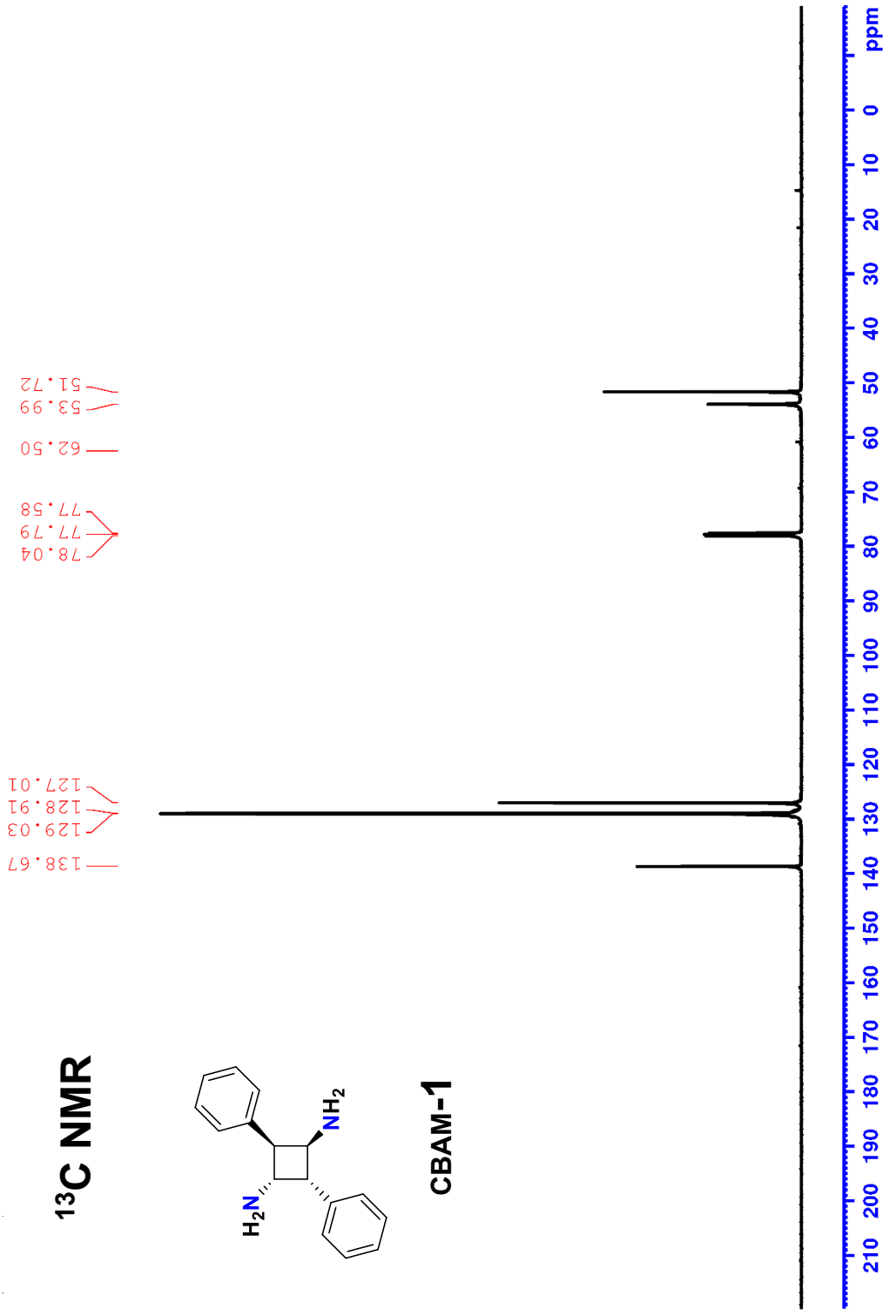

Figure A.29. $^{13}C\{^{1}H\}$ NMR spectrum of CBAM-1 in DSMO-d_6 at room temperature.

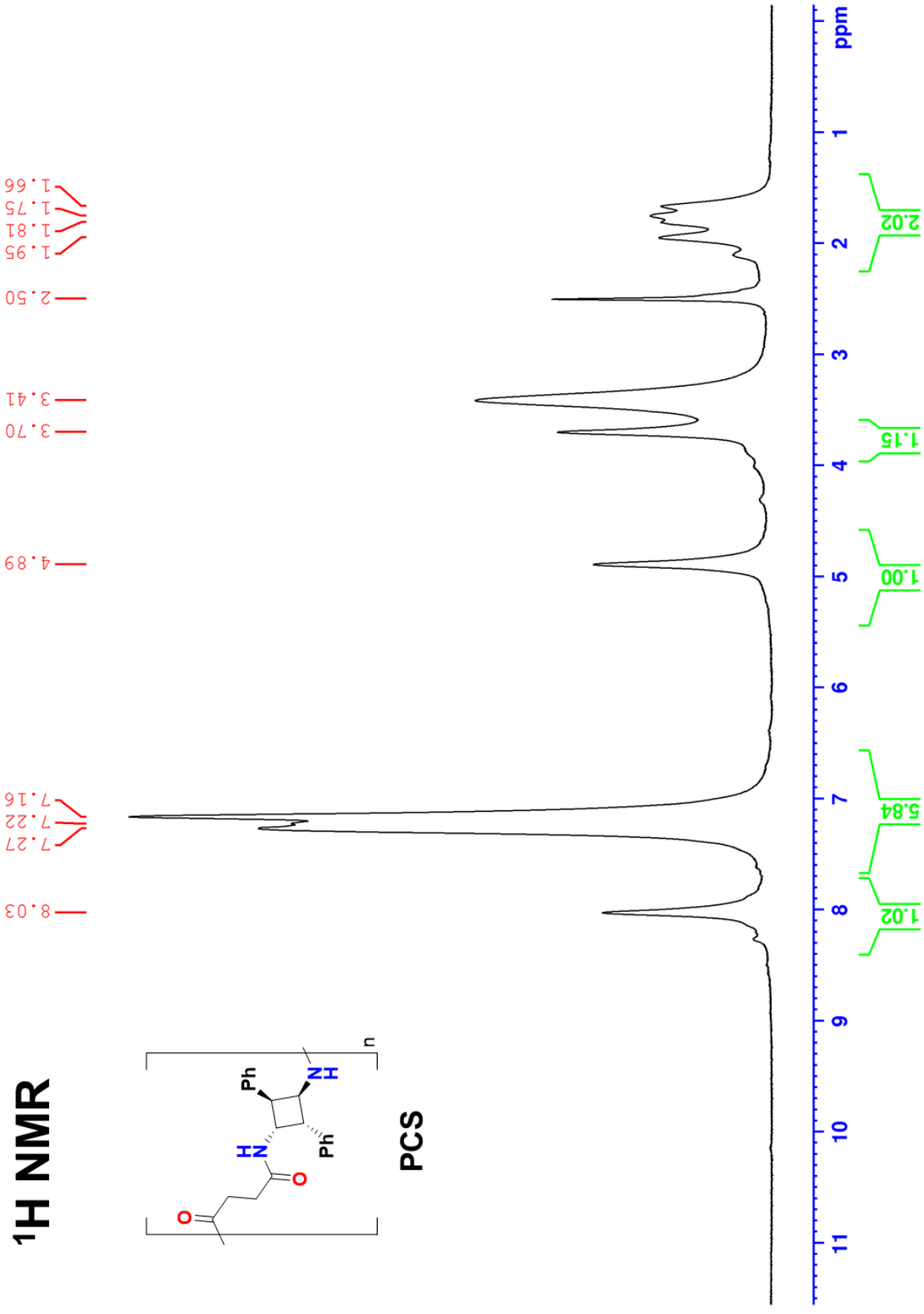

Figure A.30. ^{1}H NMR spectrum of PCS in DSMO-d_6 at room temperature.

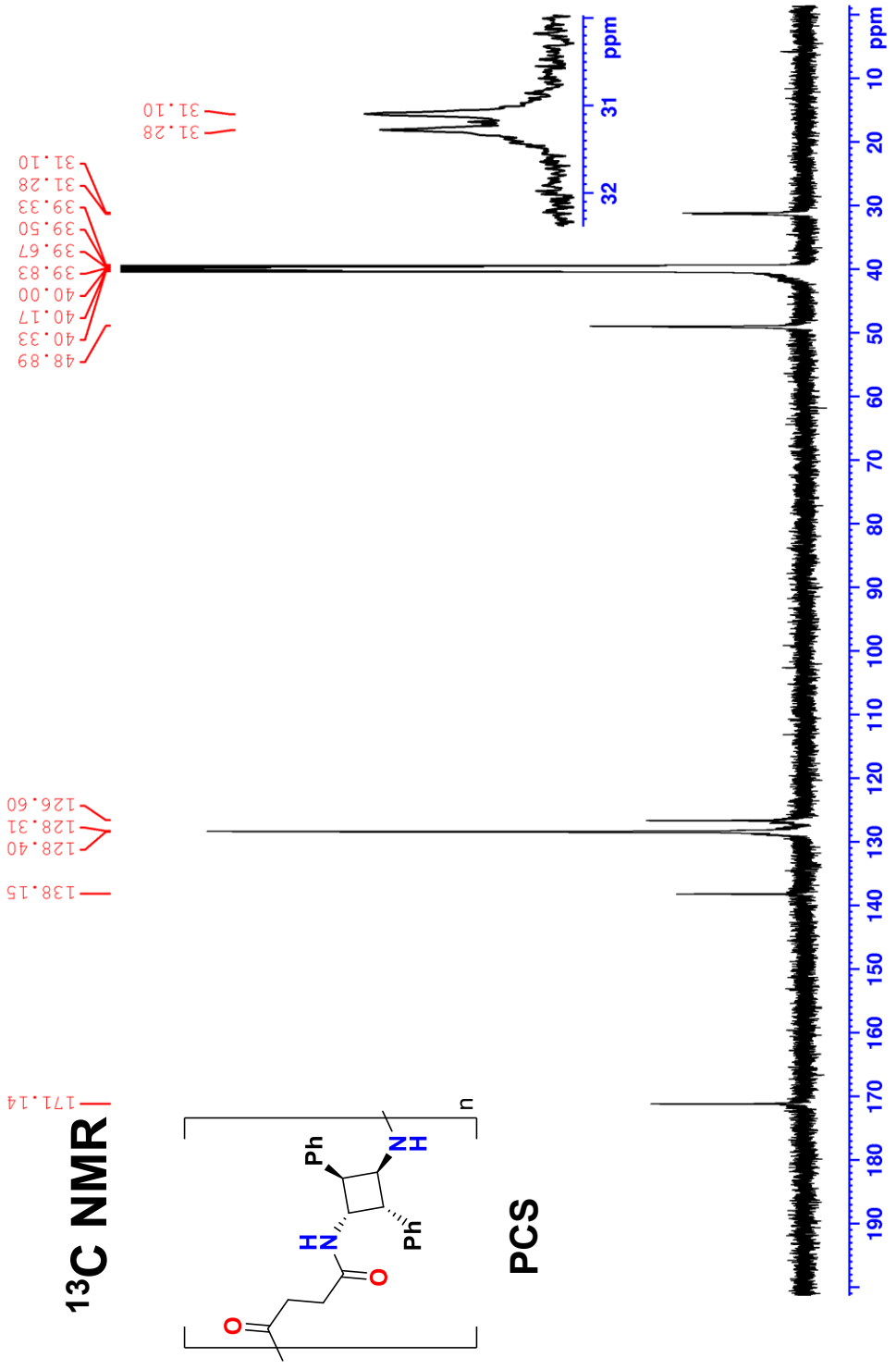

Figure A.31. $^{13}C\{^{1}H\}$ NMR spectrum of PCS in DSMO-d_6 at room temperature.

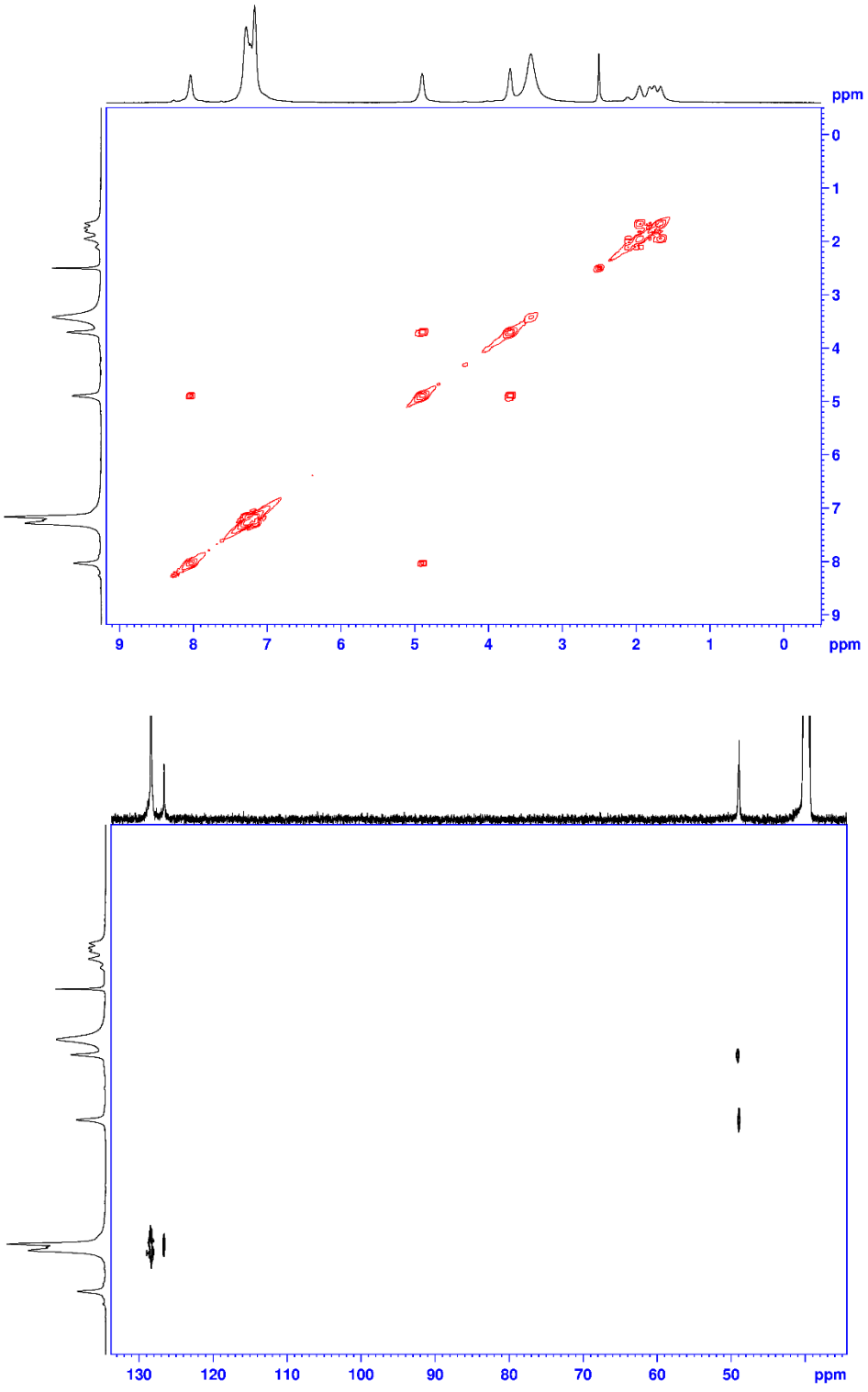

Figure A.32. COSY and CH-correlation spectra of PCS in DSMO-d_6 at room temperature.

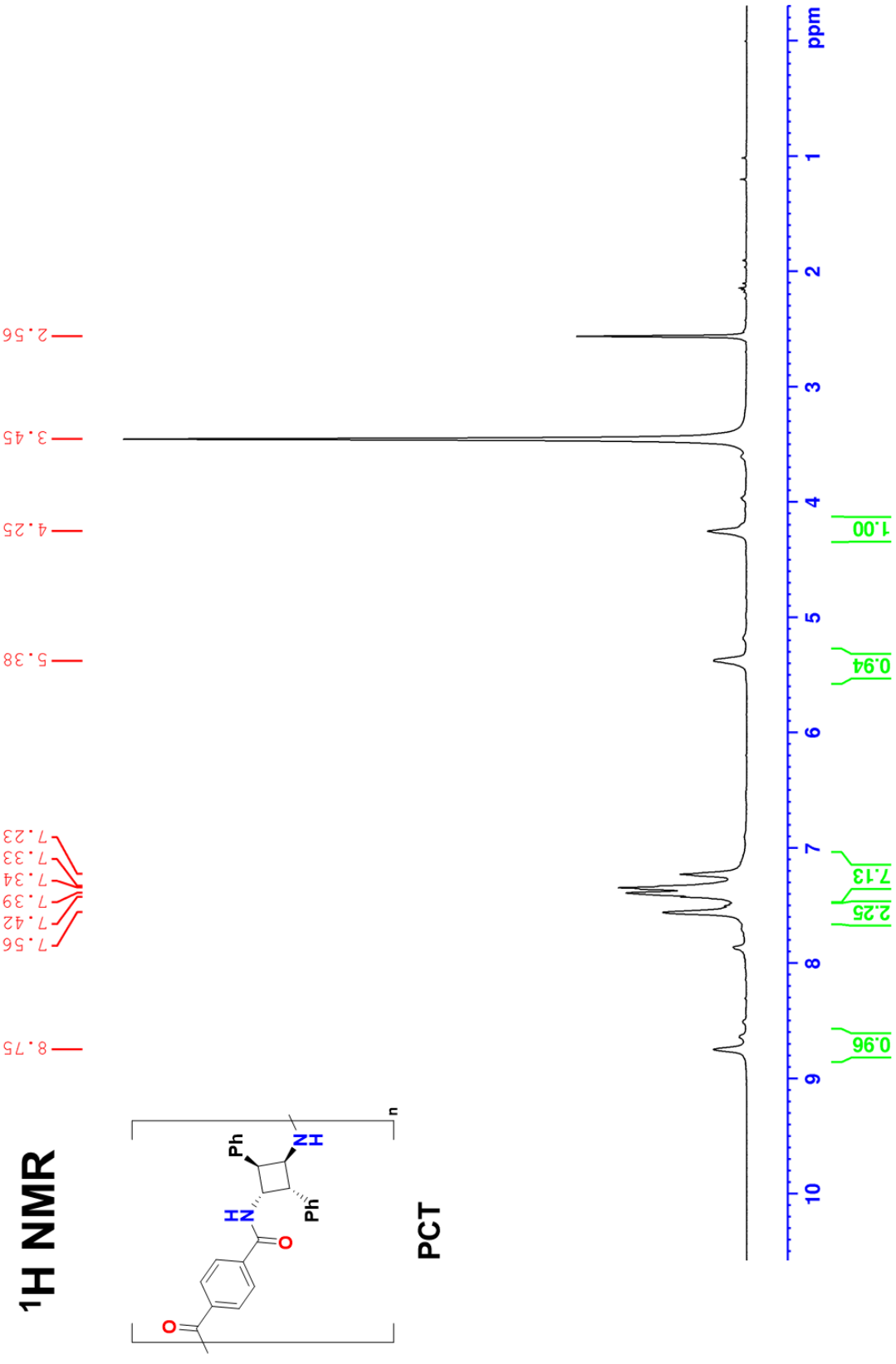

Figure A.33. ^{1}H NMR spectrum of PCT in DSMO-d_6 at room temperature.

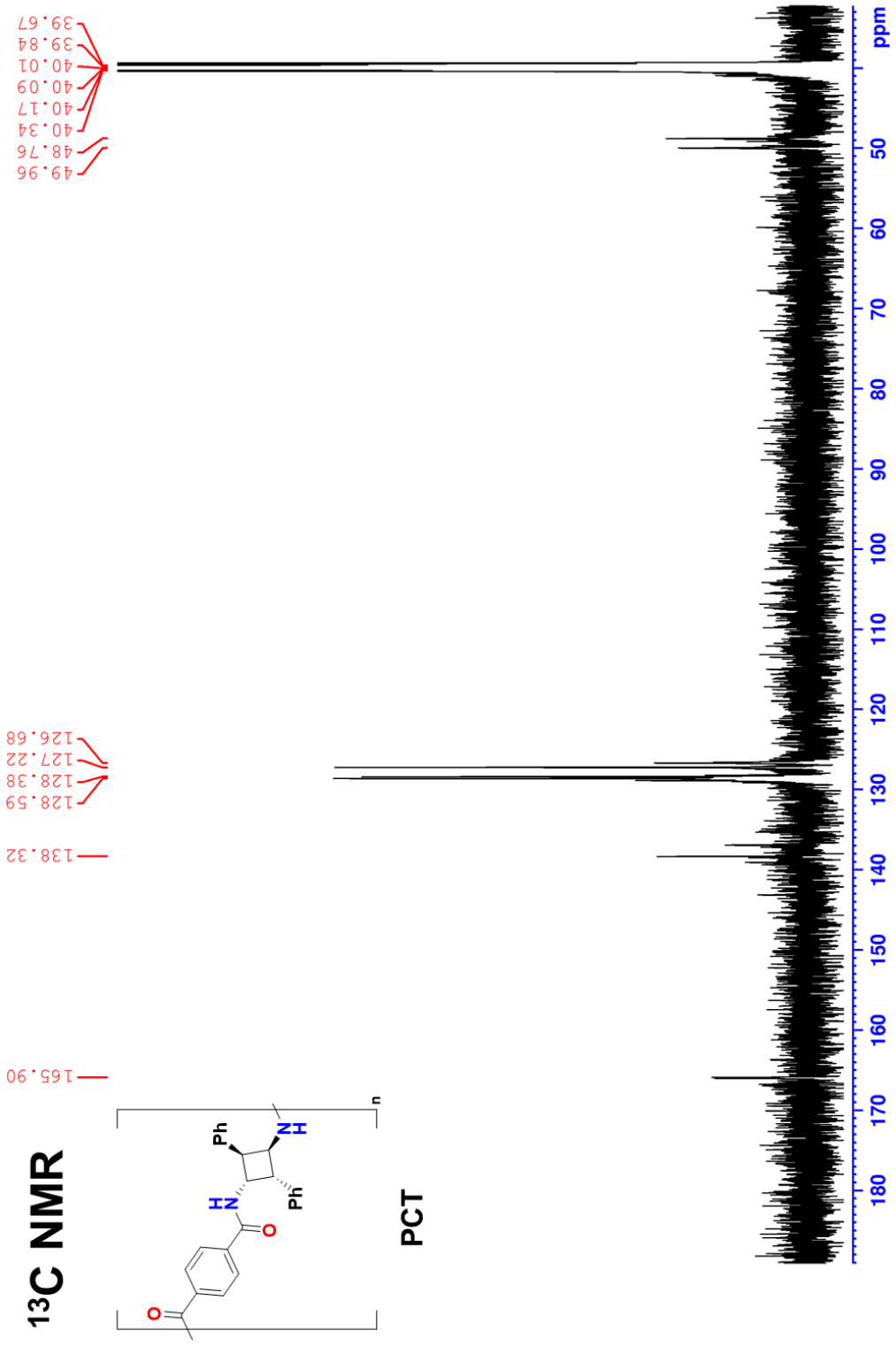

Figure A.34. $^{13}C\{^{1}H\}$ NMR spectrum of PCT in DSMO-d_6 at room temperature.

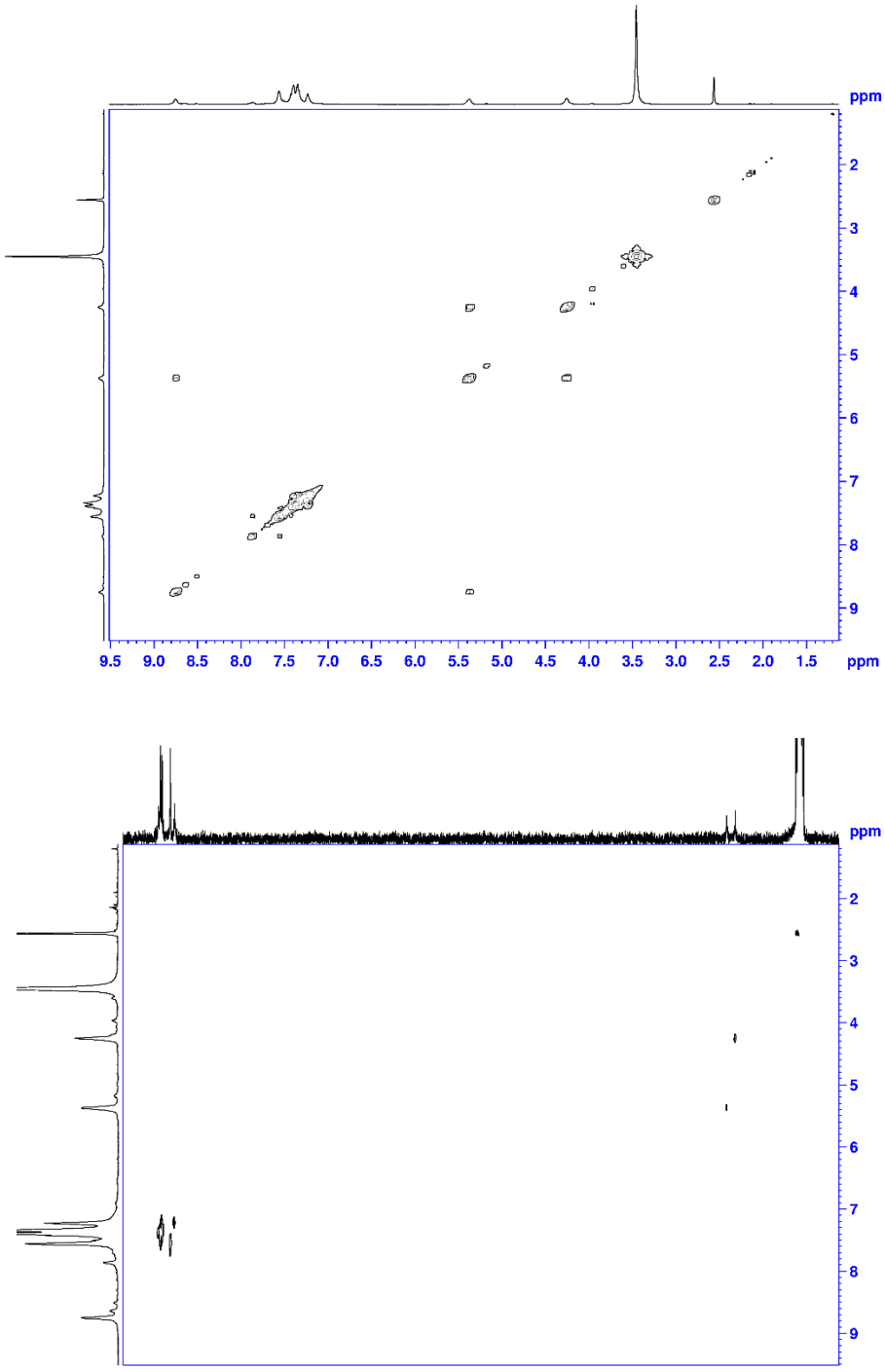

Figure A.35. COSY and CH-correlation spectra of PCT in DMSO-d_6 at room temperature.

Appendix B

Selected FT-IR spectra

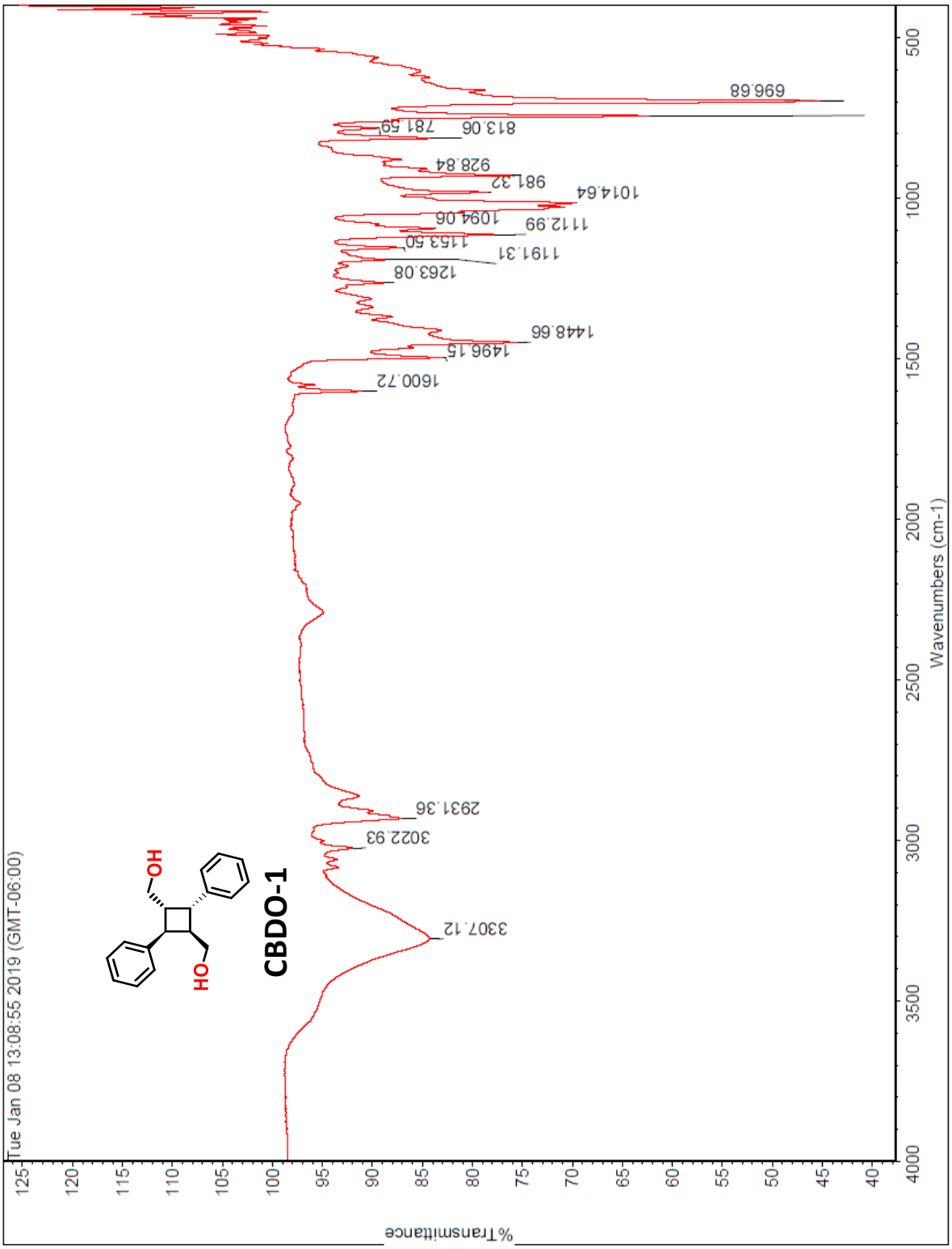

Figure B.1. FT-IR spectrum of CBDO-1 using ATR detector.

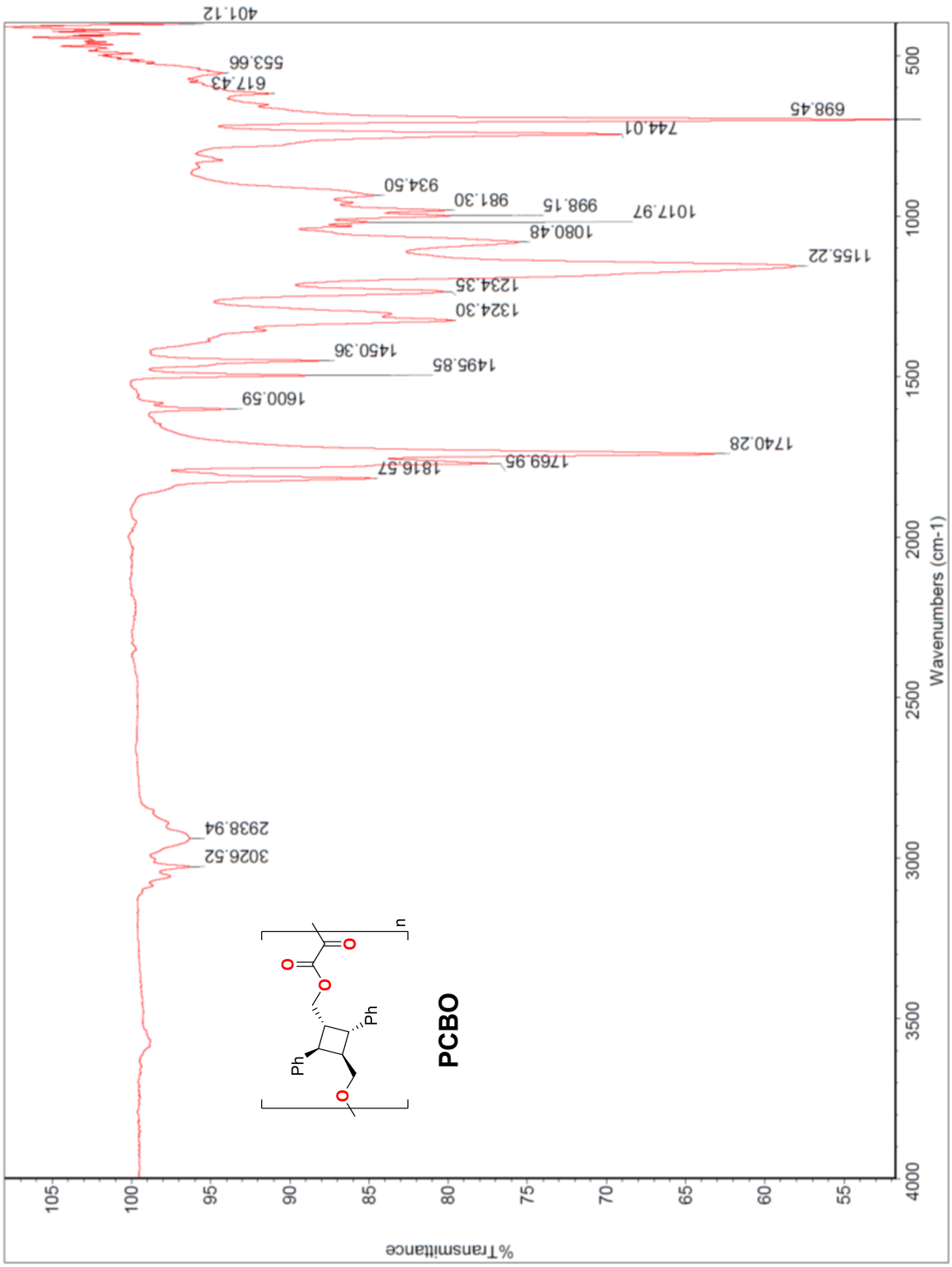

Figure B.2. FT-IR spectrum of PCBO using ATR detector.

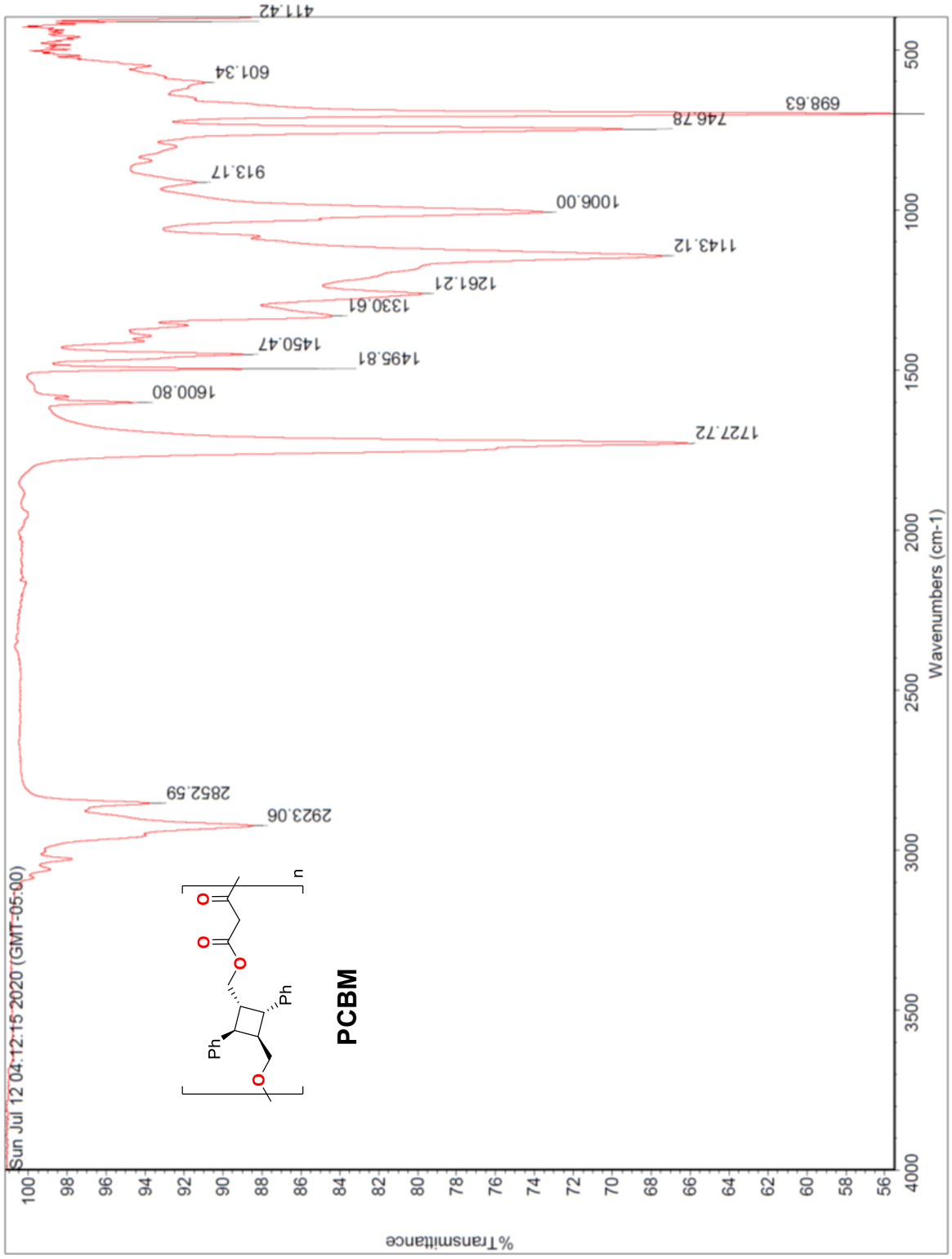

Figure B.3. FT-IR spectrum of PCBM using ATR detector.

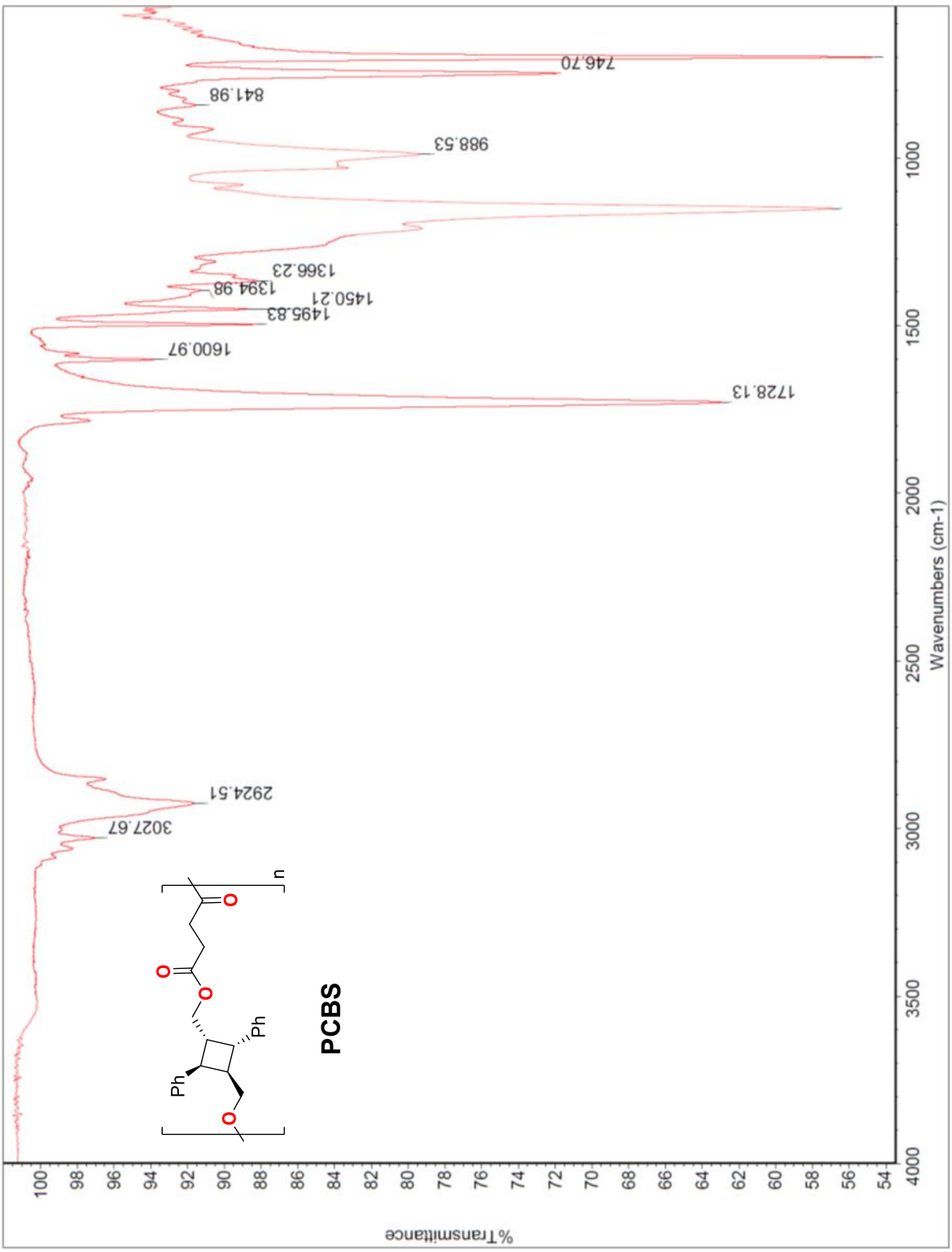

Figure B.4. FT-IR spectrum of PCBS using ATR detector.

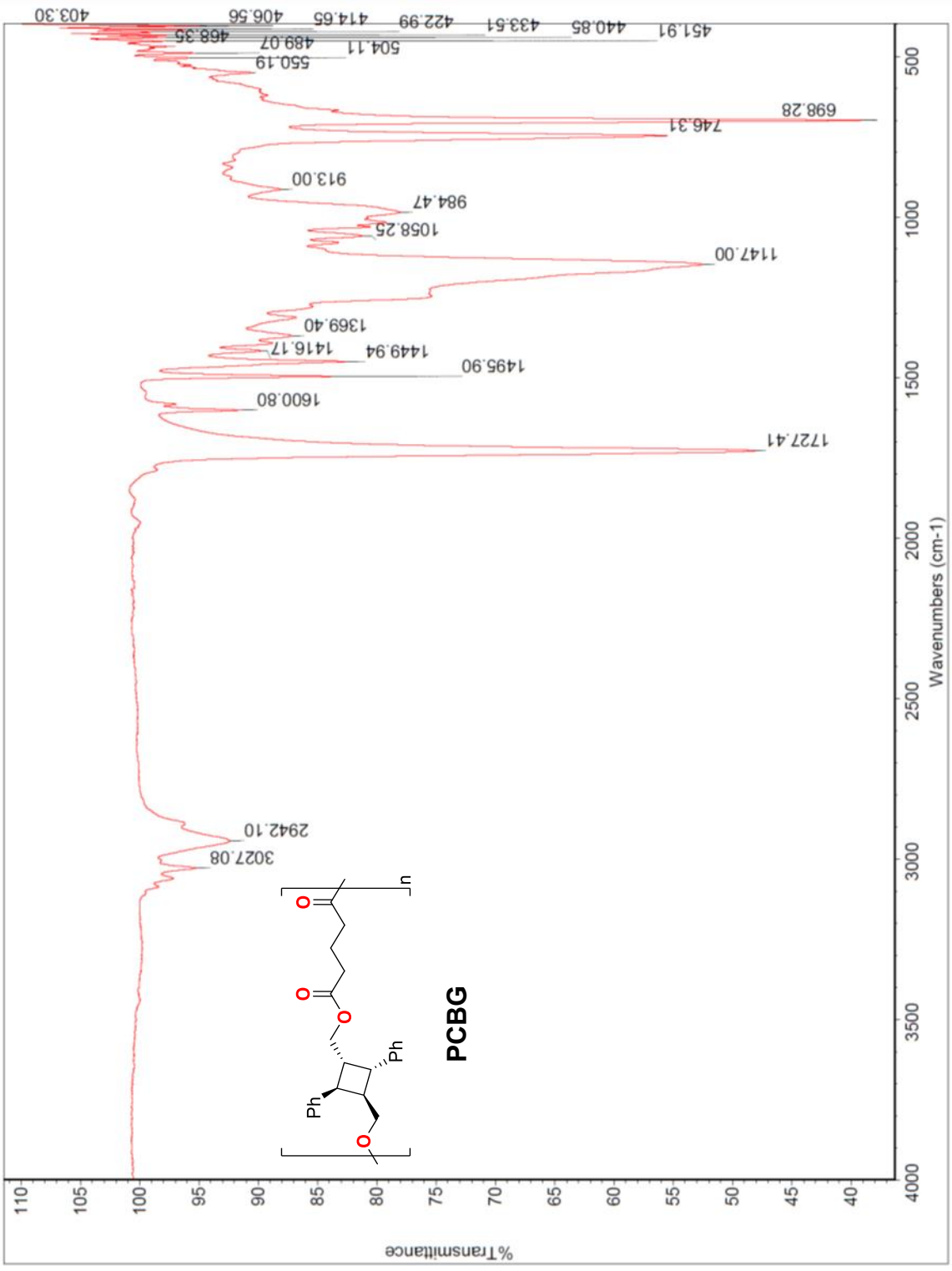

Figure B.5. FT-IR spectrum of PCBG using ATR detector.

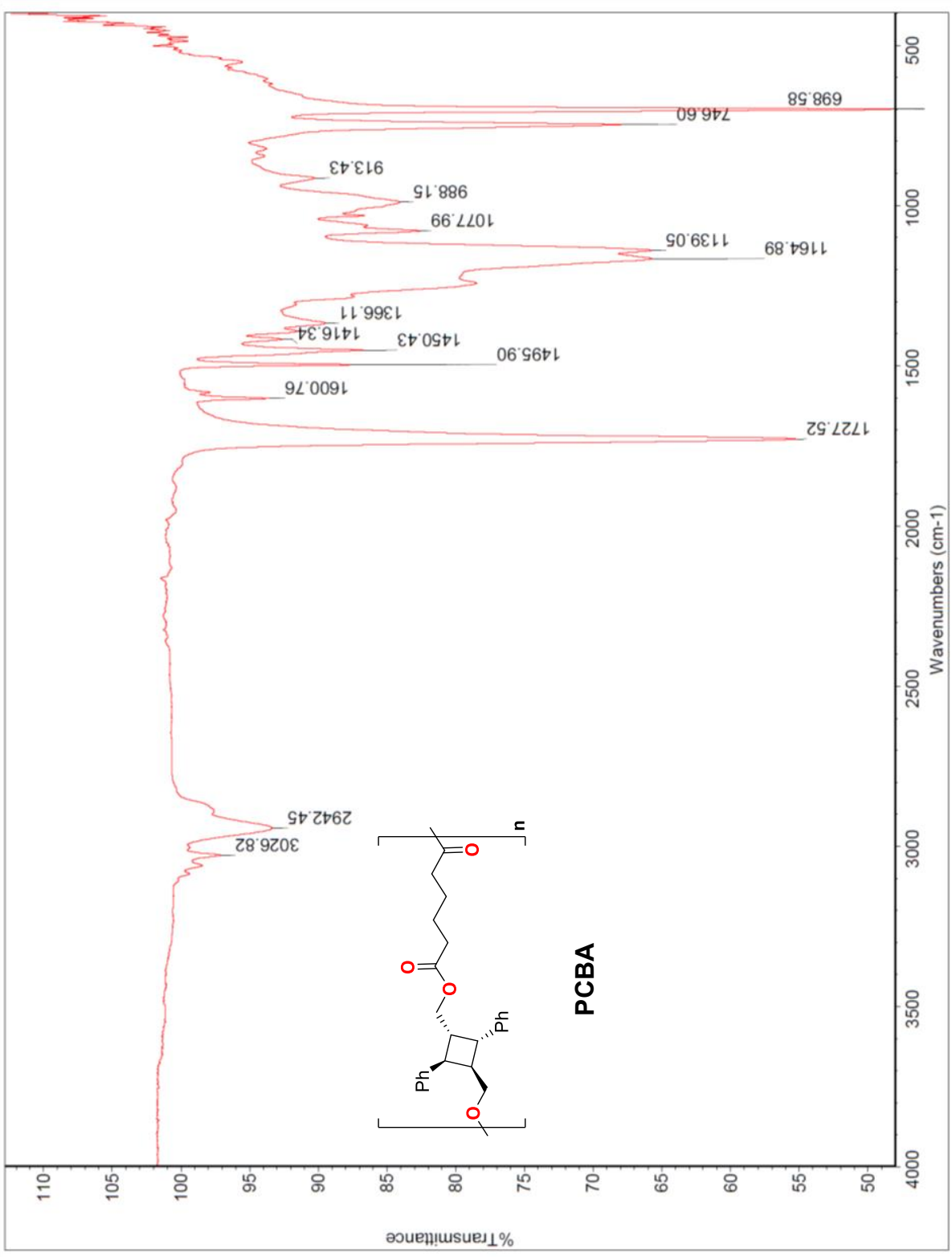

Figure B.6. FT-IR spectrum of PCBA using ATR detector.

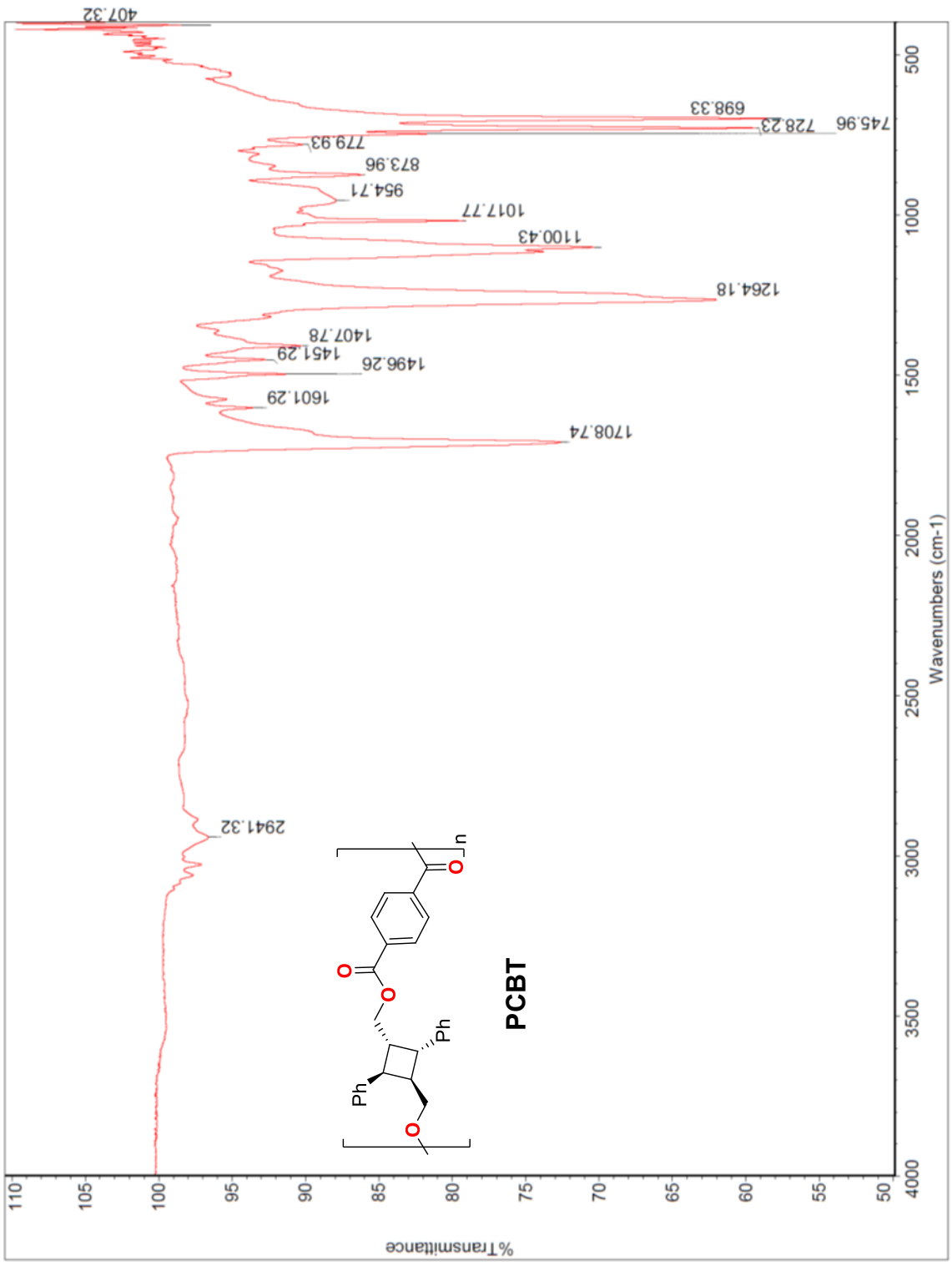

Figure B.7. FT-IR spectrum of PCBT using ATR detector.

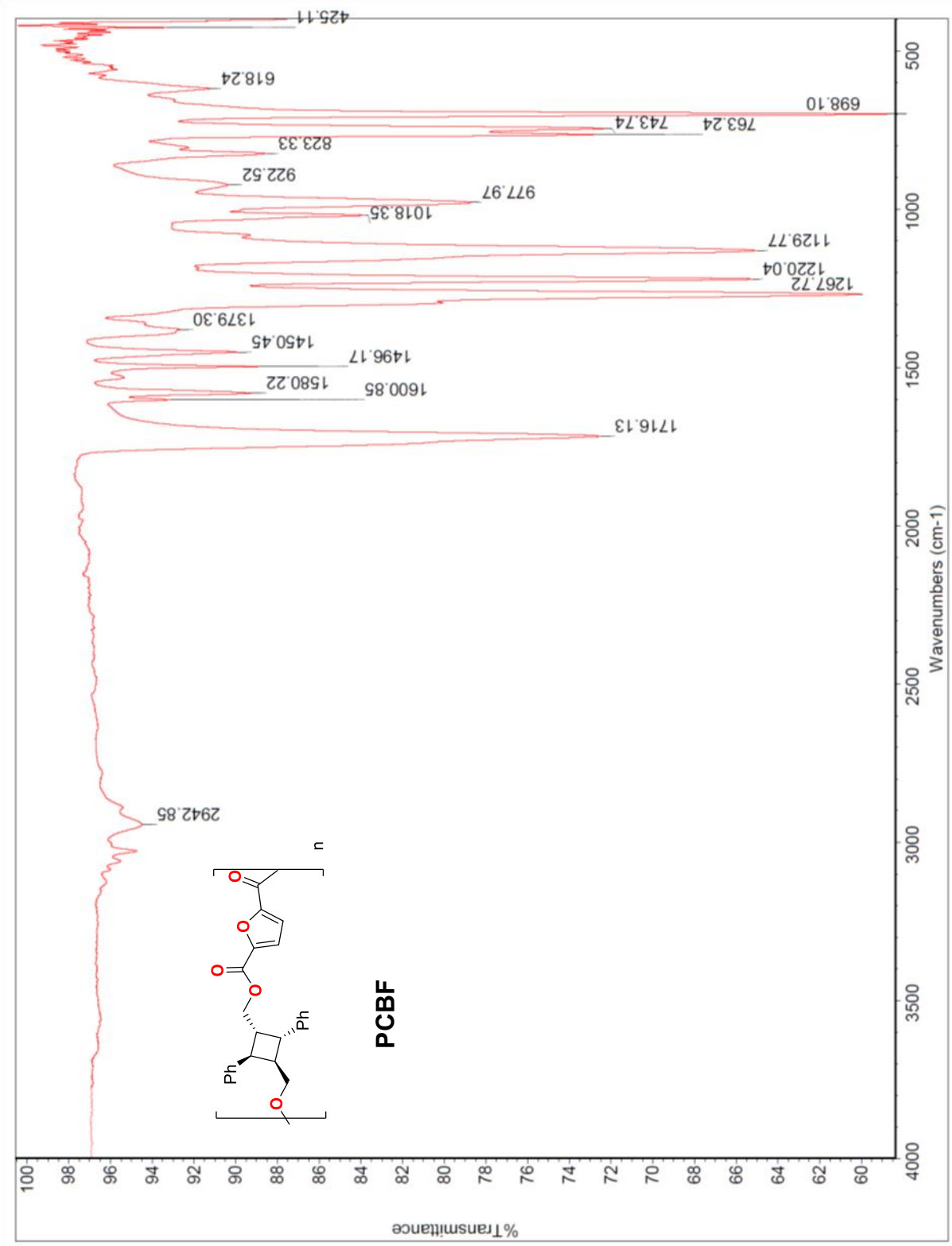

Figure B.8. FT-IR spectrum of PCBF using ATR detector.

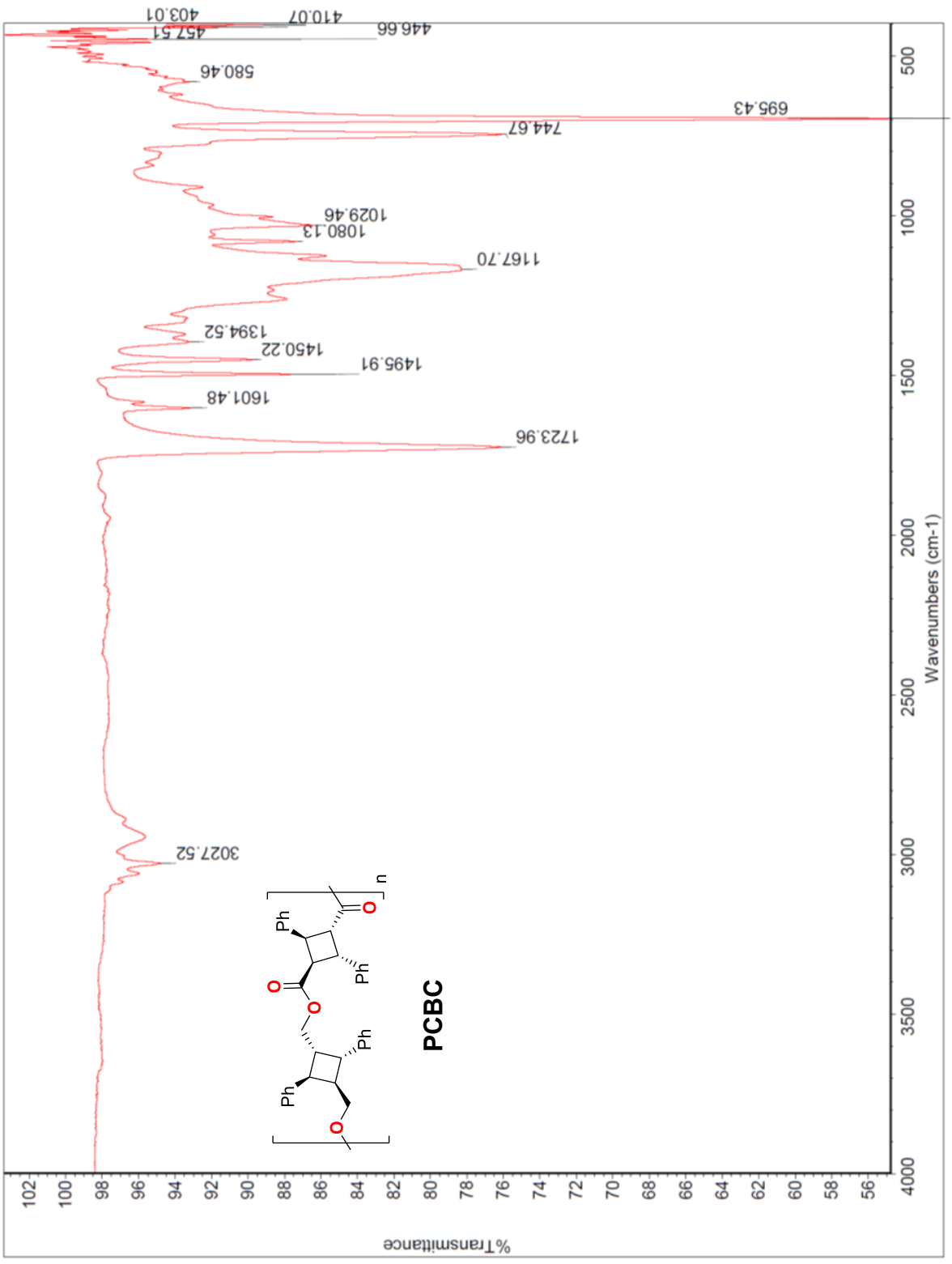

Figure B.9. FT-IR spectrum of PCBC using ATR detector.

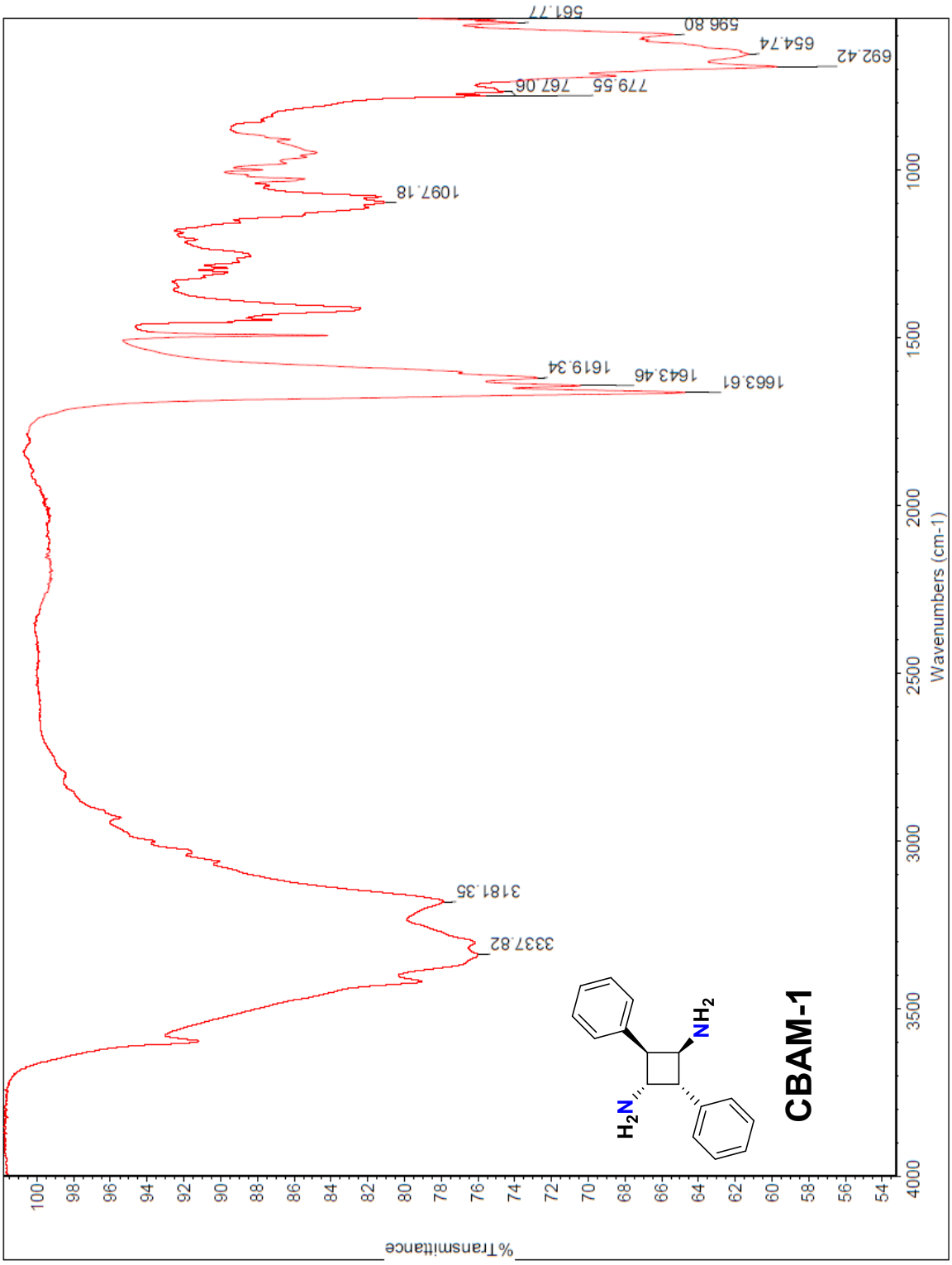

Figure B.10. FT-IR spectrum of CBAM-1 using ATR detector.

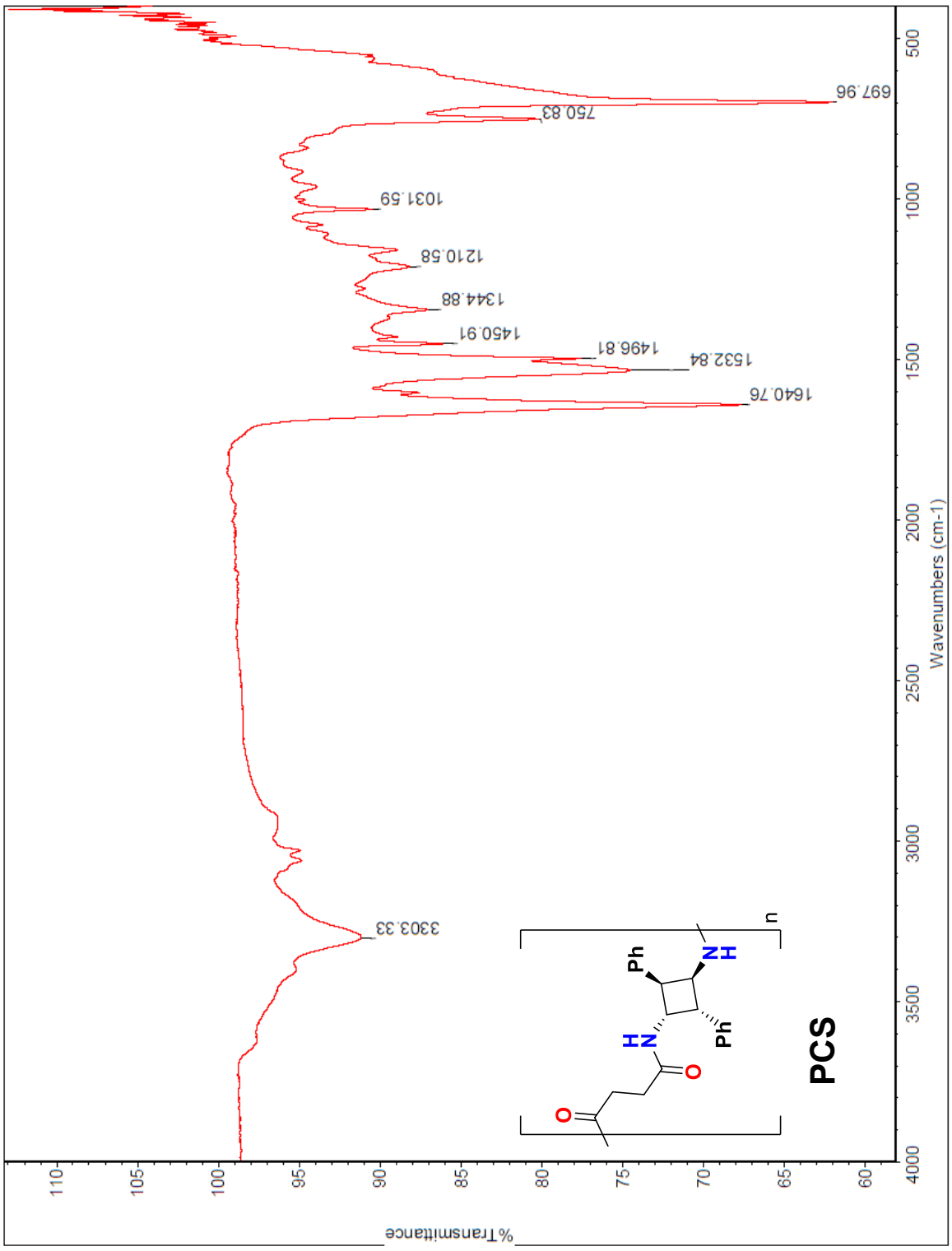

Figure B.11. FT-IR spectrum of PCS using ATR detector.

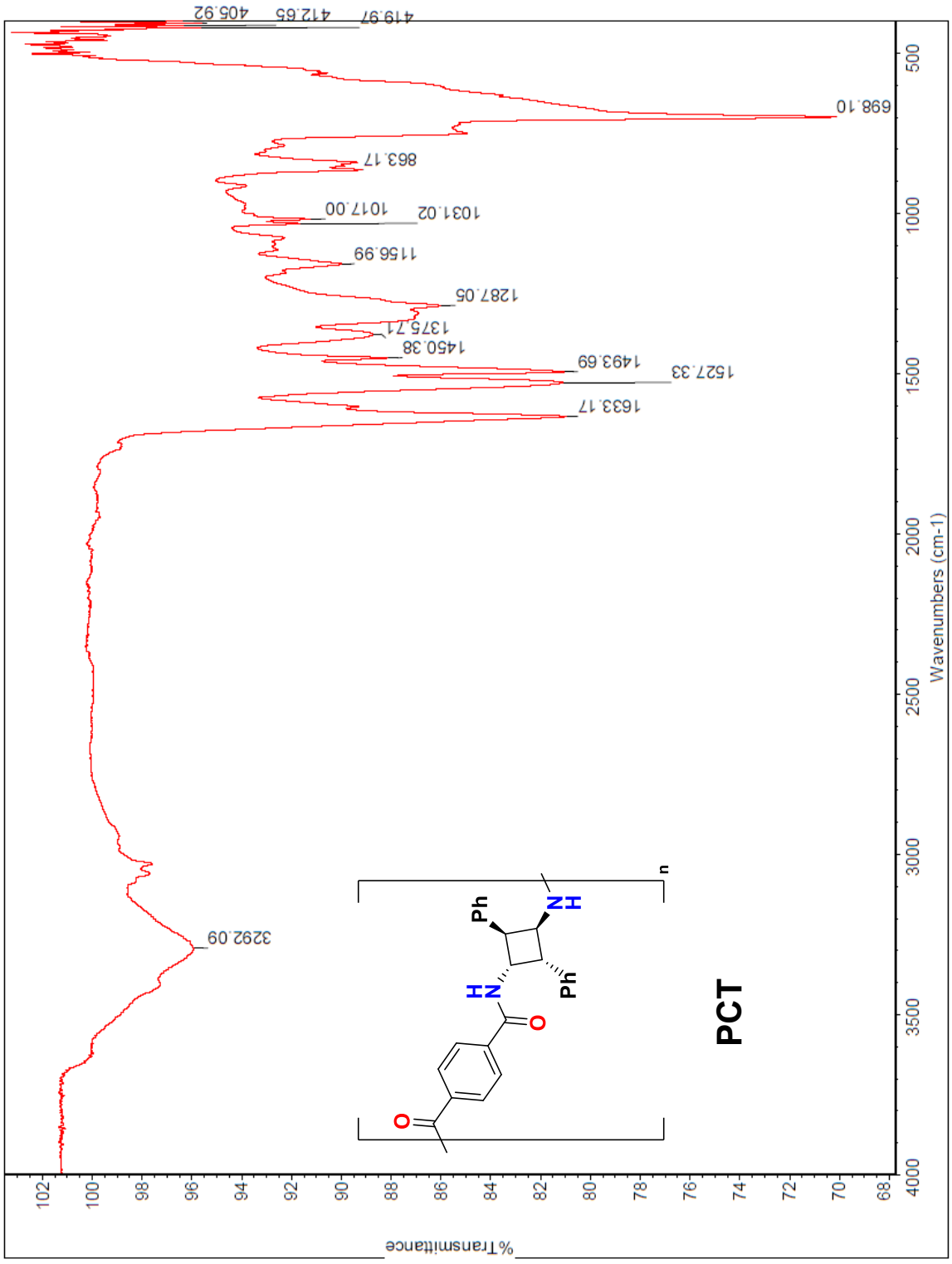

Figure B.12. FT-IR spectrum of PCT using ATR detector.

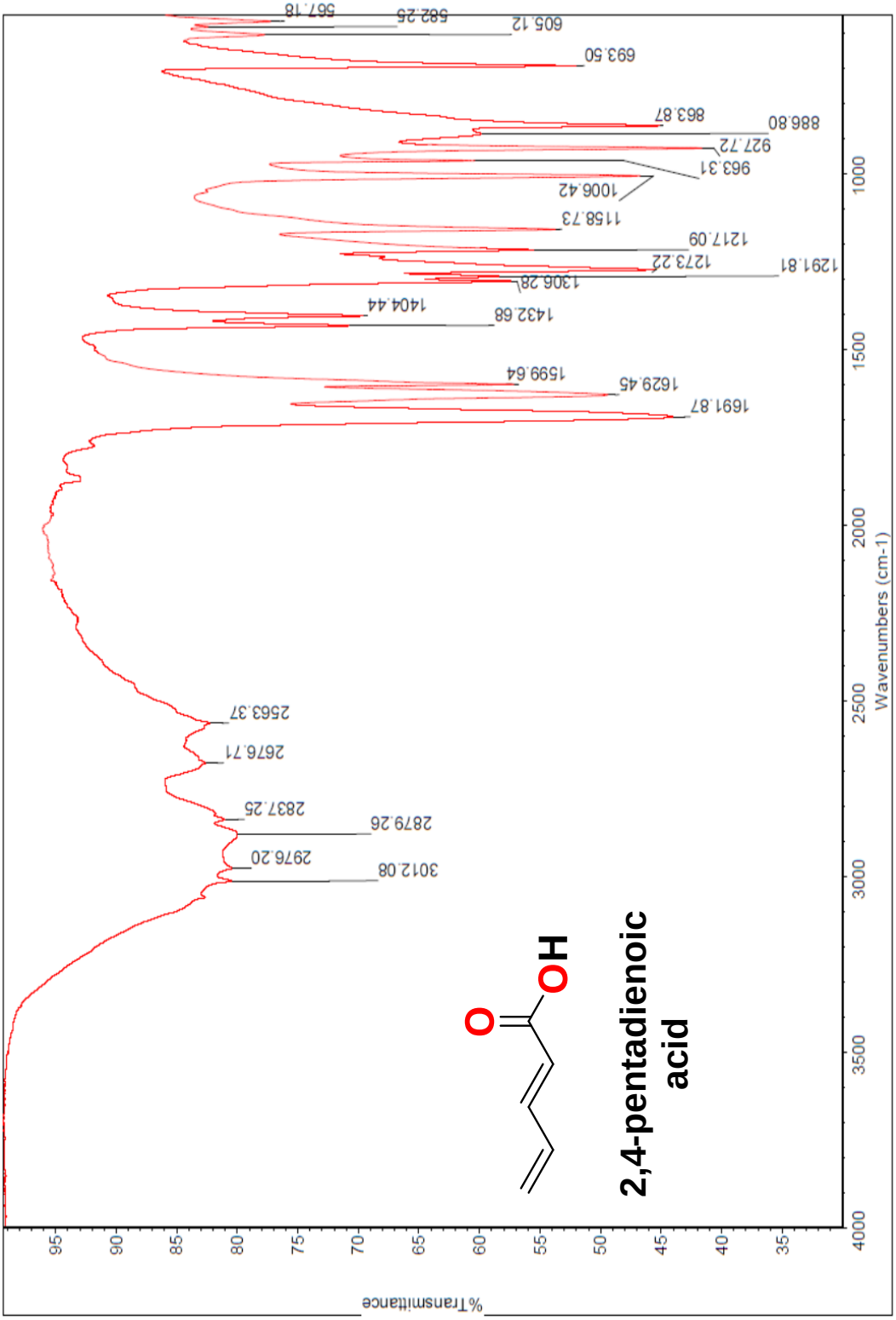

Figure B.13. FT-IR spectrum of 2,4-pentadienoic acid using ATR detector.

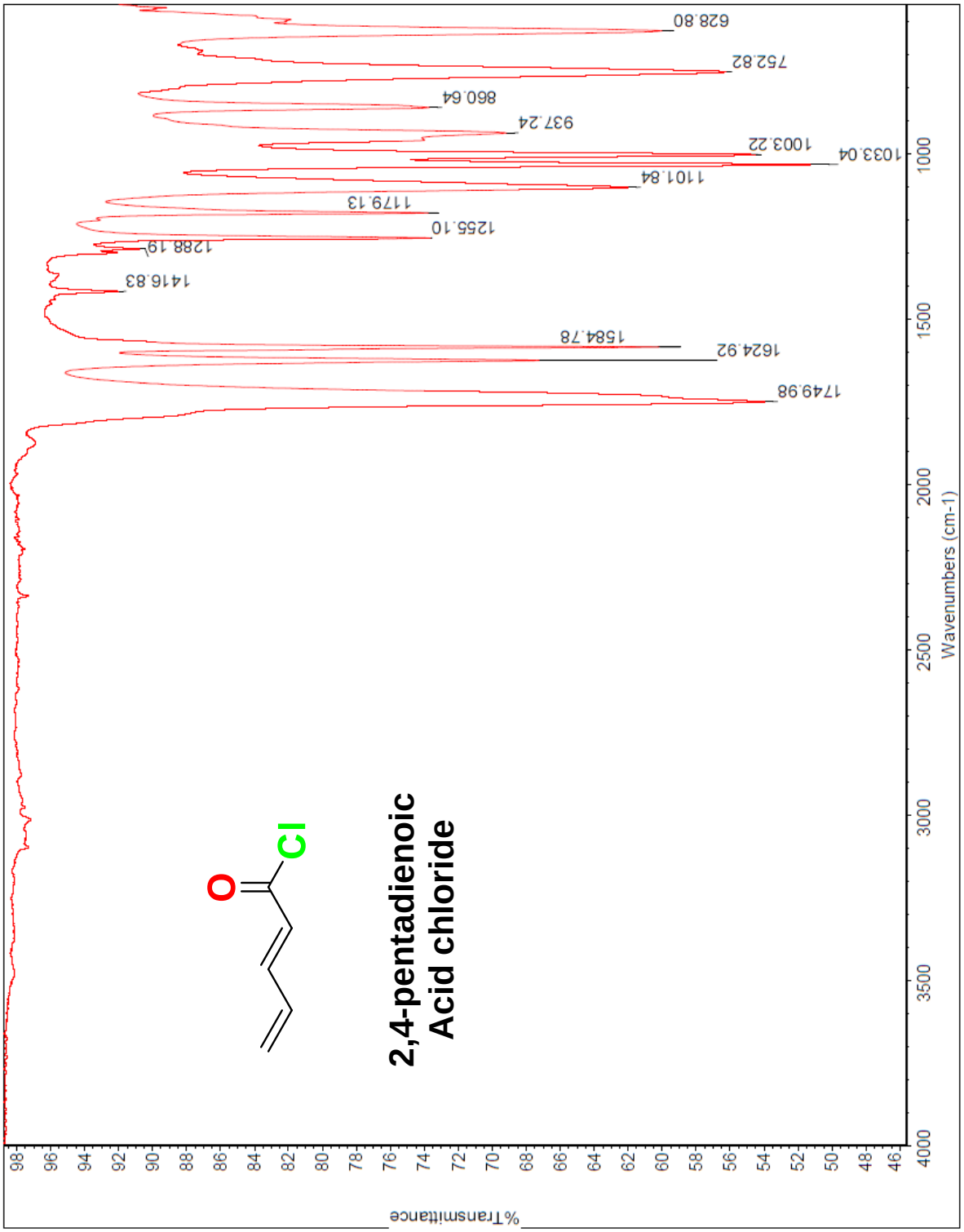

Figure B.14. FT-IR spectrum of 2,4-pentadienoic acid chloride using ATR detector.

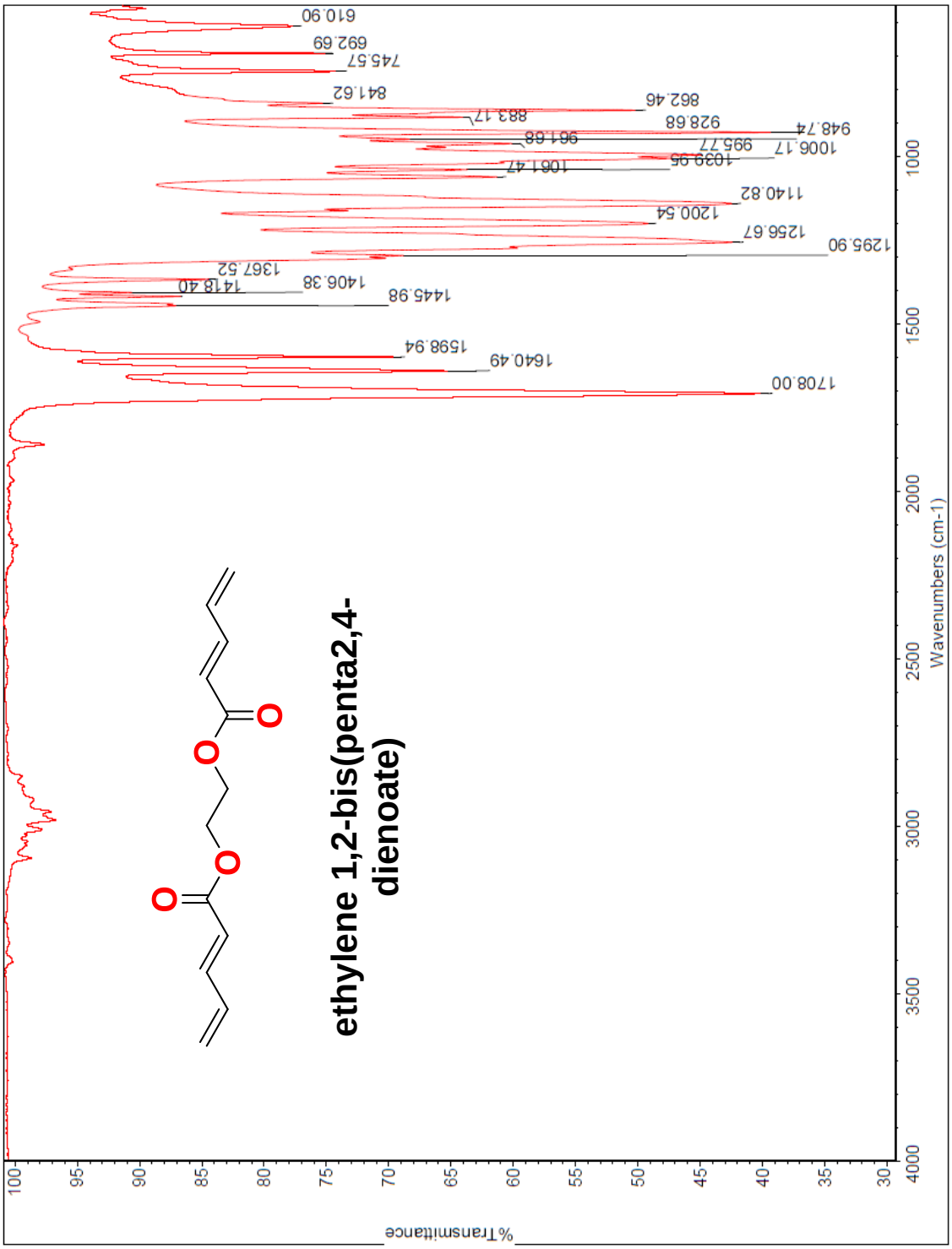

Figure B.15. FT-IR spectrum of EBP using ATR detector.

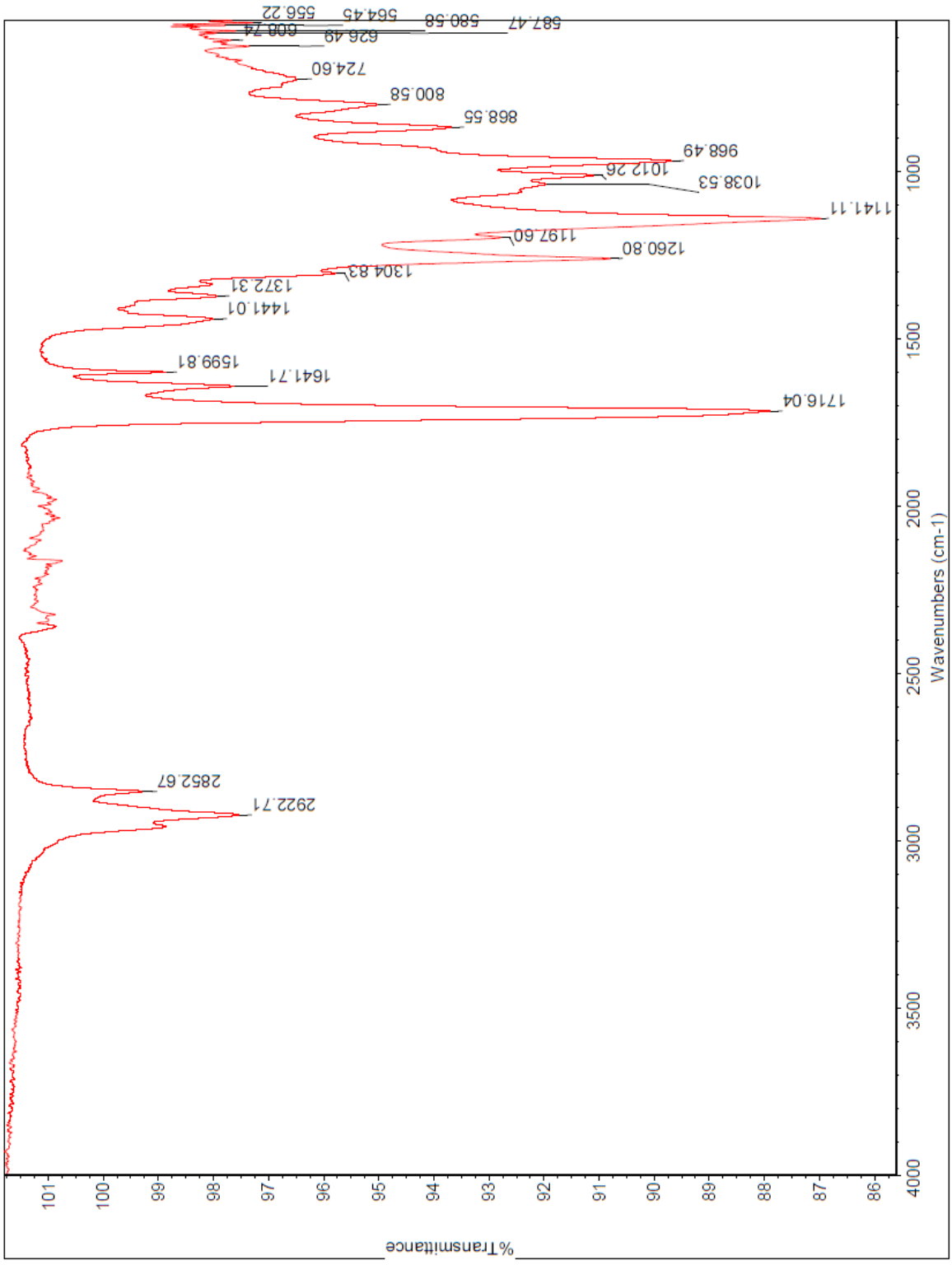

Figure B.16. FT-IR spectrum of EBP after heating at 40 °C using ATR detector.

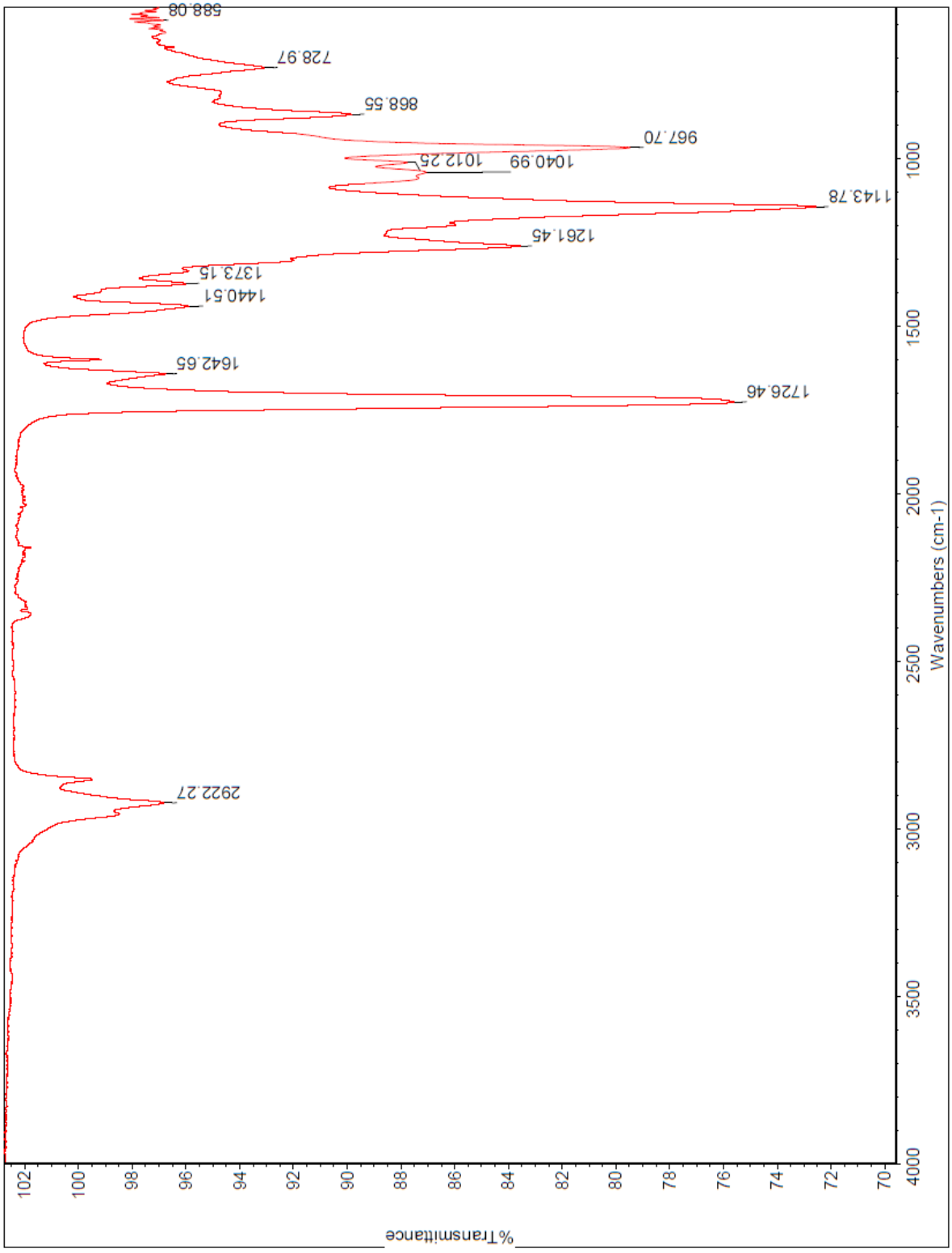

Figure B.17. FT-IR spectrum of EBP after heating at 50 °C using ATR detector.

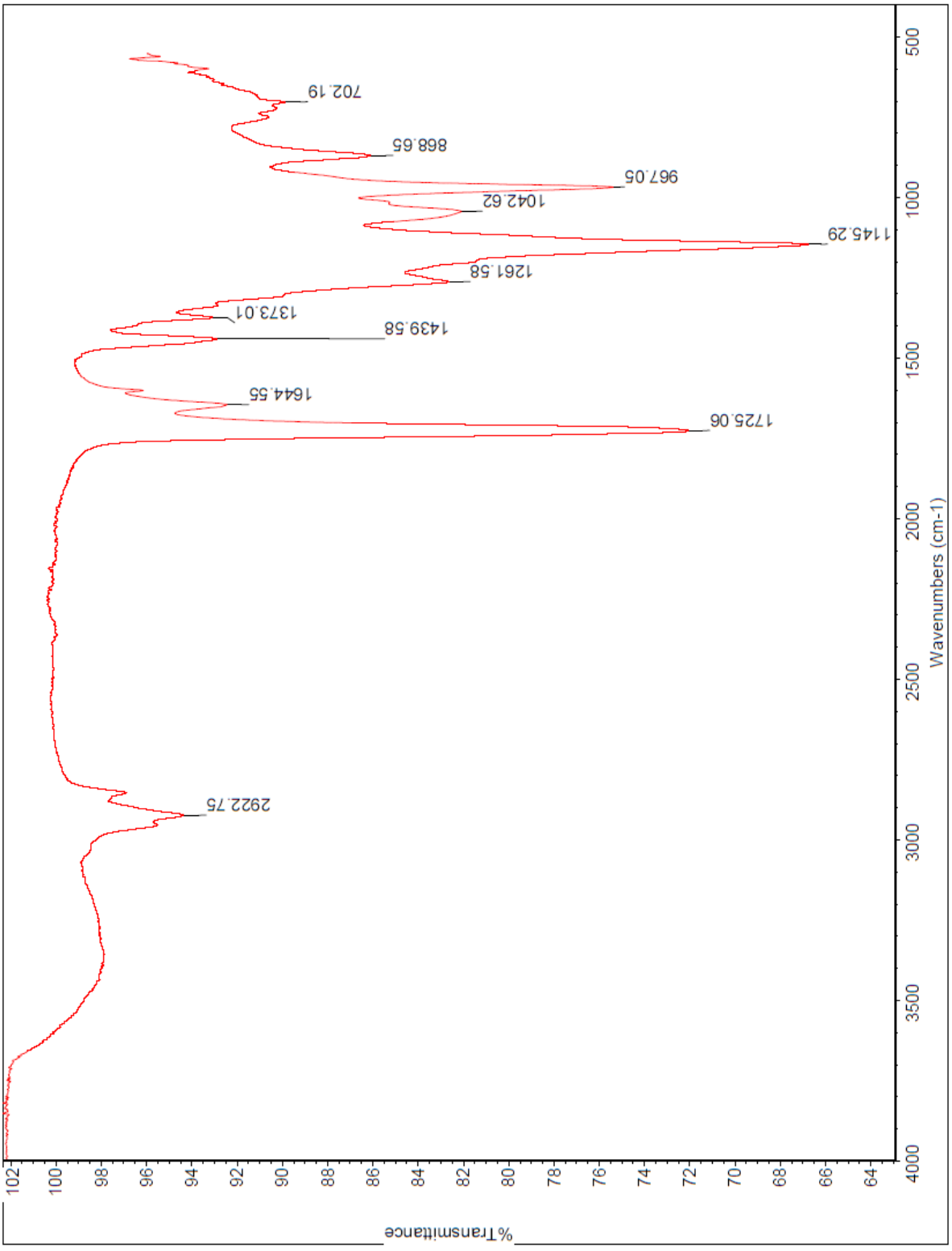

Figure B.18. FT-IR spectrum of PEBP after treating with H_2SO_4 using ATR detector.

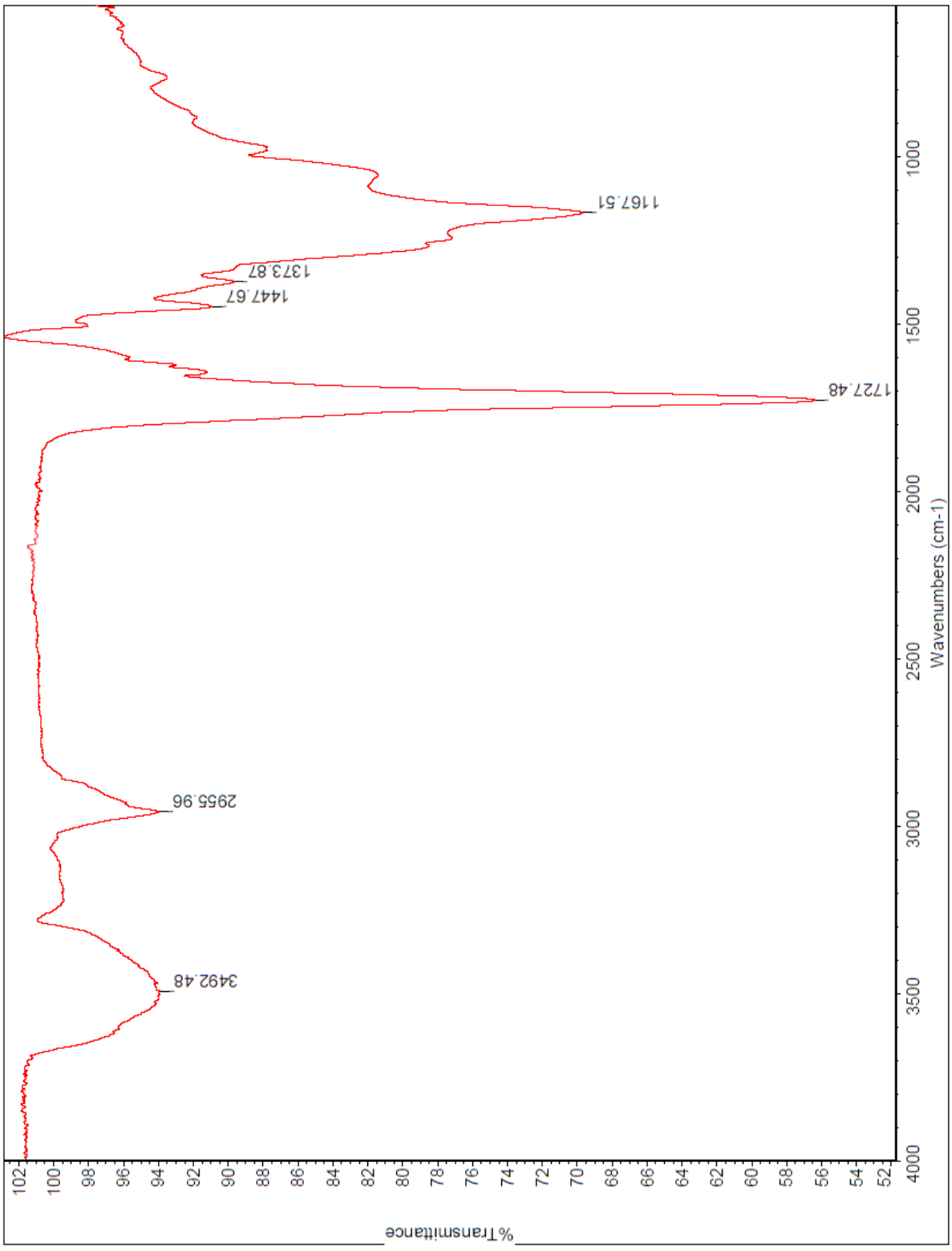

Figure B.19. FT-IR spectrum of PEBP after curing at 170 °C using ATR detector.

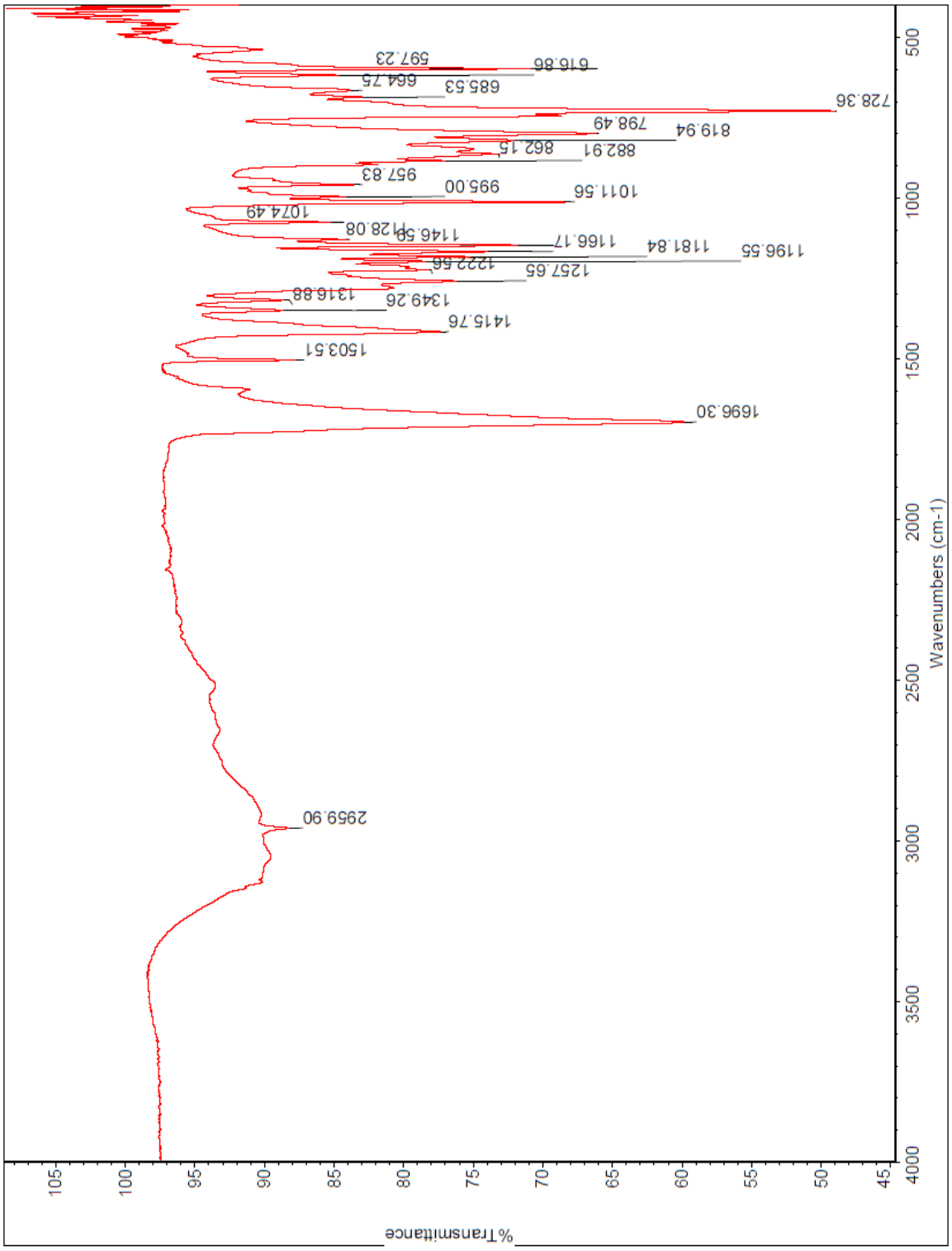

Figure B.20. FT-IR spectrum of CBDA-2 using ATR detector.

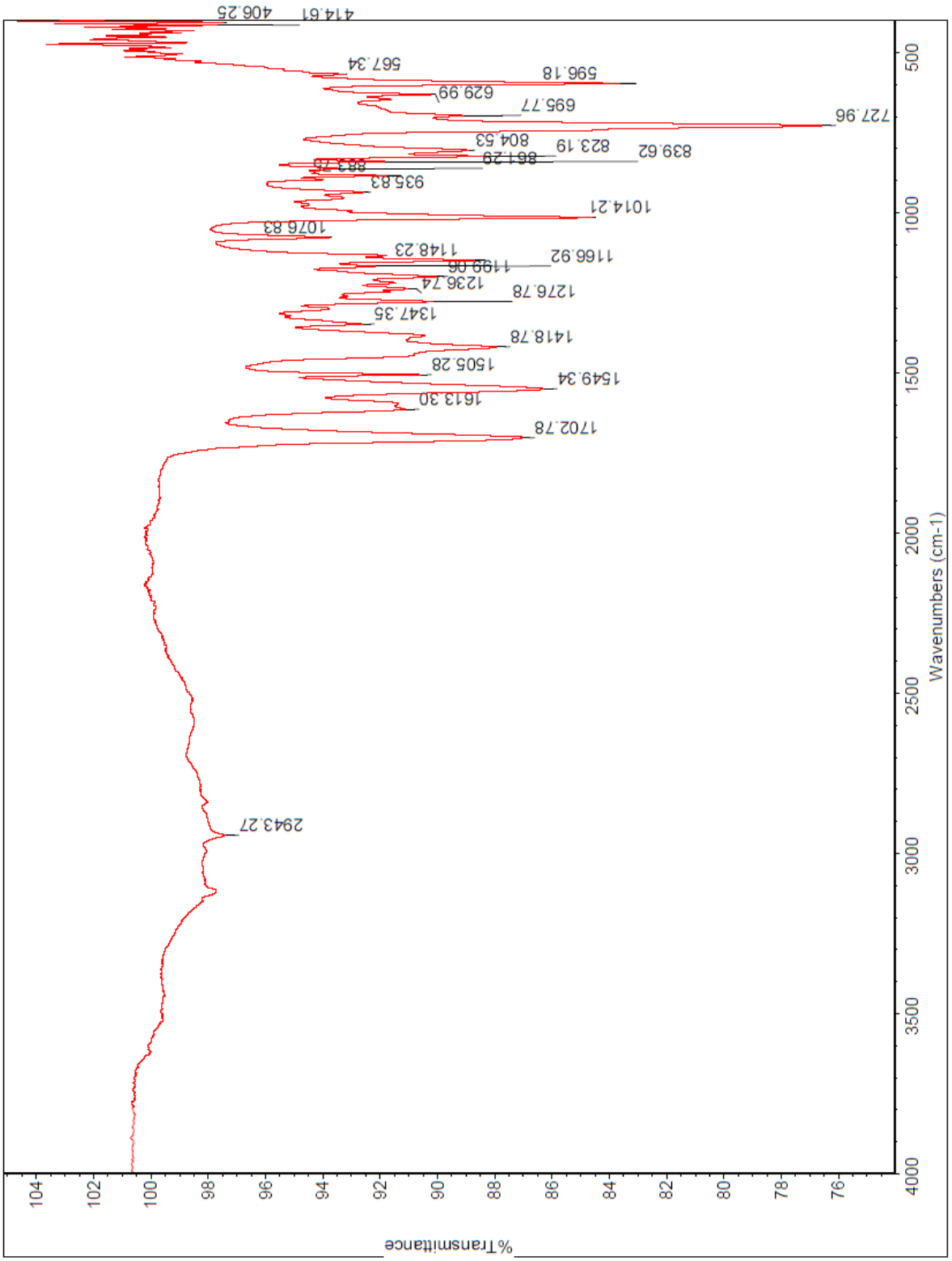

Figure B.21. FT-IR spectrum of Cu-CBDA-2 Complex (I) using ATR detector.

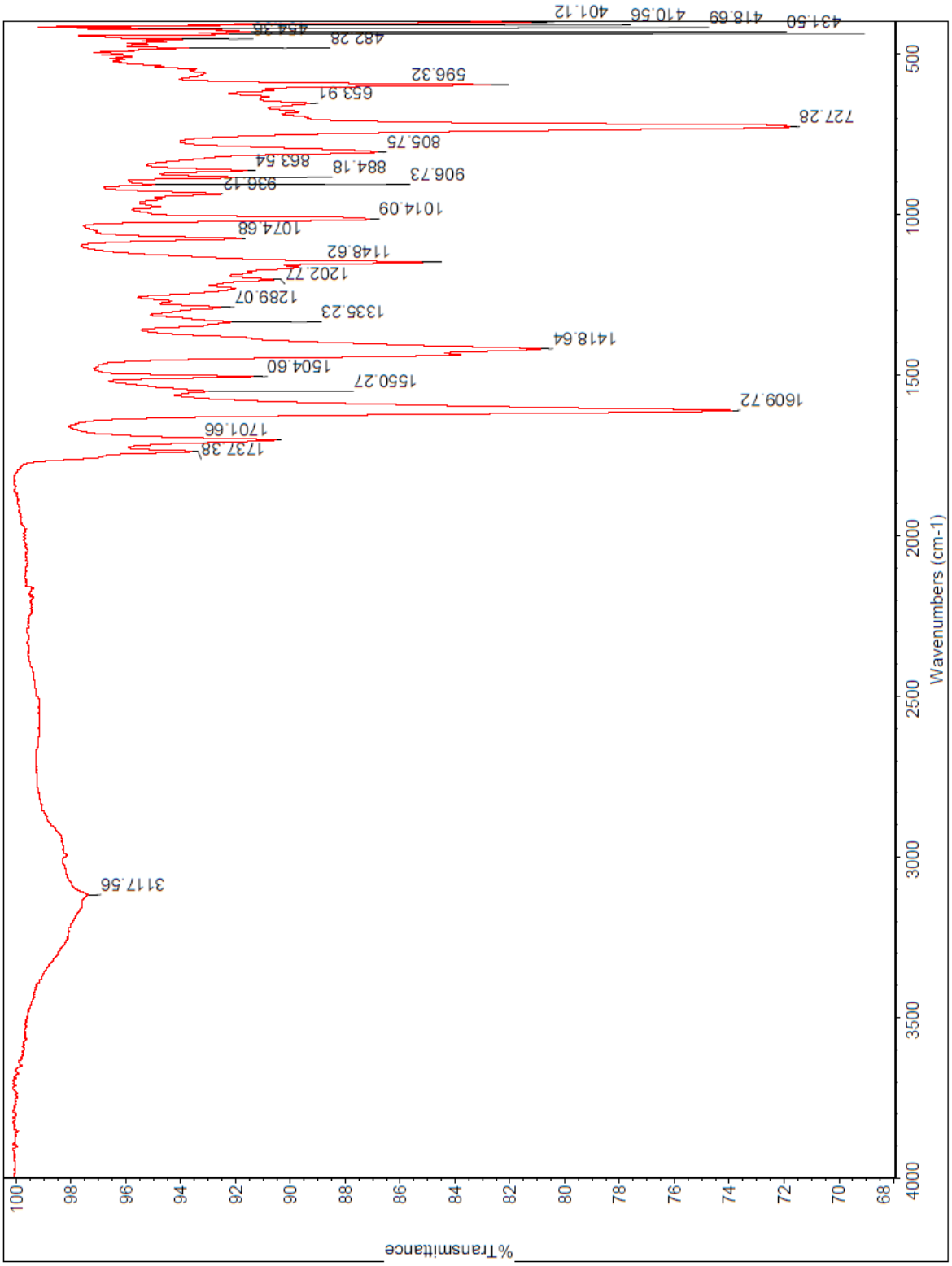

Figure B.22. FT-IR spectrum of Cu-CBDA-2 Complex (I) after heating at 200 °C in vaccume oven using ATR detector.

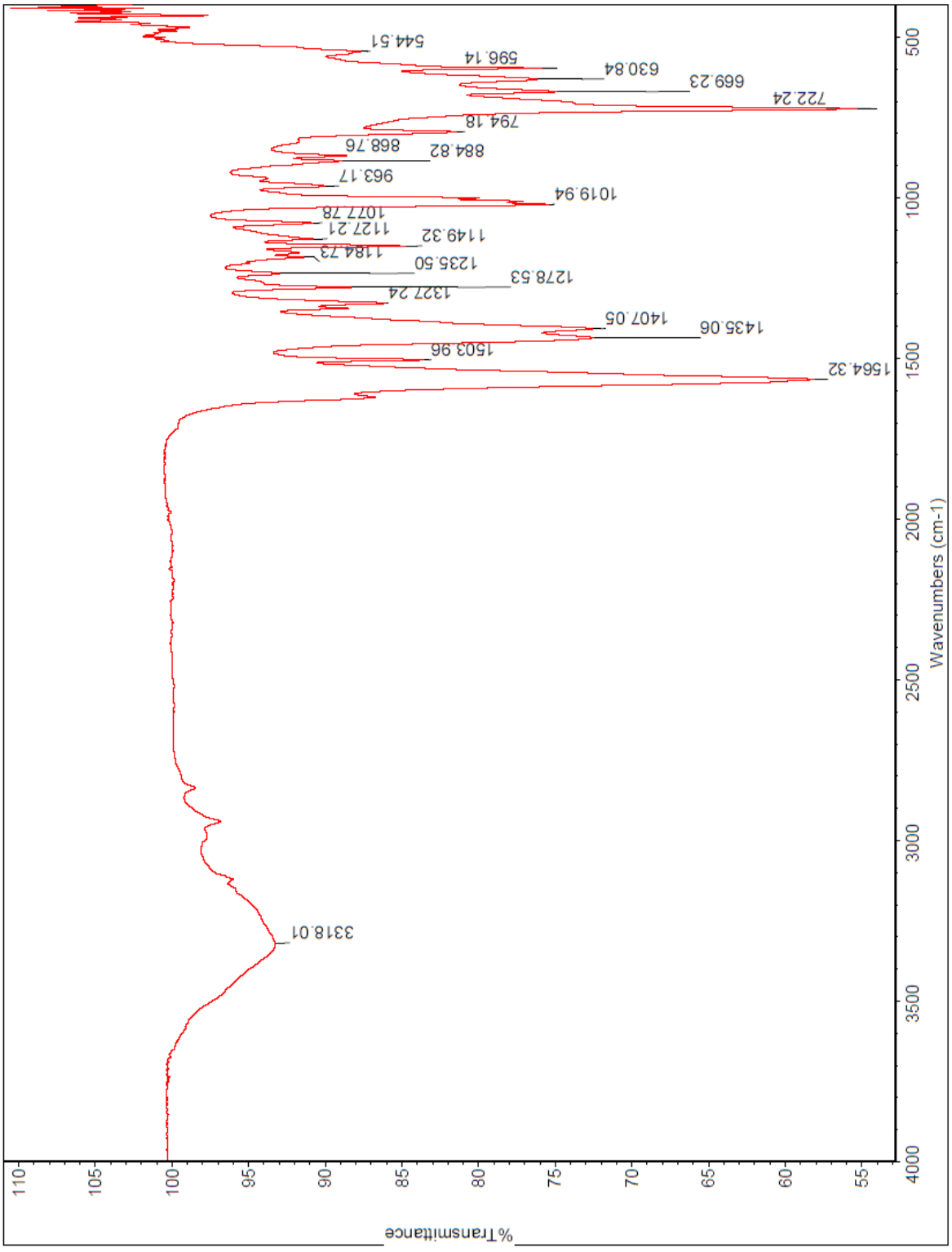

Figure B.23. FT-IR spectrum of Co-CBDA-2 Complex (II) using ATR detector.

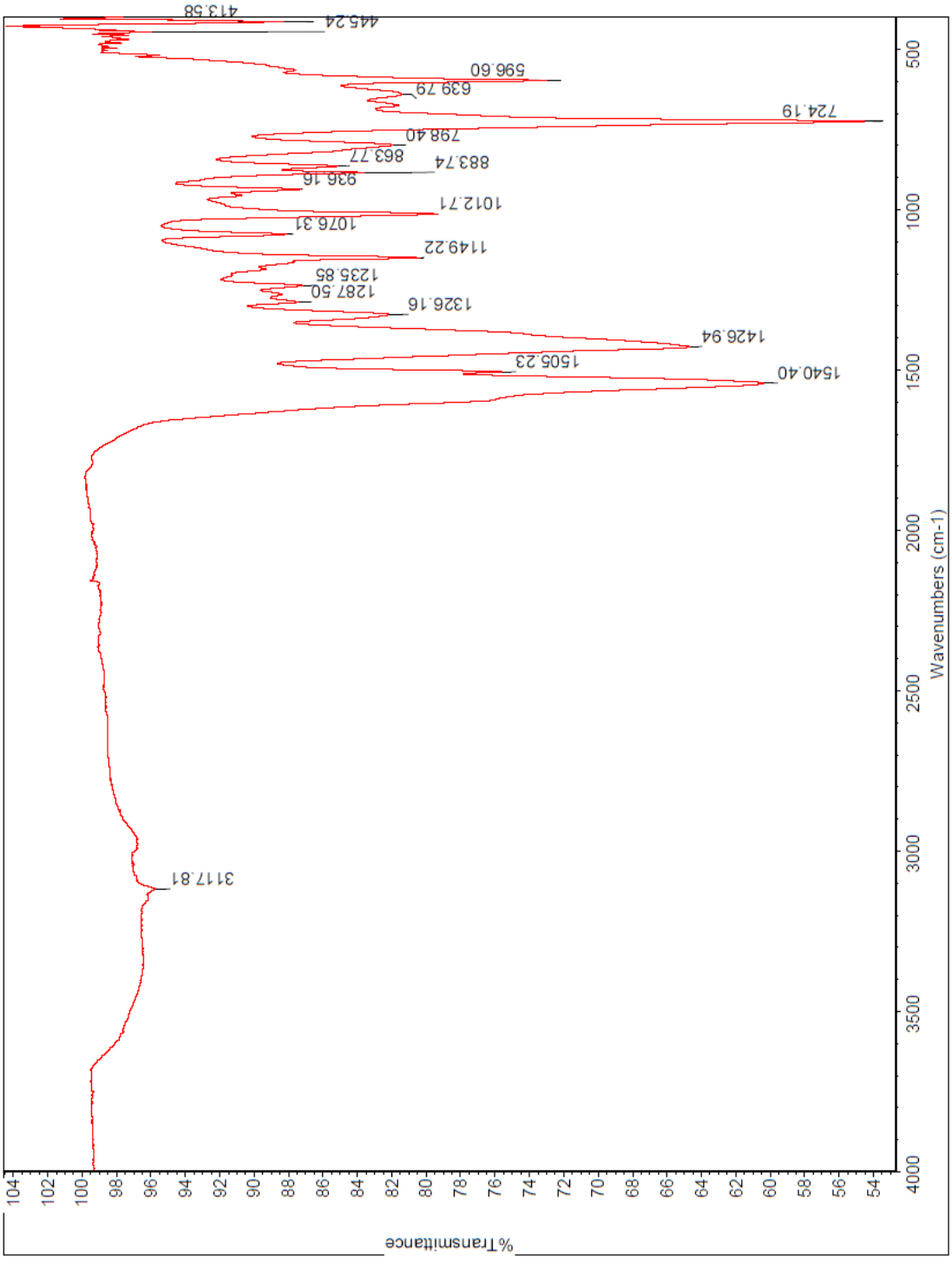

Figure B.24. FT-IR spectrum of Co-CBDA-2 Complex (II) after heating at 200 °C in vaccume oven using ATR detector.

Appendix C

Selected MALDI-TOF-MS Spectra

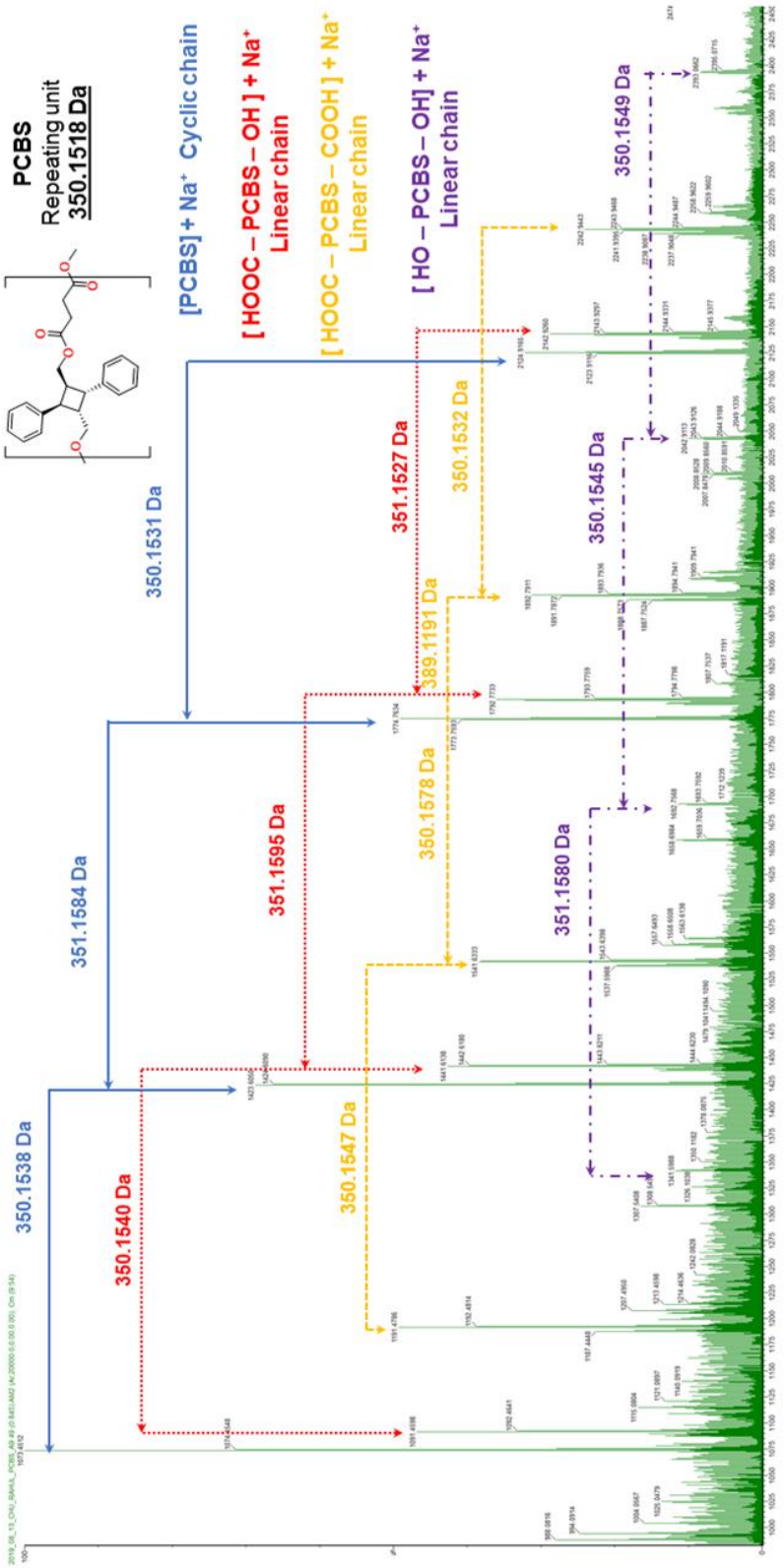

Figure C.1. MALDI-TOF-MS spectrum of PCBS.

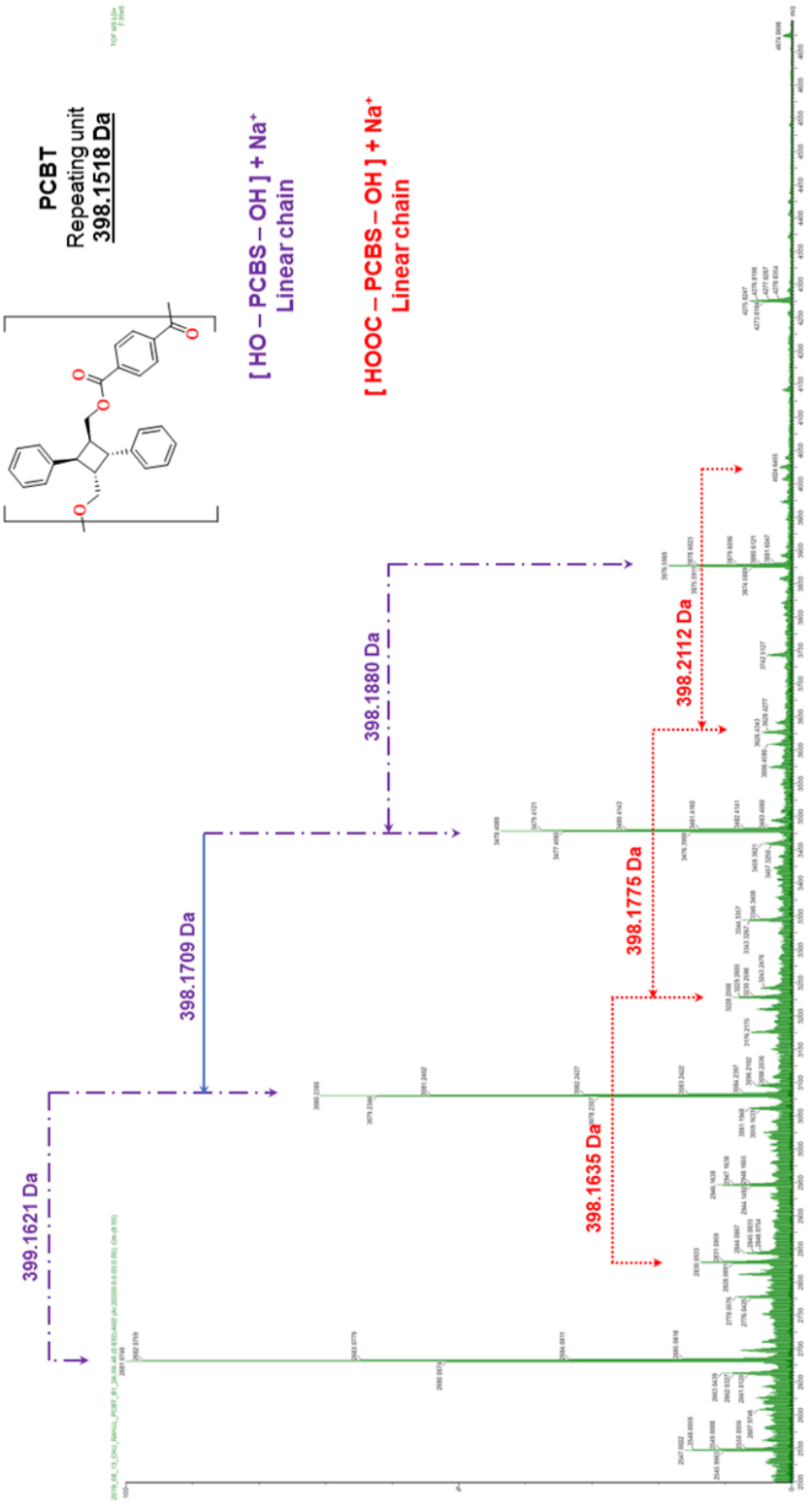

Figure C.2. MALDI-TOF-MS spectrum of PCBT.

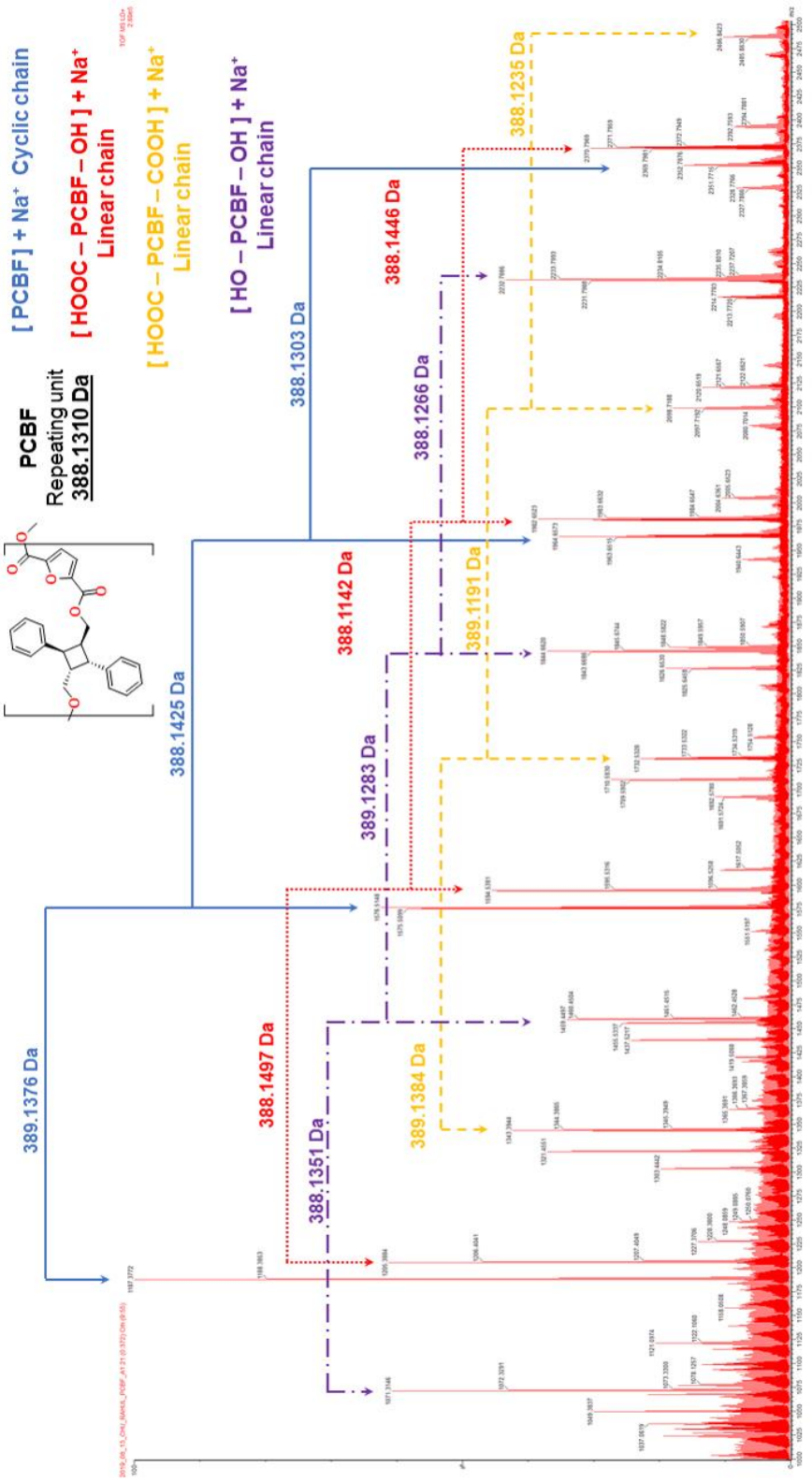

Figure C.3. MALDI-TOF-MS spectrum of PCBF.

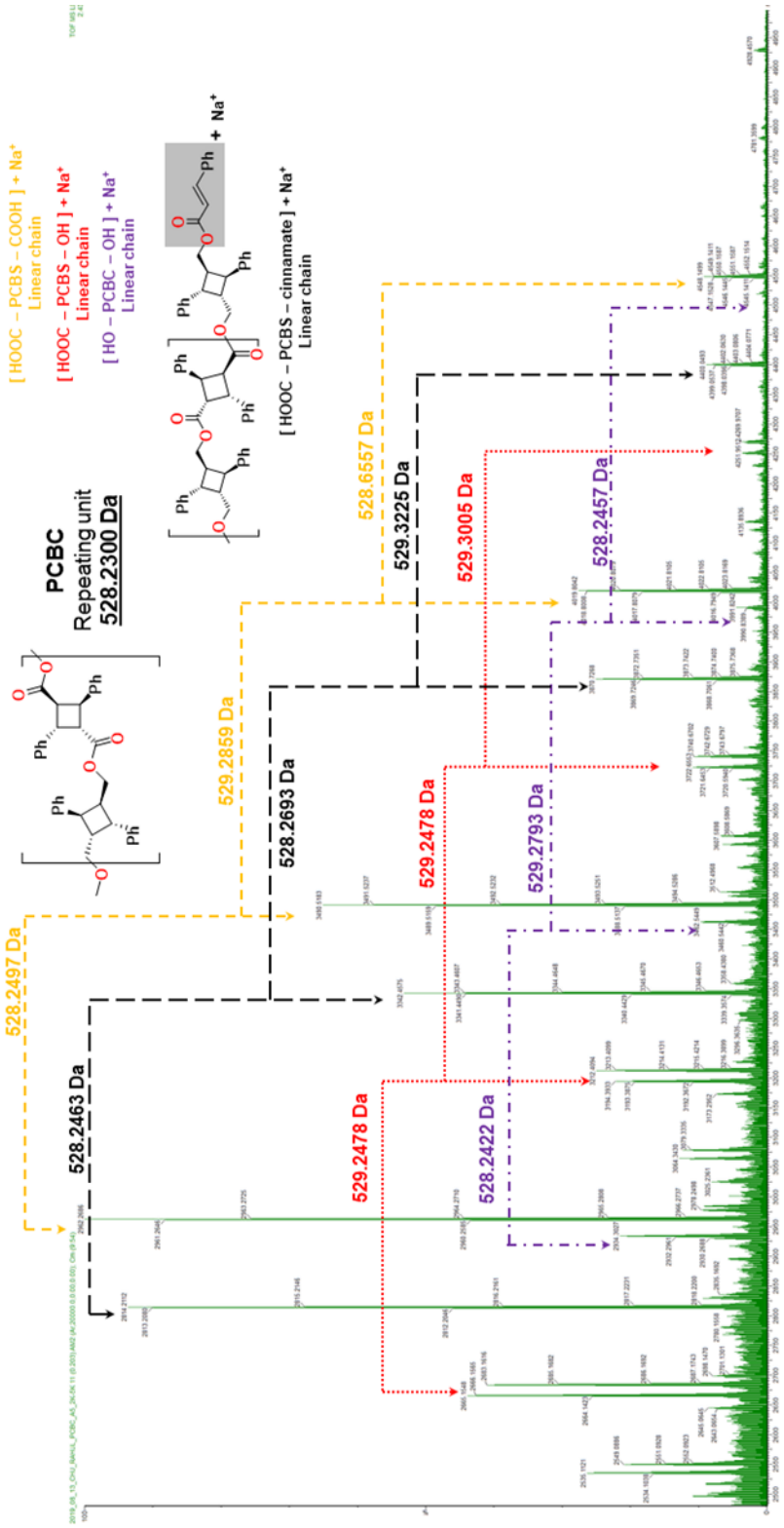

Figure C.4. MALDI-TOF-MS spectrum of PCBC.

Appendix D

Selected GPC traces

Chromatogram report

Header

Title		Data acquisition date and time	2019/07/24 23:14:21
Sample name	UND_Rahul_**PCBO**	Calculation date and time	2019/07/26 12:59:53
Database name	7-24-2019 Column2 UND-Rahul samples	Acquisition time [min]	0.000 - 30.000
Data name	RSLT0012	Sampling interval [msec]	100
Method name	STD PS for SuperHM-H(up to 6m) Column2 July2019	Cup number	10
Channel	RI	Calculation type	Molecular Weight

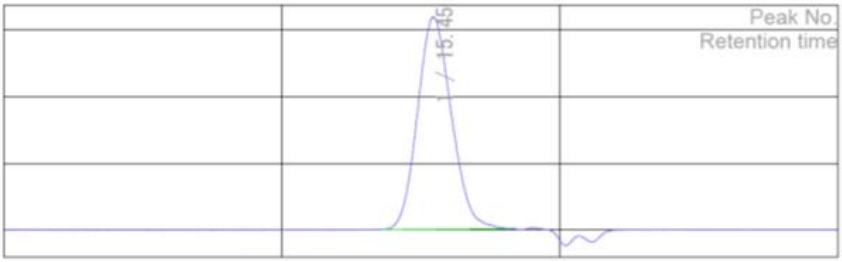

Result of molecular weight calculation (RI)
Peak 1 Base Peak

	[min]	[mV]	[mol]		
Peak start	13.595	0.640	82,702	Mn	6,285
Peak top	15.450	320.443	7,358	Mw	14,934
Peak end	18.252	1.975	165	Mz	26,555
				Mz+1	39,084
				Mv	24,821
Height [mV]			319.271	Mp	12,684
Area [mV*sec]			26973.935	Mz/Mw	1.778
Area% [%]			100.000	Mw/Mn	2.376
[eta]			8666.56556	Mz+1/Mw	2.617

Result of molecular weight calculation (RI)
Total

	[min]	[mV]	[mol]		
Peak start	13.595	0.640	82,702	Mn	6,285
Peak top	15.450	320.443	7,358	Mw	14,934
Peak end	18.252	1.975	165	Mz	26,555
				Mz+1	39,084
				Mv	24,821
Height [mV]			319.271	Mp	12,684
Area [mV*sec]			26973.935	Mz/Mw	1.778
Area% [%]			100.000	Mw/Mn	2.376
[eta]			8666.56556	Mz+1/Mw	2.617

Figure D.1. GPC chromatogram report of PCBO.

Chromatogram report

Header

Title		Data acquisition date and time	2019/07/24 21:14:16
Sample name	UND_Rahul_**PCBM**	Calculation date and time	2019/07/26 12:59:39
Database name	7-24-2019 Column2 UND-Rahul samples	Acquisition time [min]	0.000 - 30.000
Data name	RSLT0008	Sampling interval [msec]	100
Method name	STD PS for SuperHM-H(up to 6m) Column2 July2019	Cup number	6
Channel	RI	Calculation type	Molecular Weight

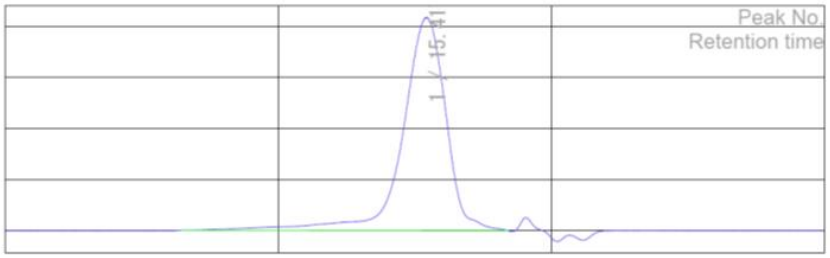

Result of molecular weight calculation (RI)
Peak 1 Base Peak

	[min]	[mV]	[mol]		
Peak start	6.450	0.992	119,513,327	Mn	4,489
Peak top	15.417	418.122	7,692	Mw	6,954
Peak end	18.438	-0.279	128	Mz	10,430
				Mz+1	14,891
				Mv	9,853
Height [mV]			418.081	Mp	5,979
Area [mV*sec]			46082.038	Mz/Mw	1.499
Area% [%]			100.000	Mw/Mn	1.549
[eta]			329980.28152	Mz+1/Mw	2.141

Result of molecular weight calculation (RI)
Total

	[min]	[mV]	[mol]		
Peak start	6.450	0.992	119,513,327	Mn	4,489
Peak top	15.417	418.122	7,692	Mw	6,954
Peak end	18.438	-0.279	128	Mz	10,430
				Mz+1	14,891
				Mv	9,853
Height [mV]			418.081	Mp	5,979
Area [mV*sec]			46082.038	Mz/Mw	1.499
Area% [%]			100.000	Mw/Mn	1.549
[eta]			329980.28152	Mz+1/Mw	2.141

Figure D.2. GPC chromatogram report of PCBM.

Chromatogram report

Header

Title		Data acquisition date and time	2019/07/24 23:44:23
Sample name	UND_Rahul_**PCBS**	Calculation date and time	2019/07/26 12:59:56
Database name	7-24-2019 Column2 UND-Rahul samples	Acquisition time [min]	0.000 - 30.000
Data name	RSLT0013	Sampling interval [msec]	100
Method name	STD PS for SuperHM-H(up to 6m) Column2 July2019	Cup number	11
Channel	RI	Calculation type	Molecular Weight

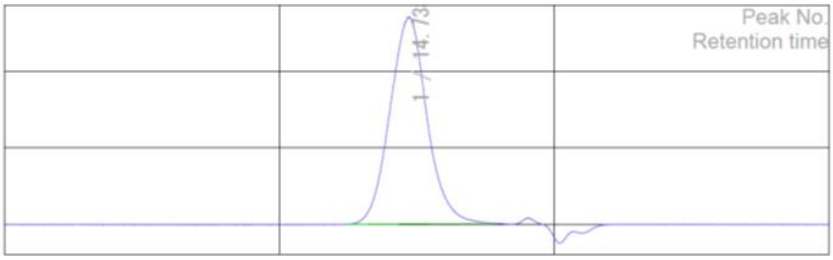

Result of molecular weight calculation (RI)
Peak 1 Base Peak

	[min]	[mV]	[mol]		
Peak start	12.472	0.544	333,622	Mn	12,112
Peak top	14.738	271.184	18,875	Mw	26,788
Peak end	17.743	1.884	330	Mz	49,222
				Mz+1	80,915
				Mv	26,788
Height [mV]			270.064	Mp	20,024
Area [mV*sec]			25195.186	Mz/Mw	1.837
Area% [%]			100.000	Mw/Mn	2.212
[eta]			26788.34657	Mz+1/Mw	3.021

Result of molecular weight calculation (RI)
Total

	[min]	[mV]	[mol]		
Peak start	12.472	0.544	333,622	Mn	12,112
Peak top	14.738	271.184	18,875	Mw	26,788
Peak end	17.743	1.884	330	Mz	49,222
				Mz+1	80,915
				Mv	26,788
Height [mV]			270.064	Mp	20,024
Area [mV*sec]			25195.186	Mz/Mw	1.837
Area% [%]			100.000	Mw/Mn	2.212
[eta]			26788.34657	Mz+1/Mw	3.021

Figure D.3. GPC chromatogram report of PCBS.

Chromatogram report

Header

Title		Data acquisition date and time	2019/07/24 20:44:15
Sample name	UND_Rahul_**PCBG**	Calculation date and time	2019/07/26 12:59:34
Database name	7-24-2019 Column2 UND-Rahul samples	Acquisition time [min]	0.000 - 30.000
Data name	RSLT0007	Sampling interval [msec]	100
Method name	STD PS for SuperHM-H(up to 6m) Column2 July2019	Cup number	5
Channel	RI	Calculation type	Molecular Weight

[...]

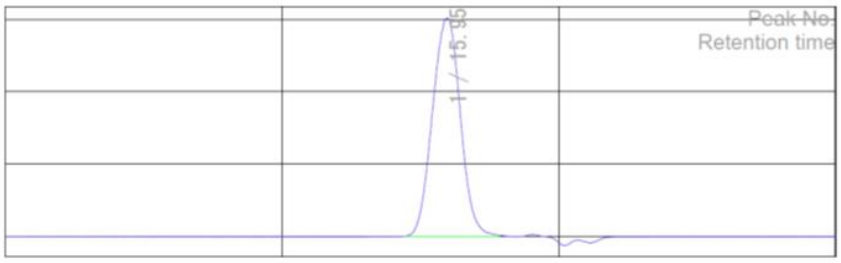

Result of molecular weight calculation (RI)
Peak 1 Base Peak

	[min]	[mV]	[mol]		
Peak start	14.455	0.712	27,345	Mn	5,393
Peak top	15.953	604.354	3,749	Mw	8,929
Peak end	17.868	2.751	279	Mz	6,331
				Mz+1	8,435
				Mv	4,513
Height [mV]			603.719	Mp	6,874
Area [mV*sec]			42329.521	Mz/Mw	1.403
Area% [%]			100.000	Mw/Mn	1.483
[eta]			4512.72088	Mz+1/Mw	1.869

Result of molecular weight calculation (RI)
Total

	[min]	[mV]	[mol]		
Peak start	14.455	0.712	27,345	Mn	5,393
Peak top	15.953	604.354	3,749	Mw	8,929
Peak end	17.868	2.751	279	Mz	6,331
				Mz+1	8,435
				Mv	4,513
Height [mV]			603.719	Mp	6,874
Area [mV*sec]			42329.521	Mz/Mw	1.403
Area% [%]			100.000	Mw/Mn	1.483
[eta]			4512.72088	Mz+1/Mw	1.869

Figure D.4. GPC chromatogram report of PCBG.

Chromatogram report

Header

Title		Data acquisition date and time	2019/07/25 16:23:57
Sample name	UND_Rahul_**PCBA**	Calculation date and time	2019/07/26 09:19:41
Database name	7-25-2019 Column2 Standard Sanjana UND-Rahul samples	Acquisition time [min]	0.000 - 30.000
Data name	RSLT0007	Sampling interval [msec]	100
Method name	STD PS for SuperHM-H(up to 6m) Column2 July2019	Cup number	9
Channel	RI	Calculation type	Molecular Weight

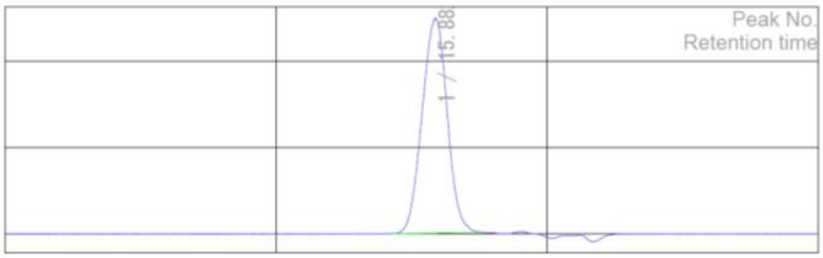

Result of molecular weight calculation (RI)
Peak 1 Base Peak

	[min]	[mV]	[mol]		
Peak start	14.318	0.481	32,666	Mn	8,805
Peak top	15.882	249.445	4,128	Mw	25,653
Peak end	17.610	1.777	396	Mz	73,778
				Mz+1	84,680
				Mv	9,147
Height [mV]			248.348	Mp	18,142
Area [mV*sec]			16026.737	Mz/Mw	2.876
Area% [%]			100.000	Mw/Mn	2.914
[eta]			4992.99996	Mz+1/Mw	3.301

Result of molecular weight calculation (RI)
Total

	[min]	[mV]	[mol]		
Peak start	14.318	0.481	32,666	Mn	8,805
Peak top	15.882	249.445	4,128	Mw	25,653
Peak end	17.610	1.777	396	Mz	73,778
				Mz+1	84,680
				Mv	9,147
Height [mV]			248.348	Mp	18,142
Area [mV*sec]			16026.737	Mz/Mw	2.876
Area% [%]			100.000	Mw/Mn	2.914
[eta]			4992.99996	Mz+1/Mw	3.301

Figure D.5. GPC chromatogram report of PCBA.

Chromatogram report

Header

Title		Data acquisition date and time	2020/02/06 18:18:38
Sample name	UND_Rahul_**PCBT**	Calculation date and time	2020/02/07 17:17:48
Database name	2-6-2020 Column1 RustOleum Ihor Standard samples	Acquisition time [min]	0.000 - 30.000
Data name	RSLT0018	Sampling interval [msec]	100
Method name	STD PS for SuperH3000(less than 20,000) Column1 Dec2019	Cup number	20
Channel	RI	Calculation type	Molecular Weight

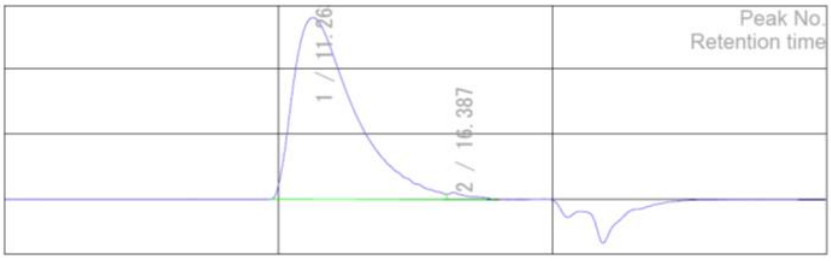

Result of molecular weight calculation (RI)
Peak 1 Base Peak

	[min]	[mV]	[mol]		
Peak start	9.742	0.265	75,698	Mn	11,071
Peak top	11.263	138.938	19,987	Mw	23,166
Peak end	16.163	3.950	965	Mz	43,793
				Mz+1	68,300
				Mv	40,471
Height [mV]			138.806	Mp	14,495
Area [mV*sec]			21493.031	Mz/Mw	1.890
Area% [%]			98.652	Mw/Mn	2.092
[eta]			16517.50692	Mz+1/Mw	2.948

Result of molecular weight calculation (RI)
Total

	[min]	[mV]	[mol]		
Peak start	9.742	0.265	75,698	Mn	11,071
Peak top	11.263	138.938	19,987	Mw	23,166
Peak end	18.010	-0.459	260	Mz	43,793
				Mz+1	68,300
				Mv	40,471
Height [mV]			144.426	Mp	14,495
Area [mV*sec]			21786.659	Mz/Mw	1.890
Area% [%]			100.000	Mw/Mn	2.092
[eta]			16303.93524	Mz+1/Mw	2.948

Figure D.6. GPC chromatogram report of PCBT.

Chromatogram report

Header

Title		Data acquisition date and time	2019/07/24 21:44:17
Sample name	UND_Rahul_**PCBF**	Calculation date and time	2019/07/26 12:59:43
Database name	7-24-2019 Column2 UND-Rahul samples	Acquisition time [min]	0.000 - 30.000
Data name	RSLT0009	Sampling interval [msec]	100
Method name	STD PS for SuperHM-H(up to 6m) Column2 July2019	Cup number	7
Channel	RI	Calculation type	Molecular Weight

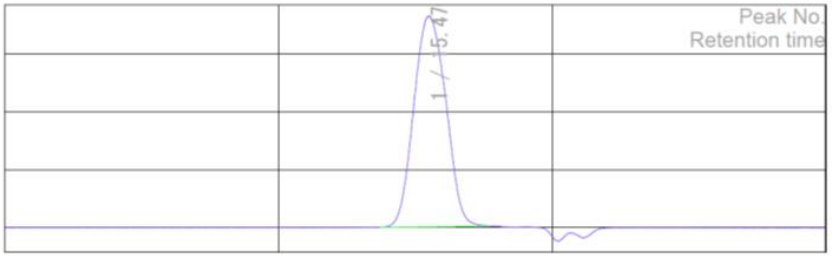

Result of molecular weight calculation (RI)
Peak 1 Base Peak

	[min]	[mV]	[mol]		
Peak start	13.702	0.418	72,214	Mn	4,971
Peak top	15.470	365.994	7,164	Mw	8,002
Peak end	17.690	2.321	355	Mz	12,059
				Mz+1	16,916
				Mv	8,002
Height [mV]			364.732	Mp	7,164
Area [mV*sec]			29670.670	Mz/Mw	1.507
Area% [%]			100.000	Mw/Mn	1.610
[eta]			8002.45563	Mz+1/Mw	2.114

Result of molecular weight calculation (RI)
Total

	[min]	[mV]	[mol]		
Peak start	13.702	0.418	72,214	Mn	4,971
Peak top	15.470	365.994	7,164	Mw	8,002
Peak end	17.690	2.321	355	Mz	12,059
				Mz+1	16,916
				Mv	8,002
Height [mV]			364.732	Mp	7,164
Area [mV*sec]			29670.670	Mz/Mw	1.507
Area% [%]			100.000	Mw/Mn	1.610
[eta]			8002.45563	Mz+1/Mw	2.114

Figure D.7. GPC chromatogram report of PCBF.

Chromatogram report

Header

Title		Data acquisition date and time	2019/07/24 20:14:14
Sample name	UND_Rahul_**PCBC**	Calculation date and time	2019/07/26 12:59:30
Database name	7-24-2019 Column2 UND-Rahul samples	Acquisition time [min]	0.000 - 30.000
Data name	RSLT0006	Sampling interval [msec]	100
Method name	STD PS for SuperHM-H(up to 6m) Column2 July2019	Cup number	4
Channel	RI	Calculation type	Molecular Weight

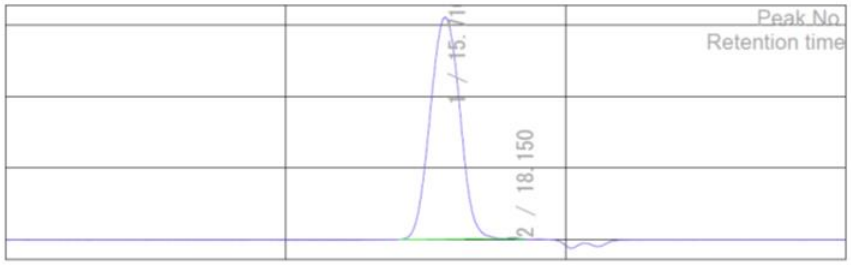

Result of molecular weight calculation (RI)
Peak 1 Base Peak

	[min]	[mV]	[mol]		
Peak start	14.050	0.650	46,220	Mn	23,454
Peak top	15.710	621.245	5,198	Mw	34,921
Peak end	17.637	3.733	382	Mz	50,006
				Mz+1	67,991
				Mv	26,364
Height [mV]			619.168	Mp	21,472
Area [mV*sec]			45510.391	Mz/Mw	1.432
Area% [%]			99.826	Mw/Mn	1.152
[eta]			6363.95753	Mz+1/Mw	1.947

Result of molecular weight calculation (RI)
Total

	[min]	[mV]	[mol]		
Peak start	14.050	0.650	46,220	Mn	23,454
Peak top	15.710	621.245	5,198	Mw	34,921
Peak end	18.492	1.938	119	Mz	50,006
				Mz+1	67,991
				Mv	26,364
Height [mV]			622.835	Mp	21,472
Area [mV*sec]			45589.688	Mz/Mw	1.432
Area% [%]			100.000	Mw/Mn	1.152
[eta]			6353.23081	Mz+1/Mw	1.947

Figure D.8. GPC chromatogram report of PCBC.

Appendix E

Selected DOSY Spectra

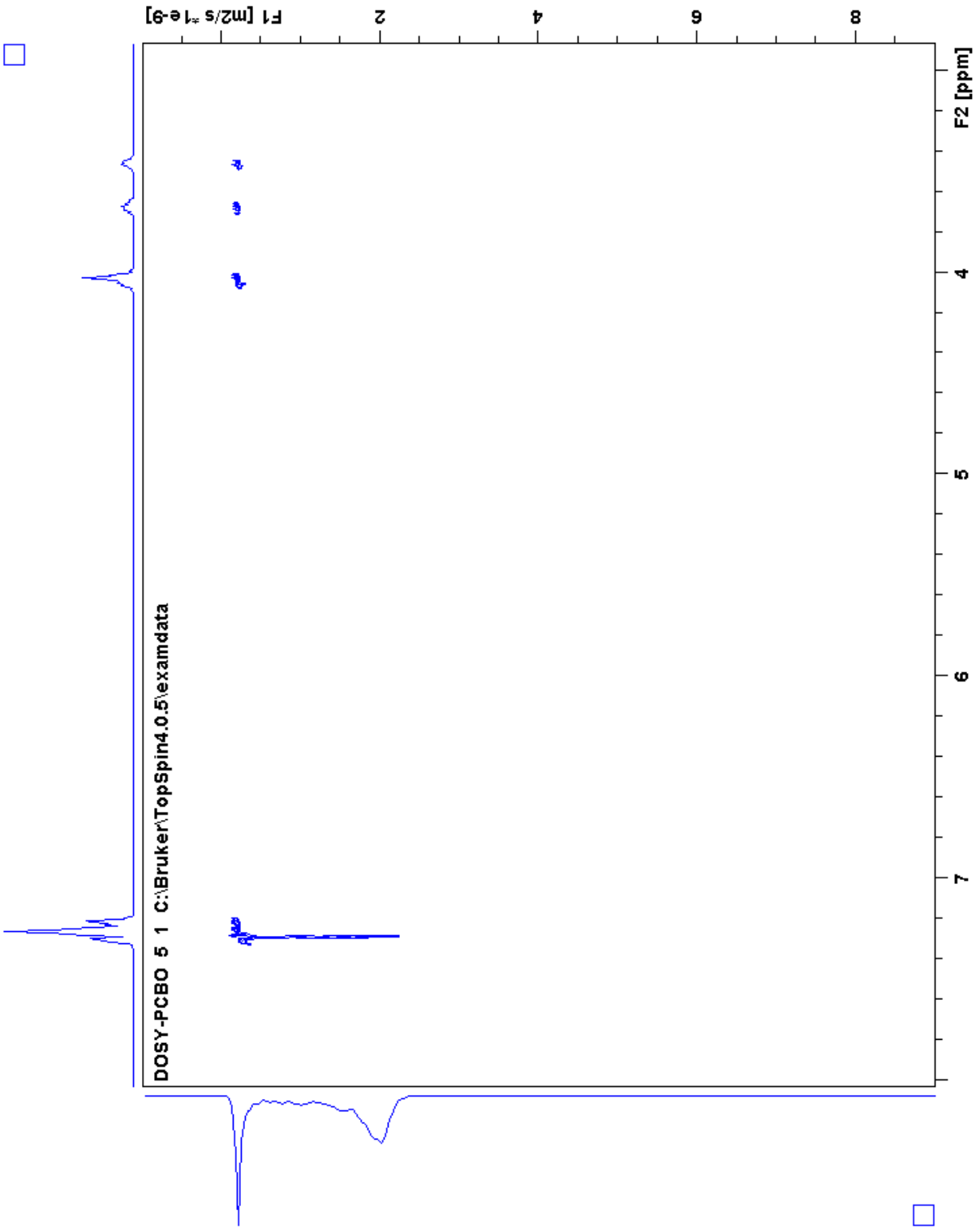

Figure E.1. 2-D DOSY spectrum of PCBO in $CDCl_3$.

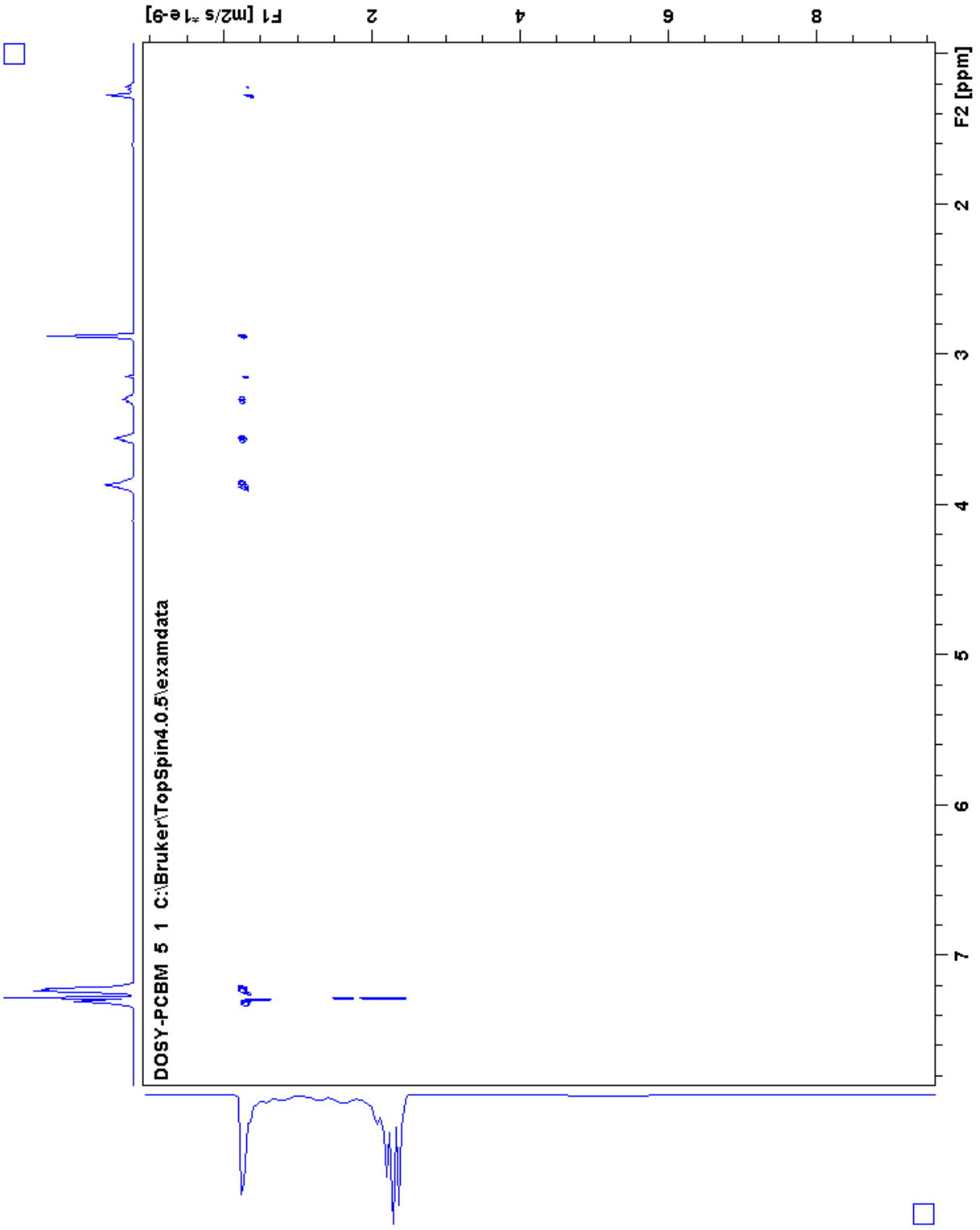

Figure E.2. 2-D DOSY spectrum of PCBM in $CDCl_3$.

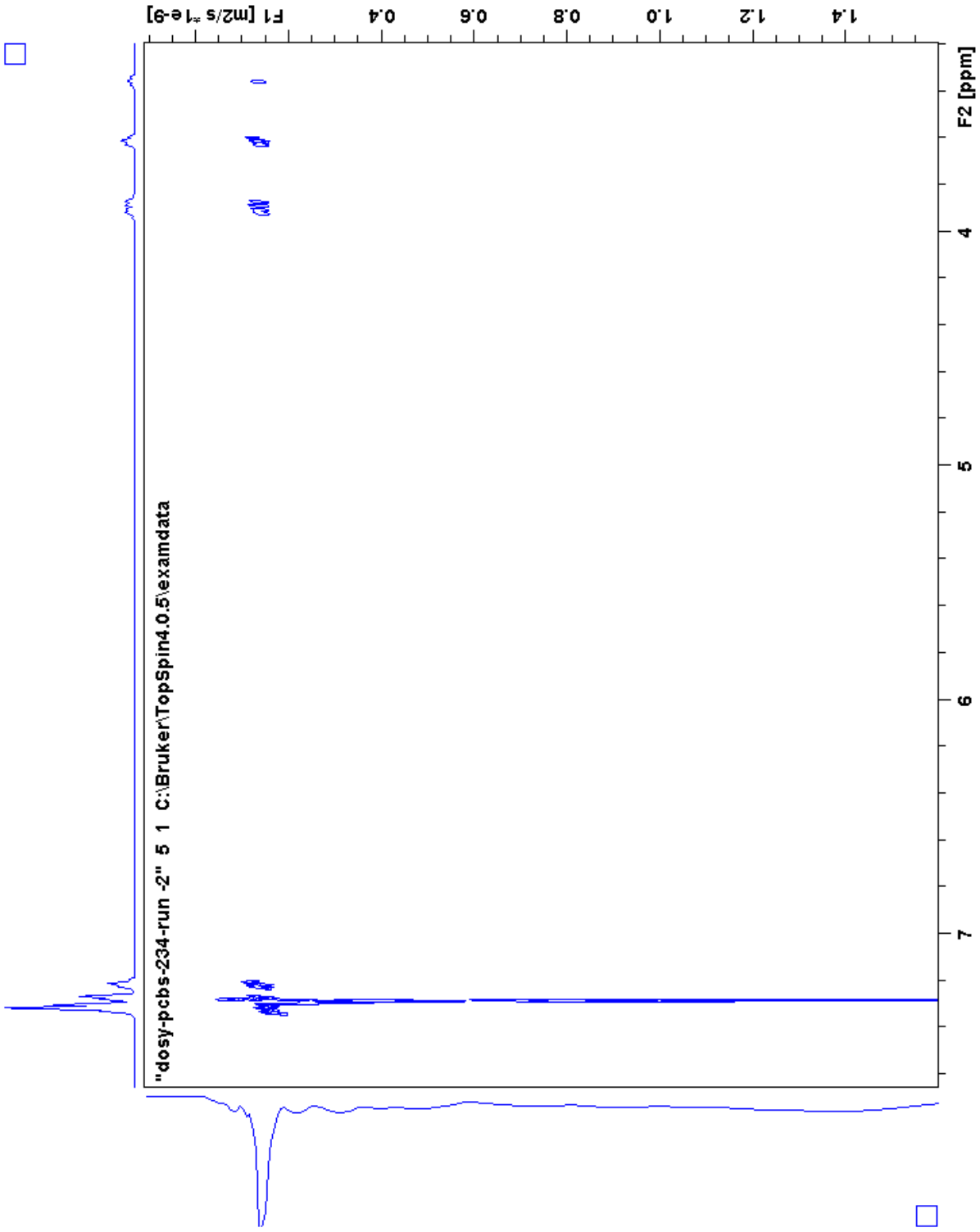

Figure E.3. 2-D DOSY spectrum of PCBS in $CDCl_3$.

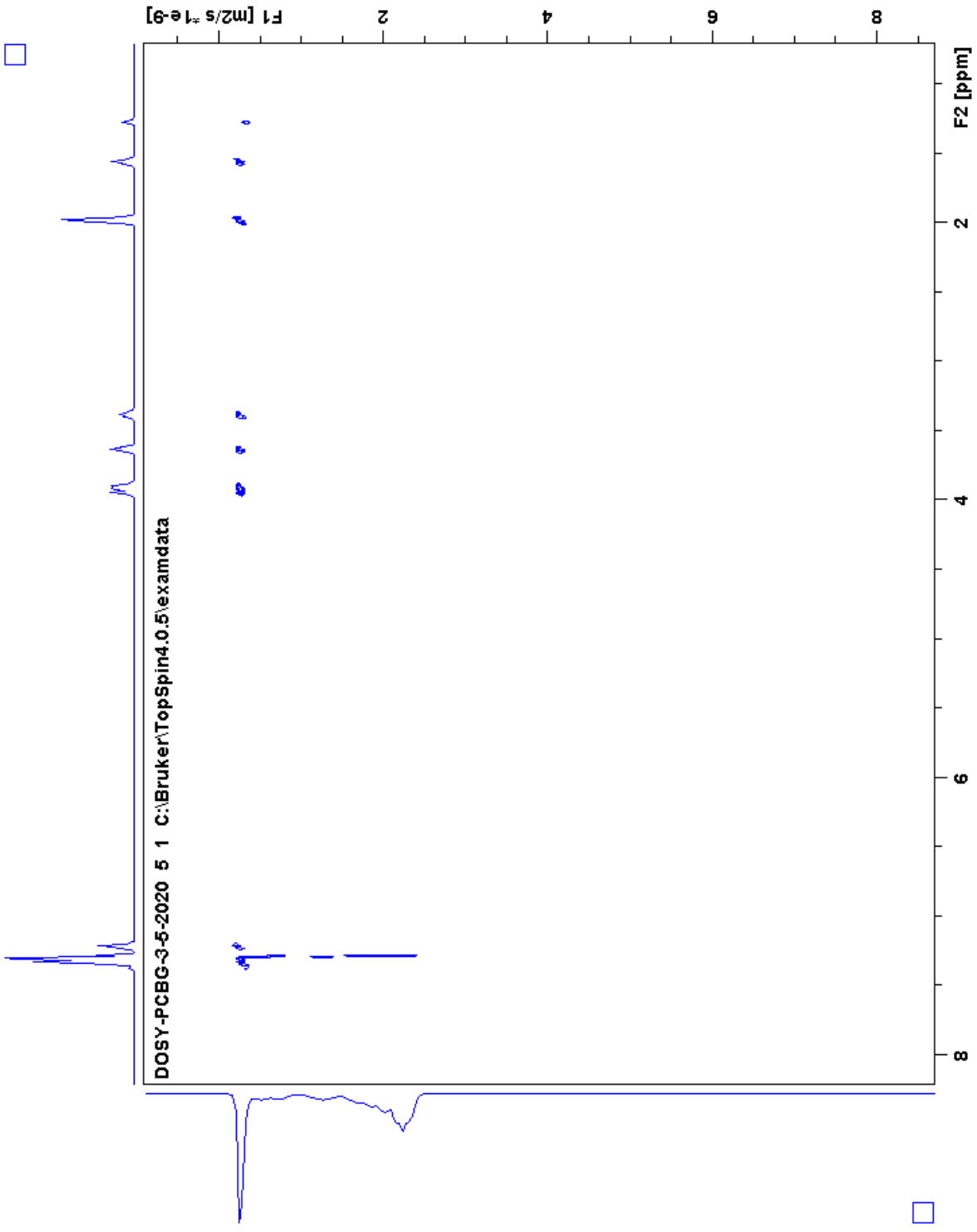

Figure E.4. 2-D DOSY spectrum of PCBG in $CDCl_3$.

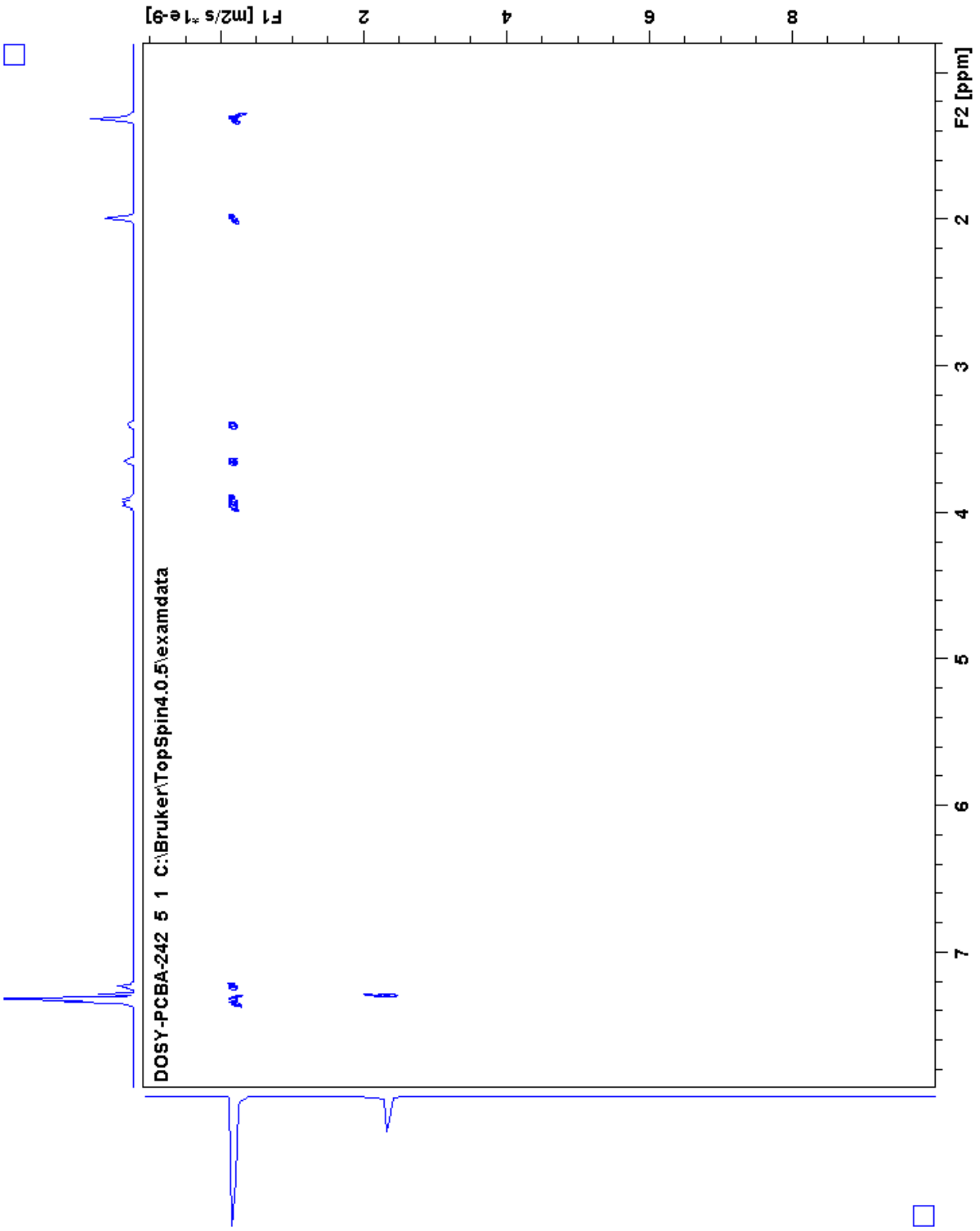

Figure E.5. 2-D DOSY spectrum of PCBA in $CDCl_3$.

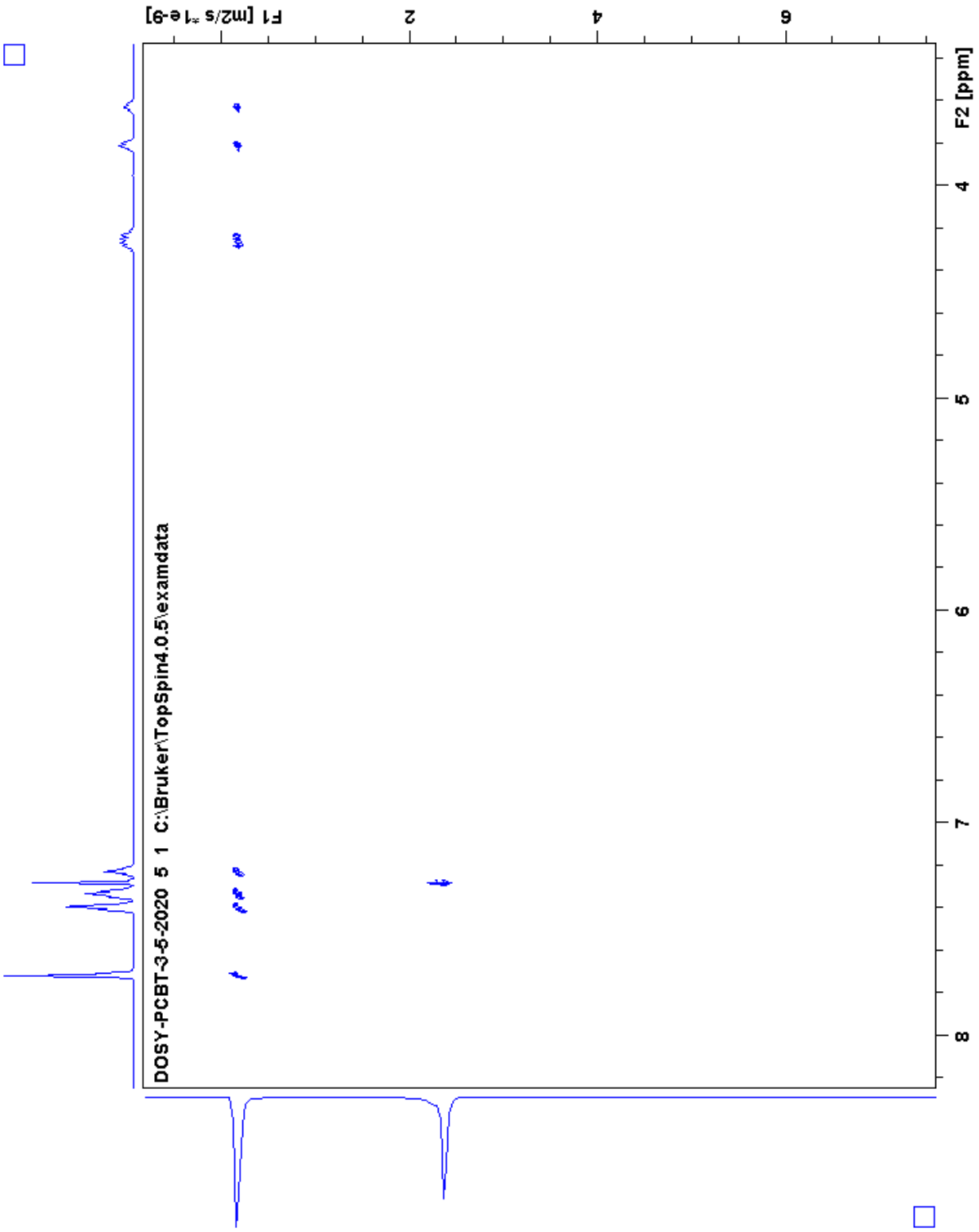

Figure E.6. 2-D DOSY spectrum of PCBT in $CDCl_3$.

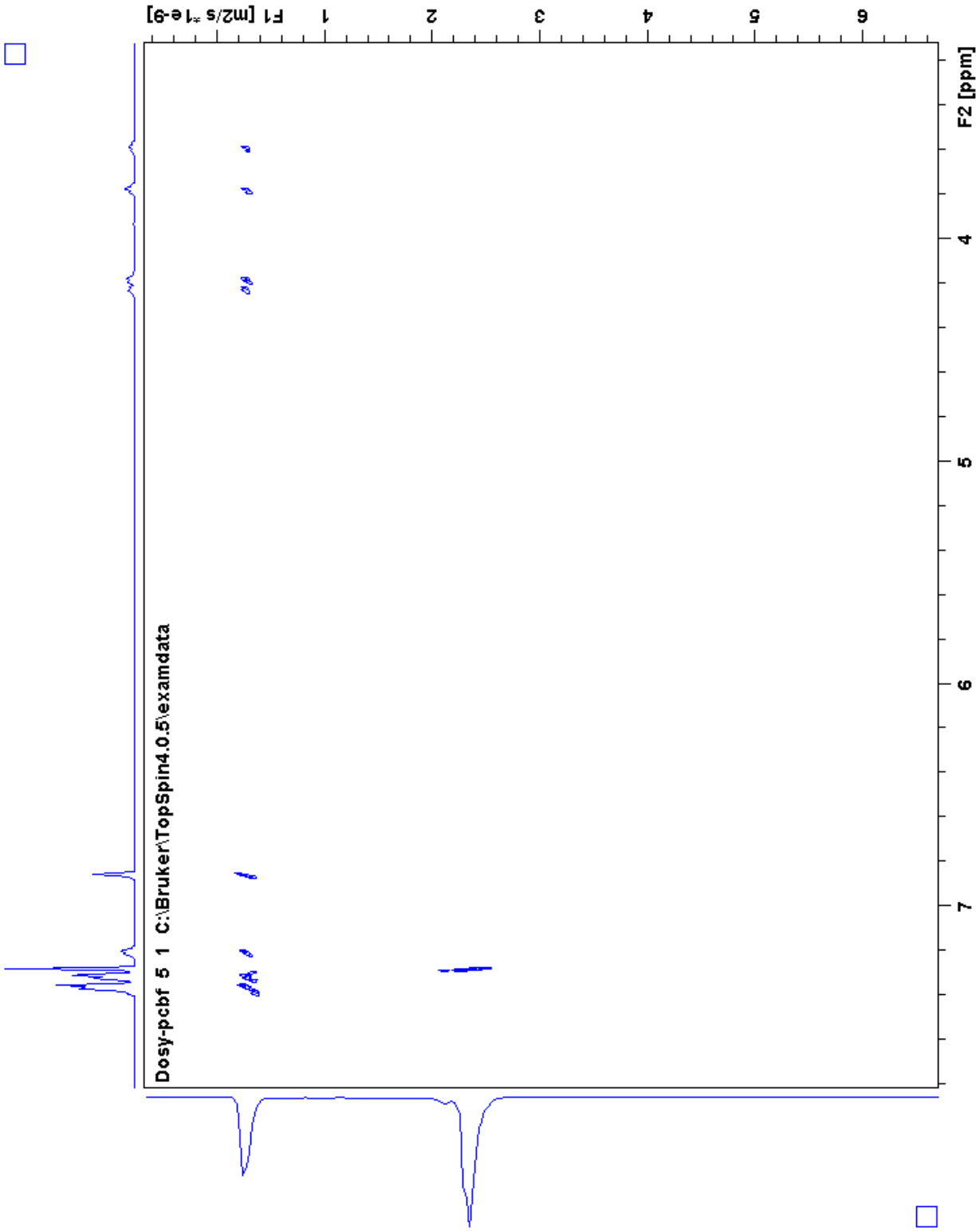

Figure E.7. 2-D DOSY spectrum of PCBF in $CDCl_3$.

Appendix F

Selected SC-XRD data

Table F.1. Crystal data of CBDO-1

Crystal Parameters	CBDO-1
Formula	$C_{36}H_{40}O_2$
FW	536.68
Cryst. Size [mm]	0.06*0.121*0.375
Crystal system	Orthorhombic
Space Group	Pna 21
a (Å)	17.9617(7)
b (Å)	7.6761(3)
c (Å)	21.5205(9)
α (°)	90
β (°)	90
γ (°)	90
V ($Å^3$)	2967.1(2)
Z	4
Temp. (K)	110
ρcalc [g/cm^3]	1.201
μ [mm^{-1}]	0.604
Radiation Type	CuKα (λ = 1.54178)
F(000)	1152.0
No of measured refl	5263
No of independent refl.	2716
No of refl. (I ≥ 2σ)	4930

Table F.2. Crystal data of *trans*-nitrostyrene

Crystal Parameters	***trans*-nitrostyrene**
Formula	$C_8H_7NO_2$
FW	149.15
Cryst. Size [mm]	0.1*0.17*0.32
Crystal system	Monoclinic
Space Group	P121/n1
a (Å)	8.003(2)
b (Å)	5.6863(15)
c (Å)	16.158(4)
α (°)	90
β (°)	94.251(3)
γ (°)	90
V ($Å^3$)	733.3(3)
Z	4
Temp. (K)	110
ρcalc [g/cm^3]	1.351
μ [mm^{-1}]	0.099
Radiation Type	CuKα (λ = 0.71073)
F(000)	312.0
No of measured refl	1727
No of independent refl.	1206
No of refl. (I ≥ 2σ)	1722

Table F.3. Crystal data of CBDN-1

Crystal Parameters	CBDN-1
Formula	$C_{16}H_{14}N_2O_4$
FW	298.29
Cryst. Size [mm]	0.17*0.18*0.19
Crystal system	Monoclinic
Space Group	P121/c1
a (Å)	9.1634(4)
b (Å)	8.1746(3)
c (Å)	10.0631(4)
α (°)	90
β (°)	110.190(2)
γ (°)	90
V ($Å^3$)	707.48(5)
Z	2
Temp. (K)	111
ρcalc [g/cm^3]	1.400
μ [mm^{-1}]	0.851
Radiation Type	CuKα (λ = 1.54178)
F(000)	312.0
No of measured refl	1248
No of independent refl.	1095
No of refl. (I ≥ 2σ)	1203

Table F.4. Crystal data of CBAM-1

Crystal Parameters	CBAM-1
Formula	$C_{17}H_{20}Cl_4N_2$
FW	394.15
Cryst. Size [mm]	0.171*0.206*0.239
Crystal system	Orthorhombic
Space Group	Pbca
a (Å)	8.2386(3)
b (Å)	17.5277(6)
c (Å)	25.7833(8)
α (°)	90
β (°)	90
γ (°)	90
V ($Å^3$)	3723.2(2)
Z	8
Temp. (K)	110
ρcalc [g/cm^3]	1.406
μ [mm^{-1}]	5.769
Radiation Type	CuKα (λ = 1.54178)
F(000)	1632.0
No of measured refl	3301
No of independent refl.	2676
No of refl. (I ≥ 2σ)	3123

REFERENCES

1. Herold, F.; Schneller, A., High-Performance Polymers. *Adv. Mater.* **1992,** *4* (3), 143−152.

2. Hergenrother, P. M.; Jensen, B. J.; Havens, S. J., Poly(arylene ethers). *Polymer* **1988,** *29* (2), 358−369.

3. Tesoro, G., Aromatic high-strength fibers, H. H. Yang, John Wiley & Sons, Inc., New York, 1989,873 pp. Price: $125.00. *J. Polym. Sci. Part C: Polym. Lett.* **1990,** *28* (8), 264−265.

4. Liaw, D.-J.; Wang, K.-L.; Huang, Y.-C.; Lee, K.-R.; Lai, J.-Y.; Ha, C.-S., Advanced polyimide materials: Syntheses, physical properties and applications. *Prog. Polym. Sci.* **2012,** *37* (7), 907−974.

5. Harris, F. W., Synthesis of aromatic polyimides from dianhydrides and diamines. In *Polyimides*, Wilson, D.; Stenzenberger, H. D.; Hergenrother, P. M., Eds. Springer Netherlands: Dordrecht, 1990; p 1−37.

6. (a) Meadway, J., Asthma and atopy in workers with an epoxy adhesive. *Br. J. Dis Chest* **1980,** *74*, 149−154; (b) Czuppon, A. B.; Kaplan, V.; Speich, R.; Baur, X., Acute autoimmune response in a case of 3yromellitic acid dianhydride-induced hemorrhagic alveolitis. *Allergy* **1994,** *49* (5), 337−341.

7. Luo, K.; Wang, Y.; Yu, J.; Zhu, J.; Hu, Z., Semi-Biobased Aromatic Polyamides from 2,5-Furandicarboxylic Acid: toward high-performance polymers from renewable resources. *RSC Adv.* **2016,** *6* (90), 87013−87020.

8. Feng, X.; East, A. J.; Hammond, W.; Jaffe, M., Sugar-Based Chemicals for Environmentally Sustainable Applications. In *Contemporary Science of Polymeric Materials*, American Chemical Society: 2010; Vol. 1061, p 3−27.

9. Feng, X.; East, A. J.; Hammond, W. B.; Zhang, Y.; Jaffe, M., Overview of advances in sugar-based polymers. *Polym. Adv. Technol.* **2011,** *22* (1), 139−150.

10. (a) Dijkman, W. P.; Groothuis, D. E.; Fraaije, M. W., Enzyme-Catalyzed Oxidation of 5-Hydroxymethylfurfural to Furan-2,5-dicarboxylic Acid. *Angew. Chem. Int. Ed.* **2014,** *53* (25), 6515−6518; (b) Liu, B.; Ren, Y.; Zhang, Z., Aerobic oxidation of 5-hydroxymethylfurfural into 2,5-furandicarboxylic acid in water under mild conditions. *Green Chem.* **2015,** *17* (3), 1610−1617.

11. Amir, S. M. M.; Sultan, M. T. H.; Jawaid, M.; Ariffin, A. H.; Mohd, S.; Salleh, K. A. M.; Ishak, M. R.; Shah, A. U. M., 16 - Nondestructive testing method for Kevlar and natural fiber and their hybrid composites. In *Durability and Life Prediction in Biocomposites, Fibre-Reinforced Composites and Hybrid Composites*, Jawaid, M.; Thariq, M.; Saba, N., Eds. Woodhead Publishing: 2019; p 367−388.

12. Zhang, Q.; Molenda, M.; Reineke, T. M., Epoxy Resin Thermosets Derived from Trehalose and β-Cyclodextrin. *Macromolecules* **2016,** *49* (22), 8397−8406.

13. Wang, Z.; Miller, B.; Butz, J.; Randazzo, K.; Wang, Z. D.; Chu, Q. R., Polyladderane Constructed from a Gemini Monomer through Photoreaction. *Angew. Chem. Int. Ed.* **2017,** *56* (40), 12155−12159.

14. (a) Hou, X.; Wang, Z.; Lee, J.; Wysocki, E.; Oian, C.; Schlak, J.; Chu, Q. R., Synthesis of polymeric ladders by topochemical polymerization. *Chem. Commun.* **2014,** *50* (10), 1218−1220; (b) Wang, Z.; Kastern, B.; Randazzo, K.; Ugrinov, A.; Butz, J.; Seals, D. W.; Sibi, M. P.; Chu, Q. R., Linear polyester synthesized from furfural-based monomer by photoreaction in sunlight. *Green Chem.* **2015,** *17* (10), 4720−4724.

15. Wang, Z.; Randazzo, K.; Hou, X.; Simpson, J.; Struppe, J.; Ugrinov, A.; Kastern, B.; Wysocki, E.; Chu, Q. R., Stereoregular Two-Dimensional Polymers Constructed by Topochemical Polymerization. *Macromolecules* **2015,** *48* (9), 2894−2900.

16. Hergenrother, P. M., The Use, Design, Synthesis, and Properties of High Performance/High Temperature Polymers: An Overview. *High Perform. Polym.* **2003,** *15* (1), 3−45.

17. May, C. A., *Chemorheology of Thermosetting Polymers*. American Chemical Society: 1982; Vol. 227, p 348.

18. (a) Kissenger, H. E., Variation of peak temperature with haeating rate in differential thermal analysis. *J. Res. Natl. Bur. Stand.* **1956,** *57*, 217 − 221; (b) Ozawa, T., A modified method for kinetic analysis of thermoanalytical data. *J. Therm. Anal.* **1976,** *9* (3), 369−373.

19. Kirschbaum, S.; Landfester, K.; Taden, A., Synthesis and Thermal Curing of Benzoxazine Functionalized Polyurethanes. *Macromolecules* **2015,** *48* (12), 3811−3816.

20. (a) Tant, M. R.; Connell, J. W.; McManus, H. L. N., *High-Temperature Properties and Applications of Polymeric Materials*. American Chemical Society: 1995; Vol. 603, p 268; (b) Tant, M. R.; McManus, H. L. N.; Rogers, M. E., High-Temperature Properties and Applications of Polymeric Materials. In *High-Temperature Properties and Applications of Polymeric Materials*, American Chemical Society: 1995; Vol. 603, p 1−20.

21. Hasegawa, M., Photopolymerization of diolefin crystals. *Chem. Rev.* **1983,** *83* (5), 507−518.

22. Pramoda, K. P.; Chung, T. S.; Liu, S. L.; Oikawa, H.; Yamaguchi, A., Characterization and thermal degradation of polyimide and polyamide liquid crystalline polymers. *Polym. Degrad. Stab.* **2000,** *67* (2), 365−374.

23. (a) Lua, A. C.; Su, J., Isothermal and non-isothermal pyrolysis kinetics of Kapton® polyimide. *Polym. Degrad. Stab.* **2006,** *91* (1), 144−153; (b) Tsanaktsis, V.; Vouvoudi, E.; Papageorgiou, G. Z.; Papageorgiou, D. G.; Chrissafis, K.; Bikiaris, D. N., Thermal degradation kinetics and decomposition mechanism of polyesters based on 2,5-furandicarboxylic acid and low molecular weight aliphatic diols. *J. Anal. Appl. Pyrolysis* **2015,** *112*, 369−378.

24. Sousa, A. F.; Matos, M.; Freire, C. S. R.; Silvestre, A. J. D.; Coelho, J. F. J., New copolyesters derived from terephthalic and 2,5-furandicarboxylic acids: A step forward in the development of biobased polyesters. *Polymer* **2013,** *54* (2), 513−519.

25. (a) Harani, H.; Fellahi, S.; Bakar, M., Toughening of epoxy resin using hydroxyl-terminated polyesters. *J. Appl. Polym. Sci.* **1999,** *71* (1), 29−38; (b) Papageorgiou, G. Z.; Tsanaktsis, V.; Bikiaris, D. N., Synthesis of poly(ethylene furandicarboxylate) polyester using monomers derived from renewable resources: thermal behavior comparison with PET and PEN. *PCCP* **2014,** *16* (17), 7946−7958.

26. https://dielectricmfg.com/knowledge-base/kapton/ (accessed July-30-2021).

27. Nandi, S.; Winter, H. H., Swelling Behavior of Partially Cross-Linked Polymers: A Ternary System. *Macromolecules* **2005,** *38* (10), 4447−4455.

28. Bozell, J. J.; Petersen, G. R., Technology development for the production of biobased products from biorefinery carbohydrates-the US Department of Energy's "Top 10" revisited. *Green Chem.* **2010,** *12* (4), 539−554.

29. Chai, S.-H.; Wang, H.-P.; Liang, Y.; Xu, B.-Q., Sustainable production of acrolein: investigation of solid acid-base catalysts for gas-phase dehydration of glycerol. *Green Chem.* **2007,** *9* (10), 1130−1136.

30. Pang, J.; Zheng, M.; Sun, R.; Wang, A.; Wang, X.; Zhang, T., Synthesis of ethylene glycol and terephthalic acid from biomass for producing PET. *Green Chem.* **2016,** *18* (2), 342−359.

31. Kristiansen, B. L., J.; Mattey, M., *Citric Acid Biotechnology*. CRC Press: 2002.

32. Liu, J.; Du, Z.; Yang, Y.; Lu, T.; Lu, F.; Xu, J., Catalytic Oxidative Decarboxylation of Malic Acid into Dimethyl Malonate in Methanol with Dioxygen. *ChemSusChem* **2012,** *5* (11), 2151−2154.

33. Werpy, T. P., G., *Top Value Added Chemicals from Biomass*. National Renewable Energy Laboratory: 2004.

34. (a) Allcock, H.; Lampe, F.; Mark, J., The Scope of Polymer Chemistry. In *Contemporary Polymer Chemistry*, Third Edition ed.; Prentice Hall: 2003; p 1−26; (b) Odian, G., Introduction. In *Principles of Polymerization*, Fourth Edition ed.; 2004; p 1−38; (c) Cowie, J. M. G.; Arrighi, V., Introduction. In *Polymers: Chemistry and Physics of Modern Materials*, Third Edition ed.; CRC Press 2007; p 1−24.

35. (a) Serini, V., Polycarbonates. In *Ullmann's encyclopedia of industrial chemistry*, Wiley VCH Verlag GmbH & Co. KGaA: Weinheim, Germany, 2000; (b) Kim, J. G.,

Chemical recycling of poly(bisphenol A carbonate). *Polym. Chem.* **2020,** *(https://doi.org/10.1039/C9PY01927H)*.

36. Ha Q. Pham; Marks, M. J., Epoxy Resins. In *Ullmann's encyclopedia of industrial chemistry*, Wiley-VCH Verlag GmbH & Co. KGaA: Weinheim, Germany, 2005.

37. (a) Krishnan, A. V.; Stathis, P.; Permuth, S. F.; Tokes, L.; Feldman, D., Bisphenol-A: an estrogenic substance is released from polycarbonate flasks during autoclaving. *Endocrinology* **1993,** *132* (6), 2279−2286; (b) Saal, F. S. v.; Hughes, C., An Extensive New Literature Concerning Low-Dose Effects of Bisphenol A Shows the Need for a New Risk Assessment. *Environ. Health Perspect.* **2005,** *113* (8), 926−933; (c) Kang, J.-H.; Kondo, F.; Katayama, Y., Human exposure to bisphenol A. *Toxicology* **2006,** *226* (2), 79−89; (d) Lang, I. A.; Galloway, T. S.; Scarlett, A.; Henley, W. E.; Depledge, M.; Wallace, R. B.; Melzer, D., Association of Urinary Bisphenol A Concentration With Medical Disorders and Laboratory Abnormalities in Adults. *JAMA* **2008,** *300* (11), 1303−1310; (e) Leranth, C.; Hajszan, T.; Szigeti-Buck, K.; Bober, J.; MacLusky, N. J., Bisphenol A prevents the synaptogenic response to estradiol in hippocampus and prefrontal cortex of ovariectomized nonhuman primates. *Proc. Natl. Acad. Sci. U.S.A.* **2008,** *105* (37), 14187−14191; (f) Benotti, M. J.; Trenholm, R. A.; Vanderford, B. J.; Holady, J. C.; Stanford, B. D.; Snyder, S. A., Pharmaceuticals and Endocrine Disrupting Compounds in U.S. Drinking Water. *Environ. Sci. Technol.* **2009,** *43* (3), 597−603; (g) Vogel, S. A., The politics of plastics: the making and unmaking of bisphenol a "safety". *Am. J. Public Health* **2009,** *99 Suppl 3* (Suppl 3), S559−S566; (h) Miller, D. E.; Hawley, R. S., Bisphenol A and the primate ovary. *Proc. Natl. Acad. Sci. U.S.A.* **2012,** *109* (43), 17315−17316.

38. (a) Fenouillot, F.; Rousseau, A.; Colomines, G.; Saint-Loup, R.; Pascault, J. P., Polymers from renewable 1,4:3,6-dianhydrohexitols (isosorbide, isomannide and isoidide): A review. *Prog. Polym. Sci.* **2010,** *35* (5), 578−622; (b) Nelson, A. M.; Long, T. E., A perspective on emerging polymer technologies for bisphenol-A replacement. *Polym. Int.* **2012,** *61* (10), 1485−1491; (c) Lavilla, C.; Gubbels, E.; Martínez de Ilarduya, A.; Noordover, B. A. J.; Koning, C. E.; Muñoz-Guerra, S., Solid-State Modification of PBT with Cyclic Acetalized Galactitol and d-Mannitol: Influence of Composition and Chemical Microstructure on Thermal Properties. *Macromolecules* **2013,** *46* (11), 4335−4345; (d) Munoz-Guerra, S.; Lavilla, C.; Japu, C.; de Ilarduya, A. M., Renewable terephthalate polyesters from carbohydrate-based bicyclic monomers. *Green Chem.* **2014,** *16* (4), 1716−1739; (e) Ma, S.; Webster, D. C.; Jabeen, F., Hard and Flexible, Degradable Thermosets from Renewable Bioresources with the Assistance of Water and Ethanol. *Macromolecules* **2016,** *49* (10), 3780−3788; (f) Lingier, S.; Spiesschaert, Y.; Dhanis, B.; De Wildeman, S.; Du Prez, F. E., Rigid Polyurethanes, Polyesters, and Polycarbonates from Renewable Ketal Monomers. *Macromolecules* **2017,** *50* (14), 5346−5352; (g) Liu, X.; Pang, C.; Ma, J.; Gao, H., Random Copolycarbonates Based on a Renewable Bicyclic Diol Derived from Citric Acid. *Macromolecules* **2017,** *50* (20), 7949−7958; (h) Son, S.; Nam, K.; Kim, H.; Gye, M. C.; Shin, I., Cytotoxicity measurement of Bisphenol A (BPA) and its substitutes using human keratinocytes. *Environ. Res.* **2018,** *164*, 655−659; (i) Avcı, D.; Altürk, S.; Sönmez, F.; Tamer, Ö.; Başoğlu, A.; Atalay, Y.; Zengin Kurt, B.; Öztürk, D.; Dege, N., A new dinuclear copper (II) complex of 2,5-Furandicarboxyclic acid with 4(5)-Methylimidazole as a high potential α-glucosidase inhibitor: Synthesis, Crystal

structure, Cytotoxicity study, and TD/DFT calculations. *Appl. Organomet. Chem.* **2019,** *33* (3), e4725.

39. (a) Dickerson, J. P.; Brink, A. E.; Oshinski, A. J.; Seo, K. S. Copolyesters based on 1,4-cyclohexanedimethanol having improved stability. US Patent 5656715, 1997; (b) Turner, S. R., Development of amorphous copolyesters based on 1,4-cyclohexanedimethanol. *J. Polym. Sci., Part A: Polym. Chem.* **2004,** *42* (23), 5847−5852; (c) Liu, Y.; Turner, S. R., Synthesis and properties of cyclic diester based aliphatic copolyesters. *J. Polym. Sci., Part A: Polym. Chem.* **2010,** *48* (10), 2162−2169; (d) Yoon, W. J.; Hwang, S. Y.; Koo, J. M.; Lee, Y. J.; Lee, S. U.; Im, S. S., Synthesis and Characteristics of a Biobased High-Tg Terpolyester of Isosorbide, Ethylene Glycol, and 1,4-Cyclohexane Dimethanol: Effect of Ethylene Glycol as a Chain Linker on Polymerization. *Macromolecules* **2013,** *46* (18), 7219−7231; (e) Wang, J.; Liu, X.; Zhang, Y.; Liu, F.; Zhu, J., Modification of Poly(ethylene 2,5-furandicarboxylate) with 1,4-cyclohexanedimethylene: Influence of composition on mechanical and barrier properties. *Polymer* **2016,** *103*, 1−8; (f) Hu, Y.; Zhao, Z.; Liu, Y.; Li, G.; Wang, A.; Cong, Y.; Zhang, T.; Wang, F.; Li, N., Synthesis of 1,4-Cyclohexanedimethanol, 1,4-Cyclohexanedicarboxylic Acid and 1,2-Cyclohexanedicarboxylates from Formaldehyde, Crotonaldehyde and Acrylate/Fumarate. *Angew. Chem. Int. Ed.* **2018,** *57* (23), 6901−6905.

40. (a) Kelsey, D. R.; Scardino, B. M.; Grebowicz, J. S.; Chuah, H. H., High Impact, Amorphous Terephthalate Copolyesters of Rigid 2,2,4,4-Tetramethyl-1,3-cyclobutanediol with Flexible Diols. *Macromolecules* **2000,** *33* (16), 5810−5818; (b) Hoppens, N. C.; Hudnall, T. W.; Foster, A.; Booth, C. J., Aliphatic–aromatic copolyesters derived from 2,2,4,4-tetramethyl-1,3-cyclobutanediol. *J. Polym. Sci., Part A: Polym. Chem.* **2004,** *42*

(14), 3473−3478; (c) Zhang, M.; Moore, R. B.; Long, T. E., Melt transesterification and characterization of segmented block copolyesters containing 2,2,4,4-tetramethyl-1,3-cyclobutanediol. *J. Polym. Sci., Part A: Polym. Chem.* **2012,** *50* (18), 3710−3718; (d) Wang, L., Heroes of Chemistry. *Chem. Eng. News* **2015,** *93* (38), 47−49.

41. Hasek, R. H.; Elam, E. U. Process of manufacturing dialkyl ketenes. US Patent 3,201,474, 1965.

42. Schiraldi, D. A., New Poly(Ethylene Terephthalate) Copolymers. In *Modern Polyesters: Chemistry and Technology of Polyesters and Copolyesters*, Scheirs, J.; Long, T. E., Eds. John Wiley & Sons, Ltd: 2004; p 267−292.

43. (a) Sumner Jr., C. E.; Gustafson, B. L.; Knight, J. R. Process for the manufacture of 2,2,4,4-tetramethycyclobutanediol. US Patent 5169994, 1991; (b) Burke, D. J.; Kawauchi, T.; Kade, M. J.; Leibfarth, F. A.; McDearmon, B.; Wolffs, M.; Kierstead, P. H.; Moon, B.; Hawker, C. J., Ketene-Based Route to Rigid Cyclobutanediol Monomers for the Replacement of BPA in High Performance Polyesters. *ACS Macro Letters* **2012,** *1* (11), 1228−1232.

44. Wang, J.; Mahmud, S.; Zhang, X.; Zhu, J.; Shen, Z.; Liu, X., Biobased Amorphous Polyesters with High Tg: Trade-Off between Rigid and Flexible Cyclic Diols. *ACS Sustainable Chem. & Eng.* **2019,** *7* (6), 6401−6411.

45. (a) Nozaki, H.; Otani, I.; Noyori, R.; Kawanisi, M., Photochemical reactions of trans-anethole. *Tetrahedron* **1968,** *24* (5), 2183−2192; (b) Campbell, N.; Macpherson, R. S.; Morris, R. A. N., 22.—Attempted Synthesis of Dibenzo[a,g]biphenylene. *Proc. R. Soc. Edinburgh, Sect. A: Math. Phys. Sci.* **1974,** *71* (4), 275−277.

46. (a) Wang, Z.; Miller, B.; Mabin, M.; Shahni, R.; Wang, Z. D.; Ugrinov, A.; Chu, Q. R., Cyclobutane-1,3-Diacid (CBDA): A Semi-Rigid Building Block Prepared by [2+2] Photocyclization for Polymeric Materials. *Sci. Rep.* **2017,** *7* (1), 13704; (b) Wang, Z. D.; Elliott, Q.; Wang, Z.; Setien, R. A.; Puttkammer, J.; Ugrinov, A.; Lee, J.; Webster, D. C.; Chu, Q. R., Furfural-Derived Diacid Prepared by Photoreaction for Sustainable Materials Synthesis. *ACS Sustainable Chem. Eng.* **2018,** *6* (7), 8136−8141; (c) Amjaour, H.; Wang, Z.; Mabin, M.; Puttkammer, J.; Busch, S.; Chu, Q. R., Scalable preparation and property investigation of a *cis*-cyclobutane-1,2-dicarboxylic acid from *beta-trans*-cinnamic acid. *Chem. Commun.* **2019,** *55* (2), 214−217; (d) Wang, Z.; Scheuring, M.; Mabin, M.; Shahni, R.; Wang, Z. D.; Ugrinov, A.; Butz, J.; Chu, Q. R., Renewable Cyclobutane-1,3-dicarboxylic Acid (CBDA) Building Block Synthesized from Furfural via Photocyclization. *ACS Sustainable Chem. Eng.* **2020,** *8* (24), 8909−8917.

47. (a) Cohen, M. D.; Schmidt, G. M. J.; Sonntag, F. I., 384. Topochemistry. Part II. The photochemistry of *trans*-cinnamic acids. *J. Chem. Soc.* **1964,** (0), 2000−2013; (b) Abdelmoty, I.; Buchholz, V.; Di, L.; Guo, C.; Kowitz, K.; Enkelmann, V.; Wegner, G.; Foxman, B. M., Polymorphism of Cinnamic and α-Truxillic Acids: New Additions to an Old Story. *Cryst. Growth Des.* **2005,** *5* (6), 2210−2217.

48. PaquetteL. A.; Ollevier, T.; Desyror, V., Lithium Aluminum Hydride. In *Encyclopedia of Reagents for Organic Synthesis*, John Wiley & Sons, Inc.: 2004.

49. Kanth, J. V. B.; Periasamy, M., Selective reduction of carboxylic acids into alcohols using sodium borohydride and iodine. *J. Org. Chem.* **1991,** *56* (20), 5964−5965.

50. (a) McKennon, M. J.; Meyers, A. I.; Drauz, K.; Schwarm, M., A convenient reduction of amino acids and their derivatives. *J. Org. Chem.* **1993,** *58* (13), 3568−3571;

(b) Simek, J. W.; Tuck, T.; Bush, K. C., Reduction of Carboxylic Acids with Sodium Borohydride and an Electrophile. *J. Chem. Educ.* **1997,** *74* (1), 107.

51. Cotton, F. A.; Frenz, B. A., Conformations of cyclobutane. *Tetrahedron* **1974,** *30* (12), 1587−1594.

52. Thiyagarajan, S.; Vogelzang, W.; J. I. Knoop, R.; Frissen, A. E.; van Haveren, J.; van Es, D. S., Biobased furandicarboxylic acids (FDCAs): effects of isomeric substitution on polyester synthesis and properties. *Green Chem.* **2014,** *16* (4), 1957−1966.

53. (a) Wang, Z.; Kastern, B.; Randazzo, K.; Ugrinov, A.; Butz, J.; Seals, D. W.; Sibi, M. P.; Chu, Q. R., Linear polyester synthesized from furfural-based monomer by photoreaction in sunlight. *Green Chem.* **2015,** *17* (10), 4720-4724; (b) Randazzo, K.; Wang, Z.; Wang, Z. D.; Butz, J.; Chu, Q. R., Lighting the Way to Greener Chemistry: Incandescent Floodlights as a Facile UV Light Source for Classic and Cutting-Edge Photoreactions. *ACS Sustainable Chem. Eng.* **2016,** *4* (9), 5053−5059; (c) Wang, Z.; Miller, B.; Butz, J.; Randazzo, K.; Wang, Z. D.; Chu, Q. R., Polyladderane Constructed from a Gemini Monomer through Photoreaction. *Angewandte Chemie International Edition* **2017,** *56* (40), 12155-12159.

54. (a) Dalli, S. S.; Tilaye, T. J.; Rakshit, S. K., Conversion of Wood-Based Hemicellulose Prehydrolysate into Succinic Acid Using a Heterogeneous Acid Catalyst in a Biphasic System. *Ind. Eng. Chem. Res.* **2017,** *56* (38), 10582−10590; (b) Zhu, W.; Tao, F.; Chen, S.; Li, M.; Yang, Y.; Lv, G., Efficient Oxidative Transformation of Furfural into Succinic Acid over Acidic Metal-Free Graphene Oxide. *ACS Sustainable Chem. Eng.* **2018,** *7* (1), 296−305.

55. Huang, Y.-T.; Wong, J.-J.; Huang, C.-J.; Li, C.-L.; Jang, G.-W. B., 2,5-Furandicarboxylic Acid Synthesis and Use. In *Chemicals and Fuels from Bio-Based Building Blocks*, Wiley-VCH Verlag GmbH & Co. KGaA: 2016; p 191−216.

56. (a) Scott, E.; Peter, F.; Sanders, J., Biomass in the manufacture of industrial products — the use of proteins and amino acids. *Appl. Microbiol. Biotechnol.* **2007,** *75* (4), 751−762; (b) Goodman, C., Metabolic engineering: A plastic pathway. *Nat. Chem. Biol.* **2011,** *7* (9), 576−576; (c) McKenna, R.; Nielsen, D. R., Styrene biosynthesis from glucose by engineered E. coli. *Metab. Eng.* **2011,** *13* (5), 544−554; (d) Spekreijse, J.; Le Notre, J.; van Haveren, J.; Scott, E. L.; Sanders, J. P. M., Simultaneous production of biobased styrene and acrylates using ethenolysis. *Green Chem.* **2012,** *14* (10), 2747−2751.

57. (a) Li, W.; Chung, H.; Daeffler, C.; Johnson, J. A.; Grubbs, R. H., Application of 1H DOSY for Facile Measurement of Polymer Molecular Weights. *Macromolecules* **2012,** *45* (24), 9595−9603; (b) Rosenboom, J.-G.; De Roo, J.; Storti, G.; Morbidelli, M., Diffusion (DOSY) 1H NMR as an Alternative Method for Molecular Weight Determination of Poly(ethylene furanoate) (PEF) Polyesters. *Macromol. Chem. Phys.* **2017,** *218* (1), 1600436.

58. (a) Li, D.; Keresztes, I.; Hopson, R.; Williard, P. G., Characterization of reactive intermediates by multinuclear diffusion-ordered NMR spectroscopy (DOSY). *Acc. Chem. Res.* **2009,** *42* (2), 270−280; (b) Li, W.; Kagan, G.; Yang, H.; Cai, C.; Hopson, R.; Sweigart, D. A.; Williard, P. G., Physically Separated References for Diffusion Coefficient-Formula Weight (D-FW) Analysis of Diffusion-Ordered NMR Spectroscopy (DOSY) in Water. *Org. Lett.* **2010,** *12* (12), 2698−2701; (c) Kagan, G.; Li, W.; Li, D.; Hopson, R.; Williard,

P. G., Characterization of Dimeric Chiral Lithium Amide Structures Derived from N-isopropyl-O- triisopropylsilyl Valinol. *J. Am. Chem. Soc.* **2011,** *133* (17), 6596−6602.

59. (a) Mishra, M. K.; Varughese, S.; Ramamurty, U.; Desiraju, G. R., Odd–Even Effect in the Elastic Modulii of α,ω-Alkanedicarboxylic Acids. *J. Am. Chem. Soc.* **2013,** *135* (22), 8121−8124; (b) Mishra, M. K.; Ramamurty, U.; Desiraju, G. R., Hardness Alternation in α,ω-Alkanedicarboxylic Acids. *Chem.: Asian J.* **2015,** *10* (10), 2176−2181.

60. (a) Chattopadhyay, D. K.; Webster, D. C., Thermal stability and flame retardancy of polyurethanes. *Prog. Polym. Sci.* **2009,** *34* (10), 1068−1133; (b) Zakharova, E.; Martínez de Ilarduya, A.; León, S.; Muñoz-Guerra, S., Sugar-based bicyclic monomers for aliphatic polyesters: a comparative appraisal of acetalized alditols and isosorbide. *Des Monomers Polym.* **2017,** *20* (1), 157−166.

61. Froidevaux, V.; Negrell, C.; Caillol, S.; Pascault, J.-P.; Boutevin, B., Biobased Amines: From Synthesis to Polymers; Present and Future. *Chem. Rev.* **2016,** *116* (22), 14181−14224.

62. (a) García, J. M.; García, F. C.; Serna, F.; de la Peña, J. L., High-performance aromatic polyamides. *Prog. Polym. Sci.* **2010,** *35* (5), 623−686; (b) Rebouillat, S., 2 - ARAMIDS: 'Disruptive', open and continuous innovation. In *Advanced Fibrous Composite Materials for Ballistic Protection*, Chen, X., Ed. Woodhead Publishing: 2016; p 11−70; (c) Maniar, D.; Hohmann, K. F.; Jiang, Y.; Woortman, A. J. J.; van Dijken, J.; Loos, K., Enzymatic Polymerization of Dimethyl 2,5-Furandicarboxylate and Heteroatom Diamines. *ACS Omega* **2018,** *3* (6), 7077−7085.

63. Crespo, L.; Sanclimens, G.; Pons, M.; Giralt, E.; Royo, M.; Albericio, F., Peptide and Amide Bond-Containing Dendrimers. *Chem. Rev.* **2005,** *105* (5), 1663−1682.

64. (a) Angelo, R. J.; Miura, H.; Gardner, K. H.; Chase, D. B.; English, A. D., Preparation and characterization of selectively isotopically labeled nylon 66 polymers. *Macromolecules* **1989,** *22* (1), 117−121; (b) Steeman, P.; Nijenhuis, A., The effect of random branching on the balance between flow and mechanical properties of polyamide-6. *Polymer* **2010,** *51* (12), 2700−2707; (c) Moran, C. S.; Barthelon, A.; Pearsall, A.; Mittal, V.; Dorgan, J. R., Biorenewable blends of polyamide-4,10 and polyamide-6,10. *J. Appl. Polym. Sci.* **2016,** *133* (45); (d) Gomes, A. C. d. O.; Soares, B. G.; Oliveira, M. G.; Machado, J. C.; Windmöller, D.; Paranhos, C. M., Characterization of crystalline structure and free volume of polyamide 6/nitrile rubber elastomer thermoplastic vulcanizates: Effect of the processing additives. *J. Appl. Polym. Sci.* **2017,** *134* (48), 45576; (e) Yuan, D.; Gao, Y.-F.; Guo, Z.-X.; Yu, J., Improved thermal conductivity of ceramic filler-filled polyamide composites by using PA6/PA66 1:1 blend as matrix. *J. Appl. Polym. Sci.* **2017,** *134* (40), 45371.

65. (a) Rao, Y.; Waddon, A. J.; Farris, R. J., Structure–property relation in poly(*p*-phenylene terephthalamide) (PPTA) fibers. *Polymer* **2001,** *42* (13), 5937−5946; (b) Ferreiro, J. J.; de la Campa, J. G.; Lozano, A. E.; de Abajo, J., Polyisophthalamides with heteroaromatic pendent rings: Synthesis, physical properties, and water uptake. *J. Polym. Sci., Part A: Polym. Chem.* **2005,** *43* (21), 5300−5311.

66. Huang, Y.-C.; Wang, K.-L.; Chang, C.-H.; Liao, Y.-A.; Liaw, D.-J.; Lee, K.-R.; Lai, J.-Y., Solvent Response and Protonation Effects of Novel Aramides Containing Pyridine and Unsymmetrical Carbazole Moieties. *Macromolecules* **2013,** *46* (18), 7443−7450.

67. (a) Hsiao, S.-H.; Chen, C.-W.; Liou, G.-S., Novel aromatic polyamides bearing pendent diphenylamino or carbazolyl groups. *J. Polym. Sci., Part A: Polym. Chem.* **2004,** *42* (13), 3302−3313; (b) Liou, G.-S.; Lin, H.-Y.; Yen, H.-J., Synthesis and characterization of electroactive hyperbranched aromatic polyamides based on A_2B-type triphenylamine moieties. *J. Mater. Chem.* **2009,** *19* (41), 7666−7673; (c) Zhang, G.; Bai, D.-t.; Li, D.-s.; Long, S.-r.; Wang, X.-j.; Yang, J., Synthesis and properties of polyamides derived from 4,6-bis(4-chloroformylphenylthio)pyrimidine and 3,6-bis(4-chloroformylphenylthio)pyridazine. *Polym. Int.* **2013,** *62* (9), 1358−1367; (d) Du, S.; Wang, W.; Yan, Y.; Zhang, J.; Tian, M.; Zhang, L.; Wan, X., A facile synthetic route to poly(*p*-phenylene terephthalamide) with dual functional groups. *Chem. Commun.* **2014,** *50* (69), 9929−9931; (e) Williams, J. C.; Meador, M. A. B.; McCorkle, L.; Mueller, C.; Wilmoth, N., Synthesis and Properties of Step-Growth Polyamide Aerogels Cross-linked with Triacid Chlorides. *Chem. Mater.* **2014,** *26* (14), 4163−4171.

68. (a) Uddin, A. J.; Ohkoshi, Y.; Gotoh, Y.; Nagura, M.; Hara, T., Influence of moisture on the viscoelastic relaxations in long aliphatic chain contained semiaromatic polyamide, (PA9-T) fiber. *J. Polym. Sci., Part B: Polym. Phys.* **2003,** *41* (22), 2878−2891; (b) Jalal Uddin, A.; Ohkoshi, Y.; Gotoh, Y.; Nagura, M.; Endo, R.; Hara, T., Melt spinning and laser-heated drawing of a new semiaromatic polyamide, PA9-T fiber. *J. Polym. Sci., Part B: Polym. Phys.* **2004,** *42* (3), 433−444; (c) Uddin, A. J.; Gotoh, Y.; Ohkoshi, Y.; Nagura, M.; Endo, R.; Hara, T., Hydration in a new semiaromatic polyamide observed by humidity-controlled dynamic viscoelastometry and X-ray diffraction. *J. Polym. Sci., Part B: Polym. Phys.* **2005,** *43* (13), 1640−1648; (d) Uddin, A. J.; Gotoh, Y.; Ohkoshi, Y.;

Nishino, T.; Endo, R., Crystal modulus of a new semiaromatic polyamide 9-T. *Polymer Engineering & Science* **2012,** *52* (2), 331−337.

69. (a) Wang, W.; Wang, X.; Li, R.; Liu, B.; Wang, E.; Zhang, Y., Environment-friendly synthesis of long chain semiaromatic polyamides with high heat resistance. *J. Appl. Polym. Sci.* **2009,** *114* (4), 2036−2042; (b) Zhang, C.; Huang, X.; Zeng, X.; Cao, M.; Cai, T.; Jiang, S.; Yi, Q., Fluidity improvement of semiaromatic polyamides: Modification with oligomers. *J. Appl. Polym. Sci.* **2014,** *131* (7).

70. Ballistreri, A.; Garozzo, D.; Giuffrida, M.; Maravigna, P.; Montaudo, G., Thermal decomposition processes in aliphatic-aromatic polyamides investigated by mass spectrometry. *Macromolecules* **1986,** *19* (11), 2693−2699.

71. Zhang, G.; Zhou, Y.-x.; Kong, Y.; Li, Z.-m.; Long, S.-R.; Yang, J., Semiaromatic polyamides containing ether and different numbers of methylene (2–10) units: synthesis and properties. *RSC Adv* **2014,** *4* (108), 63006−63015.

72. (a) Harashina, H.; Nakane, T.; Itoh, T., Synthesis of poly(ester amide)s by the melt polycondensation of semiaromatic polyesters with ethanolamine and their characterization. *J. Polym. Sci., Part A: Polym. Chem.* **2007,** *45* (11), 2184−2193; (b) Wilsens, C. H. R. M.; Deshmukh, Y. S.; Noordover, B. A. J.; Rastogi, S., Influence of the 2,5-Furandicarboxamide Moiety on Hydrogen Bonding in Aliphatic–Aromatic Poly(ester amide)s. *Macromolecules* **2014,** *47* (18), 6196−6206.

73. Zhang, G.; Huang, G.-S.; Li, D.-S.; Wang, X.-J.; Long, S.-R.; Yang, J., Facile Synthesis of Processable Semiaromatic Polyamides Containing Thioether Units. *Industrial & Engineering Chemistry Research* **2011,** *50* (11), 7056−7064.

74. Shabanian, M.; Kang, N.; Liu, J.; Wagenknecht, U.; Heinrich, G.; Wang, D.-Y., Bio-based semi-aromatic polyamide/functional clay nanocomposites: preparation and properties. *RSC Adv.* **2014,** *4* (45), 23420−23427.

75. (a) Liaw, D.-J.; Chang, F.-C.; Leung, M.-k.; Chou, M.-Y.; Muellen, K., High Thermal Stability and Rigid Rod of Novel Organosoluble Polyimides and Polyamides Based on Bulky and Noncoplanar Naphthalene−Biphenyldiamine. *Macromolecules* **2005,** *38* (9), 4024−4029; (b) Novitsky, T. F.; Lange, C. A.; Mathias, L. J.; Osborn, S.; Ayotte, R.; Manning, S., Eutectic melting behavior of polyamide 10,T-co-6,T and 12,T-co-6,T copolyterephthalamides. *Polymer* **2010,** *51* (11), 2417−2425; (c) Yang, S. H.; Fu, P.; Liu, M. Y.; Wang, Y. D.; Zhang, Y. C.; Zhao, Q. X., Synthesis, characterization of polytridecamethylene 2,6-naphthalamide as semiaromatic polyamide containing naphthalene-ring. *Express Polymer Letters* **2010,** *4*, 442−449; (d) Liu, M.; Li, K.; Yang, S.; Fu, P.; Wang, Y.; Zhao, Q., Synthesis and thermal decomposition of poly(dodecamethylene terephthalamide). *J. Appl. Polym. Sci.* **2011,** *122* (5), 3369−3376.

76. (a) Jikei, M.; Chon, S.-H.; Kakimoto, M.-a.; Kawauchi, S.; Imase, T.; Watanebe, J., Synthesis of Hyperbranched Aromatic Polyamide from Aromatic Diamines and Trimesic Acid. *Macromolecules* **1999,** *32* (6), 2061−2064; (b) Hsiao, S.-H.; Liao, W.-K.; Liou, G.-S., Synthesis and Electrochromism of Highly Organosoluble Polyamides and Polyimides with Bulky Trityl-Substituted Triphenylamine Units. *Polymers* **2017,** *9* (10), 511; (c) Salunkhe, P. H.; Patil, Y. S.; Kadam, V. N.; Mahindrakar, J. N.; Ubale, V. P.; Ghanwat, A. A., Synthesis and characterization of processable polyamides containing polar quinoxaline unit in the main chain and evaluation of its hydrophilicity. *Journal of Macromolecular Science, Part A* **2019,** *56* (4), 299−305.

77. Zhang, G.; Zhou, Y.-x.; Li, Y.; Wang, X.-J.; Long, S.-R.; Yang, J., Investigation of the synthesis and properties of isophorone and ether units based semi-aromatic polyamides. *RSC Adv.* **2015,** *5* (62), 49958−49967.

78. Moisa, S.; Landsberg, G.; Rittel, D.; Halary, J. L., Hysteretic thermal behavior of amorphous semi-aromatic polyamides. *Polymer* **2005,** *46* (25), 11870−11875.

79. Zhang, C., Progress in semicrystalline heat-resistant polyamides. *e-Polymers* **2018,** *18* (5), 373−408.

80. (a) Miller, D. B.; Flanagan, P. W.; Shechter, H., Structure and chemistry of the photodimer of *trans*-*beta*-nitrostyrene. *J. Am. Chem. Soc.* **1972,** *94* (11), 3912−3918; (b) Desiraju, G. R.; Pedireddi, V. R., Solid state dimerisation of *β*-nitrostyrene: a disordered photoreactive crystal. *J. Chem. Soc., Chem. Commun.* **1989,** (16), 1112−1113.

81. Schmidt, G. M. J., 385. Topochemistry. Part III. The crystal chemistry of some *trans*-cinnamic acids. *J. Chem. Soc.* **1964,** (0), 2014−2021.

82. Campbell, R. D.; Ofstead, R. F., The Photodimer from *β*-Nitrostyrene. *Proc Iowa Acad. Sci.* **1964,** *71* (1) 197−205.

83. Pedireddi, V. R.; Sarma, J. A. R. P.; Desiraju, G. R., Crystal engineering and solid state chemistry of some *β*-nitrostyrenes. *J. Chem. Soc. Perkin Trans. 2* **1992,** (2), 311−320.

84. Yamazaki, N.; Higashi, F.; Kawabata, J., Studies on reactions of the N-phosphonium salts of pyridines. XI. Preparation of polypeptides and polyamides by means of triaryl phosphites in pyridine. *J. Polym. Sci.: Polym. Chem. Ed.* **1974,** *12* (9), 2149−2154.

85. (a) Woodward, R. B.; Hoffmann, R., Stereochemistry of Electrocyclic Reactions. *J. Am. Chem. Soc.* **1965,** *87* (2), 395−397; (b) Woodward, R. B.; Hoffmann, R., The Conservation of Orbital Symmetry. *Angew. Chem. Int. Ed.* **1969,** *8* (11), 781−853.

86. Cherrington, R.; Liang, J., 2 - Materials and Deposition Processes for Multifunctionality. In *Design and Manufacture of Plastic Components for Multifunctionality*, Goodship, V.; Middleton, B.; Cherrington, R., Eds. William Andrew Publishing: Oxford, 2016; pp 19-51.

87. (a) Bender, T. A.; Dabrowski, J. A.; Gagné, M. R., Homogeneous catalysis for the production of low-volume, high-value chemicals from biomass. *Nat. Rev. Chem.* **2018,** *2* (5), 35−46; (b) Mika, L. T.; Cséfalvay, E.; Németh, Á., Catalytic Conversion of Carbohydrates to Initial Platform Chemicals: Chemistry and Sustainability. *Chem. Rev.* **2018,** *118* (2), 505−613.

88. (a) Díaz-Gallifa, P.; Fabelo, O.; Pasán, J.; Cañadillas-Delgado, L.; Ramírez, M. A.; Gallardo, A. G.; Ruiz-Pérez, C., Synthesis and structural characterization of six Cu(ii)-based coordination polymers using the thermally tunable 1,2,3,4-cyclobutanetetracarboxylic acid. *CrystEngComm* **2015,** *17* (27), 5081−5093; (b) Wan, X.-Y.; Jiang, F.-L.; Chen, L.; Pan, J.; Zhou, K.; Su, K.-Z.; Pang, J.-D.; Lyu, G.-X.; Hong, M.-C., Structural variability, unusual thermochromic luminescence and nitrobenzene sensing properties of five Zn(ii) coordination polymers assembled from a terphenyl-hexacarboxylate ligand. *CrystEngComm* **2015,** *17* (20), 3829−3837; (c) Xu, G.; Li, B.; Wu, H.; Zhou, W.; Chen, B., Construction of *ntt*-Type Metal–Organic Framework from C_2-Symmetry Hexacarboxylate Linker for Enhanced Methane Storage. *Cryst. Growth Des.* **2017,** *17* (9), 4795−4800; (d) Lippitt, E. M. L.; Ennis, C.; Moratti, S. C.; Hanton, L. R.,

Subtle Influences of a Flexible Tecton on an R22(8) Carboxyl Dimer Synthon: From Molecular Threading to 2D → 3D Interpenetration. *Cryst. Growth Des.* **2020,** *20* (12), 7805−7821.

89. (a) MacGillivray, L. R.; Papaefstathiou, G. S.; Friščić, T.; Hamilton, T. D.; Bučar, D.-K.; Chu, Q.; Varshney, D. B.; Georgiev, I. G., Supramolecular Control of Reactivity in the Solid State: From Templates to Ladderanes to Metal-Organic Frameworks. *Acc. Chem. Res.* **2008,** *41* (2), 280−291; (b) Dawe, L. N.; Shuvaev, K. V.; Thompson, L. K., Polytopic ligand directed self-assembly-polymetallic [n×n] grids versus non-grid oligomers. *Chem. Soc. Rev.* **2009,** *38* (8), 2334−2359; (c) Zhang, X.; Li, B.; Chen, Z.-H.; Chen, Z.-N., Luminescence vapochromism in solid materials based on metal complexes for detection of volatile organic compounds (VOCs). *J. Mater. Chem.* **2012,** *22* (23), 11427−11441; (d) Zhan, S.; De Gracia Triviño, J. A.; Ahlquist, M. S. G., The Carboxylate Ligand as an Oxide Relay in Catalytic Water Oxidation. *J. Am. Chem. Soc.* **2019,** *141* (26), 10247−10252.

90. (a) Chen, J.; Shen, K.; Li, Y., Greening the Processes of Metal–Organic Framework Synthesis and their Use in Sustainable Catalysis. *ChemSusChem* **2017,** *10* (16), 3165−3187; (b) Kumar, S.; Jain, S.; Nehra, M.; Dilbaghi, N.; Marrazza, G.; Kim, K.-H., Green synthesis of metal–organic frameworks: A state-of-the-art review of potential environmental and medical applications. *Coord. Chem. Rev.* **2020,** *420,* 213407.

91. (a) Li, X.; Jia, P.; Wang, T., Furfural: A Promising Platform Compound for Sustainable Production of C4 and C5 Chemicals. *ACS Catal.* **2016,** *6* (11), 7621−7640; (b) Mariscal, R.; Maireles-Torres, P.; Ojeda, M.; Sádaba, I.; López Granados, M., Furfural: a renewable and versatile platform molecule for the synthesis of chemicals and fuels. *Energy Environ. Sci.* **2016,** *9* (4), 1144−1189.

92. Wang, R.; Zhou, Y.; Sun, Y.; Yuan, D.; Han, L.; Lou, B.; Wu, B.; Hong, M., Syntheses and Crystal Structures of Copper(II) Coordination Polymers Comprising Discrete Helical Chains. *Cryst. Growth Des.* **2005,** *5* (1), 251−256.

93. (a) Ma, D.; Hu, P.; Qin, L.; Yan, J.; Lin, W.; Ding, W.; Lu, H.; Lin, D.; Sakiyama, H.; Liang, F., Synthesis, Characterization, and Magnetic Properties of Two Transition Metal Coordination Polymers Based on 2,5-Furandicarboxylic Acid and *N*-Donor Ligands. *J. Inorg. Organomet. Polymer Mater*. **2016,** *26* (5), 1053−1060; (b) Lagerspets, E.; Lagerblom, K.; Heliövaara, E.; Hiltunen, O.-M.; Moslova, K.; Nieger, M.; Repo, T., Schiff base Cu(I) catalyst for aerobic oxidation of primary alcohols. *Mol. Catal.* **2019,** *468*, 75−79.

94. (a) Guan, Q. L.; Gao, X.; Liu, J.; Wei, W. J.; Xing, Y. H.; Bai, F. Y., UO_{22}^{+}-polycarboxylate heterometallic complexes: structure, spectra, and photocatalytic properties. *J. Coord. Chem.* **2016,** *69* (6), 1026−1038; (b) Shi, D.; Cui, C.-J.; Hu, M.; Ren, A. H.; Song, L.-B.; Liu, C.-S.; Du, M., A microporous mixed-metal (Na/Cu) mixed-ligand (flexible/rigid) metal–organic framework for photocatalytic H_2 generation. *J. Mater. Chem. C* **2019,** *7* (33), 10211−10217; (c) Thuéry, P.; Atoini, Y.; Harrowfield, J., Uranyl Tricarballylate Triperiodic and Nanotubular Species. Counterion Control of Nanotube Diameter. *Inorg. Chem.* **2020,** *59* (10), 6953−6962.

95. Essex, L. A.; McSkimming, A.; Thompson, N. B.; Kelty, M. L.; Hill, E. A.; Harman, W. H., η^2-Arene Binding at High-Spin Fe(I) Enabled by a Sterically Accommodating Tris(pyrazolyl)hydroborate Ligand. *Organometallics* **2020,** *39* (13), 2545−2552.

96. Shahni, R. K.; Mabin, M.; Wang, Z.; Shaik, M.; Ugrinov, A.; Chu, Q. R., Synthesis and Characterization of BPA-Free Polyesters by Incorporating a Semi-Rigid Cyclobutanediol Monomer. *Polym. Chem.* **2020,** *11* (37), 6081-6090.

97. (a) Hou, X.; Schober, M.; Chu, Q., A Chiral Nanosheet Connected by Amide Hydrogen Bonds. *Cryst. Growth Des.* **2012,** *12* (11), 5159−5163; (b) Hou, X.; Wang, Z.; Overby, M.; Ugrinov, A.; Oian, C.; Singh, R.; Chu, Q. R., A two-dimensional hydrogen bonded organic framework self-assembled from a three-fold symmetric carbamate. *Chem. Commun.* **2014,** *50* (40), 5209−5211; (c) Wang, Z.; Lee, J.; Oian, C.; Hou, X.; Wang, Z.; Ugrinov, A.; Singh, R. K.; Wysocki, E.; Chu, Q. R., An unsaturated hydrogen bonded network generated from three-fold symmetric carbamates. *CrystEngComm* **2014,** *16* (31), 7176−7179.

98. (a) Mishra, A.; Ali, A.; Upreti, S.; Whittingham, M. S.; Gupta, R., Cobalt Complex as Building Blocks: Synthesis, Characterization, and Catalytic Applications of $\{Cd^{2+}–Co^{3+}–Cd^{2+}\}$ and $\{Hg^{2+}–Co^{3+}–Hg^{2+}\}$ Heterobimetallic Complexes. *Inorg. Chem.* **2009,** *48* (12), 5234−5243; (b) Renfrew, A. K.; O'Neill, E. S.; Hambley, T. W.; New, E. J., Harnessing the properties of cobalt coordination complexes for biological application. *Coord. Chem. Rev.* **2018,** *375*, 221−233; (c) Yang, X.-D.; Zhu, R.; Yin, J.-P.; Sun, L.; Guo, R.-Y.; Zhang, J., Bipyridinium-Bearing Multi-stimuli Responsive Chromic Material with High Stability. *Cryst. Growth Des.* **2018,** *18* (5), 3236−3243; (d) Xie, X.; He, C.; Li, B.; He, Y.; Cullen, D. A.; Wegener, E. C.; Kropf, A. J.; Martinez, U.; Cheng, Y.; Engelhard, M. H.; Bowden, M. E.; Song, M.; Lemmon, T.; Li, X. S.; Nie, Z.; Liu, J.; Myers, D. J.; Zelenay, P.; Wang, G.; Wu, G.; Ramani, V.; Shao, Y., Performance enhancement and

degradation mechanism identification of a single-atom Co–N–C catalyst for proton exchange membrane fuel cells. *Nat. Catal.* **2020,** *3* (12), 1044−1054.

99. (a) Chen, C.-L.; Goforth, A. M.; Smith, M. D.; Su, C.-Y.; zur Loye, H.-C., $[Co_2(ppca)_2(H_2O)(V_4O_{12})_{0.5}]$: A Framework Material Exhibiting Reversible Shrinkage and Expansion through a Single-Crystal-to-Single-Crystal Transformation Involving a Change in the Cobalt Coordination Environment. *Angew. Chem. Int. Ed.* **2005,** *44* (41), 6673−6677; (b) Takaoka, K.; Kawano, M.; Tominaga, M.; Fujita, M., In Situ Observation of a Reversible Single-Crystal-to-Single-Crystal Apical-Ligand-Exchange Reaction in a Hydrogen-Bonded 2D Coordination Network. *Angew. Chem. Int. Ed.* **2005,** *44* (14), 2151−2154; (c) Fu, S.-J.; Cheng, C.-Y.; Lin, K.-J., A Reversible Octahedral to Trigonal−Bipyramidal Cobalt Coordination Change in an Aquo-Accessible Coordination Network. *Cryst. Growth Des.* **2007,** *7* (8), 1381−1384; (d) Lasanta, T.; Olmos, M. E.; Laguna, A.; López-de-Luzuriaga, J. M.; Naumov, P., Making the Golden Connection: Reversible Mechanochemical and Vapochemical Switching of Luminescence from Bimetallic Gold–Silver Clusters Associated through Aurophilic Interactions. *J. Am. Chem. Soc.* **2011,** *133* (41), 16358−16361; (e) Shen, C.; Sheng, T.; Zhu, Q.; Hu, S.; Wu, X., Four new Cobalt(II) Coordination Complexes: Thermochromic Switchable Behavior in the Process of Dehydration and Rehydration. *CrystEngComm* **2012,** *14* (9), 3189−3198.

100. Payne, G., Threads of Evidence: Thermochromic threads are used to protect important documents from counterfeiting. *Chem. Ber.* **2002,** *38*, 37−39.

101. Nicholls, J., Smart Coatings: a Bright Future. *Mater. World* **1996,** *4*, 19−21.

102. Sacripante, G.; Kittelberger, S., Worth the paper New types of inks will make recycling office paper more feasible. *Chem. Ber.* **2001,** *37*, 52−55.

103. White, G. D.; Zartman, D. A.; Bonicamp, J. M., A Serious Look at Changeable Silly Putty. *Chem. Educator* **2000,** *5* (1), 2−7.

104. Horváth, I. T., Introduction: Sustainable Chemistry. *Chem. Rev.* **2018,** *118* (2), 369−371.

105. Chu, Q.; Duncan, A. J. E.; Papaefstathiou, G. S.; Hamilton, T. D.; Atkinson, M. B. J.; Mariappan, S. V. S.; MacGillivray, L. R., Putting Cocrystal Stoichiometry to Work: A Reactive Hydrogen-Bonded "Superassembly" Enables Nanoscale Enlargement of a Metal-Organic Rhomboid via a Solid-State Photocycloaddition. *J. Am. Chem. Soc.* **2018,** *140* (14), 4940−4944.

106. Stavila, V.; Talin, A. A.; Allendorf, M. D., MOF-based Electronic and Opto-Electronic Devices. *Chem. Soc. Rev.* **2014,** *43* (16), 5994−6010.

107. (a) Chen, J.; Wu, X.; Hou, X.; Su, X.; Chu, Q.; Fahruddin, N.; Zhao, J. X., Shape-Tunable Hollow Silica Nanomaterials Based on a Soft-Templating Method and Their Application as a Drug Carrier. *ACS Appl. Mater. Interfaces* **2014,** *6* (24), 21921−21930; (b) Lee, K. J.; Lee, J. H.; Jeoung, S.; Moon, H. R., Transformation of Metal–Organic Frameworks/Coordination Polymers into Functional Nanostructured Materials: Experimental Approaches Based on Mechanistic Insights. *Acc. Chem. Res.* **2017,** *50* (11), 2684−2692.

108. (a) Bucholtz, K. M.; Gareiss, P. C.; Tajc, S. G.; Miller, B. L., Synthesis and Evaluation of the First *cis*-Cyclobutane-Containing Receptor for Lipid A. *Org. Biomole. Chem.* **2006,** *4* (21), 3973−3979; (b) Byrne, N.; Strous, M.; Crépeau, V.; Kartal, B.; Birrien, J.-L.; Schmid, M.; Lesongeur, F.; Schouten, S.; Jaeschke, A.; Jetten, M.; Prieur, D.; Godfroy, A., Presence and activity of anaerobic ammonium-oxidizing bacteria at deep-sea

hydrothermal vents. *J. Int. Soc. Microb. Ecol.* **2009,** *3* (1), 117−123; (c) Dembitsky, V. M., Naturally occurring bioactive Cyclobutane-containing (CBC) alkaloids in fungi, fungal endophytes, and plants. *Phytomedicine* **2014,** *21* (12), 1559−1581; (d) Fan, Y.-Y.; Gao, X.-H.; Yue, J.-M., Attractive natural products with strained cyclopropane and/or cyclobutane ring systems. *Science China Chemistry* **2016,** *59* (9), 1126−1141; (e) Goodman, C., Cyclobutanes prove charlatans. *Nature Chemical Biology* **2012,** *8* (8), 678−678; (f) Rosa, M. O.; Albertina, G. M.; Graciela, Y. M., Cyclobutane Biomolecules: Synthetic Approaches to Amino Acids, Peptides and Nucleosides. *Curr. Org. Chem.* **2005,** *9* (3), 237−259.

109. (a) Warnecke, A.; Fichtner, I.; Garmann, D.; Jaehde, U.; Kratz, F., Synthesis and Biological Activity of Water-Soluble Maleimide Derivatives of the Anticancer Drug Carboplatin Designed as Albumin-Binding Prodrugs. *Bioconjugate Chem.* **2004,** *15* (6), 1349−1359; (b) Figueras, A.; Miralles-Llumà, R.; Flores, R.; Rustullet, A.; Busqué, F.; Figueredo, M.; Font, J.; Alibés, R.; Maréchal, J.-D., Synthesis, anti-HIV activity studies, and in silico rationalization of cyclobutane-fused nucleosides. *ChemMedChem* **2012,** *7* (6), 1044−1056; (c) Sittiwong, W.; Zinniel, D. K.; Fenton, R. J.; Marshall, D. D.; Story, C. B.; Kim, B.; Lee, J.-Y.; Powers, R.; Barletta, R. G.; Dussault, P. H., Development of cyclobutene- and cyclobutane-functionalized fatty acids with inhibitory activity against Mycobacterium tuberculosis. *ChemMedChem* **2014,** *9* (8), 1838−1849; (d) Sproul, C. D.; Mitchell, D. L.; Rao, S.; Ibrahim, J. G.; Kaufmann, W. K.; Cordeiro-Stone, M., Cyclobutane Pyrimidine Dimer Density as a Predictive Biomarker of the Biological Effects of Ultraviolet Radiation in Normal Human Fibroblast. *Photochem. Photobiol.* **2014,** *90* (1), 145−154; (e) Zheng, Y.; Tice, C. M.; Singh, S. B., The use of spirocyclic scaffolds in drug

discovery. *Bioorg. Med. Chem. Lett.* **2014,** *24* (16), 3673−3682; (f) Chernykh, A. V.; Radchenko, D. S.; Chernykh, A. V.; Kondratov, I. S.; Tolmachova, N. A.; Datsenko, O. P.; Kurkunov, M. A.; Zozulya, S. X.; Kheylik, Y. P.; Bartels, K.; Daniliuc, C. G.; Haufe, G., Synthesis and Physicochemical Properties of 3-Fluorocyclobutylamines. *Eur. J. Org. Chem.* **2015,** *2015* (29), 6466−6471.

110. Carey, F. A.; Sundberg, R. J., *Advanced Organic Chemistry*. Springer US: 1990; p 832.

111. (a) Gao, X.; Friščić, T.; MacGillivray, L. R., Supramolecular Construction of Molecular Ladders in the Solid State. *Angew. Chem. Int. Ed.* **2004,** *43* (2), 232−236; (b) MacGillivray, L. R.; Papaefstathiou, G. S.; Friščić, T.; Hamilton, T. D.; Bučar, D.-K.; Chu, Q.; Varshney, D. B.; Georgiev, I. G., Supramolecular Control of Reactivity in the Solid State: From Templates to Ladderanes to Metal−Organic Frameworks. *Acc. Chem. Res.* **2008,** *41* (2), 280−291; (c) Papaspyrides, C. D.; Vouyiouka, S. N., Fundamentals of Solid State Polymerization. In *Solid State Polymerization*, 2009; p 1−37; (d) Sonoda, Y., Solid-State [2+2] Photodimerization and Photopolymerization of α,ω-Diarylpolyene Monomers: Effective Utilization of Noncovalent Intermolecular Interactions in Crystals. *Molecules* **2011,** *16* (1), 119−148; (e) Biradha, K.; Santra, R., Crystal engineering of topochemical solid state reactions. *Chem. Soc. Rev.* **2013,** *42* (3), 950−967.